NTNU
Norwegian University of
Science and Technology

Reducing Energy Consumption in the Production of Hydrogen from Natural Gas

Avinash Shankar Rammohan Subramanian

Natural Gas Technology
Submission date: June 2017
Supervisor: Truls Gundersen, EPT
Co-supervisor: Rahul Anantharaman, SINTEF Energy Research

Norwegian University of Science and Technology
Department of Energy and Process Engineering

NTNU

Norwegian University
of Science and Technology

Department of Energy
and Process Engineering

EPT-M-2017-65

MASTER THESIS

for

Student Avinash Shankar Rammohan Subramanian

Spring 2017

Reducing Energy Consumption in the Production of Hydrogen from Natural Gas

Redusert energiforbruk ved produksjon av hydrogen fra naturgass

Background and objective

Hydrogen is expected to play an important role in a decarbonized energy scenario, particularly in light of the agreement by all parties involved at COP21. Almost all H_2 production is from fossil fuels today, and this results in significant CO_2 emissions. In order to transition to a future energy system where H_2 is produced from renewable sources, fossil based H_2 production with CO_2 capture is important. This is especially true from a Norwegian perspective where H_2 production from natural gas with CO_2 capture and storage (CCS) will be relevant.

This Master thesis project is a continuation of a Specialization project in the Fall 2016 by the same candidate, where new methodologies for analyzing and designing energy efficient chemical process were tested. In particular, the so-called G-H methodology (G is Gibbs free energy, while H is enthalpy) developed by Professor Hildebrandt and her research group in South Africa was tested for hydrogen production from natural gas, an important production to support the transition from fossil to renewable energy sources. Carbon capture and storage must of course be part of any such production of hydrogen.

The above-mentioned Specialization project focused on energy penalties in the production of hydrogen from natural gas with special emphasis on the steam reforming processes. The approach used was to identify irreversibilities and corresponding exergy losses in the process.

The ***main objective*** of this Master thesis project is to develop novel energy efficient processes for hydrogen production from natural gas with CCS.

The following tasks are to be considered:

1. Provide a brief summary of the main results from the Specialization project (since a concluding chapter was missing).
2. Examine the trade-offs between the different possible ways to achieve conversion and process irreversibility.

3. Extend the investigation on the use of recycles in the model used in the Specialization project.
4. Separation of products is important to meet purity specifications, and this would change the operating point in the G-H space, since the separation process requires work. Investigate ways to achieve separation, including integrated separation of products.
5. Use the G-H methodology to design a new model for a highly efficient steam methane reforming process for the Integrated Reforming Combined Cycle (IRCC).
6. Investigate alternative ways of adding and recovering work from the process.
7. Add more realism to the above models, such as more realistic operating temperatures, finite heat exchanger approach temperatures and real gas deviation from ideal gas. Simulate these models with Aspen HYSYS.

Tasks 2-6 should be solved in an order of priority to be determined in discussion with the supervisors. Also, these tasks should be considered to the extent that time allows.

-- " --

Within 14 days of receiving the written text on the master thesis, the candidate shall submit a research plan for his project to the department.

When the thesis is evaluated, emphasis is put on processing of the results, and that they are presented in tabular and/or graphic form in a clear manner, and that they are analyzed carefully.

The thesis should be formulated as a research report with summary both in English and Norwegian, conclusion, literature references, table of contents etc. During the preparation of the text, the candidate should make an effort to produce a well-structured and easily readable report. In order to ease the evaluation of the thesis, it is important that the cross-references are correct. In the making of the report, strong emphasis should be placed on both a thorough discussion of the results and an orderly presentation.

The candidate is requested to initiate and keep close contact with his/her academic supervisor(s) throughout the working period. The candidate must follow the rules and regulations of NTNU as well as passive directions given by the Department of Energy and Process Engineering.

Risk assessment of the candidate's work shall be carried out according to the department's procedures. The risk assessment must be documented and included as part of the final report. Events related to the candidate's work adversely affecting the health, safety or security, must be documented and included as part of the final report. If the documentation on risk assessment represents a large number of pages, the full version is to be submitted electronically to the supervisor and an excerpt is included in the report.

Pursuant to "Regulations concerning the supplementary provisions to the technology study program/Master of Science" at NTNU §20, the Department reserves the permission to utilize all the results and data for teaching and research purposes as well as in future publications.

The final report is to be submitted digitally in DAIM. An executive summary of the thesis including title, student's name, supervisor's name, year, department name, and NTNU's logo and name, shall be submitted to the department as a separate pdf file. Based on an agreement with the supervisor, the final report and other material and documents may be given to the supervisor in digital format.

☐ Work to be done in lab (Water power lab, Fluids engineering lab, Thermal engineering lab)
☐ Field work

Department of Energy and Process Engineering, 15 January 2017

Truls Gundersen
Academic Supervisor

Research Advisor:
Dr. Rahul Anantharaman, SINTEF Energy Research

Acknowledgements

I would like to thank my supervisor, Truls Gundersen, for his guidance over the course of this Masters project. In particular, I am grateful that he took the time to provide painstaking feedback on sections of this thesis. In addition, I would like to thank my co-supervisor, Rahul Anantharaman, for his valuable advice on the finer details of the project. It was very encouraging that he understood exactly what questions I had in my mind, and provided useful suggestions.

Contents

List of Figures

List of Tables

Abstract

Hydrogen is a clean fuel and is thus expected to play an important role as an energy carrier in a future decarbonized energy scenario that has a high share of renewable energy. However, global hydrogen production currently is dominated by fossil fuel-based processes with significant inefficiencies. Quantifying the source of these inefficiencies and designing novel efficient processes is essential to realizing a hydrogen-based energy economy. Further, these novel processes have to include carbon dioxide capture and storage (CCS).

Natural gas (containing predominantly methane) is a common feedstock for hydrogen production processes that use the steam-methane reforming (SMR) reaction followed by a water-gas shift (WGS) reaction. Methane is combusted in a furnace to provide heat for the endothermic reforming reaction. In the specialization project, a state-of-the-art hydrogen production process was simulated in Aspen HYSYS, and then an exergy analysis was performed in order to pinpoint the unit operations responsible for the largest sources of inefficiency. The exergy analysis included physical as well as mixing and chemical exergy parameters that were obtained using user-defined subroutines programmed into Aspen HYSYS. The results of the analysis show that the source of largest exergy destruction (and hence inefficiency) is the furnace (47.42 %), followed by the steam generation boiler (20.89%) and the reformer unit (13.72%). Using insight from the exergy analysis, it was deduced that the cause of inefficiencies was incorrect operating conditions (flow rates and compositions of feed streams, temperatures, and pressures) of different unit operations such as the furnace, SMR and WGS reactors. However, it is not practical to design a more efficient process by merely changing the operating conditions of one unit operation since all interconnected unit operations would also be affected by this change. Thus, it is necessary to employ a systematic methodology for conceptual design of an efficient hydrogen production process. This methodology should use a "systems-level" approach, i.e. it should concurrently consider all the unit operations in the process as well as their interconnections.

The objective of this Master's project is to use the systematic "G-H" methodology for conceptual design of a novel efficient hydrogen production process. The G-H methodology uses information about the change in Gibbs free energy (G) and enthalpy (H) at standard conditions to derive the heat and work balances of the corresponding reactor. The heat and work balances of the overall process are then obtained by summing up the contributions of each reactor unit operation weighted by the extent of the reaction taking place. A desirable adiabatic operating point is chosen for the overall process and this fixes the operating conditions for the unit operations as well. The operating temperature for each unit is given by its "Carnot temperature" or "reversible temperature", which is defined as the temperature at which the reaction work requirements are provided exactly by the heat supplied such that both requirements are met concurrently. Units operating at their Carnot temperatures are reversible and hence are efficient since they do not destroy any exergy. Herein lies the value of the G-H methodology: It uses the concept of reversibility to provide a target for the operating conditions that give the highest efficiency from the enormous choice of reactor unit operating conditions. In addition, the G-H methodology is applied at the systems-level ensuring that the entire process is highly efficient rather than focusing on the efficiency of individual unit operations.

However, the G-H methodology is not directly applicable to all design scenarios. For instance, it makes the assumption that complete conversion is achieved in all reactors. This assumption may not hold for all reactors. Thus, this Master's project also proposes extensions to the G-H methodology in order to account for incomplete conversion in the reactors. Thus, a methodological contribution is made in addition to a process design contribution.

With this extended G-H methodology five different hydrogen production processes were designed at the conceptual phase. Four of these processes used the SMR and WGS reactions. These could be distinguished based on the method they used to achieve a certain conversion in the reactors. The four processes were: A process for hydrogen production using 100 % recycle of unreacted feed to achieve complete conversion, a process with 80 % recycle of unreacted feed that achieves lower conversion, a process that supplies one of the components of the feed in excess, and a process that uses membrane reactors with continual removal of the formed product to increase conversion. In order to extend the G-H methodology to the case of using membrane reactors (MRs) in the SMR and WGS unit operations, a novel sequential model was developed to estimate the conversion. Different permeation models were used in the MRs and these were used to obtain upper-bound and lower-bound estimates of conversion. With these conversion estimates the extended G-H methodology was used to design a hydrogen production process with an SMR and WGS MR unit operation. The fifth process uses a highly intensified "1-step" reaction for hydrogen production. The processes were simulated using Aspen HYSYS and an exergy analysis performed. In order to provide a fair basis for comparison, the overall exergetic efficiency was also calculated for each process.

The results showed that all the designed processes had higher overall exergetic efficiencies compared to the state-of-the-art process. The process with 100 % recycle of unreacted feed had the highest overall exergetic efficiency (87.28 %), followed by the process with 80 % recycle (83.07 %). The 1-step process and the process with membrane reactors also show great promise as energy and cost-efficient hydrogen production processes. This is because they represent highly intensified processes, and as a result may have fewer units.

The scope of this Master's project was limited to the conceptual design phase. Future work would involve detailed modeling of each unit operation to include realism considerations. Inclusion of these considerations would result in a decrease in exergetic efficiency. Thus, the processes designed in this thesis represent ideal targets that set the direction for future detailed design stages.

Nomenclature

Abbreviations

F	Permeation molar flow rate of hydrogen
N	Number of blocks in MR
BFW	Boiler Feed Water
MR	Membrane Reactor
P	Pressure in [bar] or [Pascals]
SMR	Steam Methane Reforming reaction
T	Temperature in [°C] or [K]
WGS	Water-Gas Shift reaction

Symbols

Δc_i	Conversion in the reactor stage of block i of the MR
$\Delta G^0_{process}$	Change in standard Gibbs energy
$\Delta H^0_{process}$	Change in standard Enthalpy
$\eta_{overall}$	Overall process exergetic efficiency
A_{stage}	Membrane area of each separation stage of MR
A_{sub}	Membrane area of each separation sub-stage of MR
A_{total}	Total membrane area of MR
f	Multiple of simplest stoichiometric feed
J	Hydrogen flux in [mol/m^{2}s]
P	Permeability of the hydrogen membrane in [Barrers]
p_h	Partial pressure of hydrogen on the feed side in [Pascals]
p_l	Partial pressure of hydrogen on the permeate side in [Pascals]
R	Universal gas constant = 8.314 $[Jmol^{-1}K^{-1}]$
x_i	Mole fraction of component i

L Thickness of the palladium layer in [m]

M Number of sub-stages of each separation stage

N Number of moles of a substance

n Index denoting rate-determining step

P_{perm} Permeate pressure of MR

Q Heat supplied or removed

S Entropy

W Work supplied or removed

Subscripts or Superscripts

i denotes the block number considered

j denotes the separation sub-stage number considered

0 Denotes that quantity is in standard state

comb Combustion reaction

phase Water phase change reaction

Organization of Chapters in the thesis

- Chapter 1 provides an introduction for the Master's project to design a novel efficient hydrogen production process from natural gas. The motivation, scope and approach are described. In addition, Chapter 1 provides a brief literature review on existing processes for hydrogen production from natural gas, as well as on systematic methodologies for designing chemical processes. Finally, a summary of the results of the specialization project is presented. In this way, Chapter 1 addresses Task 1.

- Chapter 2 provides a technical background of the G-H methodology used in subsequent chapters.

- Chapter 3 presents the G-H methodology as a series of steps. It shows why it is necessary to consider the conversion of the reactions taking place, and it outlines several methods to increase conversion.

- Chapter 4 investigates the use of recycling of both components of the unreacted feed as a method of increasing conversion. Two case studies are presented: One with complete conversion and another with 80 % conversion. The G-H methodology is modified to account for incomplete conversion. In this way, Chapter 4 addresses Task 3.

- Chapter 5 investigates changing the feed as a method of increasing conversion.

- Chapter 6 investigates the use of membrane reactors in order to increases conversion. A model to estimate the conversion is presented. With the results of this model, the extended G-H methodology is used to design a hydrogen production process with membrane reactor unit operations. Chapter 6 addresses Task 4.

- Chapter 7 uses a highly intensified 1-step reaction for hydrogen production. Chapter 7 addresses Task 5.

- In Chapters 4 - 7, work recovery from the process is also studied. With the G-H methodology, different processes for hydrogen production are designed and simulated using Aspen HYSYS. An exergy analysis is also done on the different processes. In this way, Tasks 6 and 7 are addressed in the respective sections of Chapters 4 - 7. The overall exergetic efficiency is also calculated in order to provide a fair basis for comparison between the different methods of achieving conversion. Thus, Task 2 is also addressed in these chapters.

- Chapter 8 provides conclusions and lists opportunities for future work.

Contributions

These are divided into methodological contributions and process design contributions. The methodological contributions include:

- The G-H methodology was extended to include scenarios in which incomplete conversion is achieved. To explain this, a case study with a target of 80 % conversion in the Steam Methane Reforming (SMR) and Water-Gas Shift (WGS) reactions was presented in Chapter 4.
- A novel procedure for conceptual design of membrane reactors was developed and explained in Chapter 6. First models were developed to estimate the conversion of membrane reactors. With these conversion estimates, the extended G-H methodology was applied to design a hydrogen production process with membrane reactors for the SMR and WGS processes.

As process design contributions, 5 hydrogen production processes were developed using the G-H methodology. 4 of the processes used the SMR and WGS reaction to produce hydrogen. They were distinguished based on the method used to achieve conversion:

- A process that uses 100 % recycling of both components of the unreacted feed of the SMR and WGS reactors to achieve complete conversion, designed in Chapter 4.
- A process that uses 80 % recycling of both components of the unreacted feed of the SMR and WGS reactors to achieve incomplete conversion, designed in Chapter 4.
- A process that changes the feed to the SMR and WGS reaction, designed in Chapter 5.
- A process that uses membrane reactors for the SMR and WGS reaction, designed in Chapter 6.

In addition:

- A process that uses a highly intensified 1-step reaction for hydrogen production was designed in Chapter 7.

Chapter 1

Introduction

1.1 Motivation

Hydrogen is expected to play an important role as an energy carrier in a future clean energy scenario that has a high share of renewable energy. A hydrogen molecule is converted in the presence of oxygen to water with release of heat and work. This makes it a clean fuel. In Energy Technology Perspectives (ETP) 2016, the International Energy Agency (IEA) highlights the importance of leveraging the heightened low-carbon ambition of the COP 21 in Paris to accelerate clean energy technology research and development [1]. Implementing an energy system with a larger share of hydrogen is a vital step in decarbonizing energy generation.

However, global hydrogen production is currently dominated by fossil fuels, with the most significant technologies being steam reforming of hydrocarbons such as natural gas. While hydrogen can also be produced from renewable energy sources through the electrolysis of water or gasification of biomass, these technologies are energy intensive and still at an early stage of development. Hydrogen production from fossil fuels has the disadvantage of producing significant carbon dioxide emissions. In order to realize a clean hydrogen-based energy economy, hydrogen production with carbon dioxide capture and storage (CCS) is essential. This is especially true from a Norwegian perspective where hydrogen production from natural gas with CCS will be relevant.

While there has been some focus on improving the efficiency of hydrogen production processes with CCS, the emphasis has been on the CCS process. However, unit operations other than CCS may also be inefficient. The main objective of the specialization project [2], done prior to this Master's project, was to perform an exergy analysis on a state-of-the-art hydrogen production process in order to pinpoint the unit operations responsible for the largest sources of inefficiency. This state-of-the-art process uses natural gas (containing predominantly methane) as the feedstock for the Steam Methane Reforming (SMR) reaction that produces hydrogen and carbon monoxide. The carbon monoxide formed is fed into a High Temperature Water-Gas Shift (WGS) reactor. Methane is also combusted in a furnace to provide heat for the endothermic reforming reaction. Further details of the state-of-the-art process are given in Section 1.3. The results of the exergy analysis show that the source of largest exergy destruction (and hence inefficiency) is the furnace (47.42%), followed by the steam generation heat exchanger (20.89%) and the reformer unit (13.72%) [2]. A summary of the procedure used for the exergy analysis in [2] is

given in Appendix A. The most important results obtained are presented in Section 1.3.

Using insight from the exergy analysis, it is deduced that the cause of inefficiencies is incorrect operating conditions (flow rates and compositions of feed streams, temperatures and pressures) of different unit operations such as the furnace, SMR and WGS reactors. However, it is not practical to design a more efficient process by merely changing the operating conditions of one unit operation since all interconnected unit operations would be affected by this change. Thus, it is necessary to employ a systematic methodology right from the conceptual design stage of the novel hydrogen production process. This methodology should use a "systems-level" approach, i.e. it should concurrently consider all the unit operations in the process as well as their interconnections.

1.1.1 Objective, Study Approach and Tools used

This project uses insight from thermodynamics as a tool for the systematic design of a novel hydrogen production process. Specifically, the 2nd law of thermodynamics is applied with the aim of designing as reversible a process as possible. The approach used follows the work done in the research group of Professors Diane Hildebrandt and David Glasser at the University of Witwatersrand. They developed a novel "G-H methodology" that uses thermodynamic insight to design efficient chemical processes. The G-H methodology involves a series of steps used to determine the operating conditions (flow rates and compositions of feed streams, temperatures and pressures) of the unit operations that would result in an overall efficient chemical processes. The main objective of this Master's project is to use the systematic "G-H methodology" to design a novel efficient hydrogen production process. However, the G-H methodology is not directly applicable to all design scenarios. For instance, it does not adequately account for the conversion of reversible chemical reactions. For this reason, this Master's project also proposes extensions to the G-H methodology. Thus, a methodological contribution is made in addition to a process design contribution. In the results section, several process designs are proposed, and an exergy analysis is done to compare between these designs.

1.1.2 Scope

The scope of this project is limited to the conceptual design phase of the hydrogen production processes. Very little information is available and only very few parameters such as the feed and final hydrogen product flow rate and composition are fixed. In the conceptual design phase, a "systems-level" approach is used to develop a process flowsheet that is overall efficient. After this conceptual design phase, detailed modeling and design of unit operations is done. This detailed design phase and onwards is not within the scope of this Masters project.

The next sections in this chapter are organized as follows: Section 1.2 provides a brief literature review on actual processes for hydrogen production from natural gas, Section 1.3 describes the state-of-the-art process used as a case study for the exergy analysis in [2], and also presents the most important results of the exergy analysis, Section 1.4 provides a brief literature review of systematic methodologies used for design of chemical processes.

1.2 Actual Processes for Hydrogen Production from Natural gas

This section provides a brief description of the most important processes for hydrogen production from Natural Gas. The scope is limited to commercially available methods, with a short summary of novel emerging technologies. Figure 1.1 provides an overview of the different processes described. The hydrogen production process commonly includes the following unit operations: The Reforming process, a Water-Gas Shift (WGS) process, the Hydrogen separation process and the Carbon dioxide separation process. Each of these are described in the following subsections.

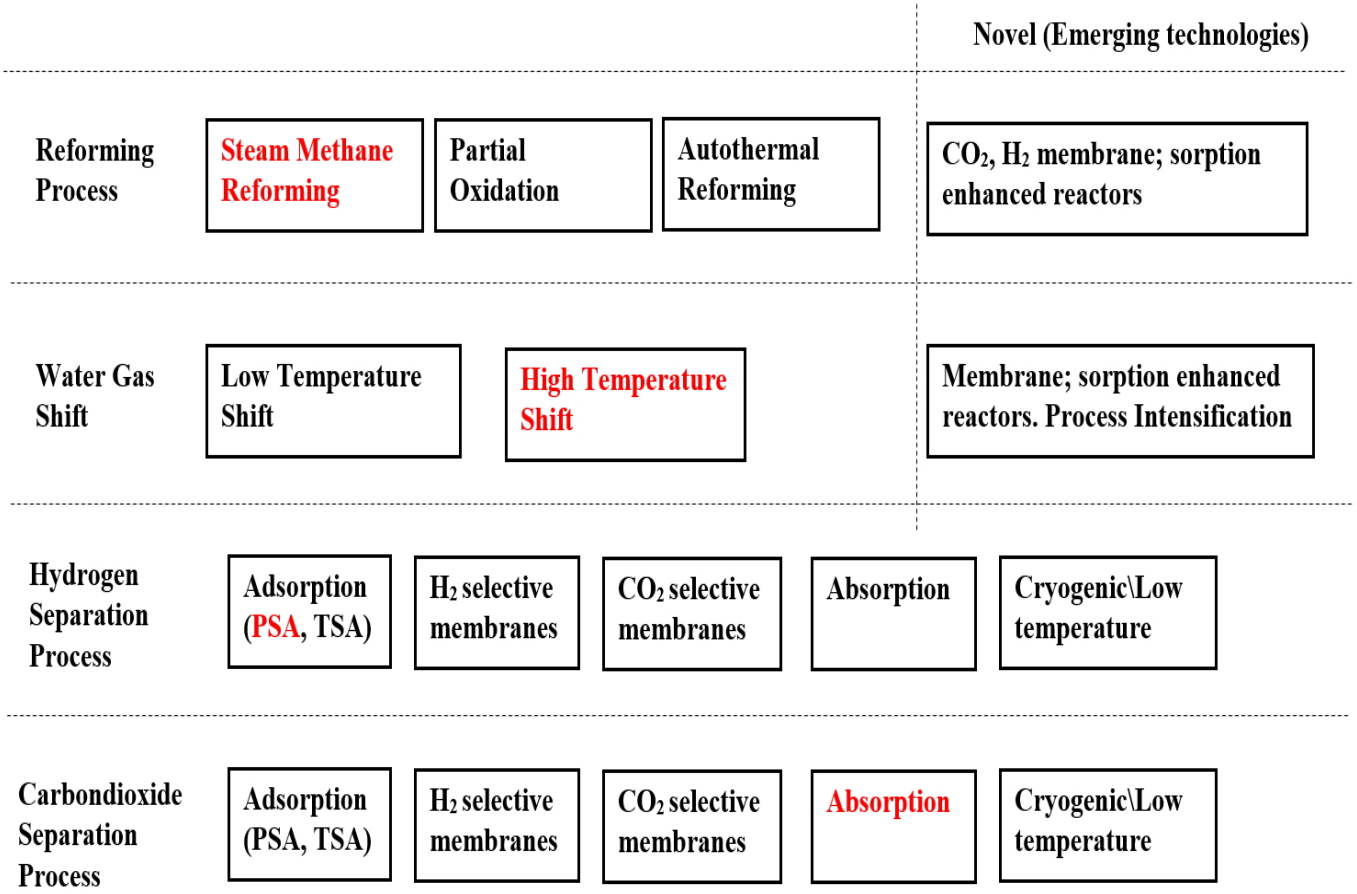

Figure 1.1: Overview of important unit operations for Hydrogen Production Processes. The state-of-the-art process uses the unit operations marked in red

1.2.1 Reforming Processes

The natural gas feed is pretreated and pre-reformed prior to the reforming process. The pretreatment process includes desulphurization in order to prevent poisoning catalysts downstream [3], [4]. Pre-reforming converts the ethane and heavier hydrocarbons which may be present in the natural gas feed to methane. The most common reforming processes of methane are: Steam Methane Reforming (SMR), Partial Oxidation (POX) and Autothermal Reforming (ATR) [4]. Only the SMR reaction is discussed. Further details are available in [2].

Steam Methane Reforming (SMR)

The desulphurized and pre-reformed natural gas then enters the steam reforming reactor where it reacts with steam to produce CO and H_2. The main chemical reaction that occurs is given by Equation 1.1. This equation is equilibrium limited and highly endothermic. It is typically achieved over a nickel-based catalyst operating at high temperatures (500-900 °C) and low pressures (5-25 bar) [4], [5].

$$\mathrm{CH_4(g) + H_2O\,(g) \rightleftharpoons CO\,(g) + 3\,H_2(g)} \tag{1.1}$$

The standard enthalpy and standard Gibbs energy of reaction are given as $\Delta H_{SMR} = 206.12$ kJ/mol, $\Delta G_{SMR} = 142.16$ kJ/mol [6].

In SMR, the heat required for the reforming process is provided from an external furnace in which fuel is burnt. The most commonly used fuel is natural gas itself since it is already available on site. The combustion reaction is exothermic and the heat released is supplied to the SMR reactor. Alternatives for heat supply include hydrogen firing and exhaust gas firing as discussed in [7].

Emerging technologies for reforming include the following:

- Membrane reactors: These continuously remove one of the products in the reforming reaction. They may either be carbon dioxide membrane reactors or hydrogen membrane reactors depending on the product removed. The rationale for integrating a membrane in the active zone of a reactor is to shift the equilibrium leading to higher conversion rates. A systematic methodology for design of a membrane reactor is proposed in Chapter 6.

- Sorption enhanced reforming reactors: These use selected adsorbents to remove one of the products formed at equilibrium so as to shift the equilibrium and achieve higher conversion [4].

1.2.2 Water-Gas Shift Processes

The gas exiting the reformer is cooled to about 350 °C and then subjected to the water-gas shift reaction (WGS). In the WGS, CO reacts with steam to produce CO_2 and additional H_2. This reaction is important because it both maximizes the hydrogen yield and produces CO_2 which can be captured [4]. The WGS is also equilibrium limited but is exothermic as shown in Equation 1.2.

$$\mathrm{CO\,(g) + H_2O\,(g) \rightleftharpoons CO_2(g) + 3\,H_2(g)} \tag{1.2}$$

The standard enthalpy and standard Gibbs energy of reaction are given as:
$\Delta H_{WGS} = -41.19$ kJ/mol, $\Delta G_{WGS} = -28.59$ kJ/mol [6].
Since the number of moles are unchanged in the WGS reaction, pressure has no impact on chemical equilibrium but higher pressures favor faster reaction kinetics.

Emerging technologies for WGS include using membrane reactors and sorption enhanced reactors which operate with the same principle as described in the reforming processes section.

1.2.3 Hydrogen and Carbon dioxide Separation processes

Several options exist for separation and purification of hydrogen from carbon dioxide in the exhaust stream. Hydrogen and carbon dioxide separation processes rely on the same technology so are discussed together in this subsection. The alternative technologies include: Adsorption, absorption, membranes, and cryogenic or low temperature processes [4].

Adsorption

Adsorption is the most technologically mature option. It uses molecules to which one of the product components selectively sticks. Adsorption processes may be divided into Pressure Swing Adsorption (PSA), Temperature Swing Adsorption (TSA). Very pure hydrogen is produced (sometimes exceeding 99.999 mol % [4]).

Absorption

Absorption processes are more widespread for carbon dioxide capture. The most widely used absorbent is MEA, which is commercially proven. Gas separation is achieved by bringing the product stream from the WGS in contact with the solvent in a scrubber. The rich solvent is continuously pumped out and replaced with lean solvent. Regeneration normally occurs by heating but may also occur by pressure swing.

Membranes

Membranes are physical barriers that let certain components pass through easier than others. The part of the feed that passes through the membrane is called the permeate while the part that does not pass through is the retentate. The transport of molecules through the membrane is driven by pressure difference across the membrane implying compression of the feed stream may be necessary to achieve adequate separation. A schematic is shown in Figure 1.2.

For hydrogen production with carbon dioxide capture, both hydrogen and carbon dioxide selective membranes are relevant [4]. Hydrogen selective membranes produce a permeate consisting of high-purity hydrogen, and a retentate with carbon dioxide. Carbon dioxide selective membranes produce a permeate containing carbon dioxide and a retentate containing a majority of hydrogen. Further details are available in [4].

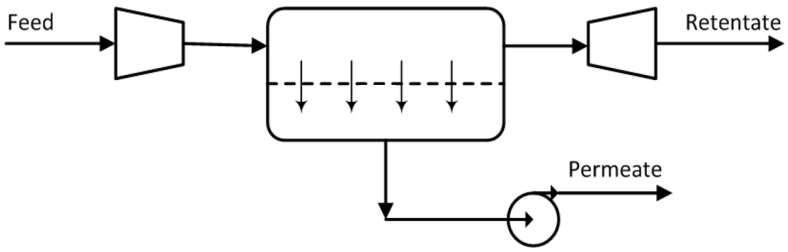

Figure 1.2: Schematic of membrane used in a separation process

Low temperature and cryogenic processes

Low temperature and cryogenic processes use the difference in boiling points of the different components of the exhaust stream for separation. The exhaust gas is compressed and cooled to temperatures close to -55 °C at which carbon dioxide liquefies and is separated out. Further details are available in [4].

1.3 Summary of Exergy Analysis of the state-of-the-art process

1.3.1 Description of process

The previous section gave an overview of different alternatives for unit operations in a typical hydrogen production process, with further details given in [2]. The options indicated in red in Figure 1.1 are selected for the state-of-the-art process that was used as a case study for the exergy analysis performed in [2]. Thus, Steam Methane Reforming, High Temperature WGS, PSA for adsorption of Hydrogen, and MEA for Absorption of carbon dioxide were used. The purpose of this section is to provide a further description of this process.

The case study process was simulated in Aspen HYSYS during previous work at SINTEF Energy. Further details of the simulation are available in [8]. Figure 1.3 shows a flowsheet of this case study.

The natural gas feed is at a pressure of 70 bar and temperature of 25.0 °C. It is expanded and preheated before mixing with steam generated on site. The boiler feed water (BFW) is pumped into a steam generating heat exchanger where it is converted to steam. The steam and natural gas feed are mixed in a mixer. Before the mixed stream enters the preformer, it is heated in the pre-reformer heat exchanger to a temperature of 437.1 °C. The pressure of the pre-reformer is 26.07 bar. The pre-reformer converts heavier hydrocarbons to methane and also reforms some of the natural gas as discussed. The stream leaving the pre-reformer is heated to a temperature of 850 °C before entering a reformer, where the steam methane reforming process occurs. Reformer pressure is 23.28 bar. The product stream is cooled to a temperature of 425.7 °C. This heat is recovered to provide thermal energy for the steam generating heat exchanger. After cooling, the stream enters a high temperature water-gas shift reactor to convert some of the carbon monoxide formed to hydrogen. After cooling, the reformed stream is fed to the hydrogen separation and purification section.

Hydrogen separation occurs with PSA. The feed stream is at a temperature of 25.0 °C and pressure of 22.34 bar. There is a known difficulty in accurately simulating the PSA adsorption and regeneration process in Aspen HYSYS. For this reason, the separation process is modeled as a simple component splitter. The produced hydrogen then undergoes conditioning where it is compressed with intercooling to a temperature of 20 °C and pressure of 80 bar. The separated hydrogen stream is 99.99 % pure.

The purge gas from the PSA component splitter is compressed from a pressure of 0.3447 bar to a pressure of 1.013 before entering a furnace. Air is also preheated before entering the furnace. Combustion occurs at the furnace, which supplies heat to the reformer. The flue gas is at a temperature of 1050 °C. Heat is recovered from the flue gas to supply thermal energy to the natural gas preheater, steam generating heat exchanger, pre-reformer preheater, reformer preheater and feed air preheater. After heat recovery, the flue gas is at a temperature of 106 °C as it enters an absorption unit for removal of carbon dioxide.

Carbon dioxide is removed using an absorption process with MEA. Once again this is modeled with a simple component splitter. The captured carbon dioxide is then conditioned i.e. it is compressed and intercooled to give liquid carbon dioxide at a temperature of 20.31 °C and a pressure of 110.0 bar for transportation to the storage site. Since the carbon dioxide capture unit is located after the furnace, this process is termed a “post-combustion carbon dioxide capture process”.

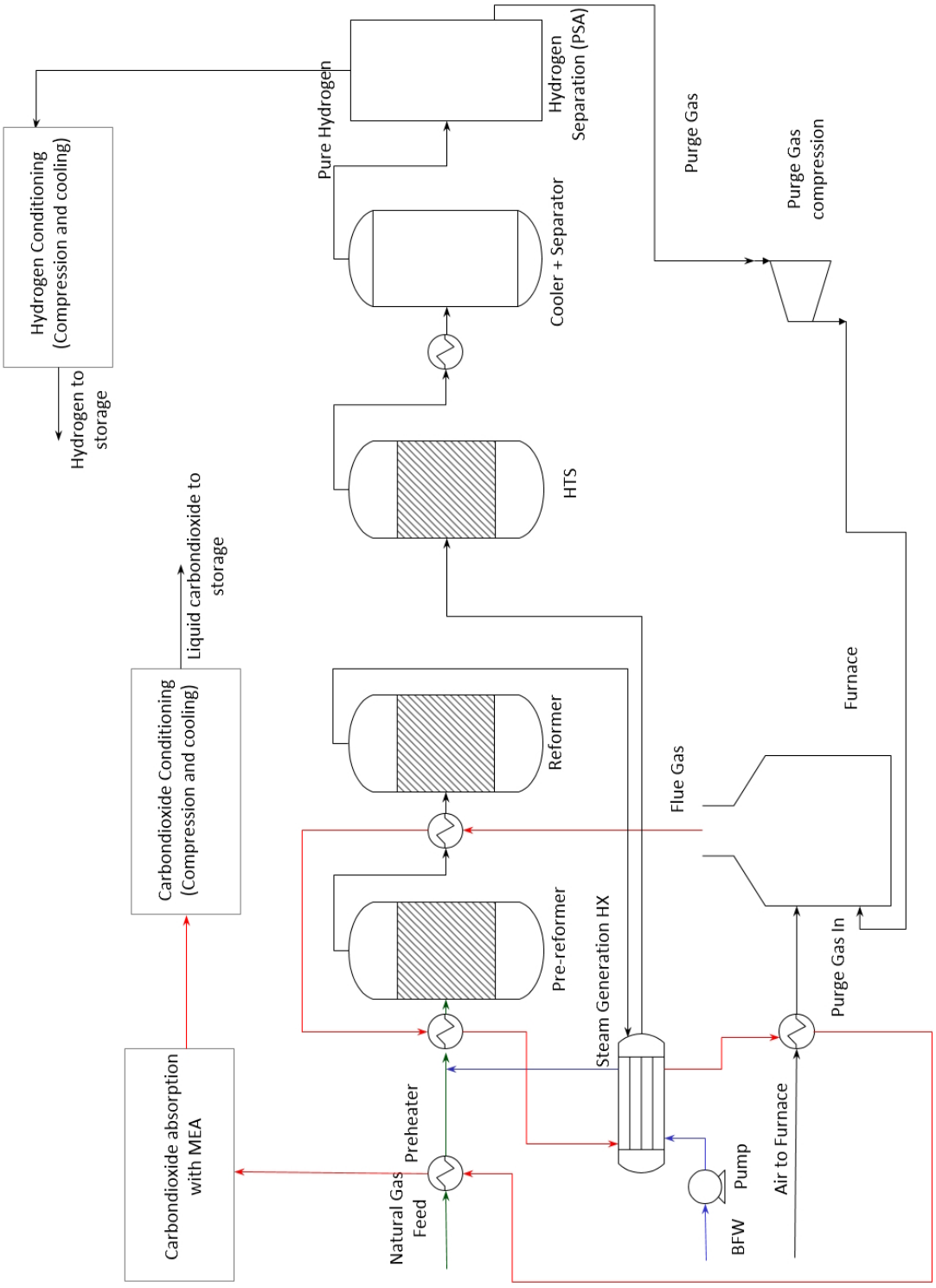

Figure 1.3: Flowsheet of state-of-the-art process used as a case study for the exergy analysis

1.3.2 Overview of Exergy Analysis Results

Full results of the exergy analysis are available in [2], Appendix A contains a summary of the procedure used. An overview of the most important results is presented below. Table 1.1 shows the percentage of exergy destroyed in the different unit operations. The sources of major process irreversibilities are the furnace (47.2 %), the steam generating heat exchanger (20.89 %) followed by the reformer (13.72 %). These results follow a similar trend to the results obtained by Simpson and Lutz in [9]. Simpson and Lutz obtain a percentage exergy destruction of 36.35 % in the furnace, 13.03 % in the reforming process, and 23.51 % in the steam generation process [9]. Note that the case study they study is significantly different which explains the deviation.

Table 1.1: Exergy analysis results of different unit operations of the state-of-the-art process

Component group	Exergy destroyed kW/kmol CH_4	Percentage %
Steam Generation Heat Exchanger	44848.99	20.89
Natural Gas Mixer	10223.17	4.76
Reformer	29466.63	13.72
Water-Gas Shift	16273.75	7.58
Furnace	101829.91	47.42
Hydrogen and carbon dioxide separation	12096.83	5.63
Total Exergy Destroyed	214739.27	

It is necessary to compare the state-of-the-art process with the novel processes designed in this Master's project. In order to get a holistic picture of the process, it is useful to calculate the "overall process exergetic efficiency" for the entire flowsheet developed. Let $\eta_{overall}$ denote this overall process exergetic efficiency with the definition given by Equation 1.3.

$$\eta_{overall} = \frac{\text{Total useful Exergy out of overall process}}{\text{Total Exergy into overall process}} \tag{1.3}$$

The only useful chemical product out of the processes is hydrogen. In addition, the state-of-the-art process is a net supplier of work. Thus, the overall process exergetic efficiency can be calculated using Equation 1.4.

$$\eta_{overall} = \frac{\text{Exergy of hydrogen produced + Work recovered}}{\text{Total Exergy into overall process}} \tag{1.4}$$

Different process configurations would have different feed streams to the overall process as well as different heat supply streams. All material and energy streams into the process must be included in the denominator. Table 1.2 shows the exergy analysis results of the overall state-of-the-art process, and the calculation of the overall process exergetic efficiency.

The material streams into the process are: Natural Gas (NG) Feed, BFW (Boiler Feed Water), and the Air Feed to the furnace while the Hydrogen product is the only useful material stream out. W_{out} represents the net work recovered . Table

Table 1.2: Exergy Analysis of overall state-of-the-art process

Stream	Units	NG Feed	BFW	Air Feed	Hydrogen out	W_{out}	$\eta_{overall}$
Temperature	°C	10	9.775	15	25		
Pressure	bar	70	1	1.013	22.34		
Physical Exergy	kW/kmol CH_4	11222.52	93.44	18.49	22759.38		
Mixing Exergy	kW/kmol CH_4	-1174.50	0.00	-5972.97	0.00		
Chemical Exergy	kW/kmol CH_4	977111.03	2689.89	6121.90	699084.33		
Total Exergy	kW/kmol CH_4	987159.05	2783.33	167.42	721843.71	21046	
			Exergy In =	990109.80	Exergy Out =	742889.71	75.03

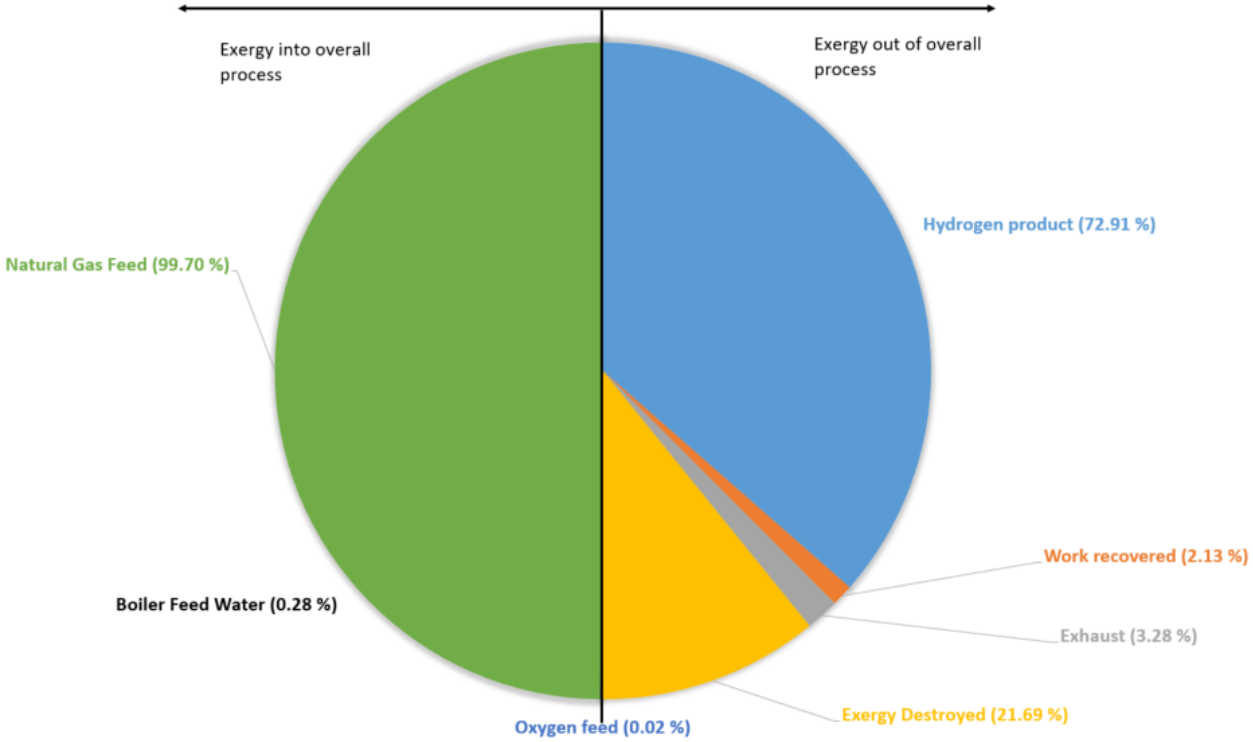

Figure 1.4: Pie chart to visualize the exergy analysis results of the overall state-of-the-art process

1.2 can be visualized in a pie chart as done in Figure 1.4. The left half of the pie chart represents the sum of exergy for the streams entering into the overall process while the right half represents the sum of exergy out of the overall process. The percentage of useful exergy in the hydrogen product stream is 72.91 %, and in the work recovered is 2.13 %. This corresponds to the $\eta_{overall}$ value of 75.03 %. The rest of the exergy out of the process is either destroyed (21.69 %) or disposed off in the exhaust streams (3.28 %). The destroyed exergy corresponds to the value given in Table 1.1, while the rest is exergy in the useless by-product streams. This holistic picture of the state-of-the-art process can be compared with other novel processes designed using the G-H methodology in later sections.

1.4 Systematic Design Methodologies for chemical processes

This chapter contains a brief literature review of systematic design methodologies for chemical processes. It provides a brief background of the main methods available in the field of Process Integration, and shows where the G-H methodology used later fits into the range of available techniques. Further details are available in [2].

1.4.1 Process Integration

The goal of a chemical process is to transform raw materials into desired chemical products. However, this usually cannot be achieved in a single step. The overall process is commonly broken down into a number of intermediate steps such as reaction, separation, mixing, heating and cooling, compression and expansion etc [10]. These steps form building blocks for the chemical process and are termed "unit operations". Unit operations are then interconnected - a procedure called Process Integration, as is explained next.

Process integration is defined by the IEA [11] as:

> "Systematic and General Methods for Designing Integrated Production Systems, ranging from Individual Processes to Total Sites, with special emphasis on the Efficient Use of Energy and reducing Environmental Effects".

This definition includes several key aspects:

- Process Integration is done using Systematic Methods. The best way to figure out and evaluate the best process out of several alternatives is with a methodical procedure. Several Systematic Design Methodologies are available and these are outlined in this section.

- Process Integration is done with a "systems-level" approach. Emphasis is put on optimizing the performance of the entire interconnected system of unit operations before details of these unit operations are fixed. This is contrasted with the "units-level" approach in which the performance of the individual unit operations is optimized before considering the effects of their interactions ([12] cited in [13]). A"systems-level" analysis gives particular targets (for example energy and mass-balance targets) for the optimized process prior to developing a detailed flowsheet of interconnections. The advantage of the "systems-level" approach is that it ensures an overall efficient process rather than a possibly inefficient process with few efficient unit operations [6].

- The goal of Process Integration is to optimize the design with respect to factors such as energy efficiency and environmental impact. The guiding principle for Process Integration is: "Combining ... [unit operations] with needs of an opposite type to give double-savings" [14]. For example, unit operations that require heating are integrated with those that require cooling (Heat integration), compression processes are integrated with expansion processes (power integration) and chemical reaction by-products are used as raw-materials (chemical integration) [14].

1.5 Systematic Design Methodologies in Process Integration

One of the pioneers of using systematic design methodologies for process design was Jim Douglas with his work in 1988 ([15] cited in [11], [16]). This field of research aims to develop methodical procedures to zero in on the most energy-efficient alternatives for the chemical process to transform a given raw material into the desired product.

The life cycle for the design and realization of an integrated chemical process begins with an initial idea. This is followed by a conceptual design phase, before basic engineering, detailed engineering and finally plant construction as shown in Figure 1.5 [17].

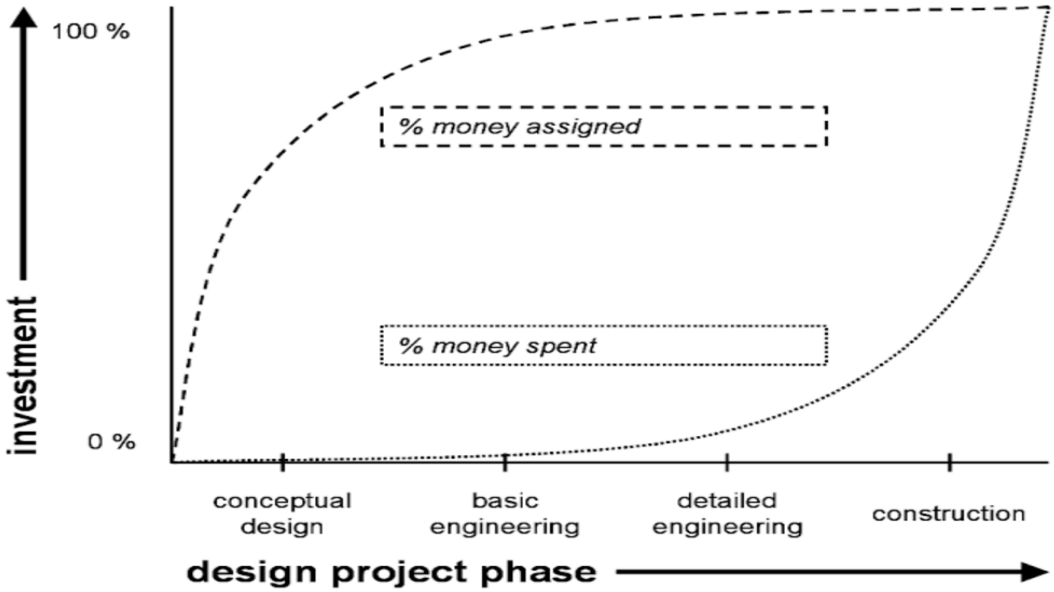

Figure 1.5: Life cycle for design and realization of a typical integrated chemical process [17]

The conceptual design phase is usually quite complex. This is because the design problem is under-defined: Very limited information is available and only very few parameters such as the feed and desired product composition, temperature and pressure are fixed [16]. Thus there exist a very large number of alternatives for possible processes. Systematic design methodologies are employed to consistently evaluate and rank these alternatives based on required criteria such as energy efficiency, capital costs and environmental impacts. Using the systematic design methodologies, informed design decisions are made to give optimized flowsheets.

Figure 1.5 also shows the investment levels at each stage in the process life cycle. It is clear that the design decisions made at the conceptual design stage have a significant impact on the costs of latter stages. However, only a small percentage of the total cost is spent on the conceptual design phase. For example, one study suggests that the conceptual design phase accounts for two or three percent of the project costs, yet the design decisions made fix approximately eighty percent of the total cost of the final plant ([12] cited in [17]). Thus, there is an incentive to "get it right from the start": Robust and rigorous design methodologies are sought to generate the most efficient flowsheets with a high degree of accuracy. Further,

this motivates implementing "systems-level" thinking right from this early stage; it is useful to include all the unit operations as well as their interconnections in the conceptual design stage to avoid surprises at later stages when more investments have been made. In this way, the inherently open-ended nature of the conceptual design phase can be turned into an advantage to explore the best design alternatives to implement in later stages.

In his seminal work of 1988, Jim Douglas proposed a systematic "Hierarchical" method which is described in the following sub-section ([15] cited in [16], [17]).

1.5.1 Hierarchical Method for design of Integrated Processes

The Hierarchical Method involves division of the complex conceptual design task into a logical sequence of levels. Several design decisions are made at each level such that the amount of detail in the design increases [17]. A more complete description of the levels in Douglas' classical Hierarchical Method can be found in [16] and [17]. A simpler visual representation of the Hierarchical Method called the "Onion Diagram" is shown in Figure 1.6 [11].

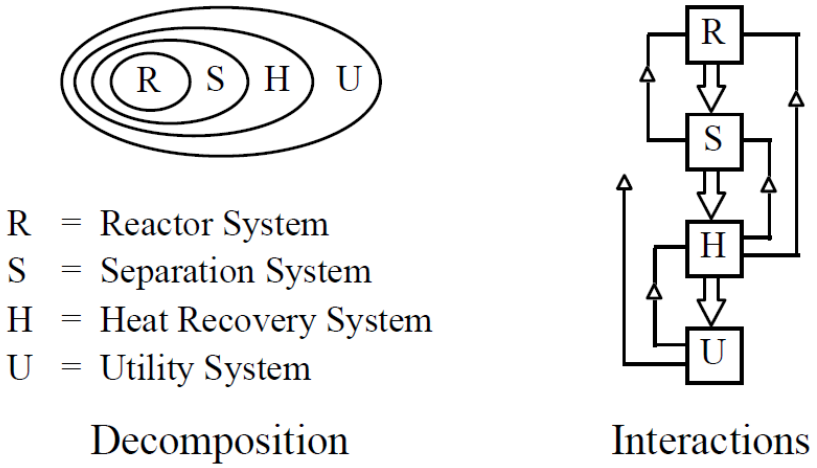

Figure 1.6: Onion diagram to represent the Hierarchical Method for Integrated Process Design [11]

The Onion diagram shows the order of design in the different levels. The Reactor System is designed first, followed by the Separation System to partition the desired product from the other by-products. Next, opportunities for heat integration are investigated to design the Heat Recovery System, followed by the Utility System to provide the balance of the heating or cooling requirement, as well as other functions. The interconnections between these different levels is also considered implying that the Hierarchical Method is a "systems-level" approach.

Systematic design methodologies that use the hierarchical method can be classified according to different frameworks. Gundersen suggests a framework for classification of these methodologies using a two-dimensional automatic vs. interactive and quantitative vs. qualitative representation shown in Figure 1.7 [11]. These are discussed below:

- "Knowledge Based Systems" use artificial intelligence concepts to automatically make decisions based on qualitative knowledge input [11].

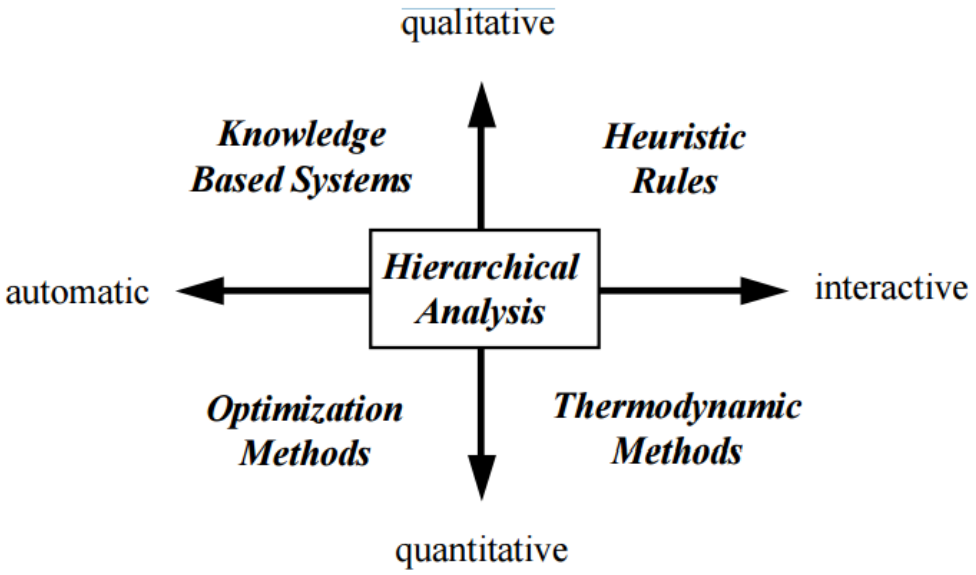

Figure 1.7: Classification of different frameworks for the Hierarchical Method [11]

- Under "Heuristic Rules", the prior experience of designers in the field is used to provide educated guesses so as to narrow down to the most promising process alternatives.

- Optimization methods use mathematical-programming concepts to determine the best process design out of several possible alternatives. Grossmann et al. summarize the approach into three steps [18]. First, the different process alternatives from which the optimal solution is to be found are generated. Second, the mathematical program to represent the process is formulated. It may involve discrete variables (for instance for decisions related to equipment) or continuous variables (for instance for decisions related to flows and operation) [14]. Then the optimal solution for the optimization model is determined by minimizing (or maximizing) the "objective function" [19]. The search process for the optimal solution is done subject to specific constraints such as material and energy balances, thermodynamic limitations, technical limitations, forbidden matches etc. [14][19].

  Optimization programs can be classified based on the nature of the objective function and the constraints: If both are linear, the program becomes a Linear Program (LP); otherwise it is a Non-Linear Program (NLP). The nature of the optimization variables can be used for further classification: Purely integer variables result in a Integer Program (IP) while a mixture of continuous and integer optimization variables could be classified as Mixed-Integer Linear Programs (MILPs) or Mixed-Integer Non-Linear Programs (MINLPs) [19]. A further discussion of these three classes is beyond the scope of this report.

  Thermodynamic Methods are used in this project so are discussed in further detail next.

1.5.2 Thermodynamic Methods

Thermodynamic insight can be used to narrow the space in which to search for optimal process design alternatives. Methods can be divided into those using the 1st law of thermodynamics and those using the 2nd law of thermodynamics. These are elaborated in further detail in the next sub-sections. However, before this can be done, it is useful to differentiate between "Targeting" and "Network Synthesis".

- In "Targeting", relevant performance targets are set or calculated for each of the levels in the Hierarchical Method prior to carrying out Network Synthesis. By setting these targets a priori, the designer reduces the search space for optimal design alternatives [20], [10] in the "Network Synthesis" stage.
- "Network Synthesis" or "Network Design" is performed after the Targeting phase. It involves determining and drawing out the location of the different unit operations as well as the interconnections between them such that the targets are met. Thus Network Synthesis deals with determining the topology of the system i.e. figuring out how the different unit operations are organized to form the overall process structure.

Systematic thermodynamic methods commonly involve an iterative procedure consisting of a series of targeting and network synthesis steps.

1st law of thermodynamics - Targeting

Historically, insight from the 1st law of thermodynamics (also known as the principle of conservation of energy) was first applied to understanding the potential for heat recovery in the chemical process (level 3 of the Onion Diagram). This was done by Linnhoff et al. with the concept of the "Heat Recovery Pinch" [11]. Targeting for the heating utility and cooling utility demand (and thus the level of heat recovery) was then possible at the "systems-level" by use of "Composite Curves" as described in [10],[11]. This approach was then extended to the Utility System (level 4 of the Onion Diagram) by the concept of "Grand Composite Curves". The "Pinch" point is central to these techniques, thus they are termed generally as "Pinch Analysis". Other Targeting approaches include Residue Curve Maps for Separation Systems (level 2 of the Onion Diagram) and the Attainable Region Theory for Reactor Systems (level 1 of the Onion Diagram) [20].

1st law of thermodynamics - Network Synthesis

Network Synthesis can then be performed using the targets obtained from "Pinch Analysis". The systematic methodology to use "Pinch" concepts for network design is called the "Pinch Design Method". Using thermodynamic insight, appropriate design decisions are taken to develop the flowsheet topology. Full details on the use of the "Pinch Design Method" for Heat Exchanger Network (HEN) design are provided in [10] and [14], with a summary in [2].

2nd law of thermodynamics - Targeting

The 2nd law of thermodynamics can be used to provide greater insight into the sources of process inefficiencies. The 1st law of thermodynamics only considers the

"quantity" of energy: It views all the different forms such as chemical energy, heat, work, electrical energy, etc. as equally useful. However, this is not the case: For instance, it can be shown that even an ideal heat engine cannot convert all the available thermal energy to work. Thus, energy has a "quality" as well as a "quantity" as demonstrated by the 2nd law of thermodynamics [21]. Exergy is the term that encompasses both the quality and quantity aspect of energy. In the specialization project, an exergy analysis was performed on a state-of-the-art hydrogen production process [2]. This exergy analysis was used to reveal the unit operations responsible for the greatest source of exergy destruction (and hence inefficiency). Unit operations that do not destroy exergy operate at their maximum possible thermodynamic efficiency. Thus, a 2nd law analysis can be used to provide a target for subsequent design stages. Appendix A contains a summary of the procedure for this exergy analysis.

2nd law of thermodynamics - Network Synthesis

After the targeting phase, insight from the 2nd law of thermodynamics can be used to design flowsheets that meet the targets. Although a substantial body of research is available on using insight from the 2nd law for analysis of existing flowsheets (for example [22],[23] and [24]), the application of the principles to network synthesis is far from developed ([24] cited in [20]). The central objective of this Master's project is to use and extend the recently developed "G-H" methodology as a procedure for network synthesis using the 2nd law of thermodynamics. The "G-H" methodology was developed by the research group of Professors Diane Hildebrandt and David Glasser at the University of Witwatersrand. Relevant research papers are [6],[13],[20],[25],[26] and [27]. A description of the G-H methodology is given in Chapter 2. Chapters 3 to 7 use and extend this systematic methodology for design of a novel efficient hydrogen production process from natural gas.

Chapter 2

Technical Background of the G-H Methodology

This chapter provides a technical background of the systematic G-H methodology as a tool that uses thermodynamic insight to design more efficient processes. The emphasis of this chapter is to provide an overview of the basic thermodynamics of the G-H methodology. In Chapter 3, these basics are used to design a process for hydrogen Production from methane.

This chapter relies heavily on the work done in the research group of Professors Diane Hildebrandt and David Glasser at the University of Witwatersrand. Relevant research papers are [6], [13], [20], [25], [26] and [27] where complete details can be found.

2.1 Simple Chemical Process

The G-H methodology begins by clearly defining a "simple chemical process". Since the G-H methodology is applied at the conceptual design phase in which very limited information is available, only the feed reactants and final product streams can be well-defined. These two streams are fixed to be at ambient conditions T_0 and P_0. The reactor can operate at any temperature T and pressure P. Figure 2.1 shows a schematic of the simple chemical process.

The following assumptions are made:

- The reactor is assumed to be the main heat sink (endothermic reaction) or main heat source (exothermic reaction); heat Q is added or removed at the reactor temperature T to satisfy these requirements.
- The reactant and products are assumed to be pure components.
- The reactants and products are assumed to be ideal gases. Thus, the ideal gas equation is assumed to hold.
- Both the mixing of reactants and separation of products into pure components take place at constant ambient temperature T_0 and pressure P_0.
- The separation process of the product into pure components is assumed to have a negligible work requirement. This assumption may not be realistic and is addressed extensively in this Master's project.

- The reactant stream at ambient pressure P_0 is brought to the reactor pressure P using isothermal compression. Similarly, the product from the reactor at P is brought to ambient pressure P_0 using isothermal expansion.
- The reactant stream at ambient temperature T_0 is brought to the reactor temperature T by internal heat exchange with the product stream, which is brought from T to T_0. Thus, it is assumed that the reactant and product streams have equal heat capacities.
- Complete conversion of reactants to products is assumed at reactor temperature T and pressure P. This assumption may not be accurate and is addressed extensively in this Master's project.
- Other process components and equipment are assumed to have a negligible heat load compared to the reactor heat load. Thus, heat (Q) is supplied to (or removed from) only the reactor.

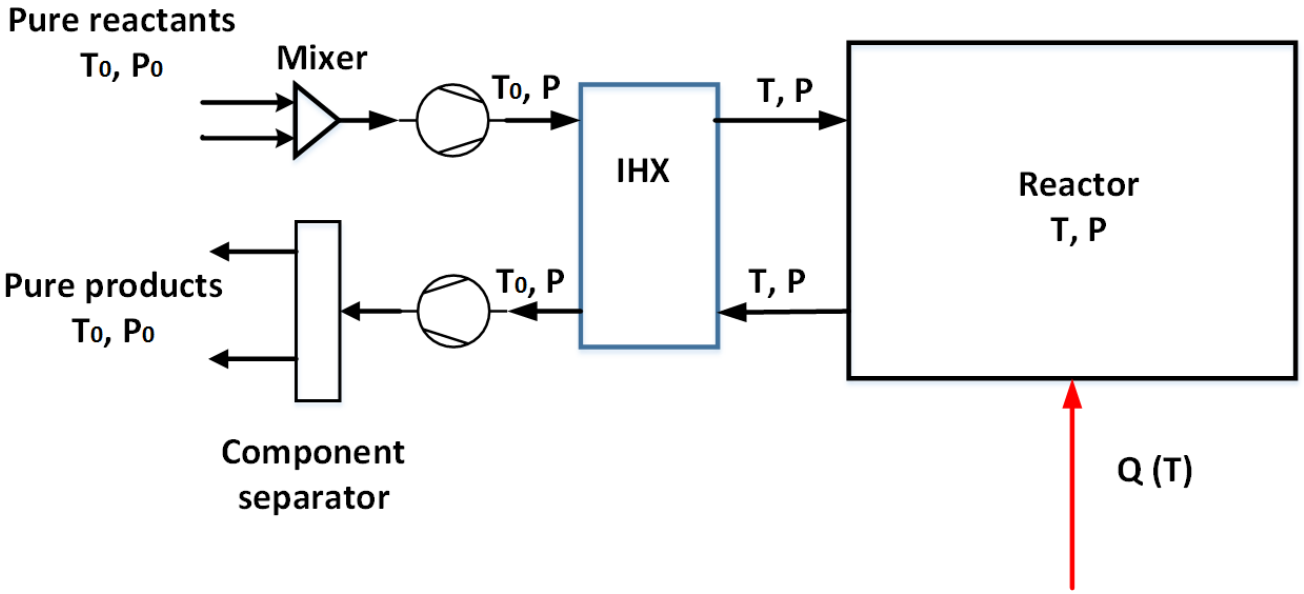

Figure 2.1: Schematic of the Simple Chemical Process. IHX is an Internal Heat Exchanger between reactant and product streams

2.1.1 Thermodynamics of the simple chemical process

Consider a reversible reaction with 2 reactants and 2 products:

$$\nu_A A + \nu_B B \rightleftharpoons \nu_C C + \nu_D D \tag{2.1}$$

where: υ_i is the stoichiometric coefficient of reactant or product component i.

1st law of thermodynamics

Using the 1st law of thermodynamics, Equation 2.2 is derived. Full details of the energy balance and derivation are available in [2].

$$Q = \Delta H^0_{process} \tag{2.2}$$

$\Delta H^0_{process}$ is the standard enthalpy change of reaction, calculated using Equation 2.3:

$$\Delta H^0_{process} = (\sum_i v_i.H^0_{f,i})_{products} - (\sum_i v_i.H^0_{f,i})_{reactants} \tag{2.3}$$

where $H^0_{f,i}$ is the enthalpy of formation of component i at standard conditions T_0 and P_0.

This result implies that the heat requirement Q of the reactor can be obtained with only information about the reactants and products. This heat demand can be supplied by a utility system or from other exothermic processes.

2nd law of thermodynamics

In a 2nd law analysis, the Gibbs energy (also called Gibbs free energy) G is relevant. The definition of Gibbs energy is given by Equation 2.4.

$$G \equiv H - TS \tag{2.4}$$

The change in Gibbs energy at standard conditions of P_0 and T_0 is given by Equation 2.5.

$$\Delta G^0 = \Delta H - T_0 \Delta S \tag{2.5}$$

As can be seen in [28], Equation 2.5 is also the definition of exergy. Exergy is thought of as the work produced by a system as it changes state to the environmental state (T_0, P_0) through a reversible process. From this equation, it is deduced that the amount of reversible work W that must be added or removed from a process is equal to the change in Gibb's energy of the process at standard conditions of temperature T_0 and pressure P_0. If the process under consideration is the simple chemical process with reactants and products at ambient conditions, then the reversible work required is given by Equation 2.6:

$$W = \Delta G^0_{process} \tag{2.6}$$

$\Delta G^0_{process}$ is given by:

$$\Delta G^0_{process} = (\sum_i v_i \Delta G^0_{f,i})_{products} - (\sum_i v_i \Delta G^0_{f,i})_{reactants} \tag{2.7}$$

where $\Delta G^0_{f,i}$ is the standard Gibbs energy of formation of component i.

The sign convention used in Equation 2.6 is defined as follows: The work required (W_{in}) by the process in order to proceed is given by the change in Gibbs energy at standard conditions of P_0 and T_0. Thus, Equation 2.6 is written more precisely in Equation 2.8:

$$W_{in} = \Delta G^0_{process} \tag{2.8}$$

Conversely, the work that can be supplied by the process (W_{out}) is given by the negative of Equation 2.8:

$$W_{out} = -\Delta G^0_{process} \tag{2.9}$$

This sign convention makes sense because a process with a positive value of $\Delta G^0_{process}$ requires work to be supplied (W_{in}) in order to proceed, while a process with a negative value of $\Delta G^0_{process}$ can supply work (W_{out}).

Equation 2.6 implies that the work requirement of the reactor can be obtained with only information about the reactants and products. Equations 2.2 and 2.6 are key results relating the heat and work requirements of the simple chemical process to the standard enthalpy change and standard Gibbs energy change of reaction. Thus, they are central to the G-H methodology and give it its name.

For convenience, the subscript "process" and superscript "0" are dropped in the following sections. It is implied that whenever ΔH or ΔG is written, this would represent the standard enthalpy change of a process and standard Gibbs energy change of a process respectively. The process heat and work requirements are only equal to ΔH or ΔG at standard conditions, not at other conditions.

2.2 The G-H space

The G-H space is a graphical tool used to visualize the heat and work requirements of a simple chemical process. Thus the standard enthalpy change ($\Delta H^0_{process}$) and the standard Gibbs energy change ($\Delta G^0_{process}$), determined for the reaction process occurring at constant temperature T_0 and pressure P_0, are plotted on a Cartesian grid.

The G-H space can be divided into 4 regions according to the sign of ΔH and ΔG. To illustrate this, consider 4 hypothetical chemical reaction processes labeled A, B, C and D each found in different regions as shown in Figure 2.2. Processes in region 1, such as A require heat and work to proceed. Processes in region 2 such as reaction B require work but have to reject heat to proceed. Processes in region 3 such as reaction C need to reject heat and do work to proceed while processes in region 4 such as reaction D need heat but have to reject work to proceed.

The extent of the chemical reaction is also readily represented on the G-H space. For instance, the extent of reaction A is proportional to the length of the line joining reaction A to the origin. This is intuitive because the ΔH and ΔG values scale in proportion to the stoichiometric amount of reactants and products participating in the reactions. As a result, vectors in G-H space represent the thermodynamics of reaction processes. The angle subtended by this vector α is discussed in a later section.

2.3 Combining simple chemical processes

Several simple chemical processes can be combined to form an overall process. Since reaction processes are represented by vectors in G-H space, it implies that the thermodynamics of the overall process can be determined by simple vector addition. For instance, consider the combination of reaction process A of extent e_A with reaction process B of extent e_B, the heat and work requirements of the overall process are given by Equation 2.10.

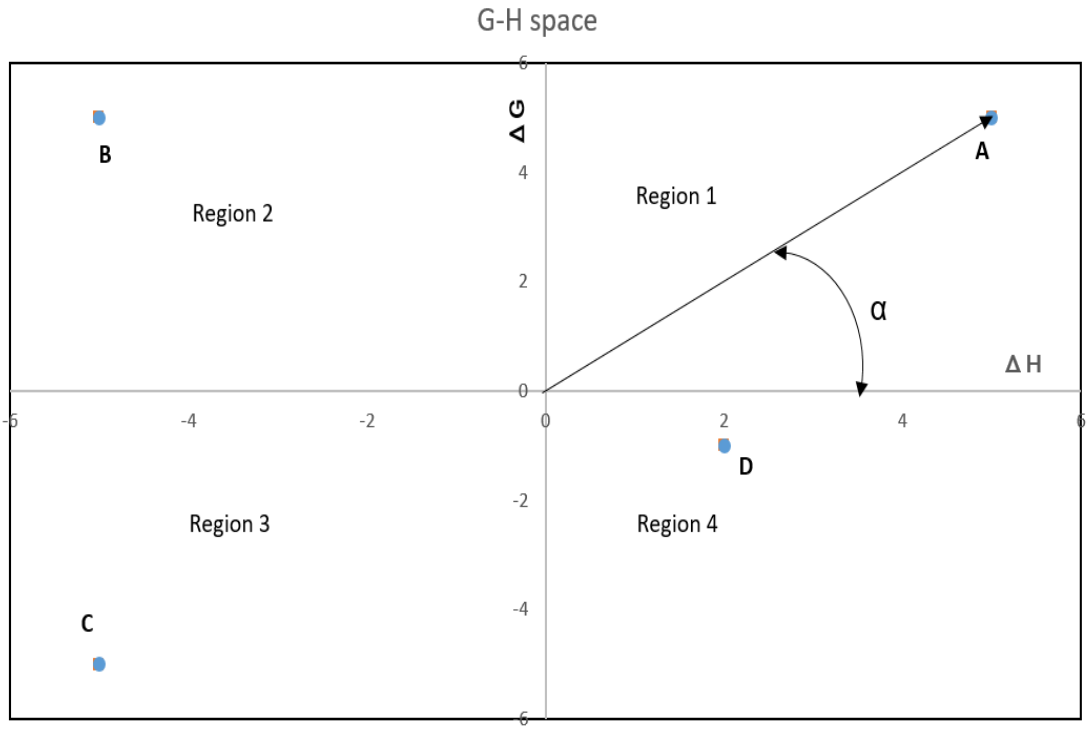

Figure 2.2: Processes in G-H space

$$\begin{pmatrix}\Delta H_{overall}\\ \Delta G_{overall}\end{pmatrix} = \begin{pmatrix}\Delta H_A\\ \Delta G_B\end{pmatrix}(e_A) + \begin{pmatrix}\Delta H_B\\ \Delta G_B\end{pmatrix}(e_B) \tag{2.10}$$

Opportunities for process integration of different reactors can be studied using the G-H space in this way. For instance, it is suitable to integrate a reactor in Region 3 with a reactor in region 1 since they have opposite needs with regards to heat and work required. Using Equation 2.10, the thermodynamics of the overall integrated process can be determined by fixing the extents of the constituent reaction processes.

2.4 The Carnot Temperature

Consider a reaction process in region 1 that requires both heat and work to be supplied from the environment in order to proceed. The supplied heat Q carries with it work which can be used to satisfy the ΔG requirements. The amount of work carried by the supplied heat depends on the temperature T at which the heat is supplied. For the special scenario in which all the required work W is supplied concurrently by the heat Q, the process is reversible. The temperature at which heat Q must be supplied is important and is called the "reversible temperature" or the "Carnot temperature". Equation 2.11 can be used to determine the Carnot temperature. The full derivation of Equation 2.11 is available in Appendix B.

$$T_{Carnot} = \frac{T_0}{1 - (\frac{\Delta G}{\Delta H})} \tag{2.11}$$

This Carnot temperature can be represented on the G-H space. Equation 2.11 shows that the Carnot temperature of the chemical reaction is independent of the extent of the reaction. The Carnot temperature is only dependent of the angle α (See Figure 2.2) which is a measure of the ratio $\frac{\Delta G}{\Delta H}$ in Equation 2.11. In Figure 2.3, the slanted tick marks on the outer box show the Carnot temperature of the reaction lying along the line joining that tick mark to the origin. The straight tick marks show the ΔH and ΔG values between -40 KJ/mol and 40 KJ/mol. From Figure 2.3 the following observations can be made:

- The figure shows that a process that lies at angle α has the same Carnot temperature as a process that lies at angle $\alpha + 180°$. Thus, the Carnot temperatures are symmetrical about the origin. Using this result, it is sufficient for the sake of clarity to label the Carnot temperatures for only half of Figure 2.3 - the Carnot temperatures for the other half can be easily obtained by drawing a line from a point in that half through the origin to the half in which the Carnot temperatures are labeled.

- Since drawing a line through the origin corresponds to a negative extent, the symmetry relation implies the Carnot temperature for the forward process in a reversible reaction is the same as the Carnot temperature for the backward process. For example, the Carnot temperature for the water-gas shift reaction is the same as the Carnot temperature for the reverse water-gas shift reaction.

- Reaction processes in regions 1B ($45° < \alpha < 90°$) and 3B ($225° < \alpha < 270°$) have negative Carnot temperatures. This suggests that it is thermodynamically infeasible to run any reaction processes that lie in these regions reversibly. For instance, combustion of coal is inherently irreversible since the reaction lies in region 3B. This information is useful at the conceptual stage of process design: If there is a choice of reaction processes, it is desirable to use reactions in other regions in order to increase process efficiency by reducing irreversibilities.

- The Carnot temperature increases to infinity at $\alpha = 45\ °$ or $\alpha = 225\ °$. At this point, ΔG and ΔH of the process are equal. Reaction processes lying close to this diagonal (with similar ΔG and ΔH values) have very high Carnot temperatures. For instance, the methane combustion reaction has a Carnot temperature of 145,866.25 K. Since, there are material limits to operating reactors at very high Carnot temperatures, lower operating temperatures are commonly chosen. These reactors operating at temperatures different from their Carnot temperature are significantly irreversible. Many fuel combustion reactions lie close to this diagonal making them inherently irreversible. Thus, if there is a choice of reaction processes, it is recommended to choose those that have reasonably low Carnot temperatures. This shows that classifying possible reactions using the G-H space tool may be useful in narrowing the search space of desirable process alternatives.

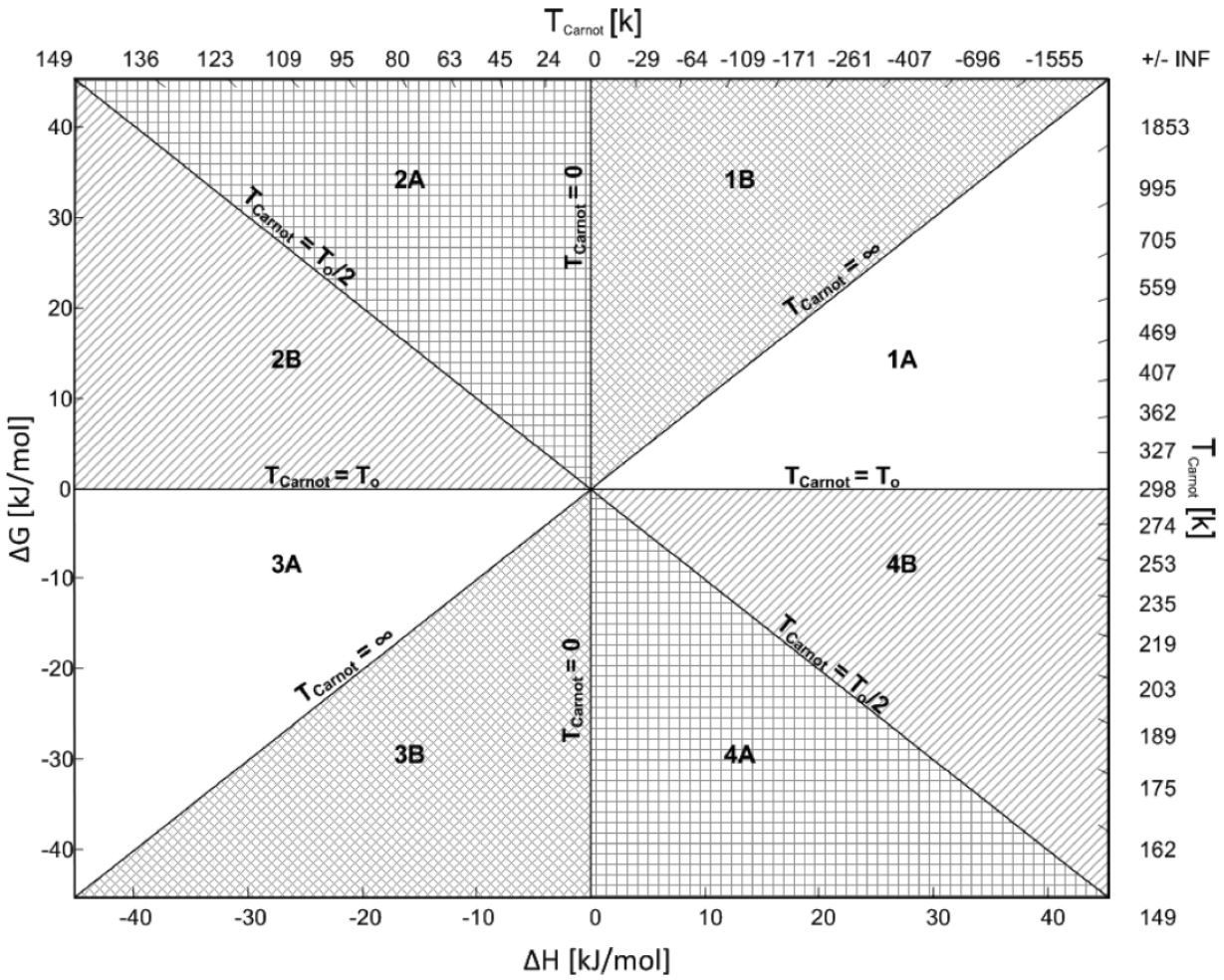

Figure 2.3: G-H space including Carnot temperatures [27]

2.5 Adding and removing work

While integration of different reaction processes of opposite needs is a useful and energy efficient way to match their work and heat requirements, there exist other ways to supply (or remove) work. These can be seen by examining Equation 2.12, in which an expression for the differential form of the Gibbs energy is provided:

$$dG = -SdT + VdP + \sum_i \mu_i dN_i \tag{2.12}$$

where:

- μ_i is the chemical potential of species i
- dN_i is the change in number of moles of species i
- S is the entropy
- dT is the temperature gradient
- V is the volume
- dP is the change in pressure. The derivation is available in [2] and [29].

The three terms correspond to three ways of adding (or removing) work: The first term $-SdT$ corresponds to addition of work by means of heat (or removal of work by cooling), the second term VdP corresponds to addition of work by means of isothermal compression (or removal of work by means of isothermal expansion), and the third term $\sum_i \mu_i dN_i$ corresponds to addition of work via separation (or removal of work via mixing). Section 2.4 discussed the method of adding work to a process by means of heat; it was shown that all the work can be supplied concurrently by the supplied heat Q if the reaction process operates at its Carnot temperature. The other two methods of adding or removing work are discussed next.

2.5.1 Isothermal compression and expansion

Isothermal compression of the feed at ambient pressure P_0 to the reactor pressure P and isothermal expansion of the product from P_0 to P is shown in Figure 2.1. Both these processes take place at ambient temperature T_0. The corresponding amount of work that can be added or removed from the process can be obtained from Equation 2.13, which gives the integral form of Equation 2.12 at constant temperature and no change in the number of moles of species i.

$$\Delta G_{compression} = (n_{in} - n_{out}) RT_0 ln \frac{P}{P_0} \tag{2.13}$$

where n_{in} and n_{out} are the number of reactant and product moles. Note that the assumption that reactants and products comply with the ideal gas law is utilized in Equation 2.13. Equation 2.13 is written for compression, $\Delta G_{expansion}$ is given by the same expression but with an opposite sign.

From Equation 2.13 it can be deduced that for compression to be able to provide work to the process, n_{in} should be greater than n_{out}. Conversely, if n_{out} is greater than n_{in}, then work can be extracted from the process.

2.5.2 Separation and Mixing

The third method of adding work to a system is using separation. This could be integrated separation and removal of the product as it is being formed using a membrane reactor, or could be separation of the product into pure components as illustrated in Figure 2.1. The case of integrated separation using membrane reactors is studied comprehensively in Chapter 6.

One of the assumptions made in the definition of the simple chemical process in Section 2.1. is that the work required to separate products into pure components is negligible. However, this may not be correct. To address this assumption, the separation work required can be calculated from the integral form of Equation 2.12. For a separation process of products into pure components at constant temperature T_0 and pressure P_0 (as in Figure 2.1), the integral form of Equation 2.12 is given by Equation 2.14 [21]:

$$\Delta G_{separation} = -n_{out} RT_0 (\sum_i x_i ln(x_i)) \tag{2.14}$$

This additional work that was not accounted for previously has to be added to the process as well. This addition is included in the process design done in subsequent chapters.

Theoretically, work can be extracted from the simple chemical process if controlled mixing is done. However, in a real mixer, this work potential is normally lost as a result of exergy destruction due to uncontrolled mixing. For this reason, mixing is not studied extensively in this project. For process designs in which it is possible to extract work, this is done instead using an isothermal expansion process as elaborated upon in subsequent chapters.

Chapter 3

Hydrogen production process design using the G-H Methodology

This chapter shows how the thermodynamic background presented in Chapter 2 can be used to develop the systematic G-H methodology. The G-H methodology is presented as a series of steps used to design a chemical process. The hydrogen production process is used as a case study to present and explain this series of steps that constitute the G-H methodology. This chapter also borrows heavily from the work done in the research group of Professors Diane Hildebrandt and David Glasser. The papers mentioned in Chapter 2 are useful to provide further details. In particular [6] is relevant to the work done in this chapter.

For simplicity, natural gas is assumed to have only one component - methane. Thus, it is not necessary to have a pre-reformer.

3.1 Step 1: Define the chemical reactions

In this step, the chemical reactions that occur in the "simple chemical process" are defined.

The goal is to reform methane to hydrogen. The steam methane reforming (SMR) reaction is used:

$$\mathrm{CH_4(g) + H_2O(g) \rightleftharpoons CO(g) + 3\,H_2(g)} \tag{3.1}$$

The standard enthalpy and standard Gibbs energy of reaction are given as $\Delta H_{SMR} = 206.12$ kJ/mol, $\Delta G_{SMR} = 142.16$ kJ/mol [6].

It is desired to have as much hydrogen as possible, thus it is necessary to convert some of the formed carbon monoxide to hydrogen. To do this, the water-gas shift (WGS) reaction is used:

$$\mathrm{CO(g) + H_2O(g) \rightleftharpoons CO_2(g) + H_2(g)} \tag{3.2}$$

The standard enthalpy and standard Gibbs energy of reaction are given as $\Delta H_{WGS} = -41.19$ kJ/mol, $\Delta G_{WGS} = -28.59$ kJ/mol [6].

Steam that is used as a feed to the SMR and WGS reactions is produced from water using a phase change reaction:

$$\mathrm{H_2O(l) \longrightarrow H_2O(g)} \tag{3.3}$$

The standard enthalpy and standard Gibbs energy of reaction are given as $\Delta H_{phase} = 44.01$ kJ/mol, $\Delta G_{phase} = 8.56$ kJ/mol [6].

The SMR reaction and phase change reaction require heat and work to proceed. Thus, a new reaction, such as a combustion reaction, that rejects heat and work is required. The fuel most convenient to combust is methane since it is already available.

$$\mathrm{CH_4(g) + 2\,O_2(g) \rightleftharpoons CO_2(g) + 2\,H_2O\,(g)} \tag{3.4}$$

The standard enthalpy and standard Gibbs energy of reaction are given as $\Delta H_{comb} = -802.35$ kJ/mol, $\Delta G_{comb} = -800.71$ kJ/mol [6].

3.2 Step 2: Plot reactions as vectors in G-H space. Determine Carnot temperatures

Figure 3.1 shows the representation of the four reactions as vectors in G-H space. For clarity, the vector is drawn only for the SMR reaction.

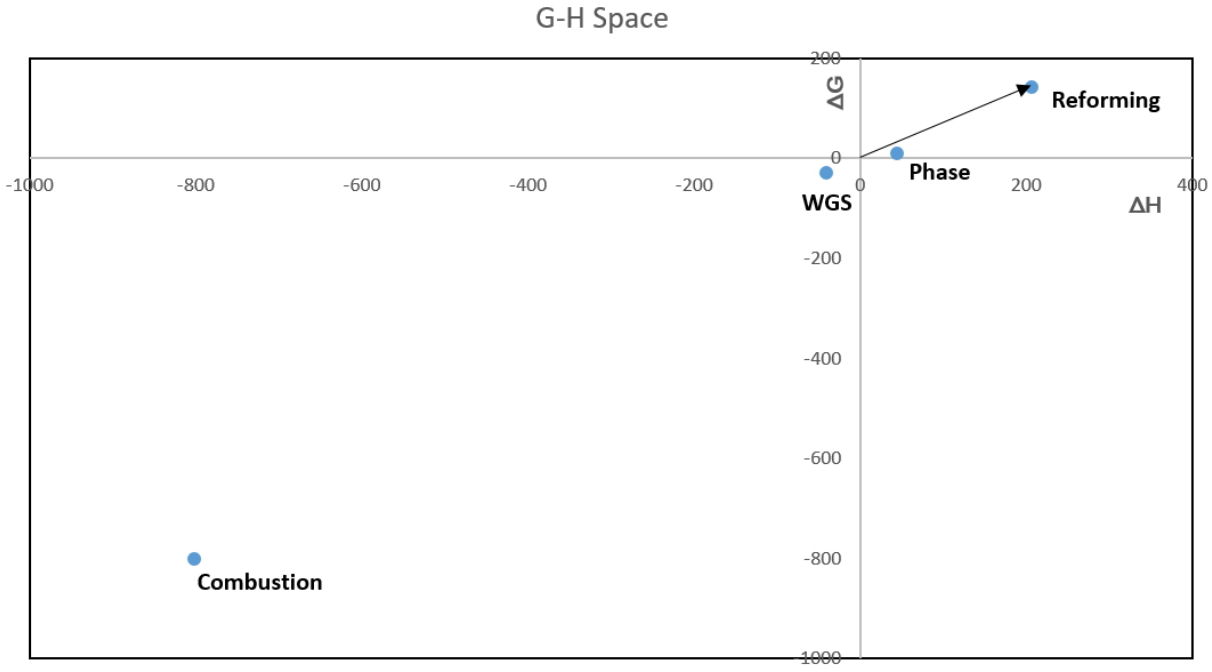

Figure 3.1: Plotting the 4 reactions on the G-H space

The Carnot temperatures for the 4 reactions are calculated using Equation 2.11:

$$\begin{aligned} T_{Carnot,SMR} &= 960.83\mathrm{K} \\ T_{Carnot,phase} &= 370.14\mathrm{K} \\ T_{Carnot,WGS} &= 974.67\mathrm{K} \\ T_{Carnot,comb} &= 145,866.25\mathrm{K} \end{aligned} \tag{3.5}$$

3.3 Step 3: Obtain relations between reaction extents

In Figure 3.1, the extent of each of the reactions is given by the length of the vector in G-H space.

Performing material balances for all the individual species, in moles:

$$N_{CH_4} = N^0_{CH_4} - e_{SMR} - e_{comb} \tag{3.6}$$

$$N_{H_2} = N^0_{H_2} + 3e_{SMR} + e_{WGS} \tag{3.7}$$

$$N_{CO} = N^0_{CO} + e_{SMR} - e_{WGS} \tag{3.8}$$

$$N_{H_2O} = N^0_{H_2O} - e_{SMR} - e_{WGS} + 2e_{comb} \tag{3.9}$$

$$N_{O_2} = N^0_{O_2} - 2e_{comb} \tag{3.10}$$

$$N_{CO_2} = N^0_{CO_2} + e_{WGS} + e_{comb} \tag{3.11}$$

The superscript "0" shows the number of moles of that component fed to the overall process, and the final number of moles out of the overall process is given by N without the superscript.

The 4 extents of reaction ($e_{SMR}, e_{WGS}, e_{phase}$ and e_{comb}) are degrees of freedom. The following design decisions are to be made to fix these degrees of freedom:

- It is required that the only feed materials are: CH_4, H_2O and O_2. Thus: $N^0_{H_2} = N^0_{CO} = N^0_{CO_2} = 0$
- The methane feed is chosen to be: $N^0_{CH_4} = 1$. This can be in any molar units, but mol/s is used here. The overall process scales with this methane feed. Also, it is desired that all the methane is used up in the process, so $N_{CH_4} = 0$. Making these design decisions, Equation 3.6 becomes:

$$e_{comb} = 1 - e_{SMR} \tag{3.12}$$

- The goal of the overall process is to produce as much hydrogen as possible, and thus utilize all the produced CO in the steam methane reforming reaction as a feed for the water-gas shift reaction. So, $N_{CO} = 0$ Thus, Equation 3.8 becomes:

$$e_{WGS} = e_{SMR} \tag{3.13}$$

- The extent of the phase change reaction, and thus the feed of water is fixed such that exactly the right amount of steam required for the other reactions is generated. No water goes to waste. So: $N_{H_2O}= 0$. Equation 3.9 becomes:

$$N^0_{H_2O} = e_{phase} = e_{SMR} + e_{WGS} - 2e_{comb} \tag{3.14}$$

Substituting and rearranging:

$$e_{phase} = 4e_{SMR} - 2 \tag{3.15}$$

Equations 3.12, 3.13 and 3.15 establish relations between the extents of the the combustion, WGS and phase change reaction and the extent of the SMR reaction. Thus, e_{SMR} is the only variable; fixing e_{SMR} fixes the extents of all the other reactions.

3.4 Step 4: Choose overall adiabatic operating conditions

In Section 2.3, the method to determine the thermodynamics of the overall process containing several simple chemical reactions was discussed. The thermodynamics of the overall process can be obtained by vector addition of the reactions in the G-H space. Equation 2.10 can be applied to get the heat and work requirements of the overall process consisting of the SMR, WGS, phase change and combustion reactions:

$$\begin{pmatrix}\Delta H_{overall}\\ \Delta G_{overall}\end{pmatrix} = \begin{pmatrix}\Delta H_{SMR}\\ \Delta G_{SMR}\end{pmatrix}(e_{SMR}) + \begin{pmatrix}\Delta H_{phase}\\ \Delta G_{phase}\end{pmatrix}(e_{phase}) + \begin{pmatrix}\Delta H_{WGS}\\ \Delta G_{WGS}\end{pmatrix}(e_{WGS}) + \begin{pmatrix}\Delta H_{comb}\\ \Delta G_{comb}\end{pmatrix}(e_{comb}) \quad (3.16)$$

Substitute in Equations 3.12, 3.13 and 3.15:

$$\begin{pmatrix}\Delta H_{overall}\\ \Delta G_{overall}\end{pmatrix} = \begin{pmatrix}\Delta H_{SMR}\\ \Delta G_{SMR}\end{pmatrix}(e_{SMR}) + \begin{pmatrix}\Delta H_{phase}\\ \Delta G_{phase}\end{pmatrix}(4e_{SMR} - 2) + \begin{pmatrix}\Delta H_{WGS}\\ \Delta G_{WGS}\end{pmatrix}(e_{SMR}) + \begin{pmatrix}\Delta H_{comb}\\ \Delta G_{comb}\end{pmatrix}(1 - e_{SMR}) \quad (3.17)$$

Substitute in values:

$$\begin{pmatrix}\Delta H_{overall}\\ \Delta G_{overall}\end{pmatrix} = \begin{pmatrix}206.12\\ 142.16\end{pmatrix}(e_{SMR}) + \begin{pmatrix}44.01\\ 8.56\end{pmatrix}(4e_{SMR} - 2) + \begin{pmatrix}-41.19\\ -28.59\end{pmatrix}(e_{SMR}) + \begin{pmatrix}-802.35\\ -800.71\end{pmatrix}(1 - e_{SMR}) \quad (3.18)$$

This equation can be plotted on the G-H space for different values of e_{SMR}, as shown by the orange line in Figure 3.2. Thus, the orange line represents the thermodynamics of the overall process. Each point on this line shows a possible operating point of the overall process. Choosing the overall process operating point is an important design decision.

In this Master's project, this operating point is chosen such that the overall process is adiabatic. Thus, the most suitable operating point on the orange line is an overall process with $\Delta H = 0$ (where the orange line crosses the y-axis). The rational for making this decision decision is explained next: An overall adiabatic process implies that that no heat is lost irreversibly to the environment, and no external heat is required for the overall process to proceed. The part of the line that has +ve ΔH would imply that the extent of the combustion reaction was

more than necessary to supply the heat required for the SMR and phase change reactions. Operating at such points would be wasteful in terms of methane input to the combustion reaction. This also implies a release of excess carbon dioxide into the atmosphere. The part of the line that has -ve ΔH would imply that the extent of the combustion reaction is too small to supply heat for the SMR and phase change reactions. Thus, external heat would be required and this is not desired.

Fixing $\Delta H = 0$, e_{SMR} is the only unknown of Equation 3.18. Solving for e_{SMR} also fixes the extents of the other reactions. The resulting heat and work balance is given in Table 3.1.

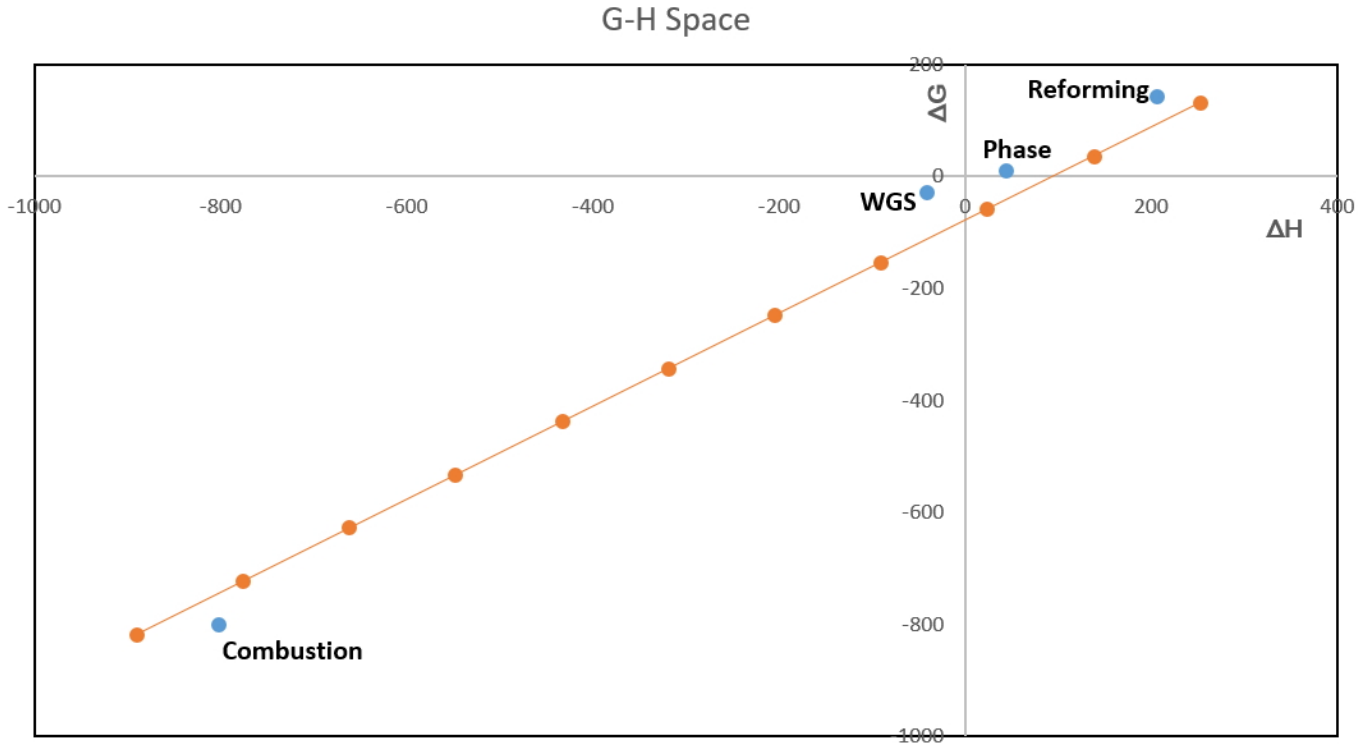

Figure 3.2: Overall process heat and work balance shown by orange line

Table 3.1: Heat and Work balance after Step 4

		SMR	WGS	phase change	Combustion	Overall Process
Temperature	K	960.83	974.67	370.14	145,866.25	
Pressure	bar	1	1	1	1	
e		0.7788	0.7788	1.1152	0.2212	
ΔH	kW	160.53	-32.08	49.08	-177.51	0
ΔG	kW	110.71	-22.27	9.55	-177.12	-79.12

The negative sign of ΔG implies that the overall process produces work (see sign convention explained by Equation 2.9). This implies the recoverable work after Step 4, $W_{out} = 79.12$ kW.

After Step 4, a block diagram of the hydrogen production process can be drawn. This is shown in Figure 3.3. Since all the reactions take place at their Carnot temperatures, this block diagram corresponds to a reversible process.

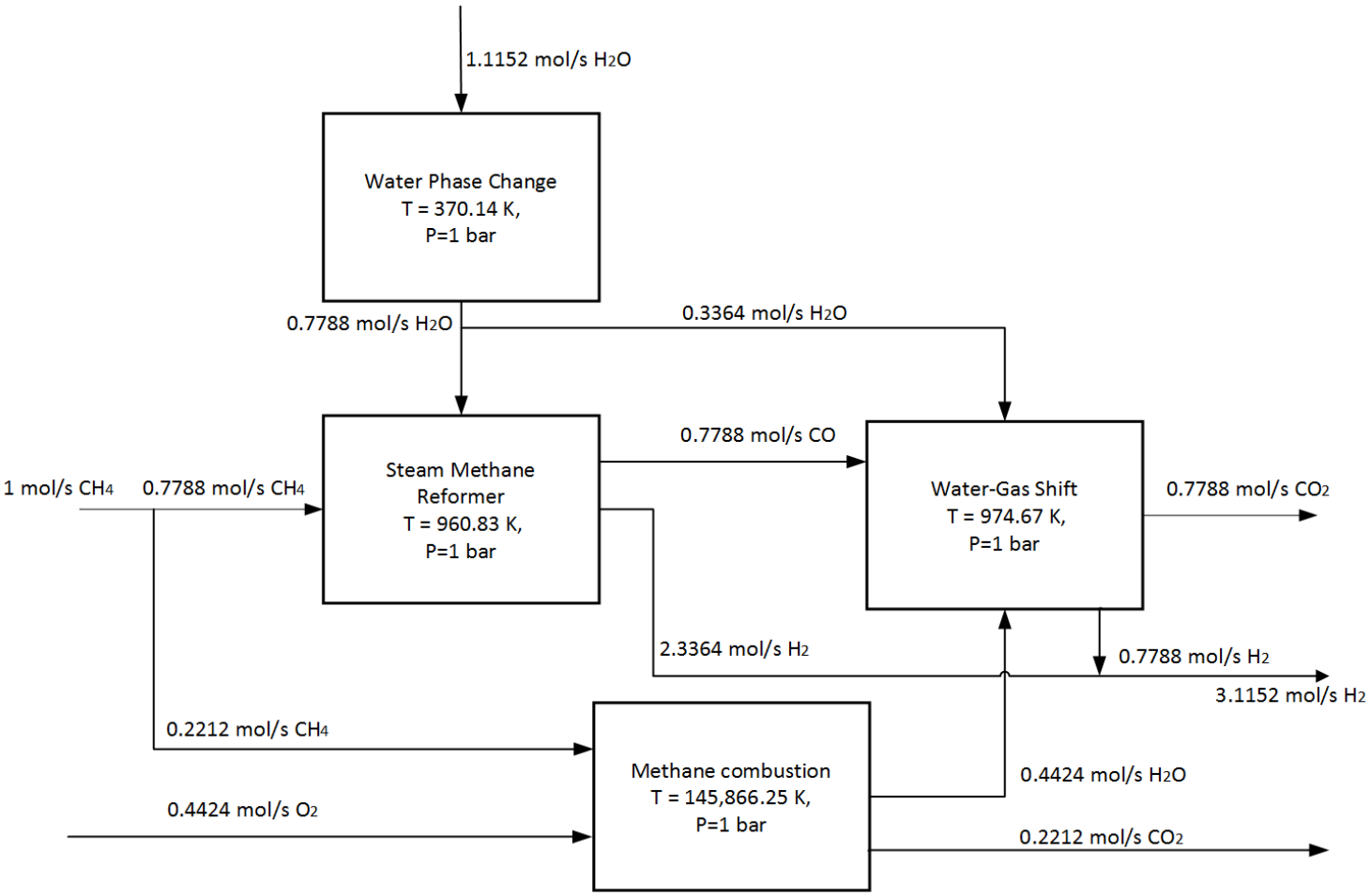

Figure 3.3: Block diagram of hypothetical Hydrogen production process before conversion and realism considerations

From the block diagram in Figure 3.3, two issues are immediately clear. First, an assumption that was made (see Section 2.1) in each of the 4 chemical reactions was complete conversion of the reactants to the products at the respective Carnot temperatures. However, there is no reason for this assumption to hold. The SMR and WGS reactions are reversible implying that it is necessary to investigate the conversion at their Carnot temperatures. This is discussed in the next section.

The second issue is that the process may not be realistically achievable. For instance, the operating temperature of the combustion reaction is 145,866.25 K - an unrealistically high value. It is necessary to design a process in which all unit operations operate at a realistic temperature. This requirement is addressed in the subsequent Chapters 4 - 7.

3.5 Conversion of SMR and WGS reactions

First, the procedure to calculate the conversion of a chemical reaction at a given temperature is presented. The difference between conversion and extent of a chemical reaction is also made explicit.

Consider a general reversible reaction with 2 reactants and 2 products:

$$\nu_A A + \nu_B B \rightleftharpoons \nu_C C + \nu_D D \tag{3.19}$$

where: v_i is the stoichiometric coefficient of reactant or product component i.

Let this chemical reaction have a "stoichiometric feed". A chemical reaction is said to have a "stoichiometric feed" if the ratio of the molar flowrates of the reactants is equal to the ratio of their stoichiometric coefficients. For instance, let the molar flowrate of reactant A be N_A^0 mol/s and the molar flowrate of reactant B be N_B^0 mol/s. Then if $\frac{N_A^0}{N_B^0} = \frac{v_A}{v_B}$, the feed is said to be a stoichiometric feed.

During a chemical reaction, the change in the number of moles of each species is proportional to v_i. The proportionality constant is termed the "extent of reaction" (e). Thus at equilibrium, $e.v_A$ moles of A react with $e.v_B$ moles of B to produce $e.v_C$ moles of C and $e.v_D$ moles of D. The dot sign (.) is used in this context to denote multiplication of the two scalars e and v_i.

Thus the equilibrium number of moles of each species can be calculated:

$$N_A = N_A^0 - e.v_A \tag{3.20}$$

$$N_B = N_B^0 - e.v_B \tag{3.21}$$

$$N_C = e.v_C \tag{3.22}$$

$$N_D = e.v_D \tag{3.23}$$

The conversion is the fraction of moles that are reacting normalized between 0 and 1. This normalization is done by dividing the number of reacting moles by the feed flowrate. For instance, the conversion with respect of component A (c_A) is given by Equation 3.24 and the conversion with respect to component B (c_B) is given by Equation 3.25.

$$c_A = \frac{e.v_A}{N_A^0} \tag{3.24}$$

$$c_B = \frac{e.v_B}{N_B^0} \tag{3.25}$$

Note however, that for a stoichiometric feed:

$$c = c_A = c_B \tag{3.26}$$

Thus, the entire reaction only has one conversion value (c) without the subscripts - this is only true if the feed is a stoichiometric feed. The difference between extent and conversion thus is that conversion is normalized between 0 and 1, while the extent scales with the feed flowrate and can be greater than 1.

The equilibrium constant at constant pressure (K_p) gives a measure of the equilibrium conversion of reactants to products at a given temperature. Assuming the reacting gases are ideal, the definition of K_p is given by Equation 3.27 [29].

$$K_P = \frac{(N_C)^{V_C}(N_D)^{V_D}}{(N_A)^{V_A}(N_B)^{V_B}} \left(\frac{\mathrm{P}}{N_{total}}\right)^{\Delta v} \tag{3.27}$$

where:

- $\Delta v = v_C + v_D - v_A - v_B$
- N_i is the number of moles of species i at chemical equilibrium
- P is the reactor pressure

- $N_{total} = N_A + N_B + N_C + N_D$

The K_p value at a temperature T can be obtained from the change in Gibbs free energy at T using Equation 3.28. The derivation can be found in [29], R is the universal gas constant.

$$K_P = e^{-\Delta G(T)/RT} \tag{3.28}$$

Equations 3.20 - 3.26 can be substituted into Equation 3.27, and the conversion value determined for any temperature T. Details are available in [2].

A plot of the variation of conversion of the SMR reaction with temperature is given in Figure 3.4. As can be seen from the dotted line, the conversion obtained at the Carnot temperature of SMR ($T_{Carnot,SMR} = 960.83$K) is equal to 0.73, which is less than full conversion previously assumed in Section 2.1 and Figure 3.3.

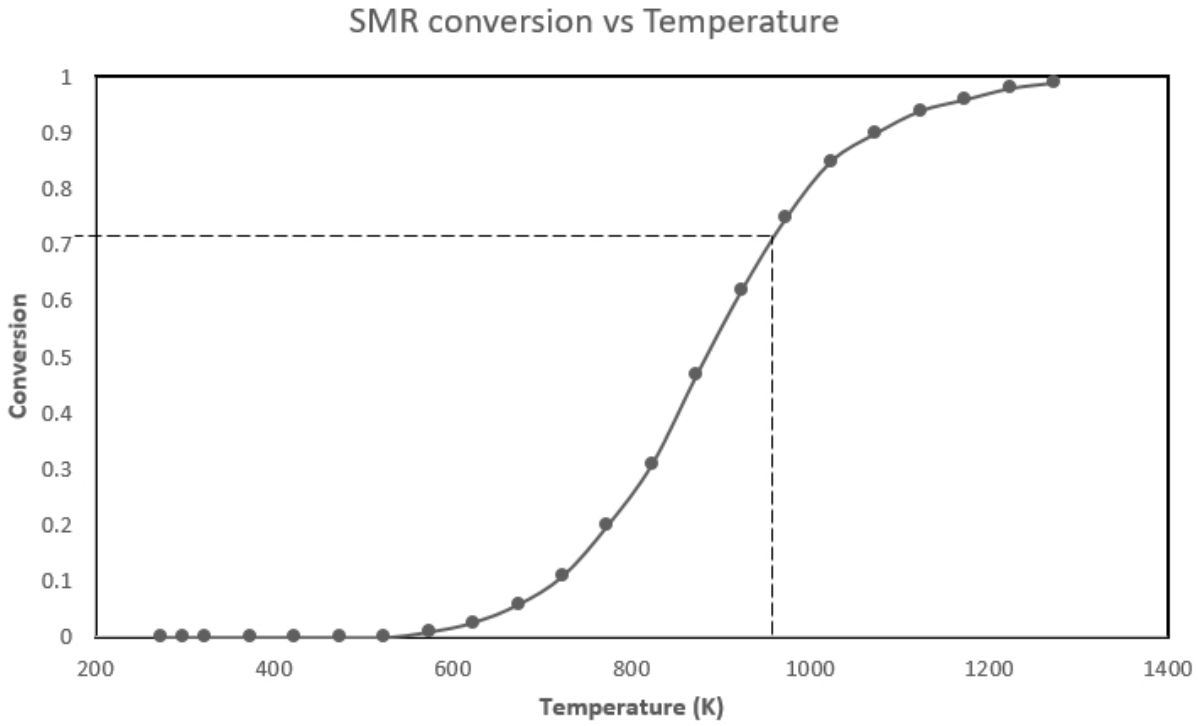

Figure 3.4: Variation of SMR conversion with Temperature

Similarly, Figure 3.5 gives a plot of the variation of conversion of the WGS reaction with temperature. As can be seen, the conversion obtained at the Carnot temperature of WGS ($T_{Carnot,WGS} = 974.67$K) is equal to 0.56, which is also less than full conversion previously assumed in Section 2.1 and Figure 3.3.

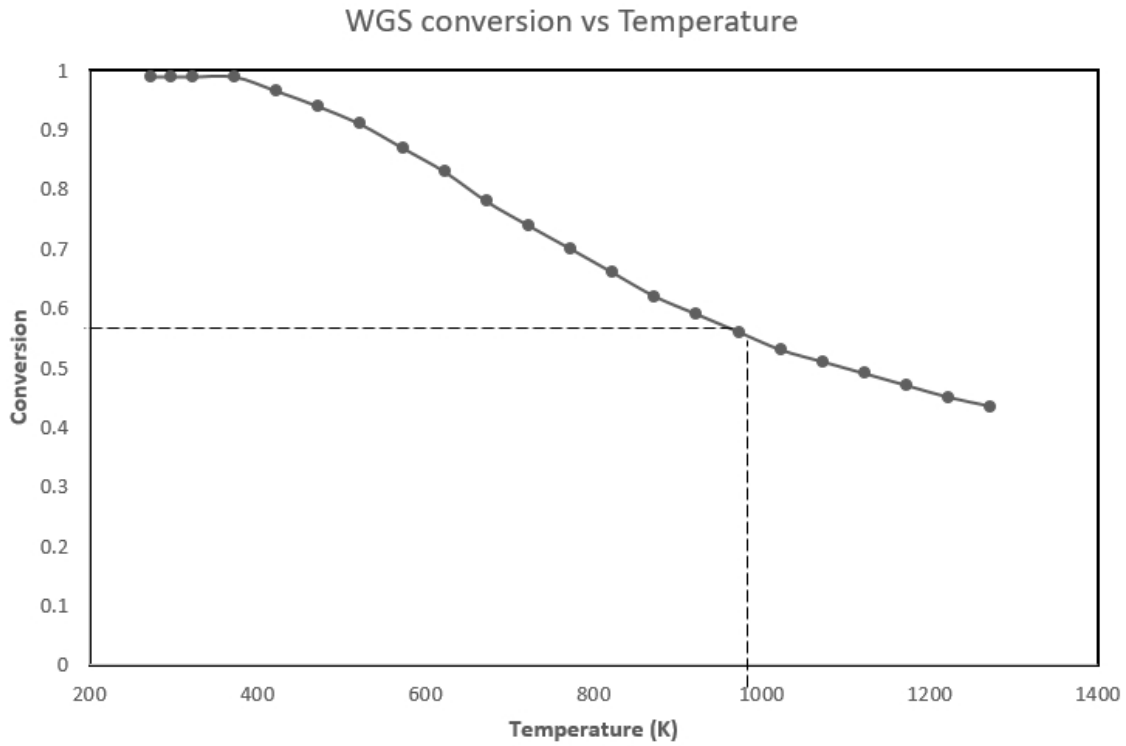

Figure 3.5: Conversion of WGS at different temperatures

The target conversion is 1, so the next step is to figure out ways to increase the conversion of the SMR and WGS reactions.

3.6 Methods of increasing conversion

Several ways are available to increase the conversion of a reaction. These are outlined next:

- Using recycling of unreacted feed: This involves separating out the unreacted feed from the product and feeding it back to the reactor. Recycling of unreacted feed is discussed extensively in Chapter 4.
- By changing the feed ratio. So far, the conversion has been calculated assuming a stoichiometric feed. However, if the molar flowrate of one of the reactant is much higher than its stoichiometric feed flowrate, more of the other reactant is converted to product. Thus, a feed with an excess of one component can be used to increase the conversion with respect to the other component. This is discussed extensively in Chapter 5.
- By using integrated separation and removal of product using a membrane reactor. A membrane reactor combines a reaction process and a membrane separation process in the same unit such that some of the product is continuously being removed as it is formed. This implies that the backward reaction is constrained from taking place, which results in a higher conversion of the forward reaction. Using a membrane reactor to increase conversion is discussed extensively in Chapter 6.

- Changing the pressure. Equation 3.27 depends on the pressure of the reactor P. Thus, changing the reactor pressure could potentially change the equilibrium conversion. The effect of changing the pressure on equilibrium conversion can be predicted by the "Le-chatelier's principle": Increasing the pressure favors the reaction that proceeds with a decrease in the system's volume [29] and vice versa. First, this implies that the reactor pressure has no impact on the conversion of the WGS since the reaction proceeds without any change in system volume. In addition, it can be seen from Equation 3.1 that the backward reaction to the SMR process proceed with a decrease in number of moles (and hence system volume), which implies the conversion of the SMR reaction is decreased as a result of increasing the pressure. Thus, the method of changing the pressure is not investigated further in this Master's project.

- By changing the temperature. Figures 3.4 and 3.5 illustrate that using reactor operating temperatures other than the Carnot temperature may result in higher conversions. For instance, an SMR reaction at approximately 1300 K would achieve complete conversion. Similarly, a WGS reaction at 300 K would achieve complete conversion. However, running these reactors at temperature significantly different from their Carnot temperatures results in significantly inefficient unit operations. Thus, it is not recommended to run the unit operations at temperatures other than their Carnot temperatures. For this reason, this method of increasing conversion is not explored further in this Master's project.

3.7 Concluding remarks

This chapter presented the first 4 steps of the G-H methodology applied to a case study of hydrogen production using the SMR and WGS reactions. Using these steps, a hypothetical block diagram was drawn with all reactors operating at their Carnot temperatures. Investigating the conversion of the WGS and the SMR process revealed that the assumption of complete conversion made in Section 2.1. is not met. Thus, in order to proceed, there are two options.

Either a method to achieve complete conversion should be used in which case the Steps 1 - 4 and the results presented are valid. The extents of reactions determined in Table 3.1 are then correct, and can be used for further design steps. In Chapter 4, complete conversion is achieved using 100 % recycle of unreacted feed - further design is done based on the results of Steps 1 - 4.

The alternative is to modify the G-H methodology to accommodate scenarios with less than complete conversion. This is also investigated in Chapter 4 with design of a process with 80 % recycle of unreacted feed.

Chapter 4

Increasing Conversion using Recycling of unreacted Feed

4.1 Introduction

Recycling of material is an essential feature of most chemical processes [10]. For reversible chemical reactions in which complete conversion does not occur, the reactor effluent contains unreacted feed in addition to the formed product [10]. The unreacted feed is usually too valuable to be disposed of, and so it can be separated from the formed product and recycled. Disposal of unreacted feed may also create an environmental problem.

Recycling of the unreacted feed is an important method to increase the conversion of the reactor system. In order to explain this, it is necessary to distinguish between the "single-pass conversion" and "overall conversion" of a reaction, separation and recycle system. Figure 4.1 shows a schematic of a general reactor, separation and recycle system. The "single-pass conversion" gives the fraction of the reactant converted on a single pass through the reactor, normalized between 0 and 1. Thus, it gives the conversion between points 2 and 3 in Figure 4.1. The "overall conversion" gives the fraction (normalized between 0 and 1) of the feed converted in the entire process taking place within the dotted red lines. Thus, it gives the conversion between points 1 and 4 in Figure 4.1. Note that its the overall conversion that is relevant in the G-H methodology; the single-pass conversion is not changed from Chapter 3 because of recycling, and is not a relevant parameter. Thus, the reactor in Figure 2.1 is now replaced by the entire reactor, separator and recycle system contained within the dotted red box in Figure 4.1. The overall conversion is directly proportional to the percentage of unreacted feed that is recycled. This means that total separation and recycle of 100 % of the unreacted feed gives complete overall conversion while a lower percentage of recycle gives lower overall conversion. Thus, the percentage of recycle is an important variable to be considered in this chapter.

Section 4.2 presents a case study of a hydrogen production process that uses 100 % recycle of the unreacted feed in order to achieve complete overall conversion while Section 4.3 presents a case study that uses 80 % recycle to achieve a corresponding overall conversion of 0.8. One of the assumptions of the G-H methodology presented in Chapter 3 was complete conversion. This implies the G-H methodology needs to be modified to account for incomplete conversion in Section 4.3. Thus, this chapter makes both a methodological contribution and a process design contribution. In

Section 4.4, the G-H methodology is extended to account for incomplete conversion. Two hydrogen production process flowsheets are developed: One with 100 % recycle and complete conversion and another with 80 % recycle of unreacted feed. These two flowsheets are then simulated using Aspen HYSYS and an exergy analysis performed.

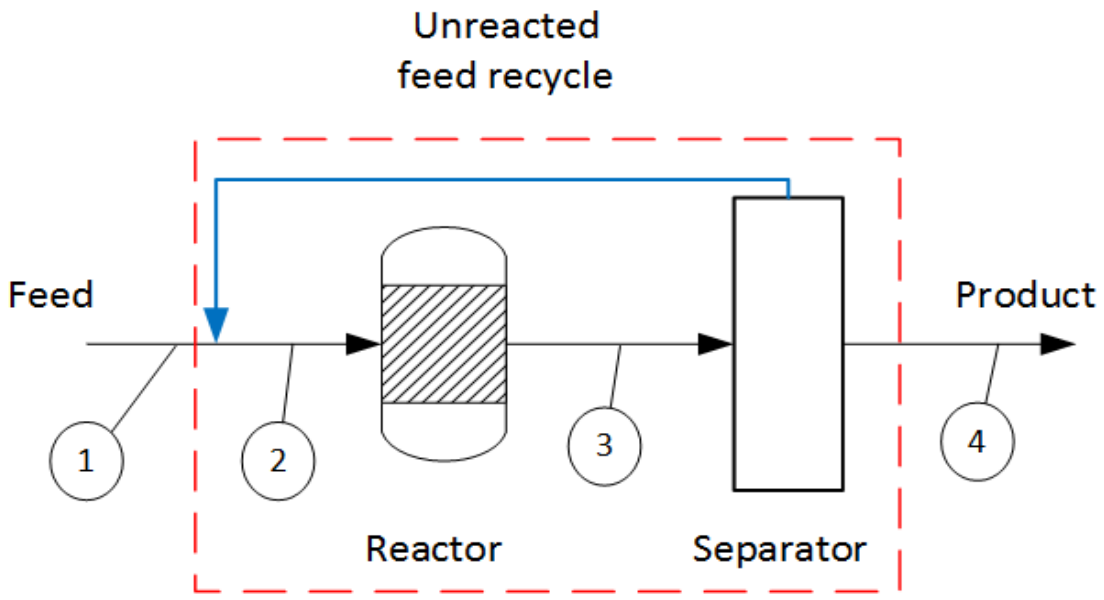

Figure 4.1: Schematic of a general reactor, separator and recycle system

4.2 Case study 1: Complete overall conversion using 100 % recycle of the unreacted feed

This section contains a case study of a hydrogen production process with 100 % recycle of the unreacted feed in the SMR and WGS reactions. This gives complete overall conversion in the SMR and WGS reactions. The G-H methodology developed in Chapter 3 assumes complete conversion in all the reactions taking place. With this assumption, the extents of the 4 reactions ($e_{SMR}, e_{WGS}, e_{phase}$ and e_{comb}) are fixed so as to result in an adiabatic overall process. With complete conversion achieved by 100 % recycle, the assumption made is valid and the extents calculated in Step 4 of Chapter 3 are correct. Thus, Steps 1 - 4 of the G-H methodology described in Chapter 3 do not need to be modified for this case study; this case study continues the design process from Chapter 3. The block process diagram shown in Figure 3.3 is redrawn in Figure 4.2 to include the recycled streams.

The heat and work balance presented in Table 3.1 is still valid at this step, provided the following additional assumption for the reactor, separation and recycle system holds:

- The work required for pumping or compression of the unreacted feed is assumed to be negligible. The unreacted feed needs to be transferred from the the separation system to the inlet to the reactor. In a real process, there exists a pressure drop through the reactor, separators, heat exchangers, control valves etc [10]. Thus, in a real process the recycle stream must be pumped or

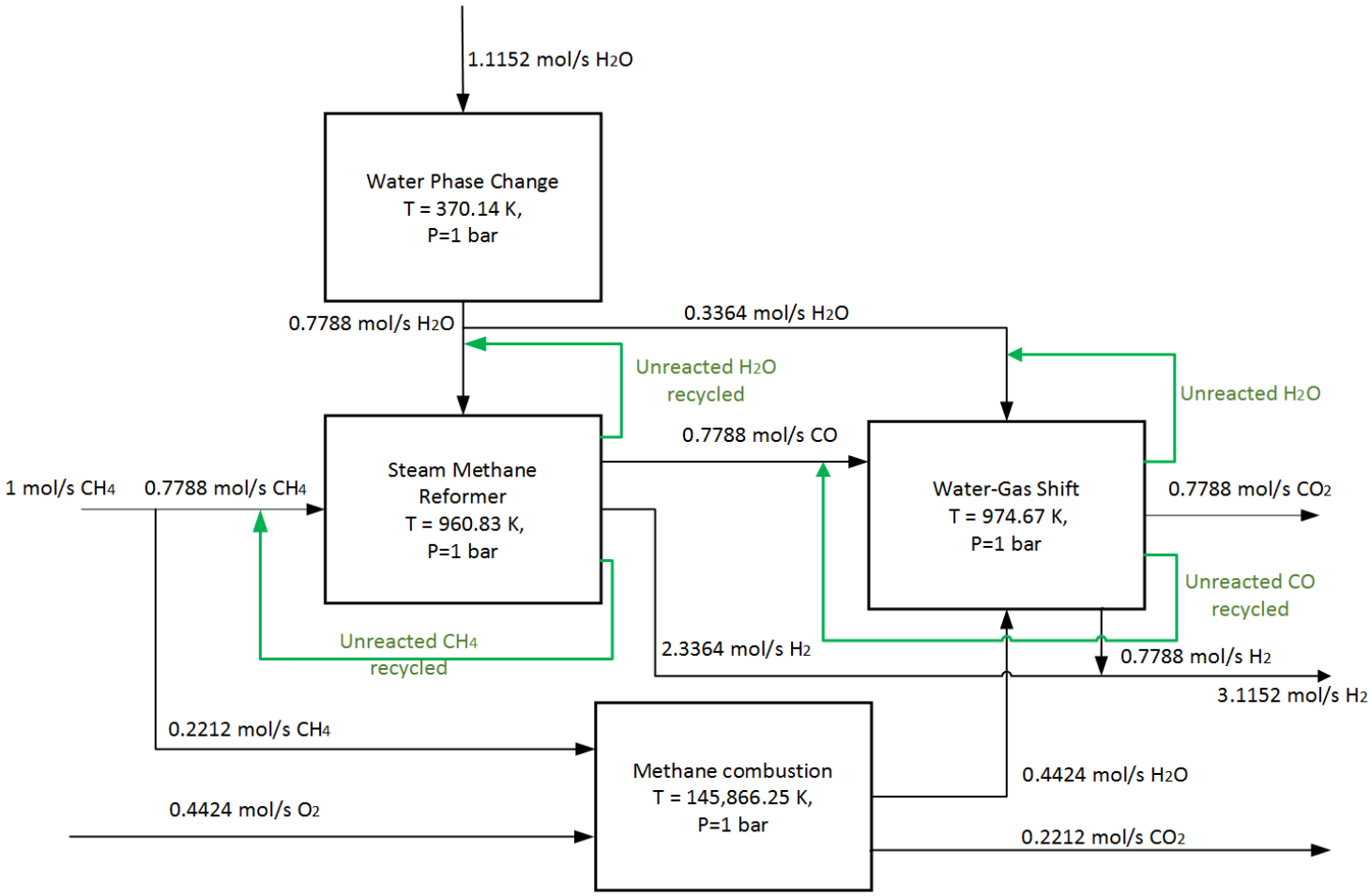

Figure 4.2: Hypothetical block flow diagram with complete conversion but before realism considerations

compressed such that this pressure drop is overcome. However, this project focuses on the conceptual design stage prior to detailed designs that would incorporate such pressure drops. It is noted that the cost to increase the pressure of unreacted gases is quite significant so this consideration is important in later design stages. However, the inclusion of this pumping or compression work would have no impact on the extents of the 4 reactions determined by the G-H methodology in Step 4 of Chapter 3. This is because the adiabatic operating point is chosen and the e_{SMR} value is calculated based on the heat balance, and not the work balance. However, the net recoverable work from the realistic overall process will be reduced to account for this pumping or compression work.

Having addressed the issue of achieving complete conversion, the second issue that needs to be handled is adding realism to the flowsheet in Figure 4.2. Specifically, all unit operations should be at realistic temperatures.

4.2.1 Step 5: Use realistic operating temperatures

The combustion reaction in the hypothetical process in Figure 4.2 has a Carnot temperature of 145,866.25 K, which is unrealistically high. A lower operating tem-

perature is to be chosen. In this Master's project, an operating temperature of 1200 K is chosen. Since the combustion reaction is used to provide heat and work to the SMR and phase change process, any temperature higher than the SMR operating temperature of 960.83 K can be chosen.

The enthalpy change of the combustion reaction is a weak function of operating temperature. For this reason, the enthalpy change is approximated to be unchanged for different operating temperatures, i.e. the enthalpy change at 1200 K is unchanged at ΔH_{comb} = -802.35 kJ/mol.

This combustion reaction is exothermic implying that the heat released from the reactor, Q is 802.35 kJ/mol. In order to determine the maximum work that can be obtained from the combustion reaction at a temperature T = 1200 K, an analogy is drawn between the reactor and the hot reservoir of a Carnot heat engine [21]. The Carnot equation can be used to determine the maximum work that can be produced from a Carnot heat engine with a hot reservoir at temperature T and cold reservoir at ambient temperature T_0 [21]:

$$W = Q(1 - \frac{T_0}{T}) \tag{4.1}$$

Substituting values:

$$W_{comb} = 802.35(1 - \frac{298.15}{1200}) = 603.01\text{kW} \tag{4.2}$$

With this value, the heat and work balance of the overall process can be updated to give Table 4.1.

Table 4.1: Heat and Work balance after Step 5

Unit Operation		SMR	WGS	Phase change	Combustion	Overall Process
Temperature	K	960.83	974.67	370.14	1200	
Pressure	bar	1	1	1	1	
e		0.7788	0.7788	1.1152	0.2212	
ΔH	kW	160.53	-32.08	49.08	-177.51	0.00
ΔG	kW	110.71	-22.27	9.55	-133.41	-35.42

Note that only the work balance changes - the heat balance remains identical to Table 3.1. This is because changing the combustion temperature is assumed to have no effect on the enthalpy change of the reaction but has a significant impact on the Gibbs energy change, and thus the work that can be extracted. The overall process operating condition is chosen to be adiabatic by setting $\Delta H = 0$ kW, and this determines the extents of the 4 reactions as explained in Step 4 of Chapter 3. In other word, the operating point of the overall process is set by the heat balance, and is independent of the work balance.

4.2.2 Step 6: Include separation work

In Section 2.1, it was assumed that the work required for separation of the product from the reactor into its pure components is negligible. However, in a realistic

process, this separation work is significant and needs to be included. This work is supplied from the overall process, thus lowering the overall work available to be extracted. Equation 2.14 is used to get the separation work of the product streams into pure components.

Separation of the products is required for the SMR, WGS and combustion reactions, the corresponding work is denoted $W_{sep,SMR}$, $W_{sep,WGS}$ and $W_{sep,comb.}$ respectively. An example to calculate $W_{sep,SMR}$ is given below:

The product stream composition is given in Table 4.2.

Table 4.2: SMR product stream

Stream	SMR products	
	Component Molar Flow rates	Mole fraction, xi
CO	0.7788	0.25
H_2	2.3364	0.75
Total	3.1152	1

$$W_{sep,SMR} = -(3.1152)(\frac{8.314}{1000})(298.15)[0.25ln0.25 + 0.75ln0.75] \tag{4.3}$$

$$W_{sep,SMR} = 4.3424\text{kW} \tag{4.4}$$

The work balance is updated to include this separation work of products into pure components.

Table 4.3: Work balance including separation work after Step 6

$W_{sep,SMR}$	$W_{sep,WGS}$	$W_{sep,comb.}$	Total separation Work	Total recoverable Work
kW	kW	kW	kW	kW
4.3424	2.6762	1.0470	8.0656	27.3573

4.2.3 Step 7: Determine overall process operating pressure required for maximum work extraction

Until this step, all the unit operations of the process were assumed to be at a pressure of 1 bar. However, the operating pressure of the process is a degree of freedom. Higher operating pressure may be desired to increase the rate of reaction. Kinetics considerations are usually done at later stages of design. This is out of the scope of this Master's thesis that focuses on the early conceptual design stage prior to detailed designs. The maximum pressure rating of the equipment available (reactors, heat exchangers, component separators etc.) may also constrain the choice of operating pressure. In this Masters project, neither of these factors are considered. Instead, the pressure of the unit operations is chosen in order to extract the maximum amount of work available. This is explained next.

The process drawn in Figure 4.2 is summarized in the overall process drawn in Figure 4.3. All the unit operations are at the same operating pressure, denoted

the overall process operating pressure $P_{overall}$. If it is desired to recover the work shown in Table 4.3 using compression of the feed and expansion of the products, the minimum $P_{overall}$ is fixed. Table 4.3 shows that the total recoverable work from the overall process $W_{out} = 27.3573$ kW. This work can be recovered from an isothermal expansion process of the products after an isothermal compression process of the the reactants into the overall process. The work recovered is the difference between the work extracted in the isothermal expansion process of products and the work required for isothermal compression of reactants to the overall process.

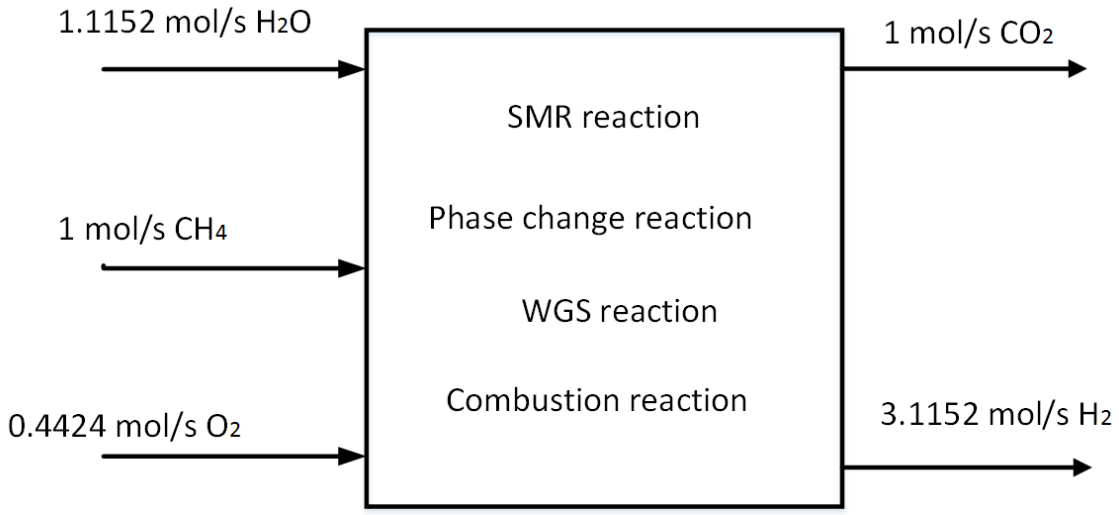

Figure 4.3: Reactants and products of overall process

Figure 4.3 shows the feed and products of the overall process. If the number of moles in the product leaving the overall process is greater than the number of moles in the feed entering the process, isothermal compression and expansion can be used to recover work. Equation 2.13 is used to determine the minimum $P_{overall}$ value. Rewriting Equation 2.13 in terms of W_{out} with the appropriate sign convention:

$$W_{out} = -(n_{in} - n_{out})RT_0 ln(P_{overall}/P_0) \tag{4.5}$$

Water is fed to the overall process at 25 °C, in liquid phase. It is assumed that the work required for liquid compression is negligible compared to the work required for gas compression. The 1.1152 moles/s of water are ignored for this reason. Thus:

$$n_{in} = 1.0 + 0.4424 = 1.4424 \tag{4.6}$$

$$n_{out} = 1 + 3.1152 = 4.1152 \tag{4.7}$$

Equation 4.5 becomes:

$$27.3573 = (4.1152 - 1.4424)(8.314/1000)298.15 ln(P_{overall}/P_0) \tag{4.8}$$

The percentage of W_{out} that can be recovered for a given overall process operating pressure $P_{overall}$ is plotted in Figure 4.4. Figure 4.4 shows that an overall process operating pressure of atleast 62.9 bar is required to completely recover all 27.3573 kW of the available work. Figure 4.4 also shows the trade-offs between

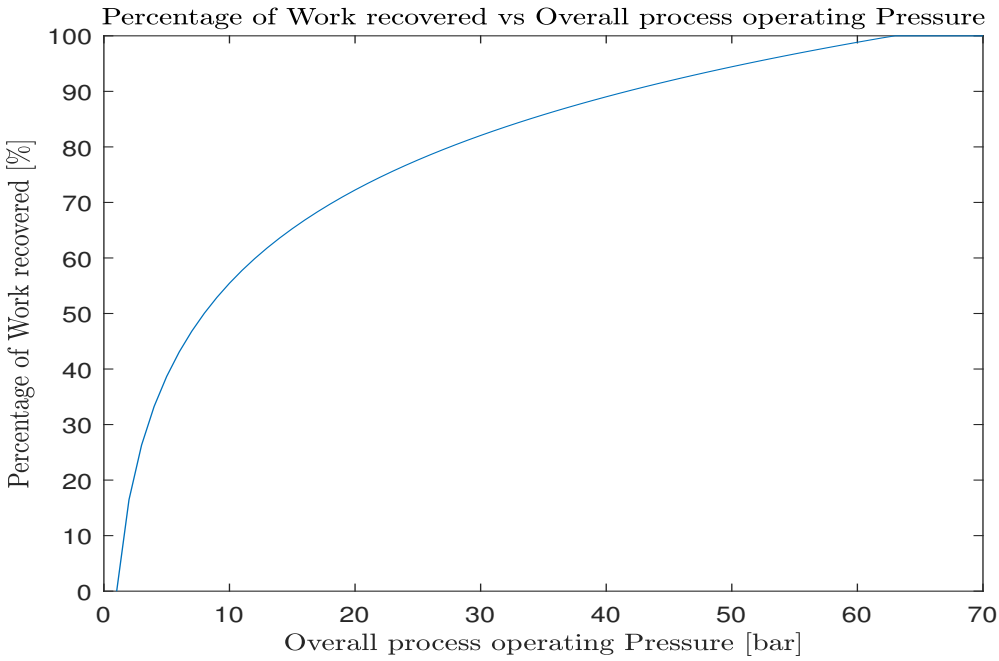

Figure 4.4: Pressure trade-offs

the percentage of work recovered and the overall process operating pressure chosen: The percentage of work recovered increases sharply from P_0 to about 20 bar and then continues to increase less sharply. Thus, it may be desirable to choose a lower $P_{overall}$ than 62.9 bar to recover most but not all of the available work. For instance, choosing $P_{overall} = 25.0$ bar recovers 77.6% of the available work.

In addition to setting the $P_{overall}$ to extract a specific percentage of the available work, other factors and trade-offs may also influence the choice of $P_{overall}$:

- The cost of manufacturing equipment such as reactors and heat exchangers increases with higher operating pressure. This is because a greater wall thickness is required for the equipment, which would require more construction material.
- Operating pressure has an influence on the kinetics of a reaction. Higher operating pressures result in higher speeds of reaction.
- In the SMR reaction, operating pressure decreases the single-pass conversion as predicted by the "K_p equation". Thus, the separation work required for the unreacted feed is increased and the pumping work of the recycle is increased.

Considering these factors is outside the scope of this Master's project, and the exact choice of the optimal $P_{overall}$ is left for later detailed design stages. In this step, the operating pressure $P_{overall} = 62.9$ bar is chosen for maximum work recovery.

With this step all the required degrees of freedom are fixed and the final block flow diagram of the process can be drawn in Figure 4.5. Note that the boiling point of water changes with pressure, thus the temperature of the phase change process has to be updated as well. The process flowsheet is presented in Figure 4.6. The stream data for both the material streams and the energy streams is provided in Appendix C. The process flowsheet is then simulated in Aspen HYSYS, and an

exergy analysis performed in order to provide a comparison with the other hydrogen production process designs. An overview of the results of the exergy analysis is presented next.

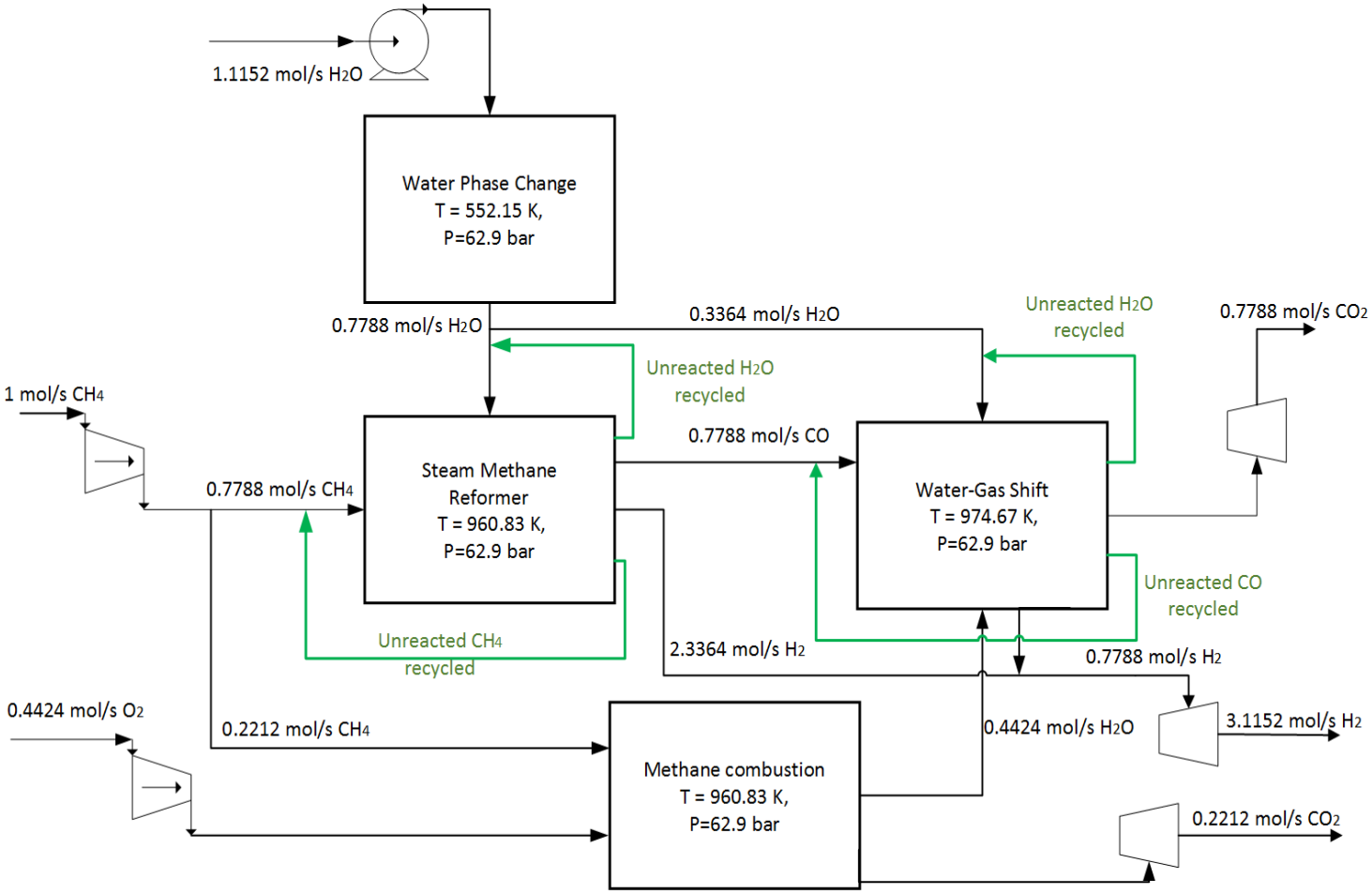

Figure 4.5: Block flow diagram of Hydrogen production process with 100 % recycle of unreacted feed in the SMR and WGS reactions

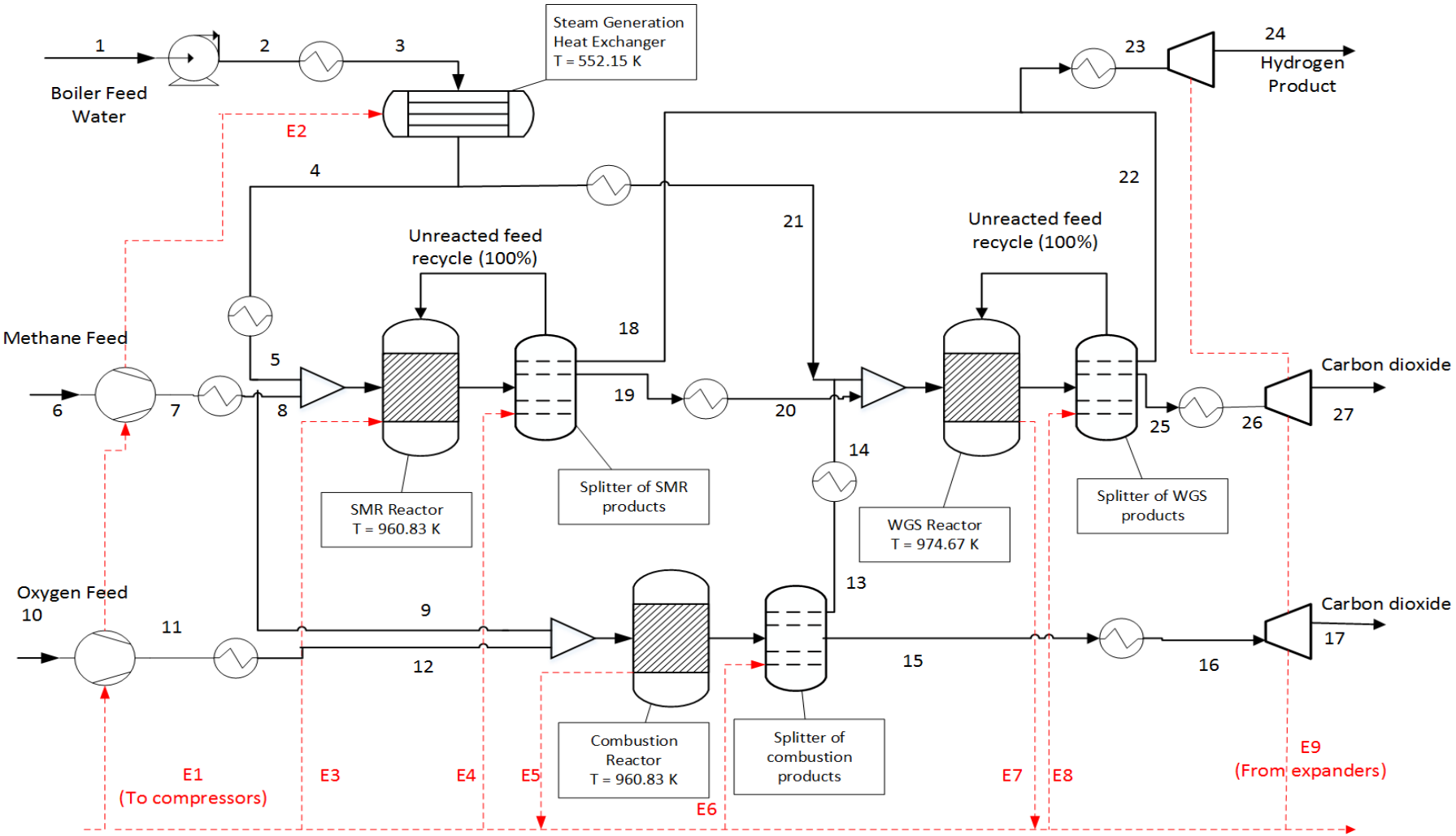

Figure 4.6: Process flowsheet of hydrogen production with 100 % recycle of unreacted feed in SMR and WGS reactions

4.2.4 Overview of Exergy Analysis Results

Table 4.4 shows the exergy destroyed in the different unit operations of the hydrogen production process with 100 % recycle of unreacted feed. A comparison with the state-of-the-art process described in Section 1.2 is also provided.

Table 4.4: Exergy Analysis of unit operations

Process: Component group	100% recycle Exergy destroyed kW/kmol CH_4	Percentage	State-of-the-art Exergy destroyed kW/kmol CH_4	Percentage
Steam Generation HX	821.00	0.79	44848.99	20.89
Feed mixers	6343.00	6.07	10223.17	4.76
Reformer	7771.06	7.43	29466.63	13.72
Water-Gas Shift	10289.72	9.84	16273.75	7.58
Furnace	43926.96	42.02	101829.91	47.42
Separation processes	35388.00	33.85	12096.83	5.63
Total Exergy Destroyed	104539.73		214739.27	

Similar to Section 1.2, an exergy analysis of the overall process can also be performed. Table 4.5 shows the exergy analysis results of the overall process, and the calculation of the overall process exergetic efficiency using Equation 1.4. Table 4.5 can be visualized in a pie chart as done in Figure 4.7.

Table 4.5: Exergy Analysis of overall process

Stream	Units	Methane In	BFW	Oxygen	Q_{in}	H_2 Out	W_{out}
Temperature	$^{\circ}C$	25	25	25		25	
Pressure	bar	62.9	62.9	62.9		62.9	
Physical Exergy	kW/kmol CH_4	9986.3	164.6	4492.6		32162.8	
Mixing Exergy	kW/kmol CH_4	0.0	0.0	0.0		0.0	
Chemical Exergy	kW/kmol CH_4	831733.2	1003.7	1756.3		735130.2	
Total Exergy	kW/kmol CH_4	841719.5	1168.3	6248.9	48782.0	767293.0	16380.0
				Exergy In =	897918.63	Exergy Out =	783673.02
					$\eta_{overall}$ =	87.28	

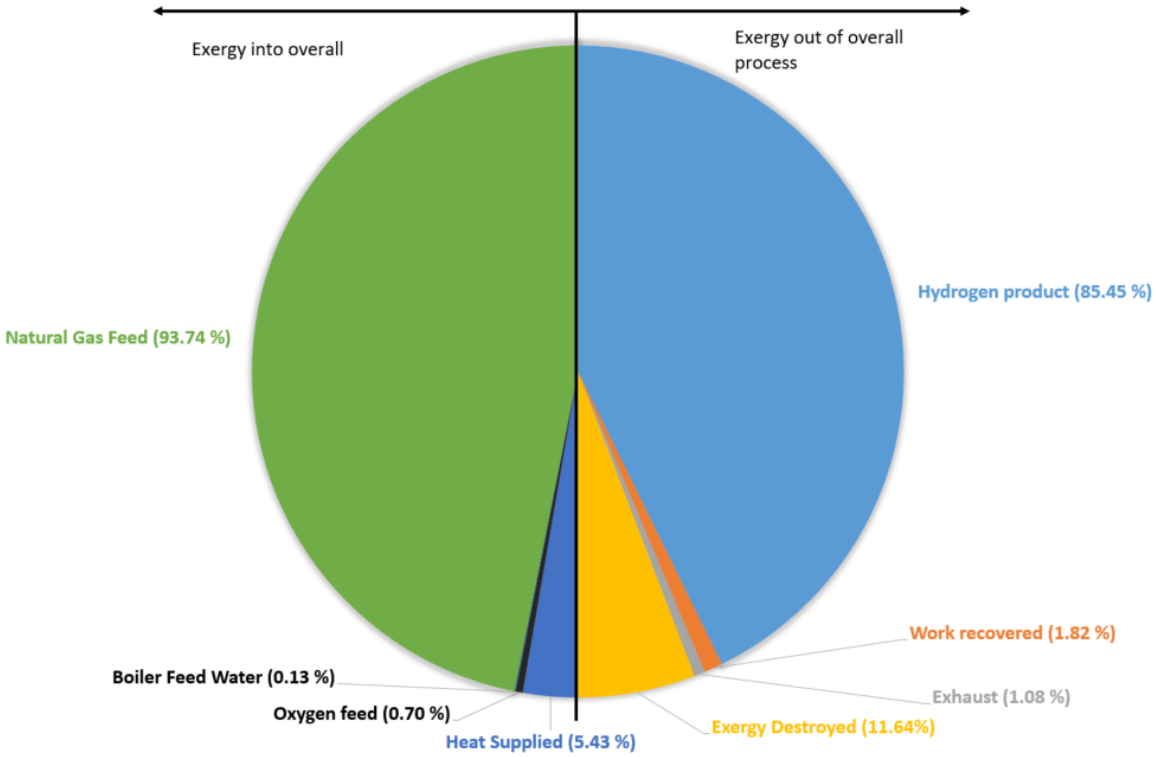

Figure 4.7: Pie chart to visualize the exergy analysis results of the overall hydrogen production process with 100 % recycle

4.2.5 Discussions

This section is presented in detail because it is the first discussion of the exergy analysis of a process designed using the G-H methodology. Discussions presented on processes designed in subsequent sections and chapters are less detailed. Table 4.4 presents a comparison between the process with 100 % recycle of unreacted feed and the state-of-the-art process, several caveats have to be made first because the two processes are considerably different:

1. A major difference between the two processes arises from the fact that the state-of-the-art process corresponds to the detailed design stage, not the conceptual design stage like the 100 % recycle process. Before developing the state-of-the-art process, each unit operation was modeled in detail in order to operate as closely as possible to a realistic unit. As a result of this detailed modeling, the state-of-the-art process included several irreversibilities that were not included in the conceptual design of the process with 100 % recycle. For instance, pressure drops were modeled for the reactors, and heat exchangers in the state-of-the-art process while a zero pressure drop was assumed in the process with 100 % recycle. This pressure drop results in significant exergy destruction in the state-of-the-art process that is not taken into account in the process with 100 % recycle. In addition, an accurate temperature difference (ΔT_{min}) was modeled between the hot and cold streams of all heat exchangers in the state-of-the-art process. This heat transfer across a finite temperature difference results in significant exergy destruction that is

not taken into account in the process with 100 % recycle. Lastly, isothermal compression and expansion was assumed in the process with 100 % recycle corresponding to a reversible process, while the compression and expansion processes in the state-of-the art process had significant irreversibilities. In a later detailed design phase, these considerations have to be taken into account and modeled. This would result in a larger exergy destruction than in presented in Table 4.4. This detailed design is outside the scope of this Master's project.

2. The flowsheet simulated in HYSYS for the state-of-the-art process is significantly different from the flowsheet simulated for the process with 100 % recycle of the unreacted feed. The heat exchanger networks of the two processes are different. In addition, the interconnections between the different unit operations is also different in the two processes.

3. The conversion in the different unit operations is different since the state-of-the-art process does not use recycling.

4. A further difference is that different reactions are taking place in the unit operations. For instance, the combustion reaction in the state-of-the-art process uses purge gas as a feed not methane as is used in the process with 100 % recycle. Thus, the reaction taking place in the furnace is different implying different heat and work released. The product composition from the furnace is also different. Similarly, the reformer reactor in the state-of-the-art model was modeled using a Gibbs reactor that determines the product composition by minimizing Gibbs free energy. Several reactions take place simultaneously and a range of product species may be formed. For instance, a reforming process of heavier hydrocarbons takes place. Even the water-gas shift reaction occurs to some extent in this reformer reactor as some carbondioxide is formed. However, the reformer unit operation for the process with 100 % recycle was constrained such that only the SMR reaction took place, and only carbon monoxide and hydrogen could be the products formed. Carbon dioxide could not be formed.

5. Finally, the thermodynamic models used in the two HYSYS simulations are different. The Peng-Robinson fluid package was used in the state-of-the-art process while the NRTL-Ideal fluid package was used in the process with 100 % recycle.

The flowrates of the feed and products in the state-of-the-art process are also different from those in the process with 100 % recycle. However, to be able to provide a fair basis for comparison, the exergy analysis was normalized with respect to the methane feed flowrate. Thus, the units of exergy in Table 4.4 are all in kW/kmol CH_4. Having made caveats 1 - 5, the following discussions can be made with regards to Table 4.4:

- The total amount of exergy destroyed is much lower in the process with 100 % recycle compared to the state-of-the-art process. This is also true for the SMR and WGS unit operations. Less exergy is destroyed in the SMR and WGS process because they operate at their Carnot temperatures in the process with 100 % recycle while they do not in the state-of-the-art process.

- One question that arises from the point above is why any exergy is destroyed by the SMR and WGS processes operating at their Carnot temperatures; processes operating at their Carnot temperatures are supposed to be reversible and not destroy any exergy. Two explanations are given for this: First, several assumptions were made in formulating the G-H methodology in Section 2.1, but these assumptions are not taken into account in the Aspen HYSYS model used to perform the exergy analysis. For instance, it was assumed that the heat capacity of the reactants matches exactly with the heat capacity of the products such that no external heating is required. This assumption is not accurate in a realistic model - the heat required to bring the reactants to the reactor temperature may not be met by the heat released by the product. Thus, the "simple chemical process" defined in Section 2.1 is not an accurate representation of the actual process but rather an idealized one. The second explanation is that the thermodynamic data and models used within Aspen HYSYS may not correspond exactly with the the heat and work balance calculations done in this case study. HYSYS uses a Gibbs energy minimization procedure to determine the reactor conversion. The thermodynamics of the reactor estimated with this procedure may not match exactly with the enthalpy change and Gibbs energy change of reaction used in this case study. Despite this, it is important to note that the exergy destroyed for example in the SMR reactor is 0.9 % of the total exergy of the SMR methane feed (Given in Table 4.5). This is a negligibly small exergy destruction in percentage terms, and within the margin of error of the exergy analysis procedure developed in the specialization project [2].

- The exergy destruction in the steam generation heat exchanger is much lower in the process with 100 % recycle than in the state-of-the-art process. However, it may not be valuable to make a conclusion based on this value because the exergy destruction may increase significantly in the detailed design phase that models accurately the temperature difference between the hot and cold streams.

- The furnace is still the unit operation responsible for the largest source of inefficiency (42.02 %). This is expected because the operating temperature of the furnace was changed significantly from its Carnot temperature in Step 5. It is thought that the furnace process will continue to be the source of largest exergy destruction because most fossil fuel combustion reactions have very high Carnot temperatures. Combustion of some fossil fuels such as coal is inherently irreversible because the Carnot temperature is negative.

- The separation processes is responsible for a large percentage of exergy destruction (33.85 %), higher than the state-of-the-art. This separation process includes both separation of the product stream into pure components and the separation of the unreacted feed from the product for the recycle process. The latter separation process is not included in the state-of-the-art process since no recycling takes place. This explains the larger exergy destruction in the 100 % recycle process.

Table 4.5 and Figure 4.7 present the main results of an exergy analysis on the overall process with 100 % recycle. The material streams into the process are:

Methane Feed, BFW (Boiler Feed Water), and the oxygen feed to the furnace while the Hydrogen product is the only useful material stream out. As described in Step 7, work W_{out} is recovered in the process. Q_{in} represents the exergy supplied as heat into the overall process. In Figure 4.7, the left half of the pie chart represents the sum of exergy for the streams into the overall process while the right half represents the sum of exergy out of the overall process. The useful exergy in the hydrogen product stream is 85.45 %, and 1.82 % is recovered in the work stream. In total, these two correspond to the $\eta_{overall}$ value of 87.28 %. The rest of the exergy out of the process is either destroyed (11.64 %) or disposed off in the exhaust streams (1.08 %). The following discussions are made:

- The exergetic efficiency of the overall process $\eta_{overall}$ is higher than that for the state-of-the-art process. The main reason for this is the smaller exergy destruction (11.64 %) versus 21.69 % for the state-of-the-art process. Thus, the more reversible SMR, WGS and furnace unit operations contribute to a higher overall exergetic efficiency. This implies that more of the methane feed is converted to hydrogen than the state-of-the-art process.

- The percentage of exergy lost in the exhaust (i.e. useless by-products) is lower (1.08 %) compared to 3.28 % in the state-of-the-art process. This is because complete conversion is achieved through 100 % recycling implying none of the unreacted feed is disposed off; as much as possible of the reactant is converted to the useful hydrogen product.

- Significant heat (Q_{in}) is supplied to the process, corresponding to 5.43 %. It is an important question to explain why this heat has to be supplied to the overall process: In Step 4 of the G-H methodology, the overall process operating point is chosen to ensure an adiabatic process. It was desired that no external heat is supplied and the flowsheet in Figure 4.6 was designed to meet this requirement. However, simulating the flowsheet using HYSYS shows that external heating is required. The reason for this is that the assumptions made in Section 2.1 are not realistic. For instance, it was assumed that the heat load of all other components except the reactor is zero, and that internal heat exchange from the products is sufficient to bring the reactants from T_0 to reactor temperature T. The HYSYS simulation showed that these assumptions are not met; it is necessary to supply external heat for the process to proceed. This situation can be addressed in later iterations of process design. The extent of the combustion process can be increased in order to provide this heat requirement. This later iteration would have a lower overall exergetic efficiency.

- From Table 4.5 it can be seen that the work recovered, $W_{out} = 16.380$ kW/mol. This is lower than the W_{out} target of 27.3573 kW/mol given in Table 4.3. The reason for the difference is the different thermodynamic data and model used within HYSYS to determine the Gibb energy change of reaction. This is illustrated in Table 4.6. This lower W_{out} implies a lower exergetic efficiency.

Table 4.6: Comparison of Gibbs energy changes of the different unit operations between HYSYS and Table 4.1

Unit Operation		SMR	WGS	Phase change	Combustion	Overall Process
Temperature	K	960.83	974.67	370.14	1200	
Pressure	bar	1	1	1	1	
e		0.7788	0.7788	1.1152	0.2212	
ΔG (Table 4.1)	kW	110.71	-22.27	9.55	-133.41	-35.42
ΔG (HYSYS)	kW	121.30	-18.69	14.60	-133.60	-16.38

In conclusion, this section used the G-H methodology to design a hydrogen production process that achieves complete conversion by recycling 100 % of the unreacted feed. This process had a lower exergy destruction than the state-of-the-art process due to running the SMR and WGS processes at their Carnot temperatures. Even though the furnace had a lower exergy destruction as well, it still remained a major source of inefficiency because it is run at an operating temperature significantly lower than its Carnot temperature. As a result of the lower exergy destruction, the designed process has a higher overall process exergetic efficiency than the state-of-the-art implying more of the methane feed is converted to valuable hydrogen product. However, it is noted that this process corresponds to the conceptual stage design - detailed and more realistic designs would have more irreversibilities and thus a lower overall process exergetic efficiency. This implies that this case study should be looked at as a best-case target for later iterations of process design.

4.3 Case study 2: Incomplete overall conversion using 80 % recycle of the unreacted feed

As explained in Chapter 3, the steps of the G-H methodology outlined assume complete conversion of all the reactions taking place. Complete overall conversion is only achieved when 100 % of the unreacted feed is separated and recycled back.

However, the percentage of the unreacted feed recycled may be an important degree of freedom in the reaction, separation and recycle system. Thus optimization of this percentage of recycle and the overall reactor conversion is necessary. Also it may be necessary to purge some of the unreacted feed in order to avoid build-up of impurities [10]. In Figure 4.8, Smith and Linnhoff explain the cost trade-offs as a function of overall reactor conversion. The annualized reactor cost depends significantly on the reactor volume, which is affected by the conversion. The separation and recycle costs as well as the Heat Exchanger Network (HEN) cost is also affected by the conversion, since these are downstream of the reactor.

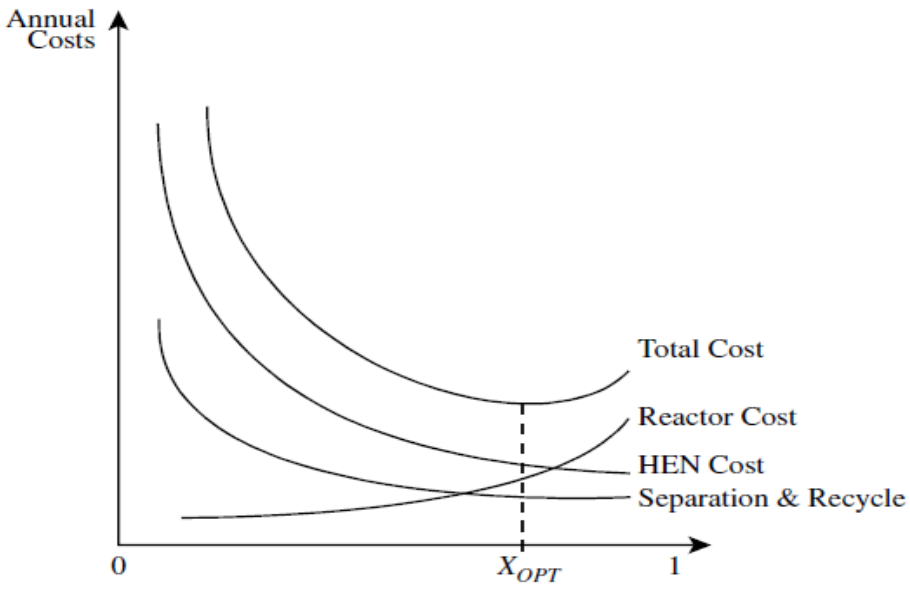

Figure 4.8: Illustration of overall cost trade-offs as a function of overall reactor conversion ([30] cited in [10]). X_{OPT} denotes the optimal conversion.

The optimal overall reactor conversion may be less than 1. This situation is considered in this case study which assumes an overall conversion of 0.8. This corresponds to an 80 % recycle of unreacted feed. For an overall conversion less than 1, the G-H methodology needs to be modified. The modifications are described in the following section.

4.4 Modifying the G-H methodology to account for less than complete conversion

In this case study, the reactions studied are unchanged. Thus, Steps 1 and 2 remain the same as Chapter 3. However, Step 3 onwards are modified.

4.4.1 Step 3: Obtain relations between reaction extents. Express extents to include conversion terms

The reversible reactions considered are the SMR and WGS reactions; complete conversion is assumed in the combustion and water phase change reactions. The conversions in the SMR and WGS reactions are termed c_{SMR} and c_{WGS} respectively. Since 80 % conversion is assumed in this case study:

$$c_{SMR} = c_{WGS} = 0.8. \tag{4.9}$$

Multiple of the simplest stoichiometric feed *(f)*

A new term "f" is introduced to denote the "multiple of the simplest stoichiometric feed". This term is introduced for convenience, and is defined next. First, the definition of f is made for any general reversible equation. Then, an example is given with the SMR reaction to clarify the definition.

In Section 3.5, the stoichiometric feed was defined for a general reversible reaction with 2 reactants and 2 products:

$$\mathrm{v_A A} + \mathrm{v_B B} \rightleftharpoons \mathrm{v_C C} + \mathrm{v_D D} \tag{4.10}$$

where: v_i is the stoichiometric coefficient of reactant or product component i.

The chemical reaction is said to have a "stoichiometric feed" if the ratio of the molar flowrates of the reactants is equal to the ratio of their stoichiometric coefficients. For instance, let the molar flowrate of reactant A be N_A^0 mol/s and the molar flowrate of reactant B be N_B^0 mol/s. Then if $\frac{N_A^0}{N_B^0} = \frac{v_A}{v_B}$, the feed is said to be the stoichiometric feed. The simplest example of a stoichiometric feed is when the molar flowrate of the reactant component is identical to its stoichiometric coefficient i.e. $N_A^0 = v_A$ mol/s and $N_B^0 = v_B$ mol/s. Such a feed can be termed the "simplest stoichiometric feed".

Since, the ratio of the flowrates of the reactant components of the simplest stoichiometric feed is fixed, all possible flowrates are a multiple of this stoichiometric feed. Thus, this multiple contains all the necessary information to define the feed flowrate, as long as its a stoichiometric feed. This multiple is denoted by "f" and termed the "multiple of the simplest stoichiometric feed".

The SMR reaction is used as an example:

$$\mathrm{CH_4(g)} + \mathrm{H_2O\,(g)} \rightleftharpoons \mathrm{CO\,(g)} + 3\,\mathrm{H_2(g)} \tag{4.11}$$

The simplest stoichiometric feed would contain 1 mol/s of CH_4 and 1 mol/s of H_2O. Any possible stoichiometric feed for the SMR reaction is a multiple of this simplest stoichiometric feed. Thus, the multiple of stoichiometric feed, f, is used to scale the actual process flow rate with respect to the simplest stoichiometric feed. For example, if the SMR process is designed with a feed of 3 mol/s of CH_4 and 3 mol/s of H_2O, $f_{SMR} = 3$.

The rationale for coining the new term is to make it more convenient to include information about conversion in the species material balance calculations. In Step 3 of Chapter 3, the extent of reaction (e) is used in the material balance equations of the species. A stoichiometric feed was assumed in Chapter 3 as well. However, the extent of reaction lumps together the scaling of this stoichiometric feed and

the conversion into one term, and it is useful to distinguish these two parameters. Conversion c is normalized between 0 and 1, and the f is used to scale the feed in order to determine the actual number of reacting moles in the chemical process. This actual number of reacting moles is extent of reaction e. Thus, the extent of reaction is given by the expression:

$$e = f.c \tag{4.12}$$

To illustrate this, return to the example of the SMR reaction with $f_{SMR} = 3$. Assume the conversion is 0.5 (i.e. c = 0.5), that is half of the feed reacts and the other half is unreacted. Thus, out of the feed of 3 mol/s of CH_4 and 3 mol/s of H_2O, 1.5 mol/s of CH_4 reacts with 1.5 mol/s of H_2O. The other half is unreacted. In this case, the extent:

$$e = f.c = 3(0.5) = 1.5 \tag{4.13}$$

With this notation, material balances can be performed for all the individual species, in moles. The extent of reaction (e) terms in Equations 3.6 to 3.11 are replaced with $f.c$ terms for the reversible SMR and WGS reactions:

$$N_{CH_4} = N^0_{CH_4} - f_{SMR}.c_{SMR} - e_{comb} \tag{4.14}$$

$$N_{H_2} = N^0_{H_2} + 3f_{SMR}.c_{SMR} + f_{WGS}.c_{WGS} \tag{4.15}$$

$$N_{CO} = N^0_{CO} + f_{SMR}.c_{SMR} - f_{WGS}.c_{WGS} \tag{4.16}$$

$$N_{CO_2} = N^0_{CO_2} + f_{WGS}.c_{WGS} + e_{comb} \tag{4.17}$$

$$N_{H_2O} = N^0_{H_2O} - f_{SMR}.c_{SMR} - f_{WGS}.c_{WGS} + 2e_{comb} \tag{4.18}$$

$$N_{O_2} = N^0_{O_2} - 2e_{comb} \tag{4.19}$$

The superscript "0" shows the number of moles of that component fed to the overall process, and the final number of moles out of the overall process is given by N without the superscript.

The following design decisions of individual unit operations are made in this case study:

- It is assumed that the only feed materials are: CH_4, H_2O and O_2. Thus: $N^0_{H_2} = N^0_{CO} = N^0_{CO_2} = 0$
- The methane feed is chosen to be: $N^0_{CH_4} = 1$. This can be any molar units but in order to be consistent with the "simplest stoichiometric feed", it is assumed to be in mol/s. The overall process scales with this methane feed. Also, it is desired that all the methane is used up in the process, so $N_{CH_4} = 0$. Equation 4.14 becomes:

$$e_{comb} = 1 - f_{SMR}.c_{SMR} \tag{4.20}$$

- Noting that the WGS reaction uses carbon monoxide produced from the SMR reactor, the feed of CO to the WGS reactor should be equal to the produced CO in the SMR MR. Thus:

$$f_{WGS} = f_{SMR}.c_{SMR} \tag{4.21}$$

Since the WGS reactor, separation and recycle system only achieves 80 % conversion, 20 % of the unreacted CO is disposed of. Thus as expected:

$$N_{CO} = 0.2 f_{WGS} \tag{4.22}$$

- Similarly, a design decision is made to set that the amount of steam produced in the phase change reaction and in the combustion reaction should equal the sum of the amount of steam that reacts in the SMR reactor and is fed to the WGS reactor.

$$e_{phase} + 2e_{comb} = f_{SMR}.c_{SMR} + f_{WGS} \tag{4.23}$$

$$e_{phase} = f_{SMR}.c_{SMR} + f_{WGS} - 2e_{comb} \tag{4.24}$$

$$e_{phase} = 4 f_{SMR}.c_{SMR} - 2 \tag{4.25}$$

Only 80 % of H_2O is converted in the WGS reactor, recycle and separation system, implying 20 % of H_2O is disposed of. This unreacted steam is not utilized. Thus, 20 % of the unreacted H_2O fed to the WGS reactor is disposed off. Thus, as expected, Equation 4.18 becomes:

$$N_{H_2O} = 0.2 f_{WGS} \tag{4.26}$$

4.4.2 Step 4: Choose overall adiabatic operating conditions

This is similar to Step 4 in Chapter 3. An overall adiabatic process is desired, thus $\Delta H = 0$ kW is chosen as the overall process operating point.

Overall heat and work balance:

$$\begin{pmatrix}\Delta H_{overall}\\ \Delta G_{overall}\end{pmatrix} = \begin{pmatrix}\Delta H_{SMR}\\ \Delta G_{SMR}\end{pmatrix}(f_{SMR}.c_{SMR}) + \begin{pmatrix}\Delta H_{WGS}\\ \Delta G_{WGS}\end{pmatrix}(f_{WGS}.c_{WGS}) + \begin{pmatrix}\Delta H_{phase}\\ \Delta G_{phase}\end{pmatrix}(e_{phase}) + \begin{pmatrix}\Delta H_{comb}\\ \Delta G_{comb}\end{pmatrix}(e_{comb}) \tag{4.27}$$

Express in terms of single variable f_{SMR}:

$$\begin{pmatrix}\Delta H_{overall}\\ \Delta G_{overall}\end{pmatrix} = \begin{pmatrix}\Delta H_{SMR}\\ \Delta G_{SMR}\end{pmatrix}(f_{SMR}.c_{SMR}) + \begin{pmatrix}\Delta H_{WGS}\\ \Delta G_{WGS}\end{pmatrix}(f_{SMR}.c_{WGS}.c_{SMR}) + \begin{pmatrix}\Delta H_{phase}\\ \Delta G_{phase}\end{pmatrix}(4 f_{SMR}.c_{SMR} - 2) + \begin{pmatrix}\Delta H_{comb}\\ \Delta G_{comb}\end{pmatrix}(1 - f_{SMR}.c_{SMR}) \tag{4.28}$$

Substitute in values:

$$\begin{pmatrix}\Delta H_{overall}\\ \Delta G_{overall}\end{pmatrix} = \begin{pmatrix}206.12\\ 142.16\end{pmatrix}(0.8 f_{SMR}) + \begin{pmatrix}-41.19\\ -28.59\end{pmatrix}(0.64 f_{SMR}) + \begin{pmatrix}44.01\\ 8.56\end{pmatrix}(4(0.8) f_{SMR} - 2) + \begin{pmatrix}-802.35\\ -800.71\end{pmatrix}(1 - 0.8 f_{SMR}) \tag{4.29}$$

Table 4.7: Heat and Work balance after Step 4 of the modified G-H methodology

Unit Operation		SMR	WGS	Phase change	Combustion	Overall Process
Temperature	K	960.83	974.67	370.14	145,866.25	
Pressure	bar	1	1	1	1	
c		0.8	0.8	1	1	
f		0.9665	0.7732	1.0927	0.2268	
e=f.c		0.7732	0.6186	1.0927	0.2268	
ΔH	kW	159.37	-25.48	48.09	-181.98	0.00
ΔG	kW	109.92	-17.68	9.35	-181.61	-80.03

Solving for f_{SMR} by setting the overall process operating point to result in an adiabatic process, the heat and work balance is calculated and presented in Table 4.7.

After Step 4, a block diagram can be drawn of the process for hydrogen production with 80 % recycle.

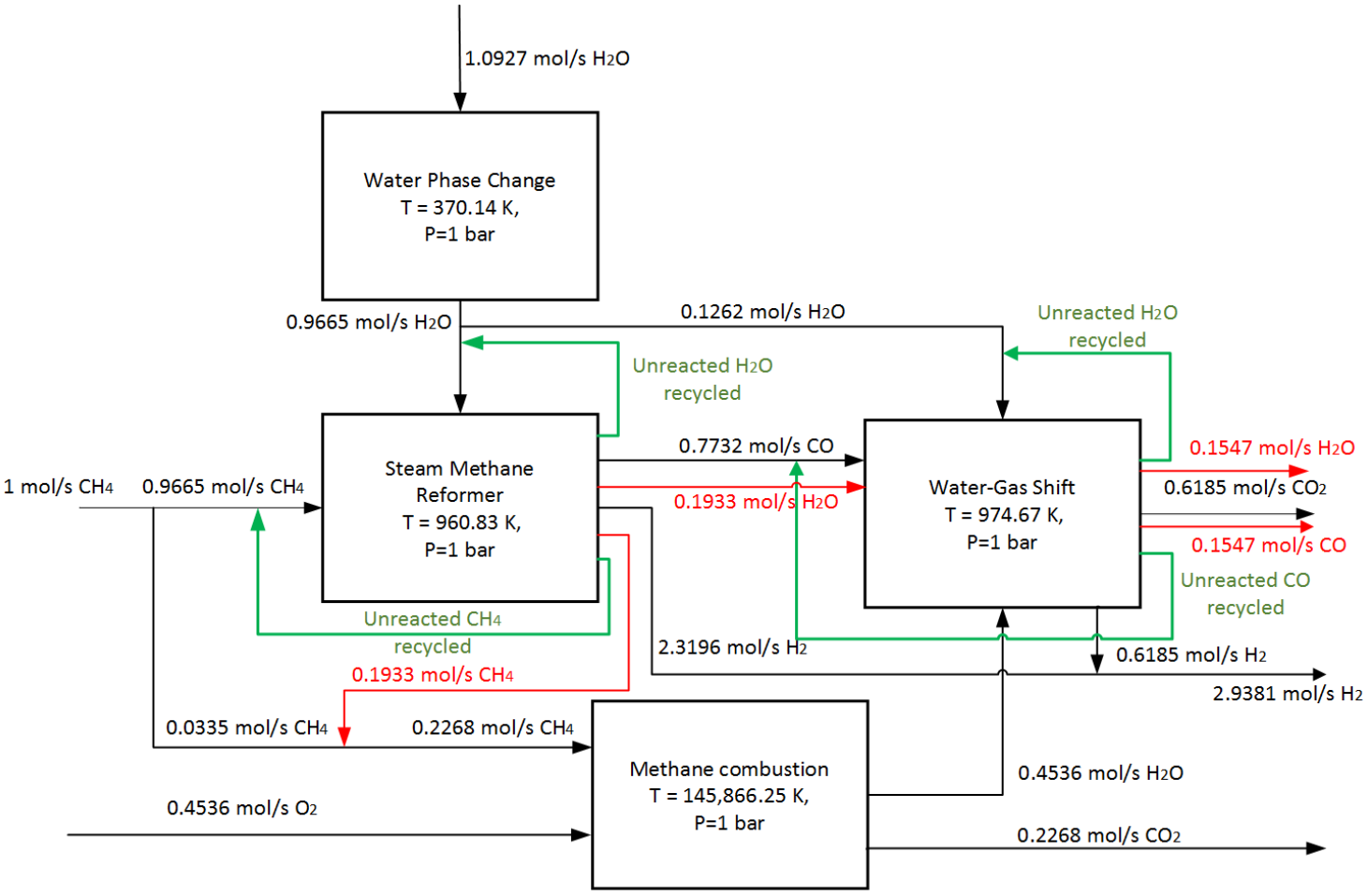

Figure 4.9: Hypothetical block flow diagram before realism considerations

4.4.3 Step 5: Use realistic operating Temperatures

For identical reasons as listed in Step 5 done in Section 4.2, a lower combustion temperature of 1200.0 K is used rather than the Carnot temperature of 145,866.25 K. This reduces the recoverable work. Table 4.8 presents the updated heat and work balance. The extents of the 4 reactions are only dependent on the heat balance so are unaffected - only the work balance changes.

Table 4.8: Heat and Work balance after Step 5

Unit Operation		SMR	WGS	Phase change	Combustion	Overall Process
Temperature	K	960.83	974.67	370.14	1200.0	
Pressure	bar	1	1	1	1	
c		0.8	0.8	1	1	
f		0.9665	0.7732	1.0927	0.2268	
e=f.c		0.7732	0.6186	1.0927	0.2268	
delta H	kW	159.37	-25.48	48.09	-181.98	0.00
delta G	kW	109.92	-17.68	9.35	-136.7704	-35.18

4.4.4 Step 6: Include separation work

This step is identical to Step 6 done in Section 4.2. Table 4.9 gives the updated work balance.

Table 4.9: Work balance of the flowsheet after including separation work

$W_{sep,SMR}$	$W_{sep,WGS}$	$W_{sep,comb.}$	Total separation Work	Total recoverable Work
KW	KW	KW	KW	KW
4.3111	2.1254	1.0735	7.5100	27.6745

4.4.5 Step 7: Determine overall process operating pressure required for maximum work extraction

This step is identical to Step 7 done in Section 4.2. Table 4.9 shows that the total recoverable work from the overall process W_{out} = 27.6745 kW.

$$W_{recovered} = -(n_{in} - n_{out})RTln(P_{overall}/P_0) \tag{4.30}$$

From Figure 4.9, ignoring the feed and outflow of $H_2O(l)$:
n_{out} = 0.6185 + 0.1547 + 2.9381 + 0.2268 = 3.9381
n_{in} = 1 + 0.4536 = 1.4536
Substituting:

$$27.6745 = (3.9381 - 1.4536)(8.314/1000)298.15ln(P_{overall}/P_0) \tag{4.31}$$

Solving: $P_{overall}$= 92.26 bar.

Thus, all the unit operations are assumed to operate at this pressure. In this step, the operating pressure $P_{overall} = 92.26$ bar is chosen for maximum work recovery.

With this step all the required degrees of freedom are fixed and the final block flow diagram of the process can be drawn in Figure 4.10. Note that the boiling point of water changes with pressure and thus the temperature of the phase change process has been updated as well. The process flowsheet is presented in Figure 4.11. The stream data for both the material streams and the energy streams is provided in Appendix C. The process flowsheet is then simulated in Aspen HYSYS, and an exergy analysis performed in order to provide a comparison with the other hydrogen production process designs. An overview of the results of the exergy analysis is presented next.

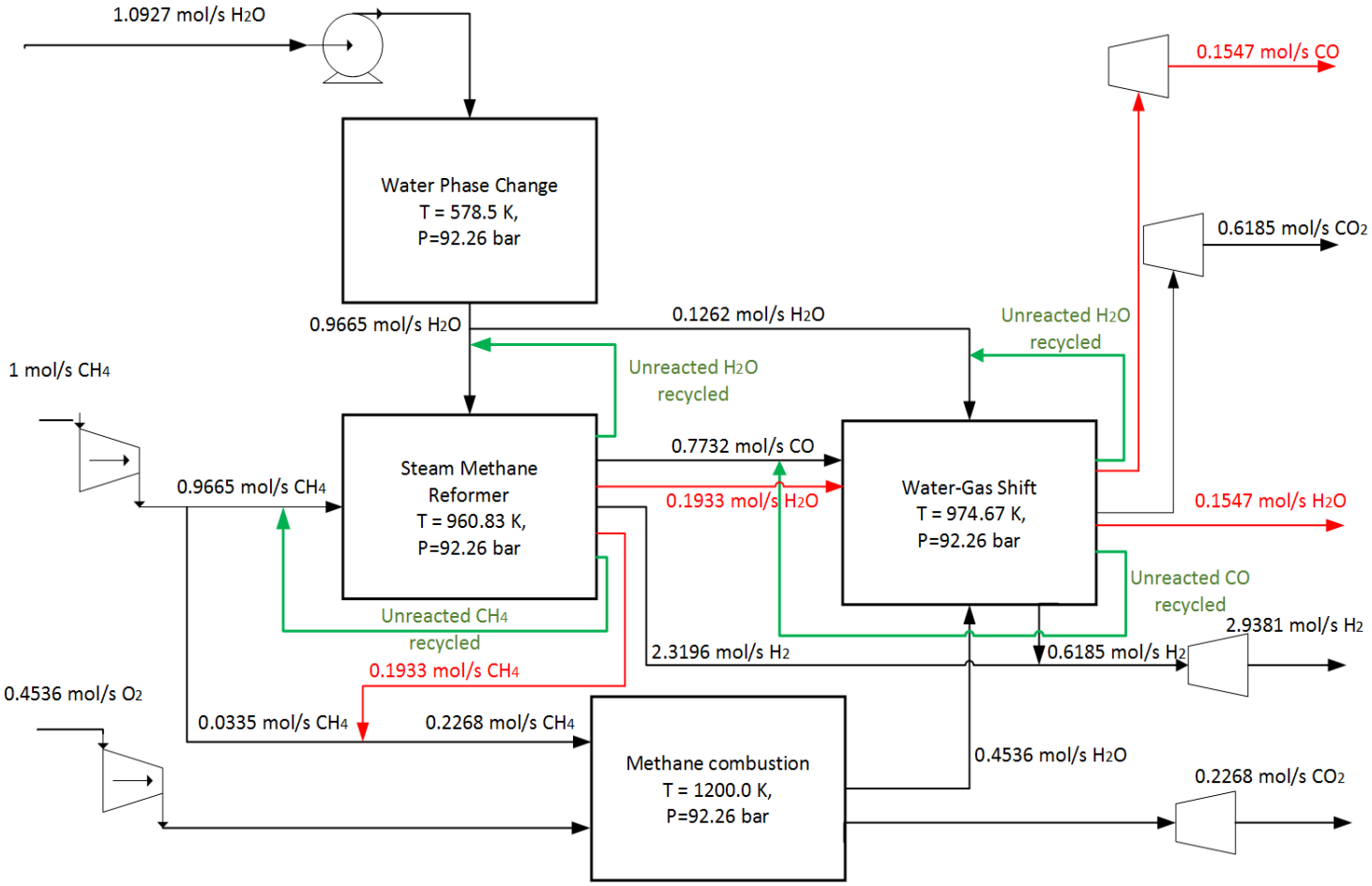

Figure 4.10: Block flow diagram of Hydrogen production process with 80 % recycle of unreacted feed in the SMR and WGS reactions

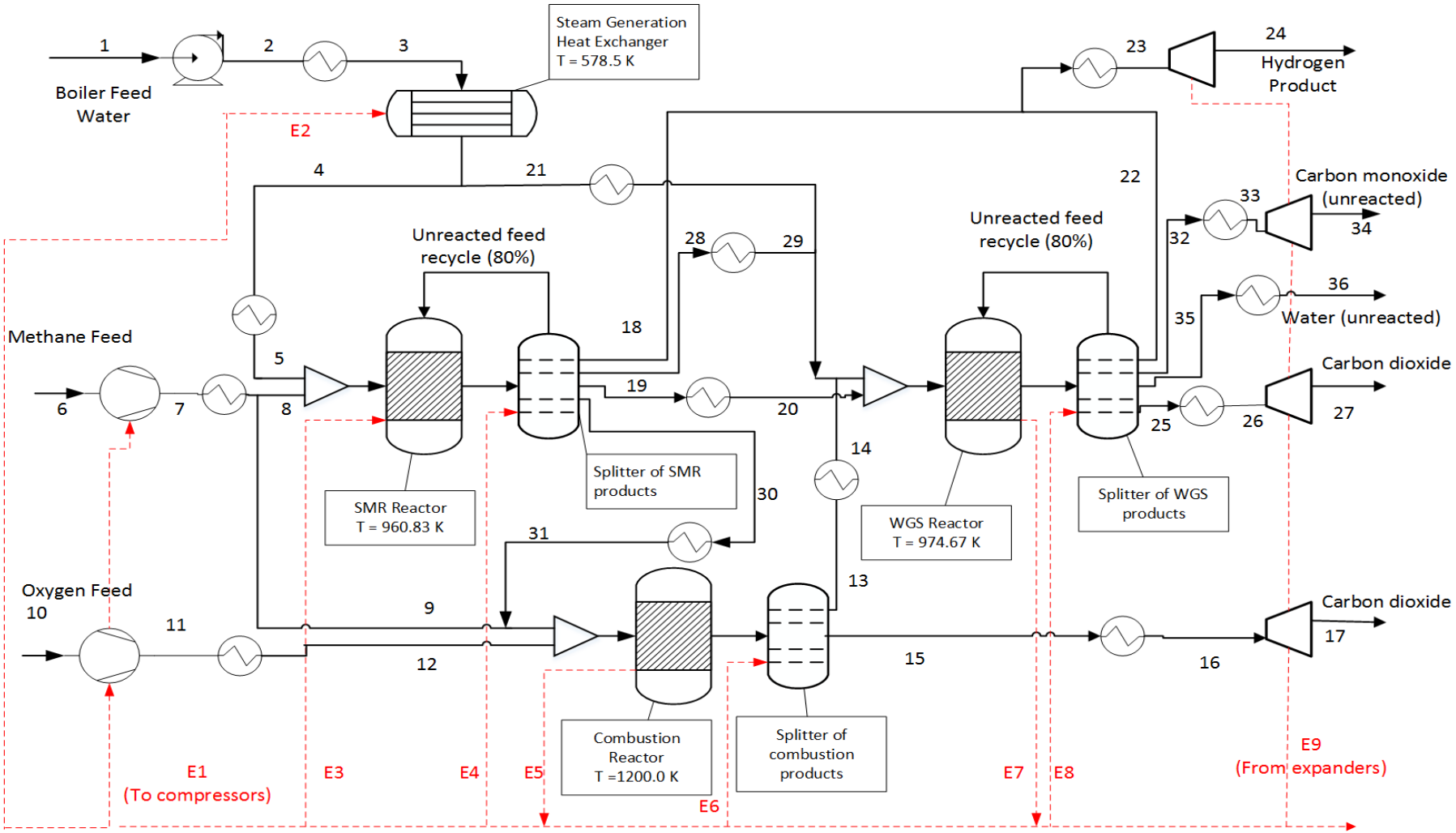

Figure 4.11: Process flowsheet of hydrogen production with 80 % recycle of unreacted feed in SMR and WGS reactions

4.4.6 Overview of Exergy Analysis Results

Table 4.10 shows the exergy destroyed in the different unit operations of the hydrogen production process with 80 % recycle of unreacted feed. A comparison with the state-of-the-art process described in Section 1.2 is also provided.

Table 4.10: Exergy Analysis of unit operations

Process: Component group	80% recycle Exergy destroyed kW/kmol CH_4	Percentage	State-of-the-art Exergy destroyed kW/kmol CH_4	Percentage
Steam Generation HX	792.00	0.87	44848.99	20.89
Feed mixers	5798	6.39	10223.17	4.76
Reformer	3271.65	3.61	29466.63	13.72
Water-Gas Shift	4885.85	5.38	16273.75	7.58
Furnace	45107.96	49.74	101829.91	47.42
Separation processes	30834.00	40.00	12096.83	5.63
Total Exergy Destroyed	90689.46		214739.27	

Similar to Section 4.2, an exergy analysis of the overall process can also be performed. Table 4.11 shows the exergy analysis results of the overall process with 80 % recycle, and the calculation of the overall process exergetic efficiency using Equation 1.4. Table 4.11 can be visualized in a pie chart as done in Figure 4.12.

Table 4.11: Exergy Analysis of overall process

Stream	Units	Methane In	BFW	Oxygen	Q_{in}	H_2 Out	W_{out}
Temperature	$^{\circ}C$	25	25	25		25	
Pressure	bar	92.26	92.26	92.26		92.26	
Physical Exergy	kW/kmol CH_4	10829.12	237.76	5023.04		33218.01	
Mixing Exergy	kW/kmol CH_4	0.00	0.00	0.00		0.00	
Chemical Exergy	kW/kmol CH_4	831650.00	983.43	1800.79		692533.73	
Total Exergy	kW/kmol CH_4	842479.12	1221.19	6823.84	44800.00	725751.74	17990.00
				Exergy In =	895324.14	Exergy Out =	743741.74
					Exergetic	Efficiency =	83.07

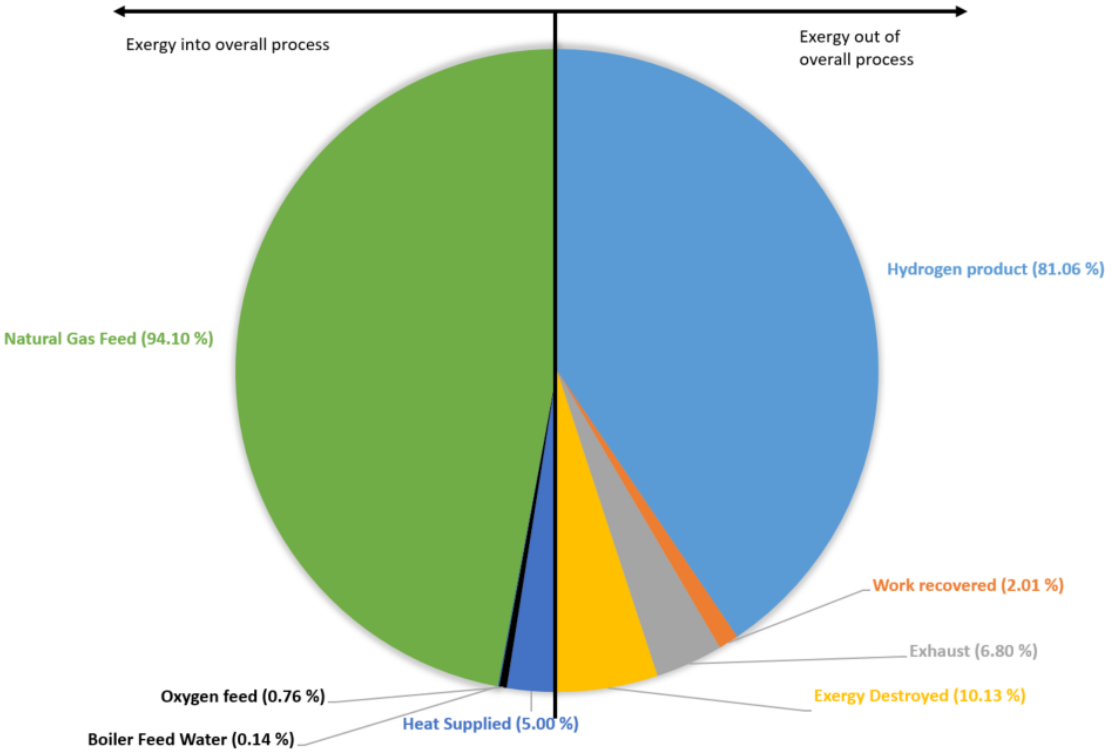

Figure 4.12: Pie chart to visualize the exergy analysis results of the overall hydrogen production process with 80 % recycle

4.4.7 Discussions

This section is brief since several of the discussions made in Section 4.2.5 are applicable here as well. The caveats 1 - 5 also hold in this section. The following comments can be made with respect to Table 4.10:

- The total exergy destroyed is less than the state-of-the art process. Note that the exergy lost in the exhaust streams is not included as exergy destroyed. Less exergy is destroyed because the SMR and WGS act more reversibly since they operate at their Carnot temperatures. Less exergy is destroyed in the furnace as well. The furnace is still the largest source of inefficiency due to identical reasons as in Section 4.2.5.

- The exergy destroyed in the SMR and WGS unit operations is smaller for the process with 80 % recycle than the process with 100 % recycle presented in Section 4.2.4. This is because the conversion of these unit operations is lower in the process with 80 % recycle, thus they have smaller reaction extents. The amount of exergy destroyed scales with reaction extent explaining why the process with 80 % recycle has lower exergy destroyed.

- Also as expected, the amount of exergy destroyed in separation is lower for the process with 80 % recycle compared to the process with 100 % recycle. This separation process is both the separation of product and separation of unreacted feed. The former process has a lower recycle percentage implying less separation of unreacted feed is required and thus lower exergy destruction.

Table 4.11 shows the results of performing the exergy analysis on the entire overall process. The following comments can be made:

- The overall exergetic efficiency is lower for the process with 80 % recycle (at 83.07 %) compared to the process with full recycle (87.28 %). This is because 20 % of the unreacted feed is disposed off in the exhaust stream, and thus does not form the valuable hydrogen product.
- The above point can also be made by comparing the exergy lost in the exhaust stream: The process with 80 % recycle loses 6.8 % of its incoming exergy in the exhaust stream which contains the remaining 20 % of unreacted feed. In contrast, the process with 100 % recycle loses only 1.08 %.
- The discussion on the heat supplied and the work recovered made in Section 4.2.5 is applicable here as well.
- The results from Tables 4.10 and 4.11 illustrate a trade-off between exergy destruction and exergy lost in the exhaust stream: The process with 100 % recycle has a greater exergy destruction but has a much lower exergy lost in the exhaust stream, and thus has a larger overall exergy efficiency. For this reason, it is recommended to aim for as much recycle as possible in order to increase the conversion of the feed to valuable hydrogen product.

4.5 Concluding remarks

In this chapter, two processes were designed at the conceptual stage using the G-H methodology. The first process used recycle of 100 % of the unreacted feed to achieve complete conversion. The second process used 80 % recycle of the unreacted feed to achieve a conversion of 0.8. Since this conversion is lower than assumed for the G-H methodology presented in Chapter 3, a modification should be made to the G-H methodology. A new term (f) denoting the "multiple of the simplest stoichiometric feed" was coined for convenience to aid the presentation of the modified G-H methodology. Both these two processes were simulated using Aspen HYSYS and an exergy analysis was performed.

The results of the exergy analysis showed that the two processes designed in this chapter had significantly lower exergy destruction values compared to the state-of-the-art process. The reason for the lower exergy destruction is that the SMR and WGS processes were running at their Carnot temperatures. In addition, a different combustion reaction was used in the furnace and this resulted in lower exergy destruction as well. However, it was noted that the furnace is still responsible for the greatest exergy destruction; it is expected that this will continue in future designs because most combustion reactions of fossil fuels are inherently irreversible.

The overall exergetic efficiency was highest in the process with 100 % recycle (87.28 %), followed by the process with 80 % recycle (83.07 %), and lastly the state-of-the-art process (75.03 %). This implies that a greater percentage of the methane feed is converted to useful hydrogen product in the two designed processes. However, it is important to note that these two processes are still at the conceptual stage of design while the state-of-the-art process corresponds to a detailed design stage. Thus there are several caveats that should be taken into account when viewing the

conclusions made from the exergy analysis. Further iterations of the two processes made after detailed design would have more irreversibilities and thus a lower exergetic efficiency. This implies that these two case studies should be looked at as ideal targets that set the direction for later detailed designs.

Chapter 5

Increasing Conversion by changing the feed

5.1 Introduction

In this chapter, the method of changing the ratio of the reactants in the feed is used to increase the conversion. Thus, the feed is no longer a stoichiometric feed. In Section 3.5, it was noted that if the feed is not a stoichiometric feed, then the conversion must be defined for each component- the entire reaction no longer has a single conversion value. This chapter continues from Chapter 3, and studies what ratio of the feed reactants is required to ensure complete conversion in the SMR and WGS reactions in Figure 3.3.

As explained in [29], increasing the feed concentration of a reactant to the reactor held at constant temperature and pressure can increase the conversion according to "Le-Chatelier's principle" which is often stated as: "In a system at equilibrium, a change in one of the variables that determines the equilibrium will shift the equilibrium in the direction counteracting the change in that variable." Thus, if an excess amount of one reactant is added in the feed, more of it reacts such that it shifts the equilibrium forwards resulting in higher conversion with respect to the other reactant. The "K_p equation" (Equation 3.27) is used to determine by how much the feed of one reactant should be increased to achieve complete conversion with respect to the other reactant.

5.1.1 Determining the required feed ratio for complete conversion

The aim is to have a conversion of 0.99. A conversion of 0.99 is used instead of 1 because the denominator in Equation 3.27 would become 0 if 1 is used, as is illustrated next.

For the SMR reaction, there is a choice between increasing the feed of water or methane. In this project the feed of water is increased while the feed of methane is kept constant. The reason for this decision is that steam is generated on site using the phase change reaction. Thus, a conversion of 0.99 with respect to methane is required.

$$\mathrm{CH_4(g) + H_2O(g) \rightleftharpoons CO(g) + 3\,H_2(g)} \tag{5.1}$$

With a conversion of 0.99, it implies that at equilibrium, 0.99 moles of CH_4 react with 0.99 moles of H_2O to produce 0.99 moles of CO and 2.97 moles of H_2. Set $N^0_{CH_4} = 1$. Assume the feed of water is varied to some value A that would result in a conversion of 0.99 thus $N^0_{H_2O} = A$. Also assume that $N^0_{CO} = N^0_{H_2} = 0$. Thus the equilibrium mole balance equations are written as:

$$N_{CH_4} = N^0_{CH_4} - e_{SMR} = 0.01 \tag{5.2}$$

$$N_{H_2O} = N^0_{H_2O} - e_{SMR} = A - 0.99 \tag{5.3}$$

$$N_{CO} = N^0_{CO} + e_{SMR} = 0.99 \tag{5.4}$$

$$N_{H_2} = N^0_{H_2} + 3e_{SMR} = 2.97 \tag{5.5}$$

Thus, $N_{total} = A + 2.98$ and $\Delta v = 2$

The superscript "0" shows the number of moles of that component fed to the SMR process, and the final number of moles out of the SMR process (i.e. the number of moles at equilibrium) is given by N without the superscript.

Thus Equation 3.27 becomes:

$$K_P = \frac{(0.99)(2.97)^3}{(0.01)(A - 0.99)} \left(\frac{\mathrm{P}_{SMR}}{A + 2.98} \right)^2 \tag{5.6}$$

Assume the reaction pressure P = 1 bar.

$$K_P = \frac{(0.99)(2.97)^3}{(0.01)(A - 0.99)} \left(\frac{1}{A + 2.98} \right)^2 \tag{5.7}$$

Keeping the temperature constant at $T_{Carnot,SMR} = 960.83$ K, $K_p = 8.025$. Thus solving

$$\frac{(0.99)(2.97)^3}{(0.01)(A - 0.99)} \left(\frac{1}{A + 2.98} \right)^2 = 8.025 \tag{5.8}$$

gives $A = 5.4924$. The implication of this result is that a 99 % conversion occurs if methane and water are fed in with a ratio of 1:5.4924.

The procedure of increasing the reactant concentration to change the conversion is repeated for the WGS reaction. Once again, it is possible to increase the feed of water. It is also possible to increase the feed of CO, however this is not feasible for a flowsheet organised like that in Figure 3.3. This is because the produced CO comes from the SMR reaction and is thus limited by this reaction. Thus once again, the choice is made to increase the feed concentration of water.

$$\mathrm{CO\,(g) + H_2O\,(g) \rightleftharpoons CO_2(g) + H_2(g)} \tag{5.9}$$

Assume an equilibrium conversion of 0.99. Thus, at equilibrium, 0.99 moles of CO react with 0.99 moles of H_2O to produce 0.99 moles of CO_2 and 0.99 moles of H_2. To normalize the conversion, set $N^0_{CO} = 1$ and let the new feed of water be $N^0_{H_2O} = B$ and $N^0_{CO_2} = N^0_{H_2} = 0$. Thus the equilibrium mole balance equations are written as:

$$N_{CO} = N^0_{CO} - e_{WGS} = 0.01 \tag{5.10}$$

$$N_{H_2O} = N^0_{H_2O} - e_{WGS} = B - 0.99 \tag{5.11}$$

$$N_{CO_2} = N^0_{CO_2} + e_{WGS} = 0.99 \tag{5.12}$$

$$N_{H_2} = N^0_{H_2} + e_{WGS} = 0.99 \tag{5.13}$$

Thus, $N_{total} = B + 1$ and $\Delta v = 0$

Thus, Equation 3.27 becomes:

$$K_P = \frac{(0.99)(0.99)}{(0.01)(B - 0.99)} \left(\frac{\mathrm{P}_{WGS}}{B+1}\right)^0 \tag{5.14}$$

Assume $P_{WGS} = 1$. The equation becomes:

$$K_P = \frac{(0.99)(0.99)}{(0.01)(B - 0.99)} \tag{5.15}$$

Solving this for the K_p value of 1.63 at the $T_{Carnot,WGS} = 974.67$ K gives:

$$\frac{(0.99)(0.99)}{(0.01)(B - 0.99)} = 1.63 \tag{5.16}$$

Solving gives $B = 6013.87$.

The implication of this result is that a 99 % conversion occurs if carbon monoxide and water are fed in with a ratio of 1:6013.87.

With these values of A and B, an issue arises: The calculation performed shows that the required flowrates of water are excessively high. For instance, it is not practical to design a flowsheet that supplies 6013.87 mol/s of water for every 1 mol/s of CO fed to the WGS reactor. For this reason, changing the feed flowrates as a method to achieve conversion is not studied further.

However, the principle of supplying one of the feed components in excess to achieve complete conversion can still be used to design a practical flowsheet if the unreacted feed component is separated from the effluent of the reactor, and recycled. This is different from recycling both components of the unreacted feed in Chapter 4. When both components of the unreacted feed are recycled as in Chapter 4, the overall conversion is increased but the single-pass conversion is unchanged. However, if only one of the components is separated and recycled back, then the single-pass conversion is increased as well. The flowsheet in Figure 3.3 is redrawn to include separation, and recycle of a single component of unreacted feed in Figure 5.1.

The heat and work balance in this flowsheet is identical to that presented in Table 3.1. This implies the operating conditions determined using the G-H methodology are independent of how the conversion is achieved; the method to achieve conversion does not affect the extents of the different unit operations. With this insight, it can be seen that Steps 5 - 7 presented in Chapter 4 are directly applicable to this scenario. The work and heat balance results are also identical in this scenario with recycle of unreacted water. For this reason, these steps and results are not presented here. The final process block diagram is similar to Figure 4.5 and the final process flowsheet is similar to Figure 4.6 - the only difference is the recycle stream contains only unreacted water not both unreacted components.

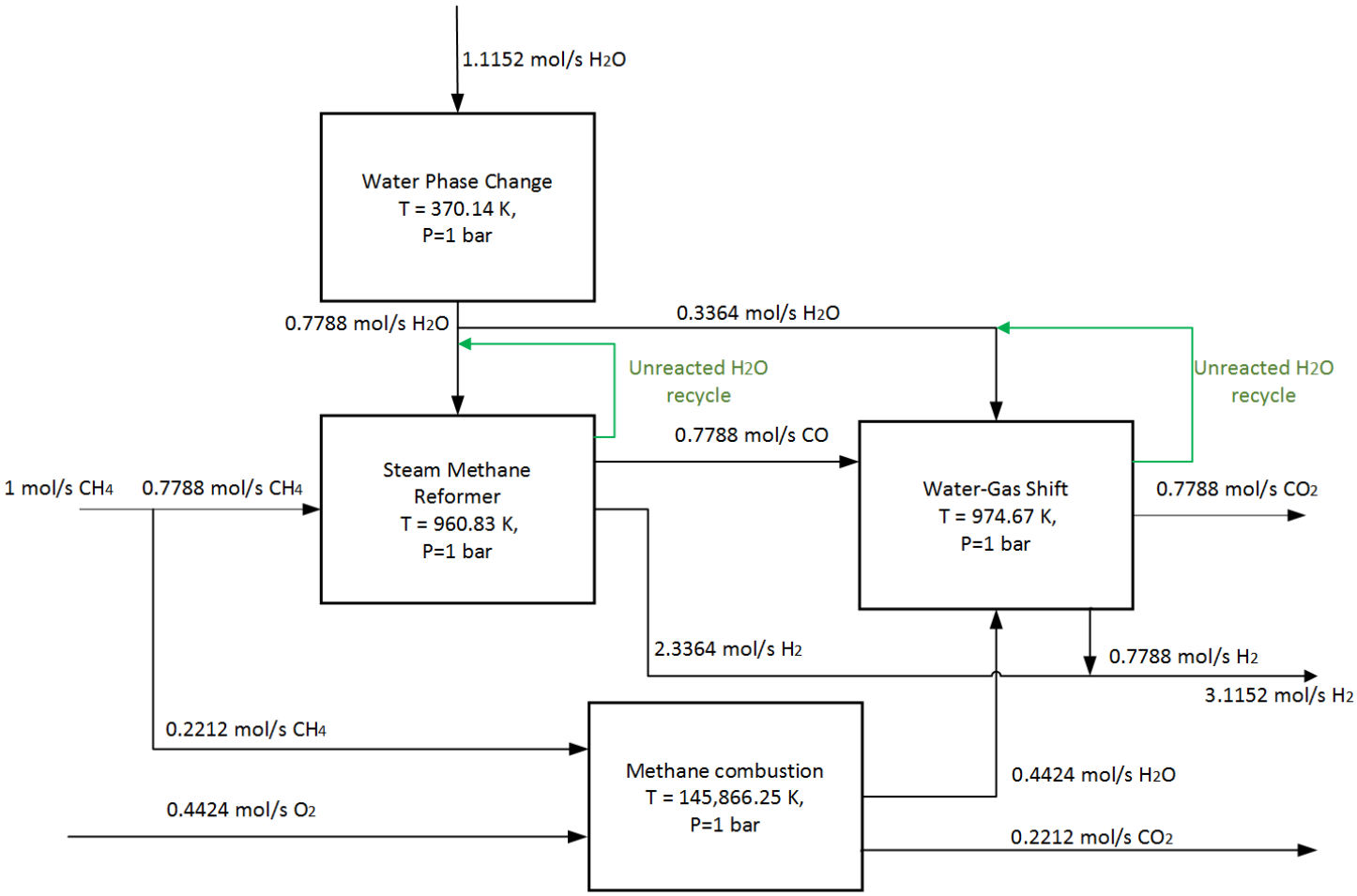

Figure 5.1: Flowsheet to achieve complete conversion by recycling one of the unreacted feed components

5.1.2 Concluding remarks

In this chapter, the method of achieving complete conversion in the SMR and WGS reactions by changing the feed was studied. One of the feed components is fed in excess such that the equilibrium shifts forward and the conversion increases. Water was chosen to be the reactant component supplied in excess, and the feed flowrates of water into the SMR and WGS reactions required to achieve complete conversion was calculated. It was found that these feed flowrates were too high to be practical. However, a flowsheet that achieves complete conversion by supplying an excess of water using recycles in drawn. In this flowsheet, the unreacted water is separated and recycled. The heat and work balance is identical to that presented in Step 4 of Chapter 3. Steps 5 - 7 in Chapter 4 are also identical, so are not presented. This implies that the operating conditions determined using the G-H methodology are dependent on the conversion but independent of the how this conversion is achieved.

Chapter 6

Increasing Conversion using Membrane Reactors

In this chapter, the systematic G-H methodology is extended to include membrane reactor unit operations. The next sections are organized as follows: First, a brief introduction is made and the approach used to study membrane reactors from a Process Systems Engineering point of view is defined. Then, the proposed models are presented together with case studies of using membrane reactors for the SMR and WGS process. Since this approach to studying membrane reactors is novel, the first case study presented is discussed in depth. Subsequent case studies are discussed briefly since they rely on insight already presented in the first case study. A flowsheet for a hydrogen production process using membrane reactors for the SMR and WGS reactions is presented. This flowsheet is simulated using Aspen HYSYS and an exergy analysis performed. The results of this exergy analysis are also presented.

6.1 Introduction

A membrane reactor (MR) is an instance of process intensification. There are several definitions of process intensification. Moulijn et al. define process intensification as the development of novel and sustainable equipment that, compared to the existing state-of-the-art, produces dramatic process improvements related to equipment sizes, waste production, and other factors ([31] cited in [32]). Reay et al. suggest that process intensification is process development that involves reduction in equipment (unit operation) sizes that lead to improvements in reaction kinetics, better energy efficiency, reduction in capital cost, and improvement in process safety ([33] cited in [32]).

These benefits of process intensification can be obtained using "hybrid/intensified unit operations". In hybrid unit operations, tasks that were previously done by several unit operations are combined so as to take place in a single unit [32]. For example, reactive distillation is a combination of reaction and separation, while a membrane reactor is a combination of reaction and in situ removal of the formed product [32].

Using membrane reactors for the steam methane reforming (SMR) and water-gas shift (WGS) has several potential advantages. First, the conversion is improved by continuously removing at least one product as it is being formed. Thus the reverse

reaction is constrained from taking place which increases the extent of the forward reaction and results in a higher equilibrium conversion. In addition, if a hydrogen-selective membrane is used, the permeate is pure hydrogen - a valuable product. Also, there are reductions in capital cost due to the reduction in the number of unit operations and reduction in equipment size as well as lower operating costs due to lower energy consumption [34].

6.1.1 Membrane Reactors: A Process Systems Engineering approach

While process intensification using membrane reactors is a prominent research field, the majority of this work focuses on detailed design of specific membrane reactor unit operations. For instance, several membrane reactors including Palladium-based hydrogen MRs for the SMR and WGS reaction are discussed in [35]. [35] also includes an experimental study of steam reforming of natural gas using a MR in a test plant. While this work is useful at a later stage of process design, it does not consider the interaction of the MR with the rest of the unit operations in the entire process right from the conceptual design phase [32]. Thus, there is need to develop a systematic methodology for design of processes with MR unit operations. The problem can be stated as follows: Given that at least one of the unit operations is a membrane reactor, develop a rigorous design methodology that includes a systems-level approach right from the conceptual design phase so as to generate the most efficient process flowsheet out of several alternatives.

Notable work on this problem has been done in the research group of Professor Rafiqul Gani at the Technical University of Denmark. The question tackled by the group is more general and includes several possibilities for process intensification in addition to membrane reactors. The procedure proposed involves first generating a design space of unit operations by combining known unit operations (such as reactors, separators etc) together with hybrid unit operations (such as membrane reactors, reactive distillation units etc) [36]. Different configurations of these unit operations form a superstructure. Computer-aided tools such as optimization techniques are used to search for the most efficient process flowsheet that may include a hybrid (intensified) unit operation [36], [37].

In this project, a different methodology based on thermodynamics is presented for the specific case of at least one MR unit operation. The systematic G-H methodology is extended so as to account for the effect of replacing a reactor unit operation with a membrane reactor unit operation. Since the design methodology must include a systems-level approach right from the conceptual phase, the conversion of the MR becomes an important parameter. This is because, in a systems-level approach, only the input and output parameters (or the transfer characteristic that relates the input parameter to the output parameter) of the different unit operations are studied without a detailed understanding of the internal functioning of the unit operation. In an MR unit operation, the relevant transfer characteristic that relates the reactant stream composition to product stream composition is the conversion. Thus, it is an important task to estimate the conversion expected in a MR unit operation.

To the best of my knowledge, no work has been done on estimating the conversion of a membrane reactor at the conceptual design phase. Thus, in this chapter, a novel

procedure to estimate the conversion of the MR is presented. With the conversion results, the systematic G-H methodology is extended to include MR unit operations. A process flowsheet for hydrogen production using membrane reactors for the SMR and WGS reactions is developed with this extended G-H methodology.

6.2 Model to estimate conversion of a hydrogen membrane reactor

This section presents a description of the model used to estimate the conversion of a hydrogen MR. Figure 6.1 shows a schematic of a hydrogen membrane reactor. The active region shown is the domain in which the reaction and separation operations take place. The reactant is fed into the membrane reactor and there is continuous removal of the formed hydrogen product as the permeate. This increases the conversion of the membrane reactor. The retentate consists of the rest of the formed product and unreacted feed.

While the reaction and separation processes in an actual MR occur simultaneously, it is easier to develop and understand a sequential model for the membrane reactor. This sequential model is discussed next. The implications of this assumption of sequentiality are discussed in Section 6.33.

6.2.1 Sequential model of the active region of a membrane reactor

In this section, a sequential model of the active region of the MR is presented based on Figure 6.2. The model developed for the membrane reactor divides the MR into a number of blocks, with each block consisting of a reactor stage followed sequentially by a separation stage. Thus the feed into the membrane reactor enters the first block in which it passes through the reaction stage 1. The conversion that occurs in reaction stage 1 is denoted by Δc_1. In the separation stage, some of the formed hydrogen permeates and the retentate is the feed to the second block's reaction stage. The removal of the hydrogen product adjusts the equilibrium such that the conversion increases by Δc_2 in the second block's reaction stage. This process continues through the N blocks.

6.3 Operation of the membrane reactor

The relevant operating conditions of the MR are: Operating pressure, operating temperature, permeate pressure, membrane permeability and selectivity, feed flow rate, feed composition and total membrane area to thickness ratio. In the model developed, the operating temperature of the MR is fixed to be the Carnot temperature of the reaction taking place, as calculated in Chapter 3. The permeate pressure is fixed at P_{perm}= 1 bar. The membrane is assumed to be infinitely selective to hydrogen i.e. only hydrogen permeates through the membrane. No other component permeates. The operating pressure, membrane permeability and total membrane area (A_{total}) are taken as variables in the model such that the conversion is estimated for different values of these variables. A standard feed flow rate and

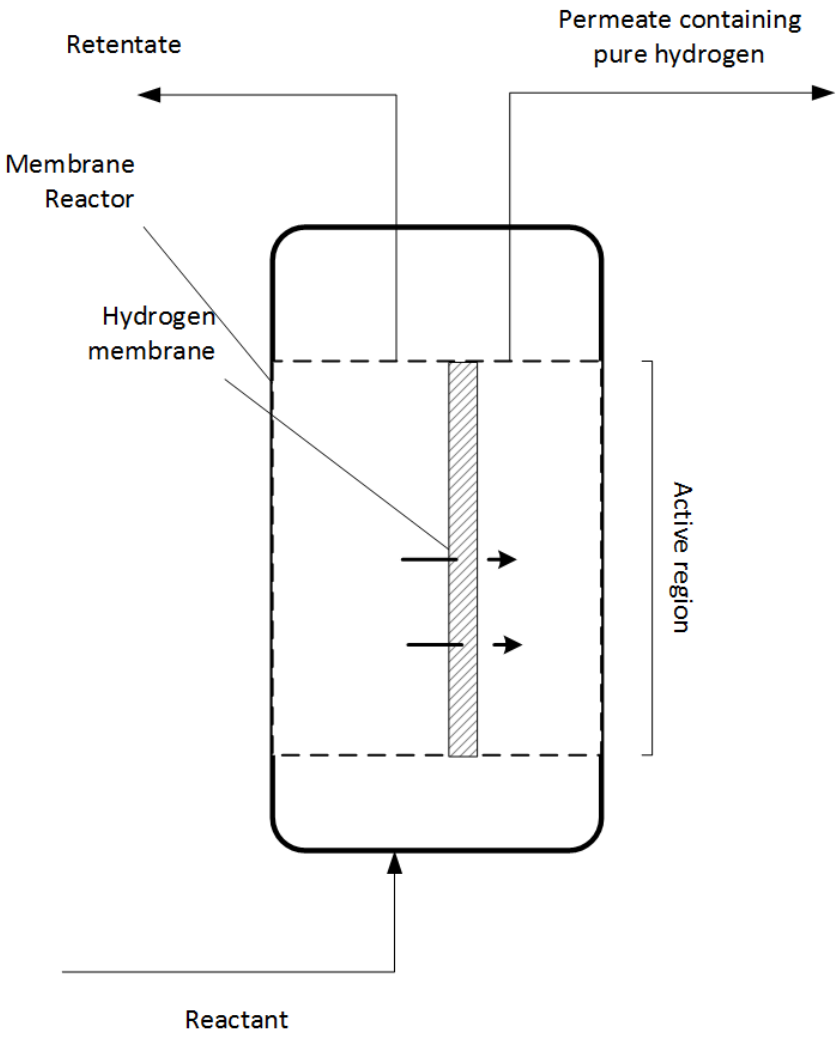

Figure 6.1: Schematic of a Hydrogen Membrane Reactor

composition is assumed. More details are given in the case studies discussed in later sections.

6.3.1 Reaction stage

The feed into a block undergoes a chemical reaction in this stage. It is assumed that only the reaction process occurs in this stage. Thus, there is no continuous separation of the formed hydrogen product. All the reaction stages within the membrane reactor occur at the operating temperature (given by the Carnot temperature in this case) and pressure. The reactions that are commonly considered in the hydrogen production process (such as SMR and WGS) are commonly reversible, thus it is possible to determine the equilibrium conversion in each reaction stage for a given feed into the block by making minimum Gibbs free energy considerations. Thus, the reaction is assumed to reach a local thermodynamic equilibrium at each stage [38]. The corresponding local increase in conversion at each reaction stage is denoted Δc_i Using Gibbs free energy considerations, the composition of the products from each reaction stage can be determined using the "K_P equation", given by Equation 3.27. This product is fed into the separation stage of the block.

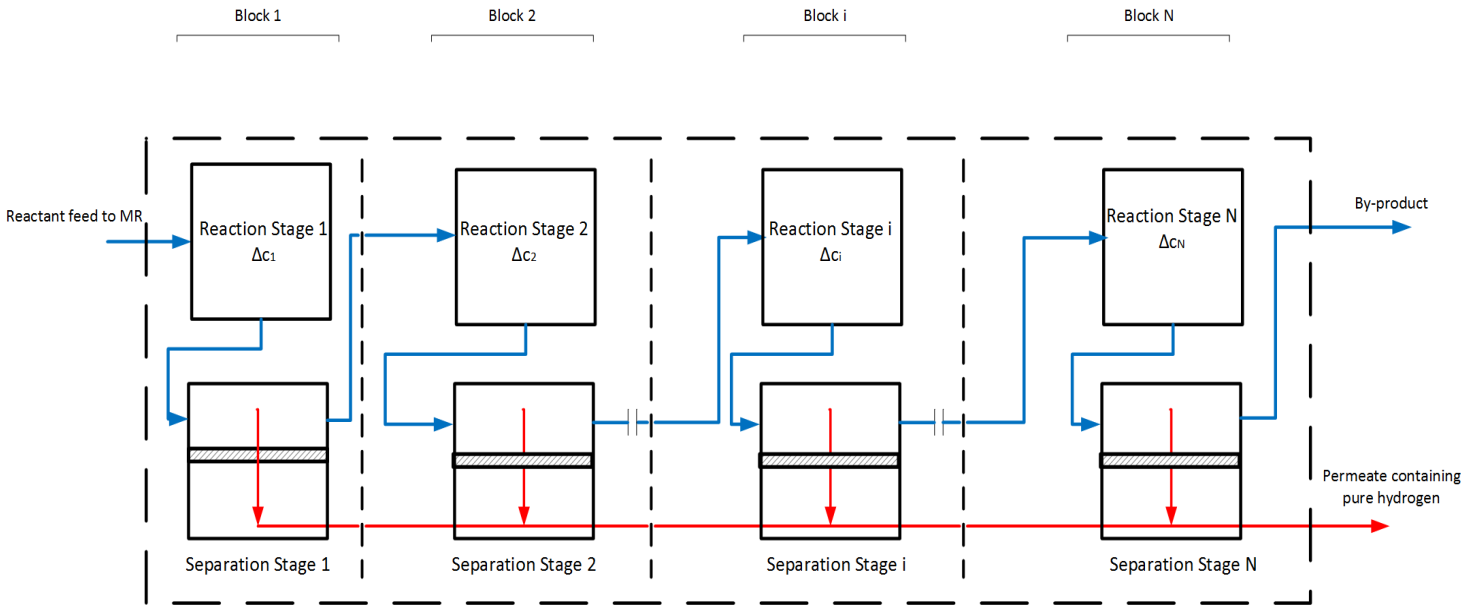

Figure 6.2: Sequential model to estimate conversion in a membrane reactor

6.3.2 Separation stage

In the separation stage, hydrogen selectively permeates through the membrane. It is assumed that no reaction occurs in this separation stage, i.e. the feed composition into the membrane is assumed to be constant. A cross-flow membrane regime is assumed such that the permeate pressure is kept constant. The feed and retentate side of the membrane are kept at the operating pressure of the membrane reactor, while the permeate is kept at a constant pressure $P_{perm} = 1$ bar. The operating temperature of the membrane is also fixed to be identical to the operating temperature of the reaction stage (given by the Carnot temperature of the reaction considered). While it is possible to design a membrane configuration with lower permeate pressure by using a vacuum pump, that scenario is not considered in this project. The retentate out of the membrane separation stage is the feed for the next block's reaction stage. The membrane area of each separation stage is determined to be $A_{stage} = A_{total}/N$. Different permeation models can be used. Using these models, the permeation molar flow rate of hydrogen, F_i in each separation stage can be calculated.

6.3.3 Assumptions of the sequential model

- The selectivity of the membrane to hydrogen with respect to other components is assumed to be infinite. This is not a realistic assumption, since there exists an upper-bound as well as trade-offs between selectivity and permeability of certain membrane types (such as polymeric membranes) as seen in the well-known "Robeson plot" shown in Figure 6.3. This Master's project does not account for this assumption. That is left for later detailed design stages.

- The rate of the separation and reaction processes is assumed to be irrelevant. Thus, it is assumed that the residence time in the reaction and separation stage is sufficiently high such that equilibrium is achieved in the respective stages.

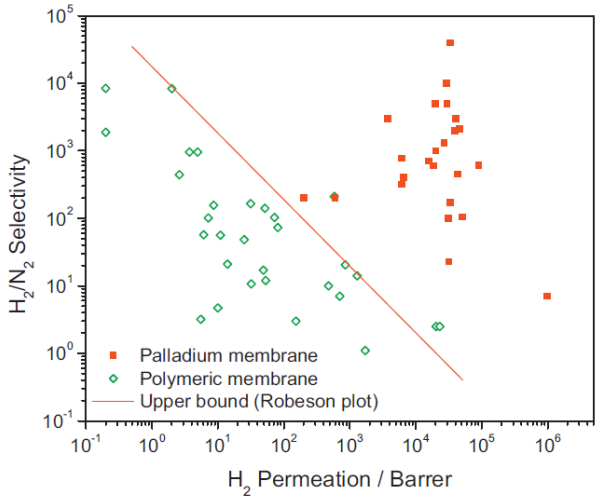

Figure 6.3: Robeson plot showing trade-offs between selectivity and permeability

Degree of sequential operation in a membrane reactor

This sub-section addresses the assumption of sequentiality of the reaction and separation process of the model developed. As mentioned, in an actual membrane reactor, there is coupling of the reaction and separation process in a single unit. Camera-Roda et al. [39] explain that the maximum effect of process intensification occurs as a result of concurrent operation of reaction and separation processes, rather than a sequential operation of a reaction stage followed by a separation stage and then the next reaction stage and so on. For example, in a membrane reactor, the maximum conversion would be estimated by a MR model in which the reaction and separation processes are occurring simultaneously rather than sequentially. However, it is easier to study and develop a MR model in which the two processes occur sequentially, as is done in this project.

Despite this, it is still desired that the MR model estimates the maximum conversion i.e. it is desired that the "degree of sequential operation" is as small as possible. Camera-Roda et al. [39] suggest that this degree of sequential operation is inversely proportional to the number of blocks, N. In other words, dividing the MR into a large number of blocks N gives a higher conversion. Thus, it is acceptable to use a sequential model to study the effect of coupling reaction and separation processes in a MR as long as the number of blocks N is sufficiently large; division of the MR into a large number of smaller blocks is used to account for the assumption of sequentiality of the MR.

Different models can be used for the permeation through the membrane. These include: 1) Sievert's law for hydrogen permeation through a palladium membrane, 2) a constant minimum flux model, and 3) a variable minimum flux model analogous to a heat exchanger. These are explained in the following sections.

6.4 Sievert's law for hydrogen permeation through a palladium membrane

Palladium is a commonly used material for manufacturing hydrogen selective membranes. This is because palladium membranes show an outstanding ability to transport hydrogen through the metal due to a much higher solubility of hydrogen in their bulk over a wide temperature range [34]. In addition, palladium can serve a dual purpose as a catalyst for reactions such as SMR in catalytic membrane reactors [34]. However, other options for hydrogen separation exist such as proton exchange membranes in fuel cells, though these are not considered in this project.

6.4.1 Mechanism of Hydrogen permeation through Palladium membranes

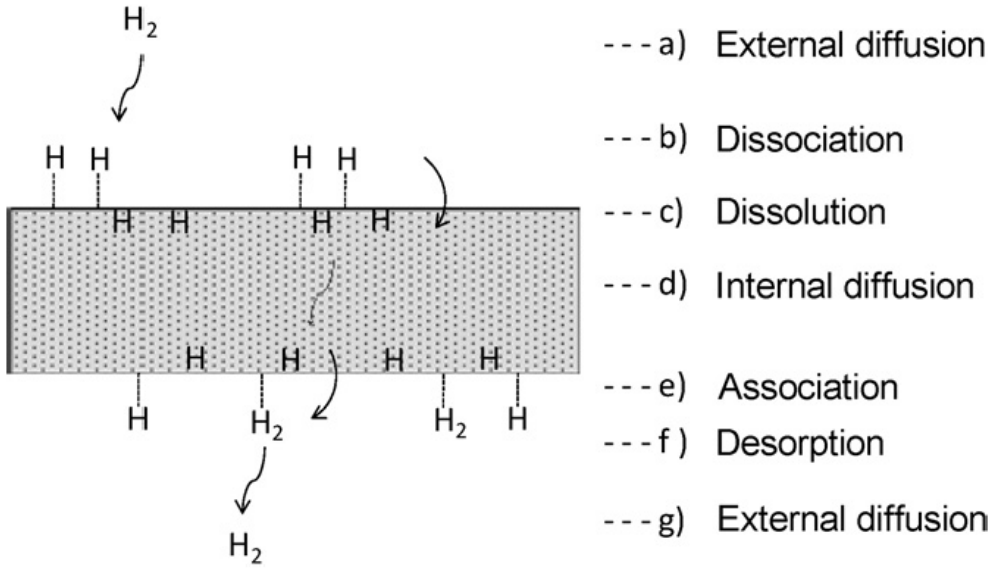

Figure 6.4: Mechanism of hydrogen permeation through Palladium membranes [34]

Hydrogen permeation through palladium membranes generally follows a solution-diffusion mechanism as seen in Figure 6.4. The steps involved in hydrogen transport from a high to a low pressure gas region are the following: (a) diffusion of molecular hydrogen to the surface of the palladium membrane, (b) reversible dissociative adsorption on the palladium surface, (c) dissolution of atomic hydrogen into the bulk metal, (d) diffusion of atomic hydrogen through the bulk metal, (e) association of hydrogen atom on the palladium surface, (f) desorption of molecular hydrogen from the surface, and (g) diffusion of molecular hydrogen away from the surface [34]. Depending on which of these steps is the slowest (i.e. the rate determining step), the hydrogen flux can be determined. Sievert's law for hydrogen permeation is described by Equation 6.1 [34]:

$$J = \frac{P(p_h^n - p_l^n)}{L} \tag{6.1}$$

where:

- J is the hydrogen flux in [mol/m^{2}s].
- P is the permeability of the hydrogen membrane in [Barrers]. 1 Barrer = $\frac{mol}{Pa.s.m}$.
- p_h is the partial pressure of hydrogen on the feed side in [Pascals].
- p_l is the partial pressure of hydrogen on the permeate side in [Pascals]. Since, the permeate contains pure hydrogen, p_l=P$_{perm}$=1 bar.
- L is the thickness of the palladium layer in [m].
- n is an index that is determined by the rate-determining step (a) to (g). Determining the value of n is done by studying the mechanism of diffusion for various palladium membranes, see [34] for full details. Commonly experimental studies are carried out to determine the value of n. A comprehensive study of these mechanisms is not in the scope of this project that focuses on conceptual stage design rather than detailed design.

Studying Equation (6.1), it is seen that for a given feed and permeate side partial pressure, the flux of hydrogen can be determined. However, as a result of this flux, the feed partial pressure drops. This would in turn change the hydrogen flux. To account for this issue it is necessary to divide the separation stage into a number of sub-stages, M as shown in Figure 6.5. In each sub-stage j, the membrane area A_{sub} is assumed to be infinitely small such that the feed partial pressure of hydrogen in each sub-stage $p_{h,j}$ remains constant. The hydrogen flux in each sub-stage J_j can then be calculated. Using a large value of M is essential to obtain accurate results; too few sub-stages would overestimate the permeation of hydrogen. This is especially important because, in this project, the equation to calculate the flux is implemented using computer code. The computer code solves Equation (6.1) at each discrete separation sub-stage, and thus the number of sub-stages has an impact on the results.

The retentate of each separation sub-stage forms the feed to the next sub-stage. Thus, the partial pressure of hydrogen in the subsequent sub-stage is lower as a result of the hydrogen flux in the previous sub-stage. This cycle continues for all separation sub-stages as shown in Figure 6.5. The retentate of the last sub-stage is the feed to next block's reaction stage as shown in Figure 6.5.

The flux J_j at each sub-stage can be calculated from Equation 6.2:

$$J_j = \frac{P(p_{h,j}^n - p_l^n)}{L} \tag{6.2}$$

The molar flowrate of hydrogen through each separation sub-stage j of the MR (termed the permeation molar flow rate at each sub-stage and denoted by F_j) is then calculated from Equation 6.3. The membrane area in each separation sub-stage A_{sub} is assumed to be a constant i.e. the separation stage is divided into sub-stages of equal area.

$$F_j = J_j A_{sub} = \frac{P A_{sub}(p_{h,j}^n - p_l^n)}{L} \tag{6.3}$$

Note that for a given membrane reactor, the values of the permeability (P) and the area to thickness ratio ($\frac{A_{sub}}{L}$) are constant. The flux is proportional to both

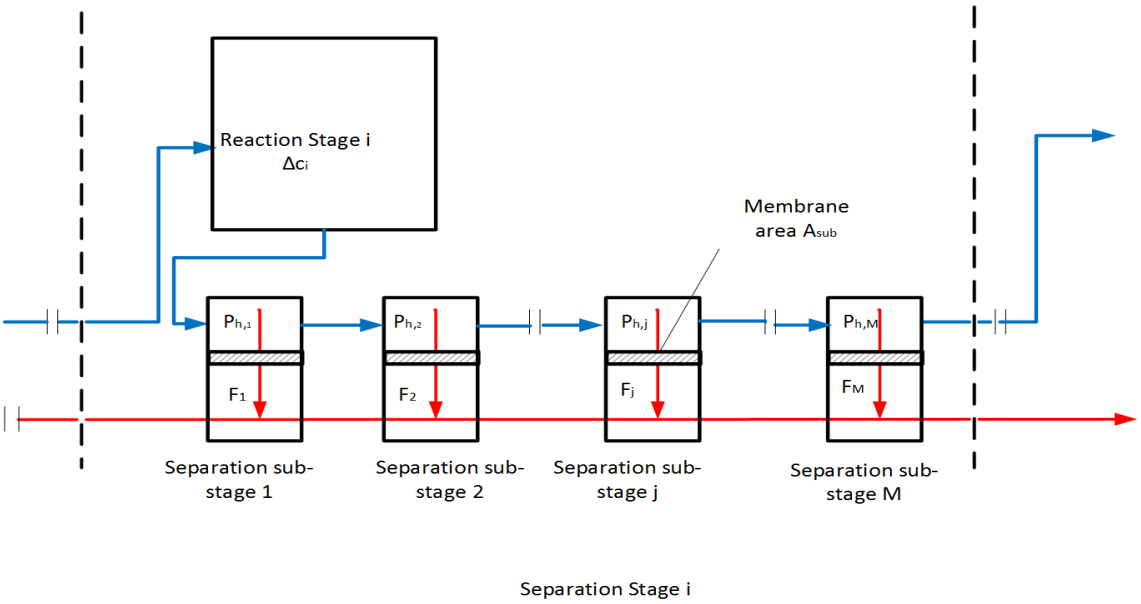

Figure 6.5: Details of block i showing subdivision of separation stage i into M sub-stages. A typical separation sub-stage is denoted by j

the permeability and the area to thickness ratio. Thus, these two parameters have similar effects: Increasing permeability while keeping the area to thickness ratio constant has a similar effect to increasing the area to thickness ratio while keeping permeability constant or an equivalent combination of the two. For this reason it is convenient to combine these parameters into a single parameter $C_1 = \frac{PA_{sub}}{L}$. Thus, the permeation molar flow rate at each sub-stage is written as:

$$F_j = C_1(p_{h,j}^n - p_l^n) \tag{6.4}$$

A case study for estimating conversion of the SMR and WGS reactions using Sievert's law of hydrogen permeation through a palladium membrane is presented in Section 6.5. Different membrane reactors are studied with a range of values for permeability and area to thickness ratio.

6.5 Estimating conversion in the SMR MR with Sievert's law hydrogen permeation model

In this section, a case study is presented to explain the model developed. Sievert's law for hydrogen permeation is used as the governing equation in the separation stages. The SMR equation is written:

$$\mathrm{CH_4(g) + H_2O(g) \rightleftharpoons CO(g) + 3\,H_2(g)} \tag{6.5}$$

The standard enthalpy and standard Gibbs energy of reaction are given as $\Delta H_{SMR} = 206.12$ kJ/mol, $\Delta G_{SMR} = 142.16$ kJ/mol [6]. The Carnot temperature of the SMR reaction, $T_{Carnot,SMR} = 960.83$ K, is the operating temperature of the SMR membrane reactor. The operating pressure of the SMR MR is denoted P_{SMR}.

Reaction Stage of the SMR MR

The feed into the membrane reactor is identical to the feed to the first reactor stage in the first block. The total number of blocks N is assumed to be equal to 100. The feed is normalized to be: $N_{CH_4,feed} = N_{H_2O(g),feed} = 1$ mol/s. Thus, the "standard stoichiometric feed" is assumed. A different flowrate can be used; the membrane area of the MR scales with the flowrate used.

Consider a general block i in the membrane reactor. Let the conversion at reaction stage i be Δc_i. Assume the molar flow rates of the components of the feed to the ith block are given by: $N^{i-1}_{CH_4}, N^{i-1}_{H_2O}, N^{i-1}_{H_2} N^{i-1}_{CO}$. As mentioned, this feed composition corresponds to the retentate composition after the separation stage of the (i-1)th block. At equilibrium, Δc_i moles of CH_4 react with Δc_i moles of H_2O to produce Δc_i moles of CO and $3\Delta c_i$ moles of H_2. The equilibrium concentrations are:

$$N^i_{CH_4,eqm} = N^{i-1}_{CH_4} - \Delta c_i \tag{6.6}$$

$$N^i_{H_2O,eqm} = N^{i-1}_{H_2O} - \Delta c_i \tag{6.7}$$

$$N^i_{H_2,eqm} = N^{i-1}_{H_2} + 3\Delta c_i \tag{6.8}$$

$$N^i_{CO,eqm} = N^{i-1}_{CO} + \Delta c_i \tag{6.9}$$

The K_P Equation 3.27 becomes:

$$K_P = \frac{(N^i_{CO,eqm})(N^i_{H_2,eqm})^3}{(N^i_{CH_4,eqm})(N^i_{H_2O,eqm})} \left(\frac{\mathrm{P}_{SMR}}{N^i_{CH_4,eqm} + N^i_{H_2O,eqm} + N^i_{H_2,eqm} + N^i_{CO,eqm}} \right)^2 \tag{6.10}$$

At $T_{Carnot,SMR}$ of 960.83 K, $K_P = 8.025$. Thus, Δc_i is the only unknown in the above equation and is calculated. The product composition is then calculated, and this is the feed to the first sub-stage of separation stage i.

Separation Stage of the SMR MR

As mentioned, in the separation stage of the SMR MR, Sievert's law for hydrogen permeation is assumed to hold. The index for the rate-determining step, n, is assumed to have a value of 0.5, which is a typical value for palladium membranes [34]. In block i, the product from reaction stage i is the feed to the first sub-stage of separation stage i. Sievert's law for hydrogen permeation (Equation 6.4) is applied to calculate the permeation molar flow rate at this sub-stage (F_j). The retentate of the first separation sub-stage is fed into the second sub-stage, and Sievert's law applied again. This procedure continues for all sub-stages. The number of sub-stages M is fixed to be 1000. A sensitivity analysis was done, and it was determined that 1000 sub-stages is adequate to give accurate results. The retentate of the last sub-stage is fed into the reaction stage of block $i + 1$. The permeate flows of all the sub-stages are combined to give the total molar permeation flow rate of the ith separation stage (F_i):

$$F_i = \sum_{j=1}^{1000} F_j \tag{6.11}$$

where F_j is given by Equation 6.4 .

Removal of some of the hydrogen product of reaction stage i in separation stage i, shifts the equilibrium in reaction stage $i+1$ resulting in a higher conversion. The procedure to estimate this conversion is implemented in Matlab, with the code used given in Appendix D. The conversion is estimated for different values of C_1 and different operating pressures of the MR. The results are presented in the next section.

6.5.1 Results: Estimates of conversion of the SMR MR

Figure 6.6 shows the contours of conversion of the SMR MR for different values of C_1 and operating pressure, P_{SMR}.

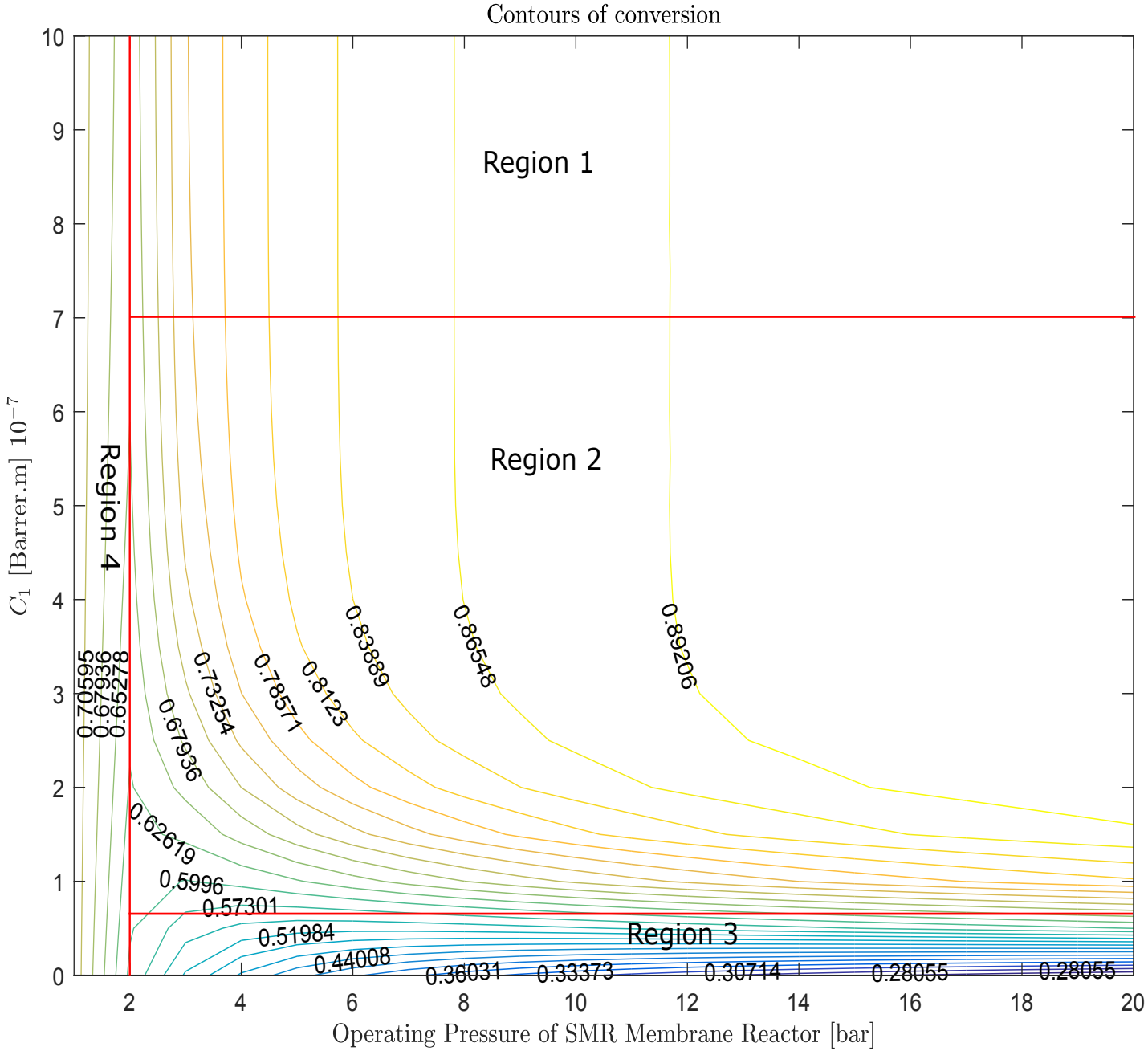

Figure 6.6: Conversion contours of the SMR MR for different operating pressures and C_1 values

6.5.2 Discussion of results

The results presented in Figure 6.6 are discussed. Several trends can be seen in different regions of the graph. Figure 6.6 is subdivided into 4 different regions in order to distinguish between the different trends. In order to stretch out the different regions of Figure 6.6, it is useful to express C_1 in terms of the membrane area to thickness ratio of each sub-stage, and the membrane permeability:

$$C_1 = \frac{P.A_{sub}}{L} \tag{6.12}$$

Before focusing on the different regions, it is first useful to understand the trade-offs associated with changing the operating pressure of the membrane reactor with regards to conversion.

Trade-offs associated with increasing the SMR MR operating pressure

There are two opposite effects of increasing the P_{SMR} on the conversion of the SMR MR. These two opposite effects are described by the "K_P equation" and "Sievert's law":

- Effect of the "K_p equation": The K_p equation 6.10 is reproduced below with the same definition of terms:

$$K_P = \frac{(N^i_{CO,eqm})(N^i_{H_2,eqm})^3}{(N^i_{CH_4,eqm})(N^i_{H_2O,eqm})} \left(\frac{\mathrm{P}_{SMR}}{N^i_{CH_4,eqm} + N^i_{H_2O,eqm} + N^i_{H_2,eqm} + N^i_{CO,eqm}} \right)^2 \tag{6.13}$$

  The K_p value is a constant for a given temperature. Thus for the same K_p value, increasing the operating pressure P_{SMR} would decrease the equilibrium concentration of the products $N^i_{H_2,eqm}$ and $N^i_{CO,eqm}$. Thus, the conversion at each stage Δc_i is lowered for higher operating pressures. This effect is consistent with the effect predicted by the "Le-chatelier's principle" i.e. increasing the pressure favors the reaction that occurs with a decrease in volume (the backward reaction in the case of SMR).

- Effect of "Sievert's law": Sievert's law (Equation (6.4)) is applied to model hydrogen permeation through a Palladium membrane at each separation sub-stage j. Equation (6.4) is reproduced below with the same definition of terms:

$$F_j = C_1.(p^n_{h,j} - p^n_l) \tag{6.14}$$

  Assume the mole fraction of hydrogen in the feed of sub-stage j is $X_{H_2,j}$, then $p_{h,j} = X_{H_2,j}.P_{SMR}$. Thus, increasing the operating pressure increases the permeation molar flow rate F_j at each sub-stage. This effect accumulates through all the 1000 sub-stages resulting in a higher permeation molar flow rate F_i in each separation stage. Thus, more of the hydrogen product is removed in the separation stage, which results in more conversion in the subsequent reaction stage in the next block. This effect is summed up across all the 100 blocks such that increasing the operating pressure increases the membrane reactor conversion.

The C_1 value determines which of the two opposing effects above dominate. As explained in the sections below, the effect predicted by Sievert's law is dominant in region 1 and 2 while the effect predicted by the K_p equation is dominant in region 3. In region 4, only the effect predicted by the K_p equation is present since there is no hydrogen permeation.

Region 1

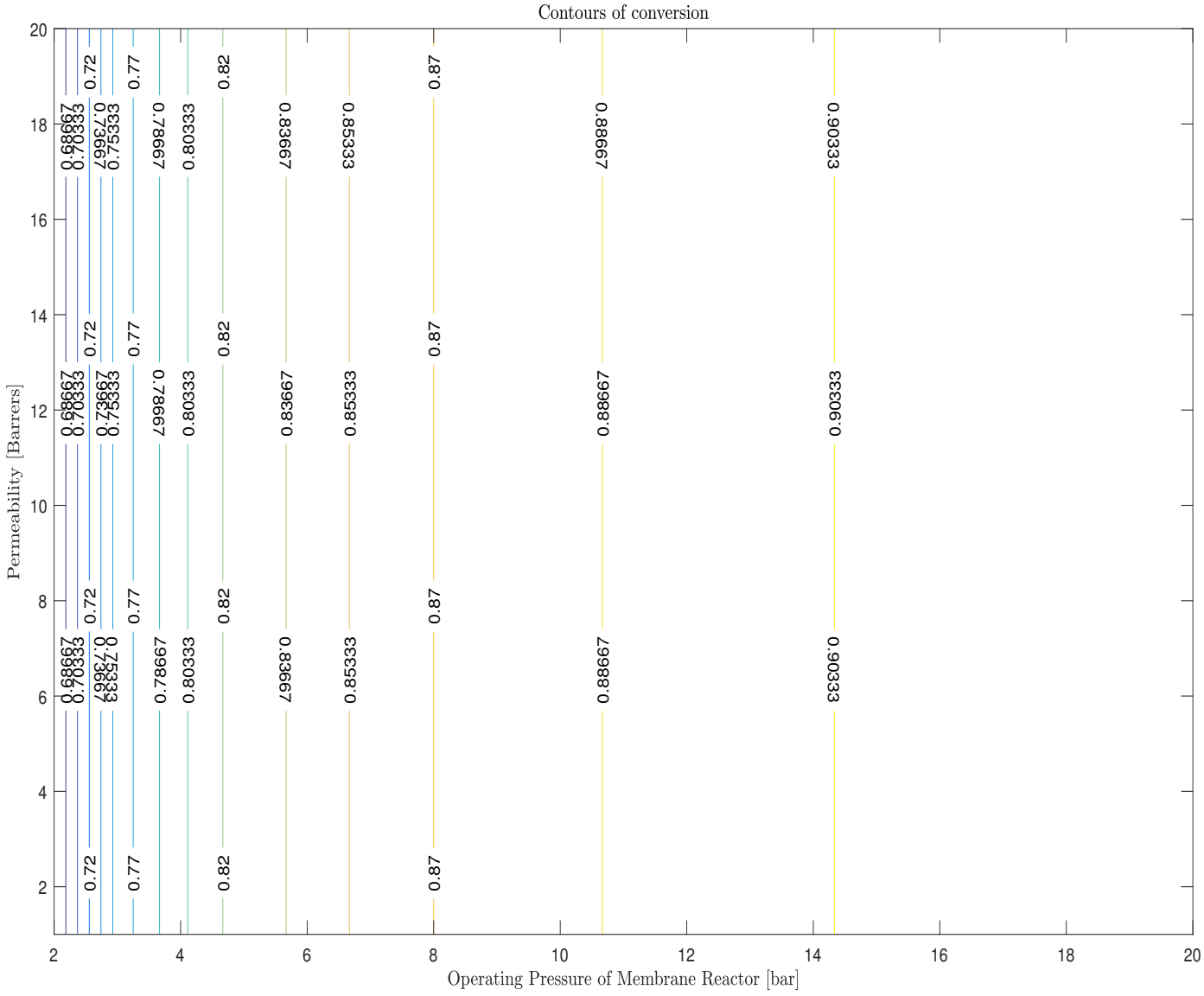

Figure 6.7: Conversion contours of SMR membrane reactors in region 1

Membrane reactors in region 1 have high C_1 values. High C_1 values are achieved when MRs have either high membrane area to thickness ratios ($\frac{A_{total}}{L}$) or high permeabilities (P) or some combination of the two parameters. In Figure 6.7, region 1 is stretched to present the trend. A high membrane area to thickness ratio

($\frac{A_{total}}{L} = 0.01$) is assumed and the permeability (P) is varied on the y-axis. It should be noted that a similar graph could also have been presented by assuming the MRs have a high permeability (P) value and varying the membrane area to thickness ratio ($\frac{A_{total}}{L}$) on the y-axis.

The operating pressures for these MRs are high enough such that there is some flux through the membrane i.e. the partial pressure of hydrogen in at least one separation stage should be higher than the permeate pressure $P_{perm} = 1$ bar. The case in which the operating pressure P_{SMR} is so low that there is no flux is discussed in a later section on region 4. The lowest operating pressure for region 1 is approximately 2 bar as shown in Figure 6.7. Region 4 exists below this operating pressure.

Two important trends are observed in Figure 6.7. First, for a given permeability (P) increasing the P_{SMR} increases the conversion. This is elaborated upon further in Figure 6.8 which compares two membrane reactors A and B with the parameters shown in Table 6.1. MR B has a higher operating pressure than MR A. As observed in Figure 6.8, MR B with the higher operating pressure has a higher conversion. Thus, "Sievert's law" has a dominant effect on conversion compared to the "K_P equation". Figure 6.8 shows that the partial pressure of hydrogen at the feed to the separation stage of any block is higher in MR B than in MR A. Sievert's law implies that there is a higher permeation molar flow rate F_i in MR B than in MR A. Since more hydrogen is removed from each stage the subsequent reaction stage has a higher conversion resulting in a higher total conversion when summed up over all blocks.

The second trend is that the permeability (and thus the C_1 value) is not the limiting factor to conversion. The conversion contours are vertical implying that increasing the permeability or area to thickness ratio (thus C_1 value) does not increase the conversion. This can be also be seen in Figure 6.8: The maximum conversion is reached at approximately the 30th stage. Thus, the remainder of the membrane reactor area, corresponding to stages 30 to 100, is not useful in increasing conversion. This trend is elaborated in Figure 6.9 in which MR A is compared with an MR C of higher permeability (and thus C_1) value. As seen the conversion, permeation molar flow rates and partial pressure profiles of hydrogen are identical in the two cases.

These trends can be used to influence design decisions. For instance, it is seen that there is no value in investing in extra membrane area or permeability for membrane reactors operating in region 1. Instead, since operating pressure (P_{SMR}) is the limiting factor of conversion, it may be useful to choose higher operating pressure.

Table 6.1: Parameters of membrane reactors in Region 1

MR	Region	$\frac{A_{total}}{L}$ [m]	Permeability [Barrer]	Pressure [bar]	C_1 [Barrer.m] 10^{-7}	Limiting Factor
A	1	0.01	8	4	8	Operating pressure only
B	1	0.01	8	14	8	Operating pressure only
C	1	0.01	12	4	12	Operating pressure only

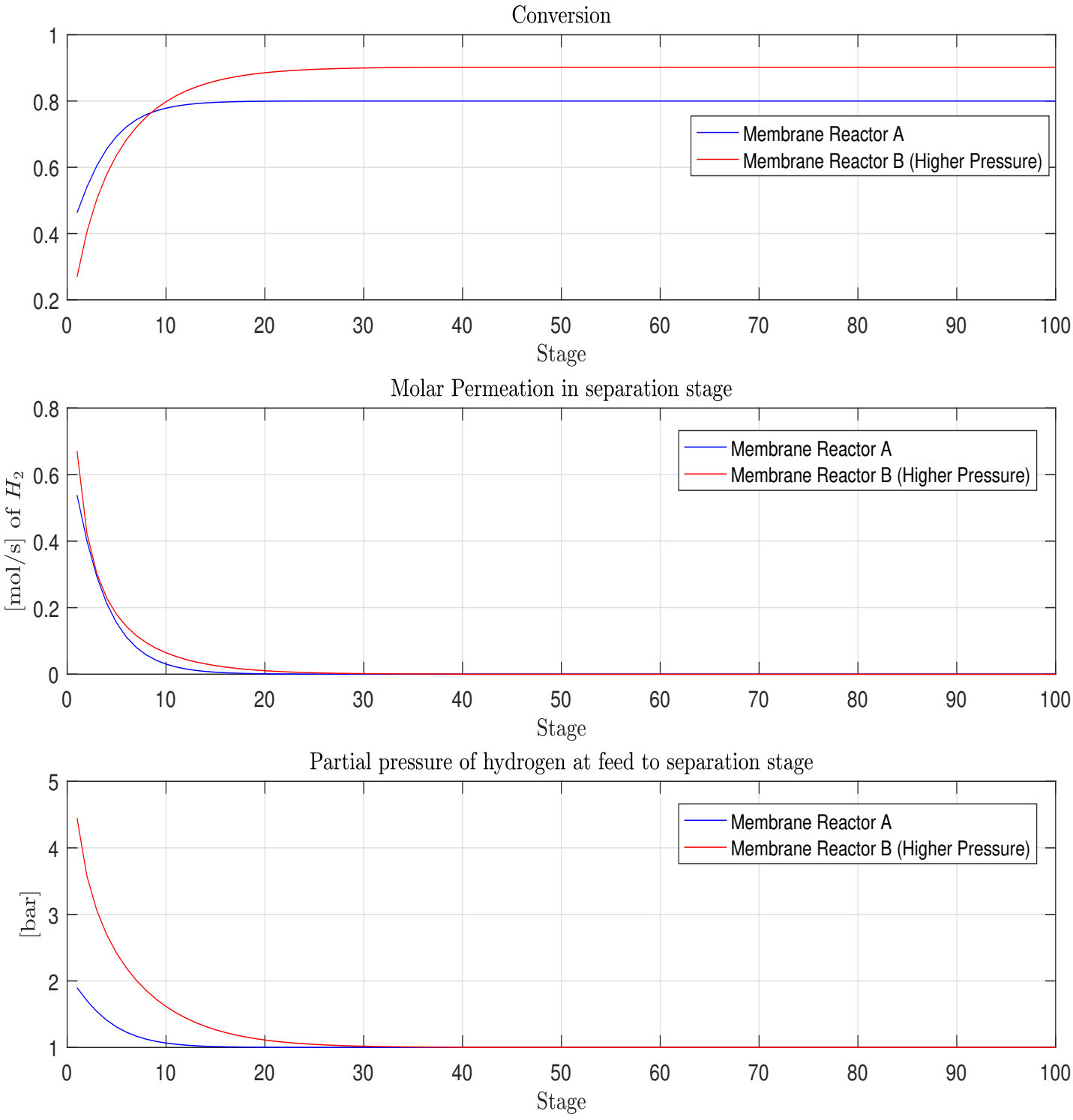

Figure 6.8: Comparison of the molar permeation, hydrogen partial pressure profile and conversion of two membrane reactors A and B. MR B operates at a higher pressure than MR A

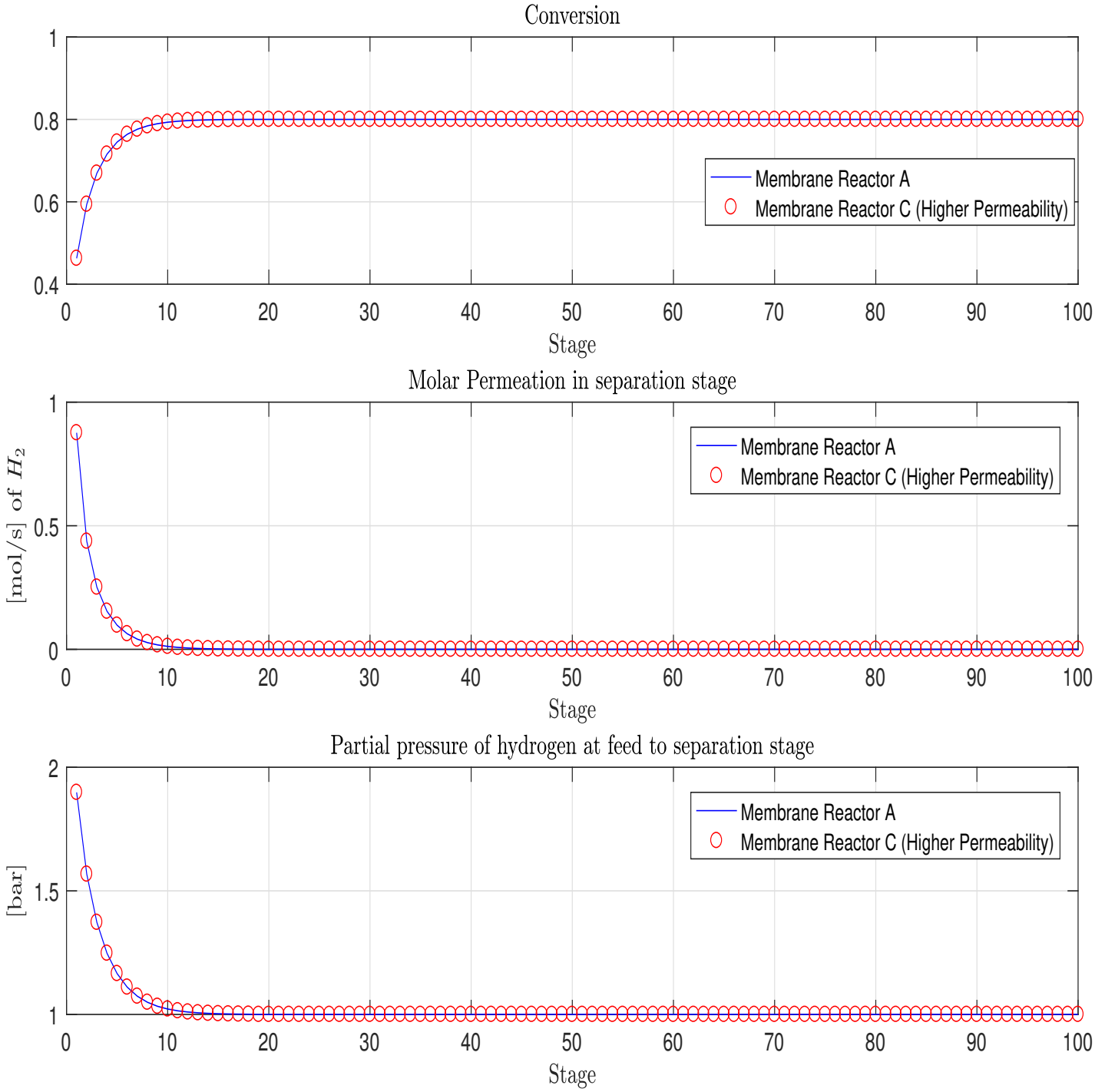

Figure 6.9: Comparison of the molar permeation, hydrogen partial pressure profile and conversion of two membrane reactors A and C. MR C has a higher permeability than MR A

Region 2

Membrane reactors in region 2 have moderate C_1 values. Moderate C_1 values are achieved when MRs have either moderate membrane area to thickness ratios ($\frac{A_{total}}{L}$)

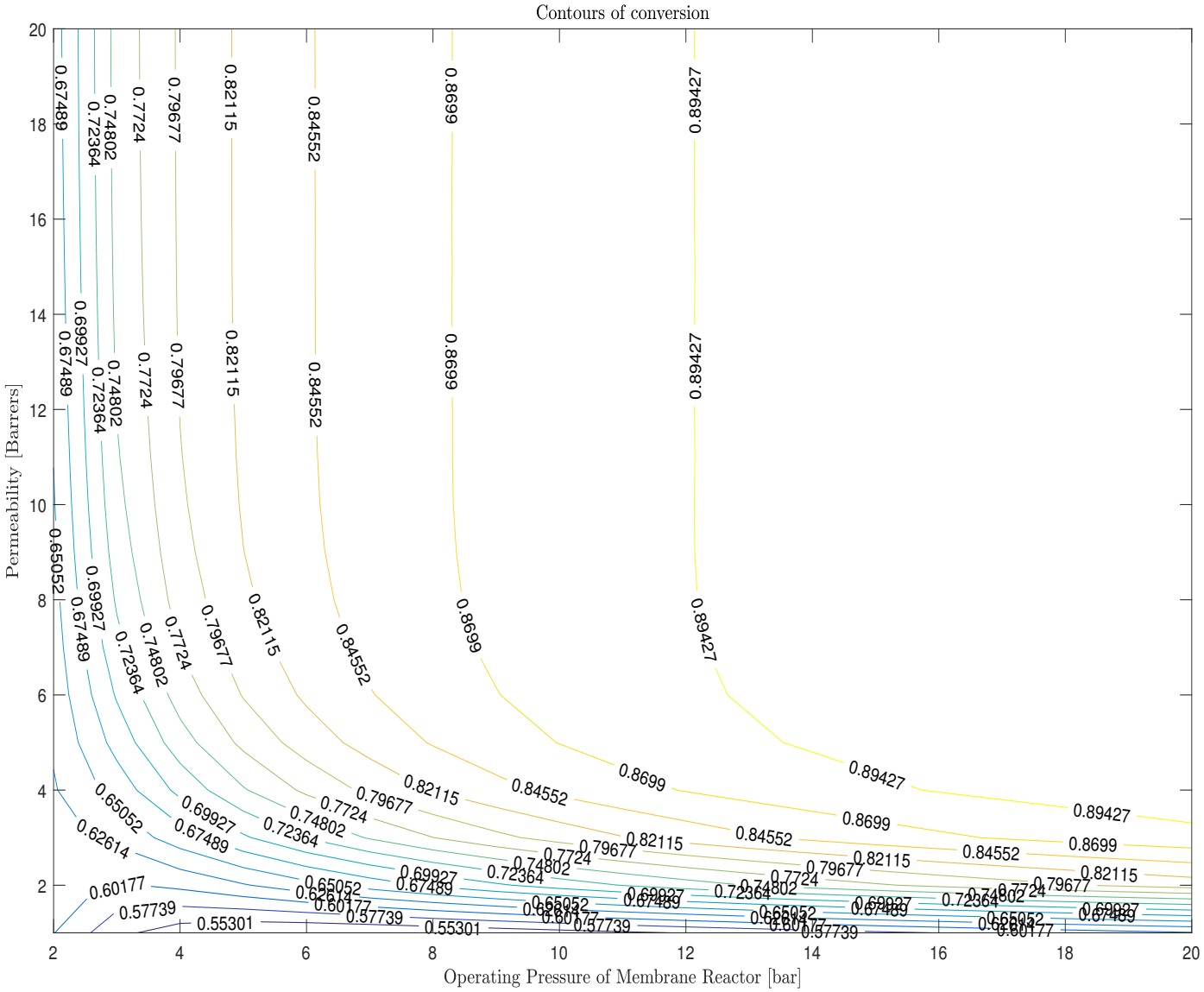

Figure 6.10: Conversion contours of SMR membrane reactor in region 2

or moderate permeabilities (P) or some equivalent combination of the two parameters. In Figure 6.10, region 2 is stretched to present the trend. A moderate membrane area to thickness ratio ($\frac{A_{total}}{L} = 0.005$) is assumed and the permeability (P) is varied on the y-axis.

Similar to region 1, the operating pressures for these MRs are high enough such that there is some flux through the membrane i.e. the partial pressure of hydrogen in at least one separation stage should be higher than the permeate pressure P_{perm} = 1 bar. The case in which the operating pressure P_{SMR} is so low that there is no flux is discussed in a later section on region 4. The lowest operating pressure for region 2 is approximately 2 bar as shown in Figure 6.10. Region 4 exists below this operating pressure.

In the entire region 2, increasing the operating pressure of the SMR MR increases

the conversion, similar to region 1. Thus, "Sievert's law" has a dominant effect on conversion compared to the "K_P equation", similar to region 1.

Figure 6.10 shows that with decreasing Permeability (and thus C_1), the conversion contours change shape from "mostly vertical" to "mostly horizontal". As explained below, this change in contour shape corresponds to a change in the limiting factor of conversion: Membrane reactors operating in the "mostly vertical" region are majorly limited by operating pressure while membrane reactors operating in the "mostly horizontal" region are majorly limited by the membrane area to thickness ratios or permeability (thus the C_1 value). Figures 6.11 and 6.12 elaborate upon this claim.

Figure 6.11 presents three membrane reactors D, E and F in the "mostly vertical region". Relevant parameters for the MRs are shown in Table 6.2. Membrane reactor E operates at a higher pressure than membrane D while F has a higher permeability. Figure 6.11 shows that increasing the pressure has a larger impact on increasing the conversion than increasing the permeability. This is because the permeation molar flow rate (F_i) is limited by the driving force of partial pressure of hydrogen at feed to the separation step in each block, rather than the membrane permeability or area to thickness ratio. In Figure 6.11, it can be seen that the feed partial pressure of hydrogen starts to approach 1 bar which is the fixed partial pressure of the permeate side. This implies that increasing the area by increasing the number of stages would not have a great impact on the conversion.

This is contrasted with Figure 6.12 showing membrane reactors G,H,I in the "mostly horizontal region". Relevant parameters for the MRs are shown in Table 6.2. Membrane reactor H operates at a higher pressure than membrane G while MR I has a higher permeability. Figure 6.12 shows that increasing the permeability has a larger impact on increasing the conversion compared to increasing the pressure in the mostly horizontal region. This is because the permeation molar flow rate is limited by the area and permeability (thus C_1 value) of the membrane reactor and not by the driving forces. This can be seen from the partial pressure profile of hydrogen at the feed to the separation step: For both membrane reactor G and H, there still exists driving forces at the last stage implying that adding membrane area or permeability would have a significant impact on conversion.

This insight can be used to influence design decisions: If a membrane reactor lies within the "mostly horizontal" region, it is recommended to focus design efforts on increasing the membrane area or permeability while if the membrane reactor lies withing the "mostly vertical" region, it is recommended to focus design efforts on increasing its operating pressure.

Table 6.2: Parameters of membrane reactors in region 2

MR	Region	$\frac{A_{total}}{L}$ [m]	Permeability [Barrer]	Pressure [bar]	C_1 [Barrer.m] 10^{-7}	Limiting Factor
D	2	0.005	6	4	3	Mostly operating pressure
E	2	0.005	6	8	3	Mostly operating pressure
F	2	0.005	8	4	4	Mostly operating pressure
G	2	0.005	2	12	1	Mostly area or permeability
H	2	0.005	2	16	1	Mostly area or permeability
I	2	0.005	4	12	2	Mostly area or permeability

Region 3

Membrane reactors in region 3 have low C_1 values. The area to thickness ratio used is $\frac{A_{total}}{L} = 0.0002$. Similar to region 1 and 2, the operating pressures for MRs in region 3 is high enough such there is some flux through the membrane. The difference between region 2 and 3 lies in the differing impact of increasing operating pressure. The influence of "Sievert's law" dominates in region 2 while the influence of the "K_P equation" dominates in region 3. Thus in region 3, as can be seen by the conversion contours in Figure 6.13, increasing the pressure decreases the conversion.

This is elaborated upon in Figure 6.14. Figure 6.14 presents two membrane reactors J and K in region 3. Relevant parameters for the MRs are shown in Table 6.3. Membrane reactor K operates at a higher pressure than membrane reactor J. While MR K has a higher permeation molar flow rate than MR J, this increase is very small and insufficient to off-set the effect of the "K_P equation".

In contrast, Figure 6.15 shows a comparison with MR L which has a higher permeability than MR J, but has the same operating pressure (P_{SMR}). Figure 6.15 shows that increasing the permeability has a big effect on increasing the conversion. This implies that, in region 3, the limiting factor is the C_1 value and thus the permeability and membrane area.

The value of this insight with respect to making design decisions is as follows: It is counter-productive to increase operating pressure of membrane reactors in region 3. Instead, it is recommended to focus design efforts on increasing the permeability and area (thus C_1 value) of the membrane.

Table 6.3: Parameters of membrane reactors in region 3

MR	Region	$\frac{A_{total}}{L}$ [m]	Permeability [Barrer]	Pressure [bar]	C_1 [Barrer.m] 10^{-7}	Limiting Factor
J	3	0.0002	4	9	0.08	Area and Permeability
K	3	0.0002	4	18	0.08	Area and Permeability
L	3	0.0002	14	9	0.28	Area and Permeability

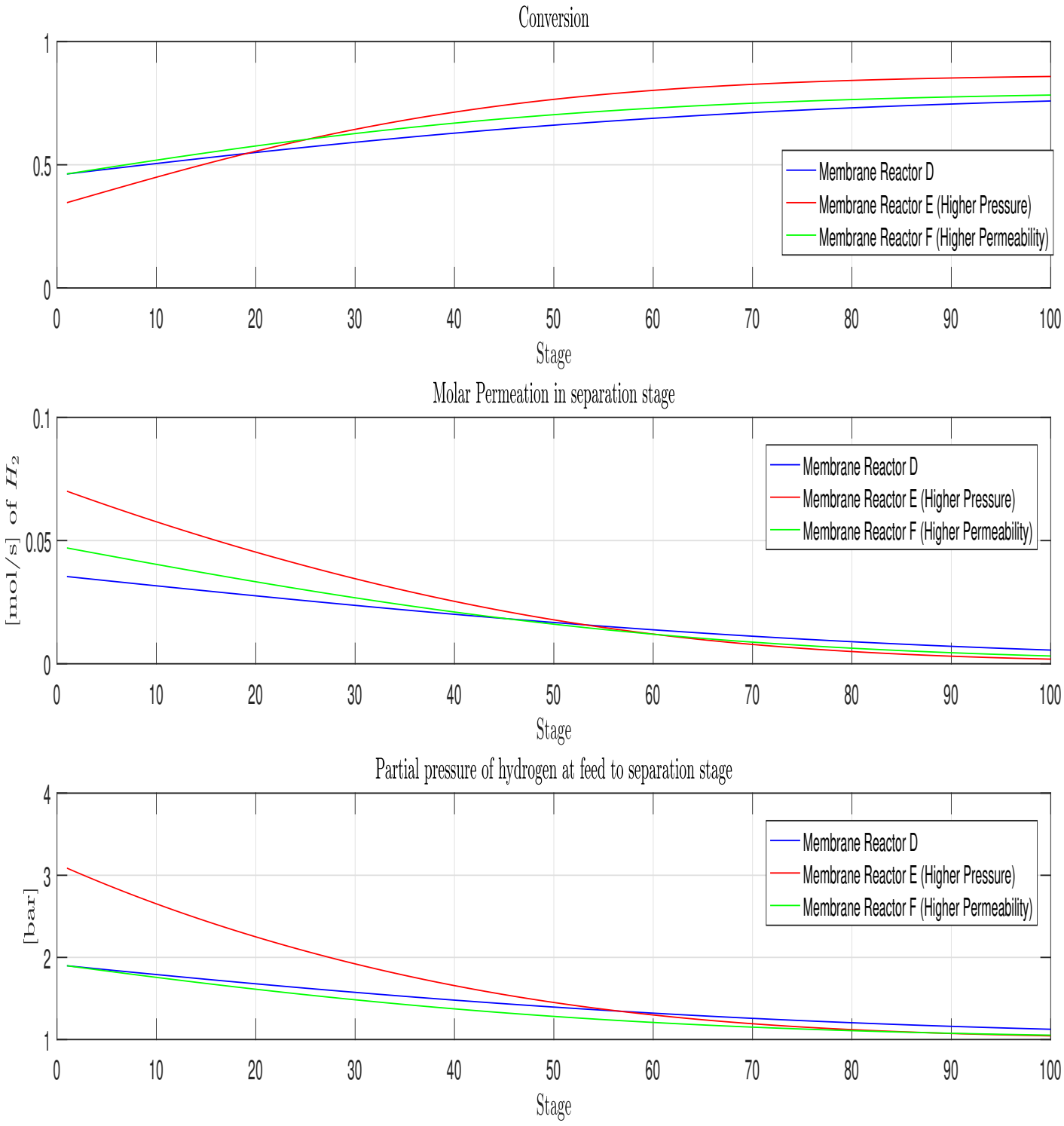

Figure 6.11: Comparison of the molar permeation, hydrogen partial pressure profile and conversion of three membrane reactors D, E and F in region 2

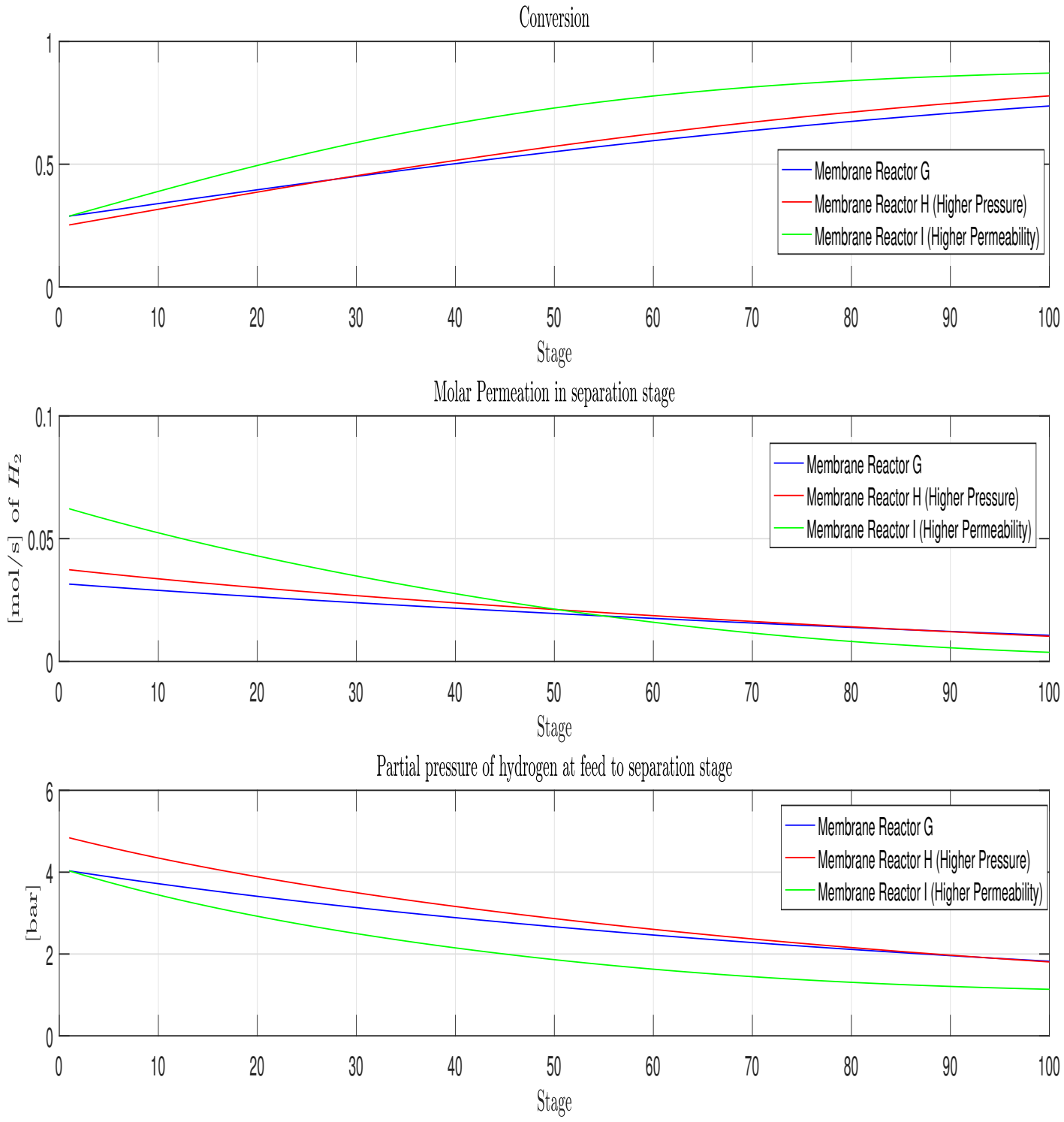

Figure 6.12: Comparison of the molar permeation, hydrogen partial pressure profile and conversion of three membrane reactors G, H and I in region 2

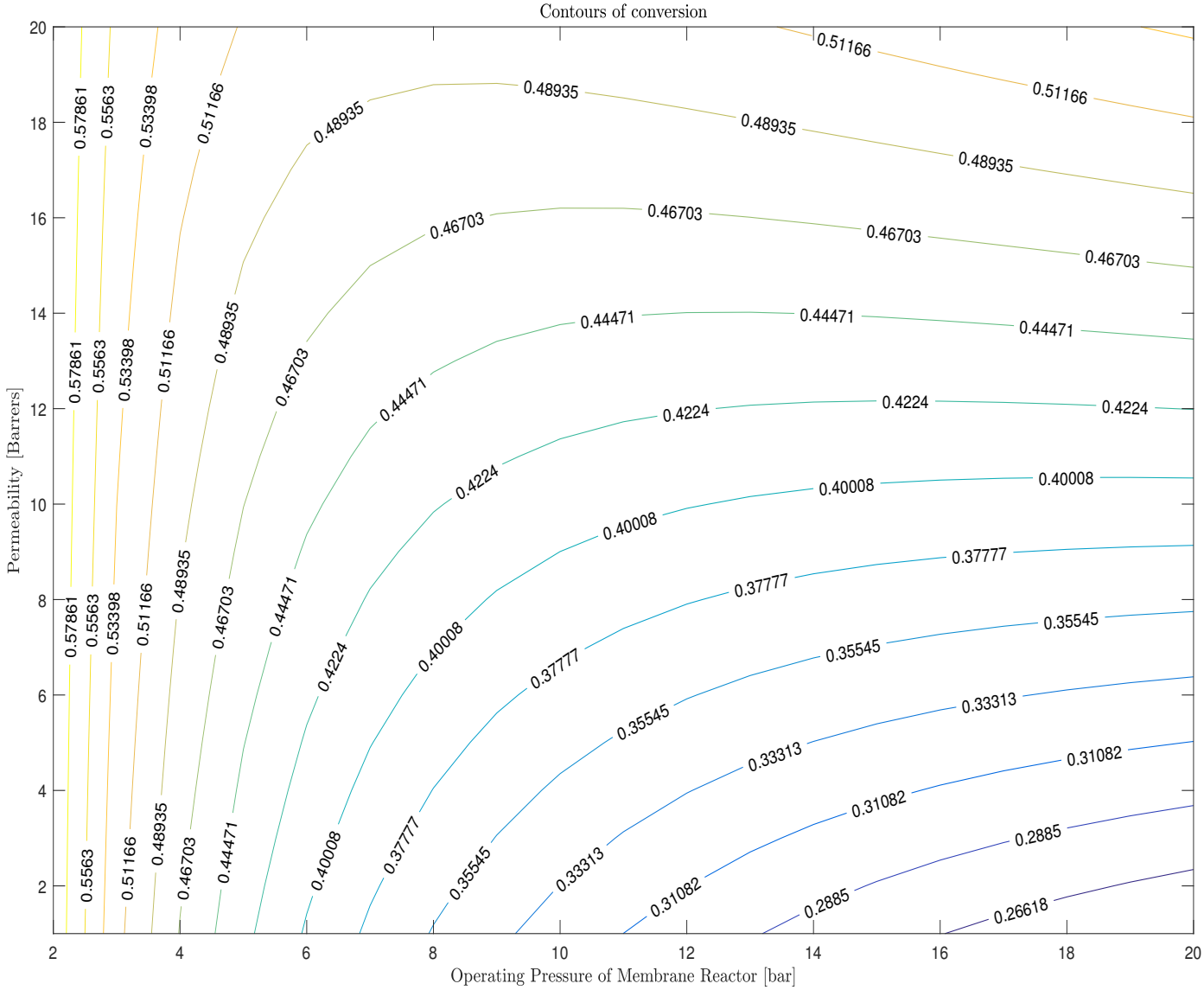

Figure 6.13: Conversion contours of SMR membrane reactor in region 3

Transition

Figure 6.16 shows the transition region between region 2 and region 3. In region 2, "Sievert's law" has a dominant effect while in region 3, the "K_P equation" has a dominant effect. The area to thickness ratio used is $\frac{A_{total}}{L} = 0.001$ The figure shows the change in the shape of the contours from region 2 to region 3.

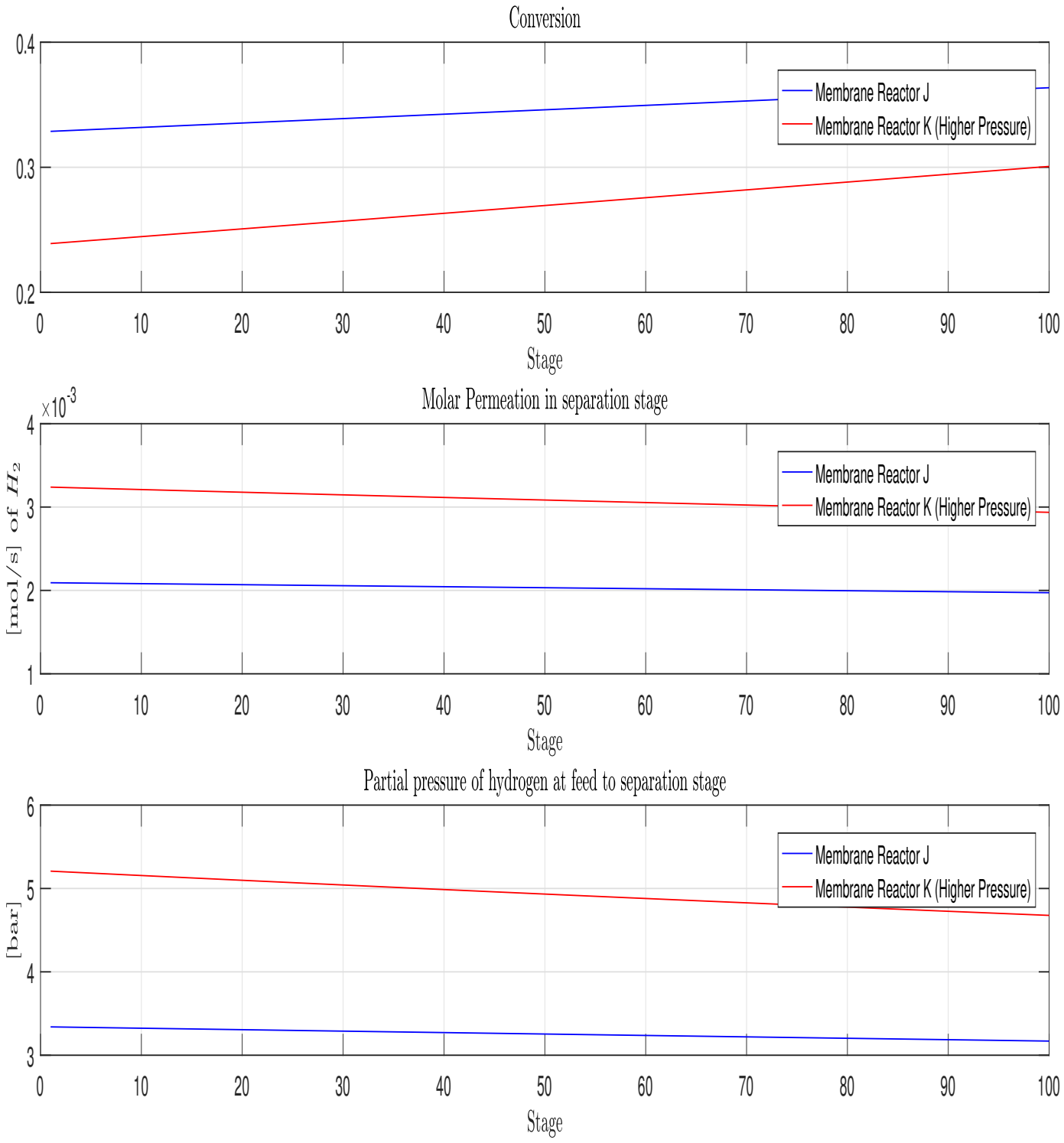

Figure 6.14: Comparison of the molar permeation, hydrogen partial pressure profile and conversion of two membrane reactors J and K in region 3

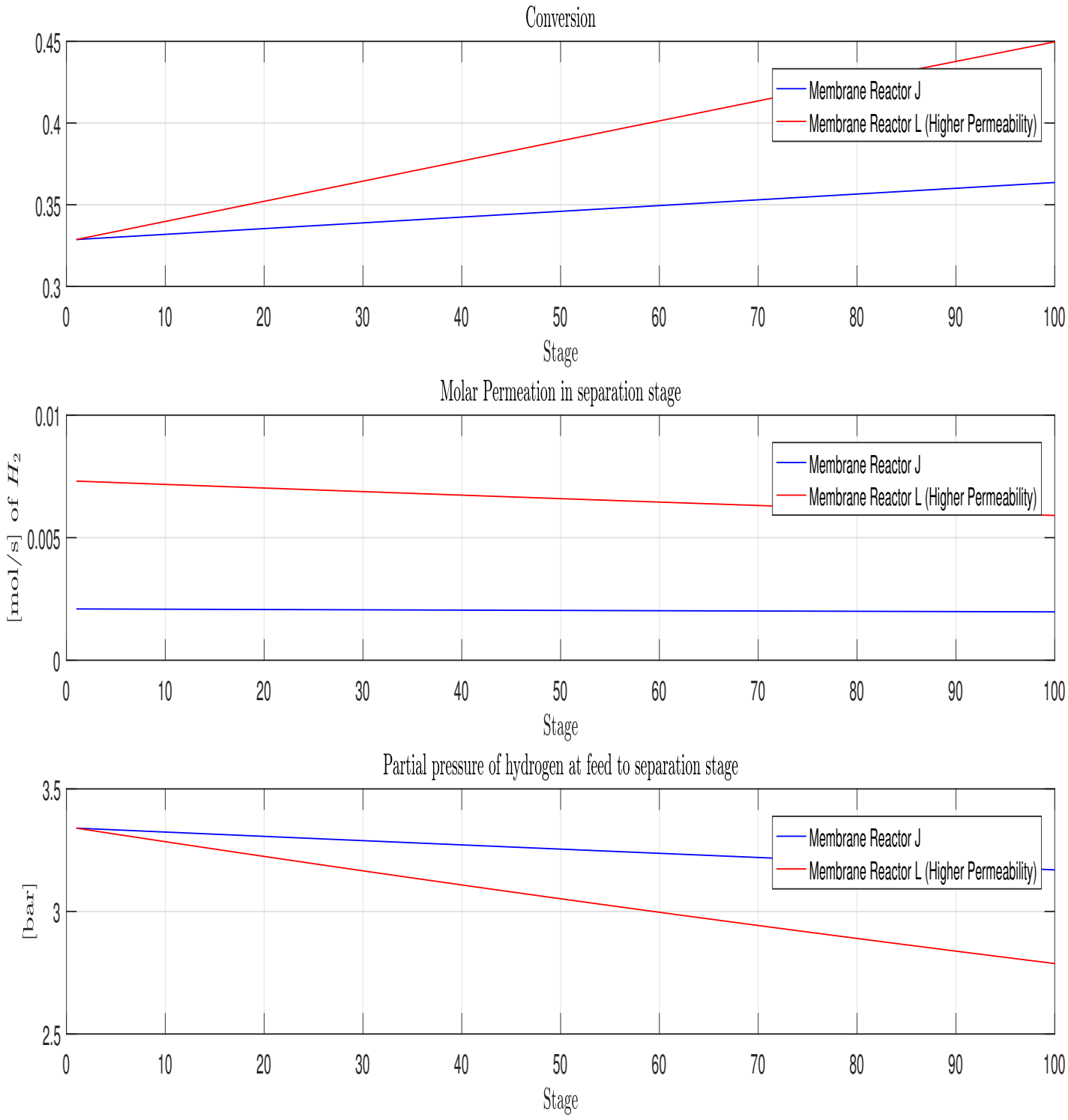

Figure 6.15: Comparison of the molar permeation, hydrogen partial pressure profile and conversion of two membrane reactors J and L in region 3

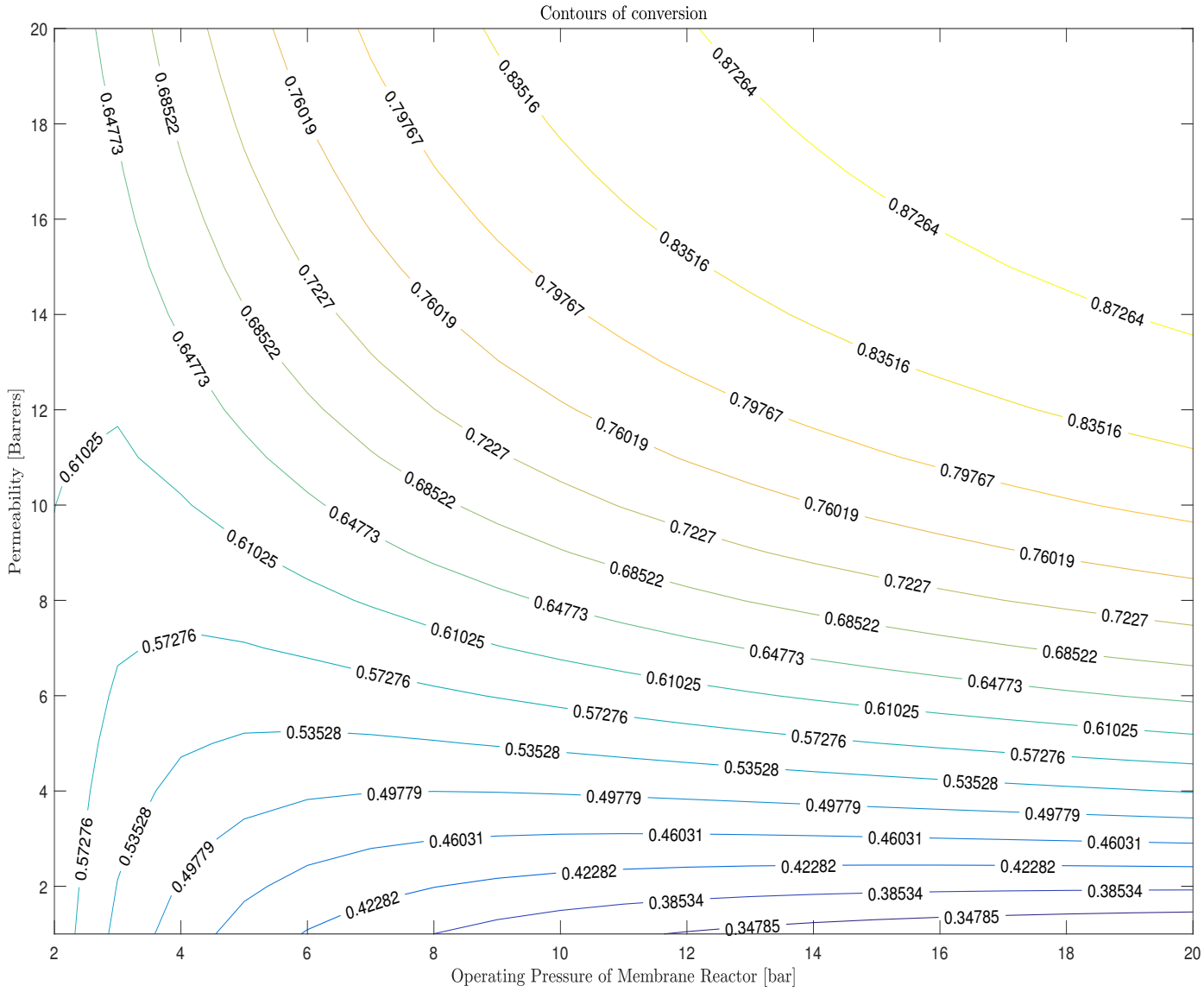

Figure 6.16: Conversion contours of SMR membrane reactor in the transition region between regions 2 and 3

Region 4

In region 4, the operating pressure of the membrane reactor is very low. Unlike other regions, the partial pressure of hydrogen on the feed side to any membrane separation stage is never higher than the permeate pressure $P_{perm} = 1$ bar. Thus, in region 4 there are zero driving forces in the separation section implying zero permeation. Membrane reactors in this region can be solely viewed as reactors. Thus, only the K_p equation has any effect; "Sievert's law" has no influence. This implies that increasing the operating pressure in region 4 decreases the conversion. Figure 6.17 shows the conversion contours of the SMR MR in region 4 varied with C_1 and operating pressure. The vertical lines correspond to membrane reactors in

region 4, while the curves correspond to membrane reactors in other regions. The transition between region 4 and other regions occurs at approximately $P_{SMR} = 1.7$ bar.

Figures 6.18 and 6.19 show the effect of increasing pressure and permeability respectively within region 4. Three membrane reactors M, N and O in region 4 are compared. The relevant properties of the MRs are given in Table 6.4. MR N has a higher pressure than MR M which results in a lower conversion as predicted by the "K_P equation". As seen in Figures 6.18 and 6.19, there is zero flux in all the three MRs implying that the "Sievert's law" is irrelevant. Thus increasing the permeability has no effect as seen in Figure 6.19. Thus, the operating pressure is the only limiting factor. The value of this insight with respect to making design decisions is as follows: The only recommendation is to increase the operating pressure for MRs in region 4. Increasing the permeability or membrane area has no effect.

Table 6.4: Parameters of membrane reactors in region 4

MR	Region	$\frac{A_{total}}{L}$ [m]	Permeability [Barrer]	Pressure [bar]	C_1 [Barrer.m] 10^{-7}	Limiting Factor
M	4	0.01	2	1.2	2	Only operating pressure
N	4	0.01	2	1.6	2	Only operating pressure
O	4	0.01	10	1.2	10	Only operating pressure

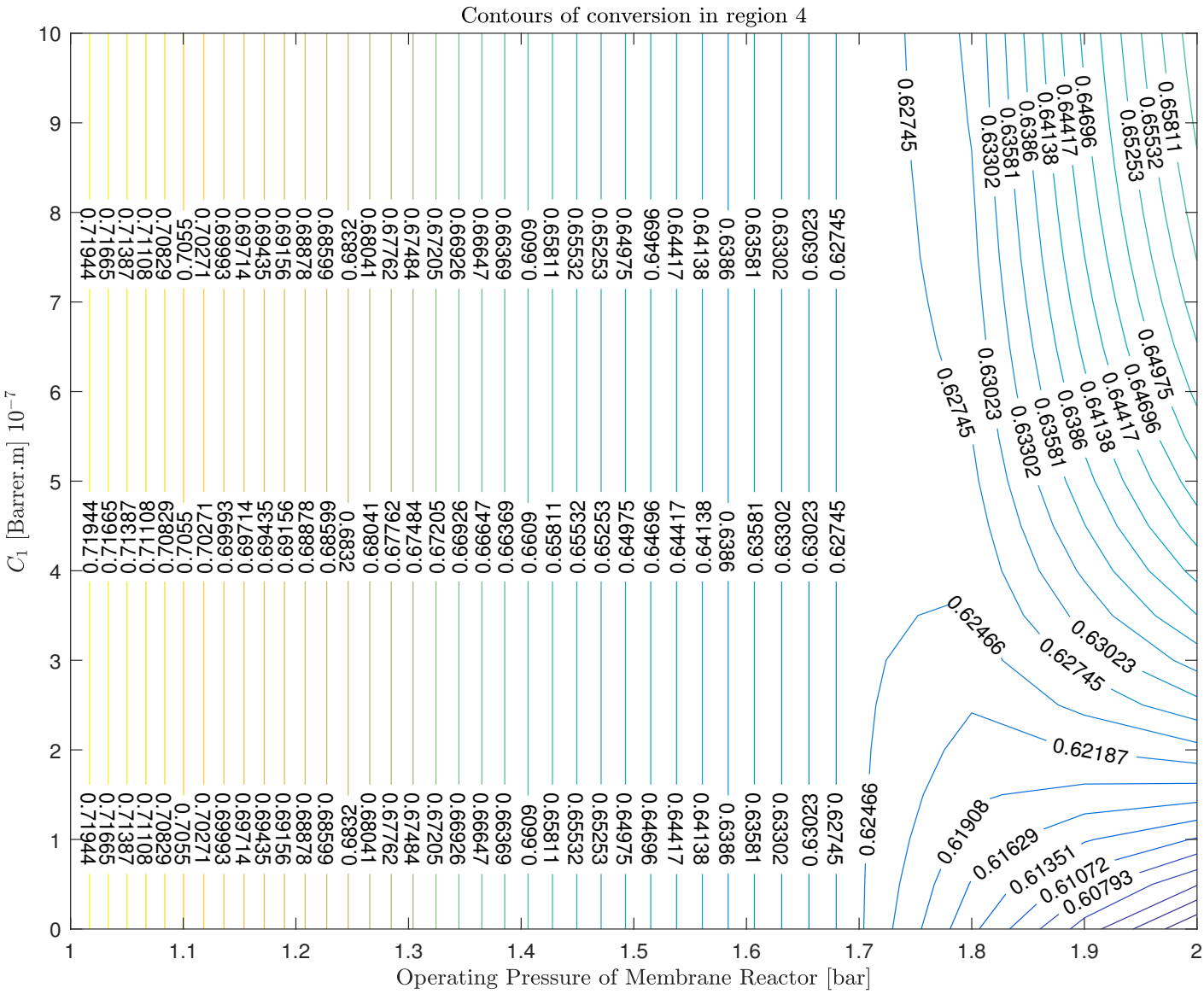

Figure 6.17: Conversion contours of SMR membrane reactor in region 4

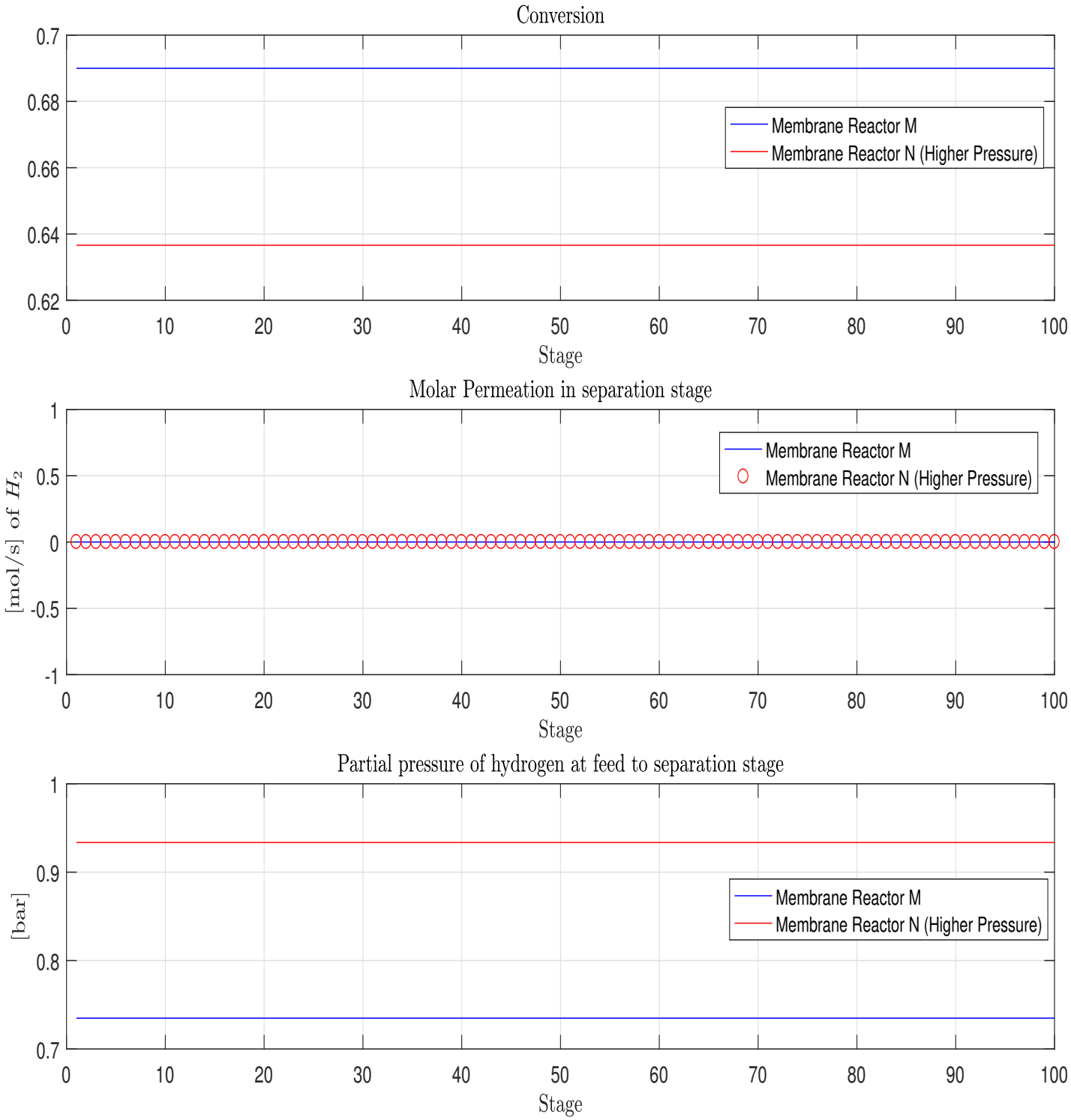

Figure 6.18: Comparison of the molar permeation, hydrogen partial pressure profile and conversion of two membrane reactors M and N in region 4

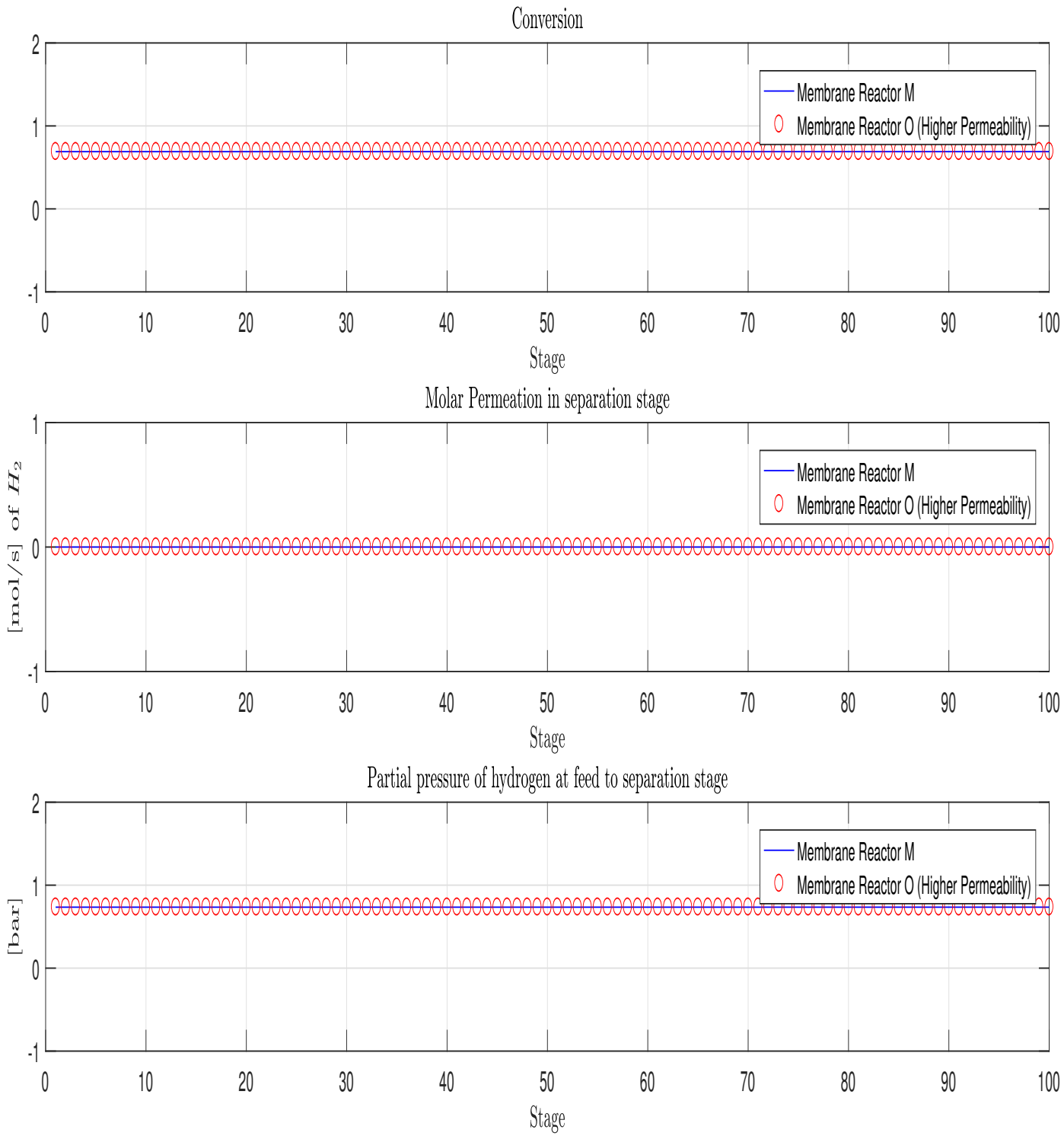

Figure 6.19: Comparison of the molar permeation, hydrogen partial pressure profile and conversion of two membrane reactors M and O in region 4

6.5.3 Area contours

.

During conceptual design of chemical processes, it is often useful to use a "black-box approach". In this, only the input and output characteristics (or transfer characteristics) of unit operations are modeled with no detailed modeling of their inner characteristics. If the unit operation is a membrane reactor, the transfer characteristic that relates the reactant and the product streams is the conversion. It is useful to target for a particular conversion in the membrane reactor. The problem can be stated as follows: Assume that a target is given for the conversion of an SMR membrane reactor operating at its Carnot temperature, what operating conditions (operating pressure, permeability, membrane area and membrane thickness) can achieve this conversion target?

The area per unit thickness ($\frac{A_{total}}{L}$) contours for three different conversion targets of 0.75, 0.80 and 0.85 are given in Figures 6.20, 6.21 and 6.22 respectively. The following observations are made:

- There is a range of operating pressure and permeability values for which achieving the target conversion is infeasible. This region is shown by the red box in Figures 6.20, 6.21 and 6.22. As expected, this infeasible region becomes larger for higher targets of conversion.

- Figures 6.20, 6.21 and 6.22 also have a region in which the area per unit thickness contours are most densely packed. Thus, in this region, the area per unit thickness required to reach the target conversion increases steeply for relatively small changes in operating conditions (operating pressure and permeability). For instance, in Figure 6.22 a MR operating at a pressure of 10 bar and with a permeability of 6 requires a membrane area per unit thickness ($\frac{A_{total}}{L}$) of approximately 0.0035 m, while a MR operating at a pressure of 6 bar and with the same permeability of 6 requires a membrane area to thickness ($\frac{A_{total}}{L}$) of approximately 100 m. Typically, the investment cost of the MR increases significantly with membrane area. This implies that given a permeability of 6, a small increase in operating pressure from 6 bar to 10 bar would have a very large reduction in the required membrane area per unit thickness ($\frac{A_{total}}{L}$) and thus investment cost required to achieve a given conversion target. Generalizing this observation, the following design decision can be made: Choose permeability and operating pressure of the MR such that it does not lie in the densely packed contour region of Figures 6.20, 6.21 and 6.22. That is: Choose permeability and operating pressure of the MR such that it lies "downhill" of the densely packed contour region where lower area to thickness ratios are required.

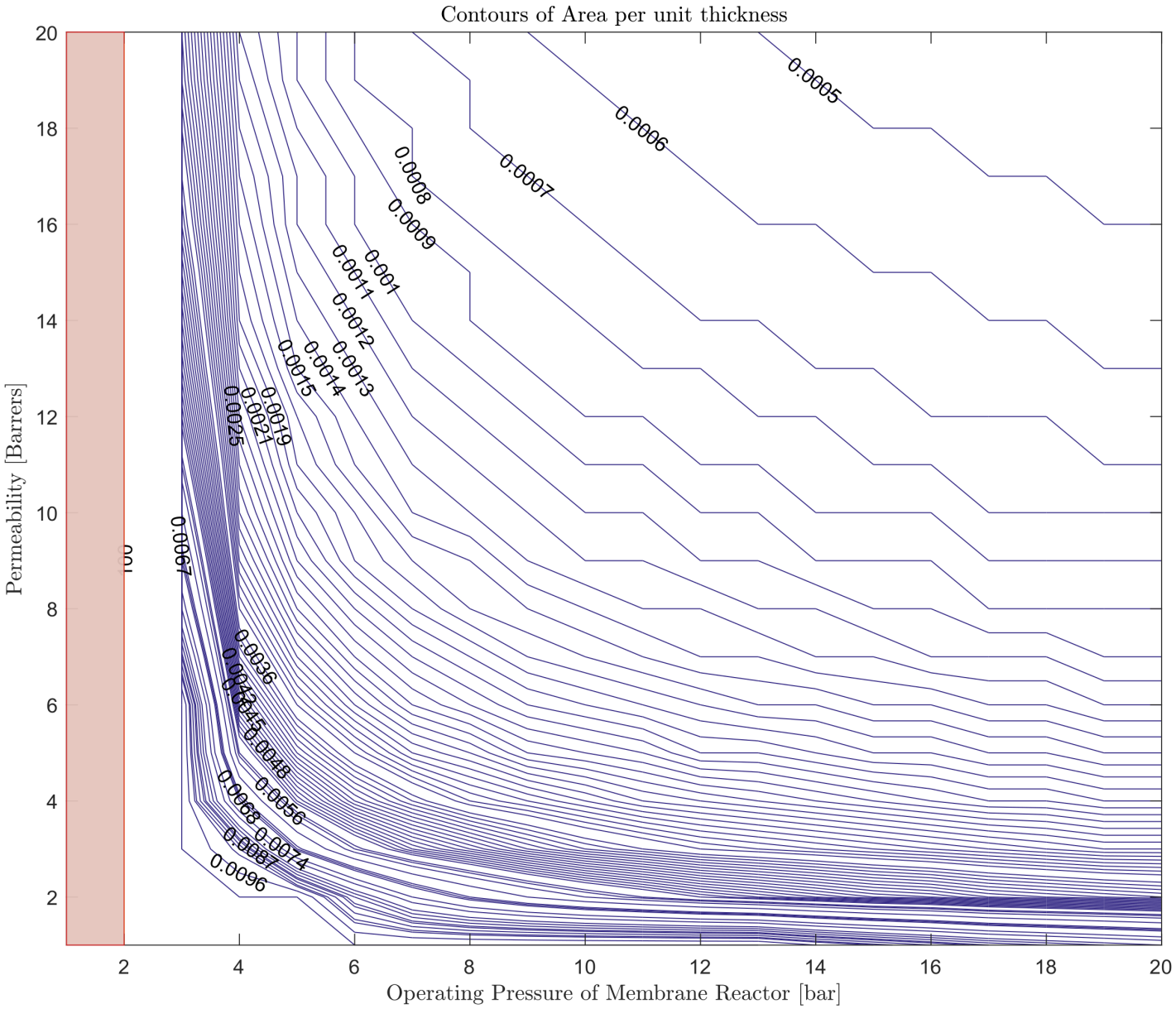

Figure 6.20: Area contours for a target conversion of 0.75 in the SMR MR. In the red region, achieving target conversion is infeasible.

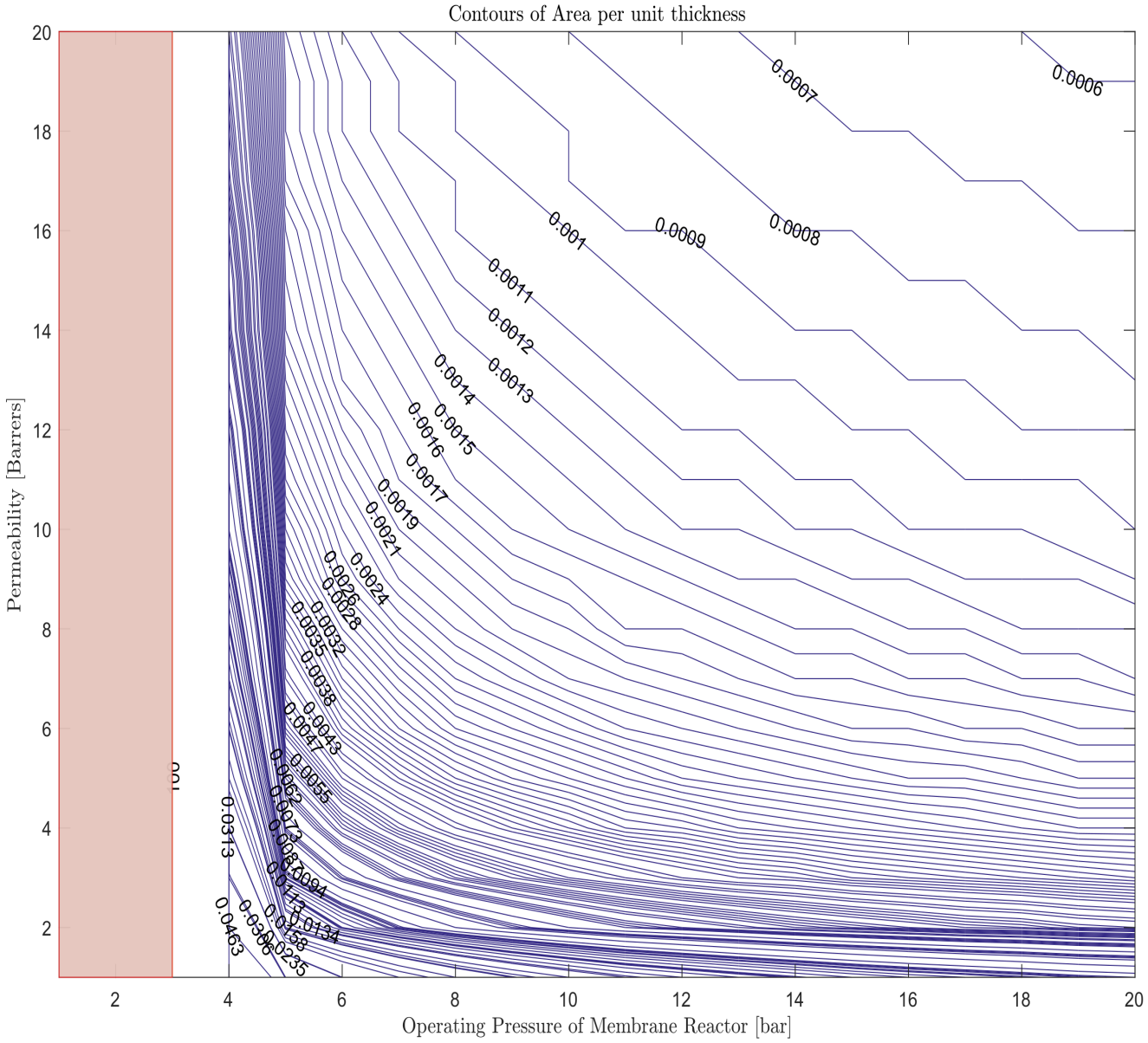

Figure 6.21: Area contours for a target conversion of 0.80 in the SMR MR. In the red region, achieving target conversion is infeasible.

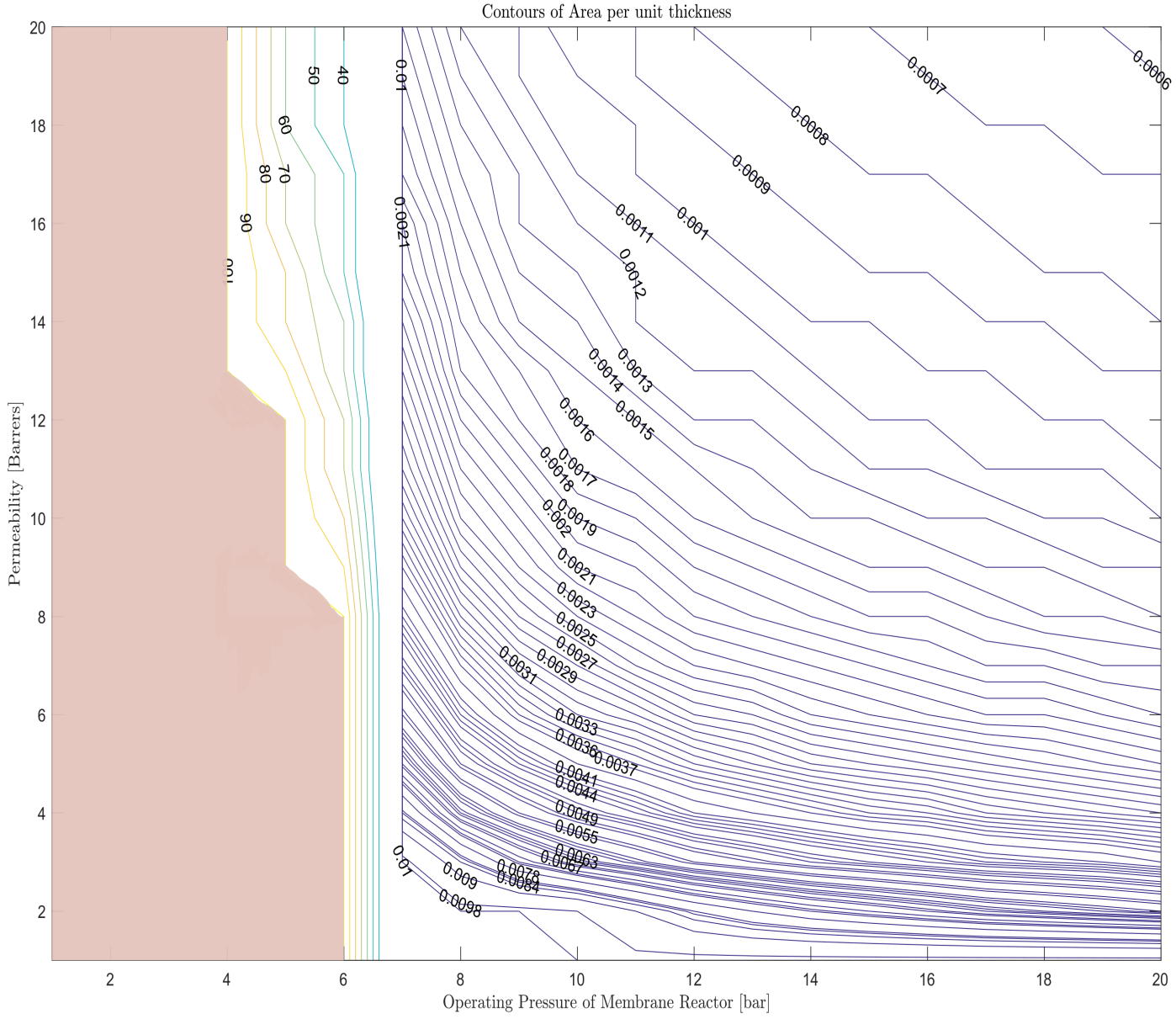

Figure 6.22: Area contours for a target conversion of 0.85 in the SMR MR. In the red region, achieving target conversion is infeasible.

6.6 Estimating conversion in the WGS MR with the Sievert's law hydrogen permeation model

In this section, the conversion of a WGS MR is estimated using the Sievert's law hydrogen permeation model. This section is brief because the procedure is similar to that for the SMR MR. The WGS equation is written:

$$\mathrm{CO\,(g)} + \mathrm{H_2O\,(g)} \rightleftharpoons \mathrm{CO_2(g)} + \mathrm{H_2(g)} \tag{6.15}$$

The standard enthalpy and standard Gibb's energy of reaction are given as $\Delta H_{WGS} = -41.19$ kJ/mol, $\Delta G_{WGS} = -28.59$ kJ/mol [6]. The Carnot temperature of WGS, $T_{Carnot,WGS} = 974.67$ K, is the operating temperature of the WGS membrane reactor. The operating pressure of the WGS MR is denoted P_{WGS}.

Only the reaction stage of the WGS MR is different from the reaction stage of the SMR MR so this is discussed below. The separation stage is identical.

Reaction Stage of the WGS MR

The feed into the membrane reactor is identical to the feed to the first reactor stage in the first block. The total number of blocks N is assumed to be equal to 100. The feed is normalized to be: $N_{CO,feed} = N_{H_2O(g),feed} = 1$ mol/s. A different flowrate can be used; the membrane area of the MR scales with the flowrate used.

Consider a general block i in the membrane reactor. Let the conversion at a reaction stage i be Δc_i. Assume the molar flow rates of the components of the feed to the ith block are given by: $N_{CO}^{i-1}, N_{H_2O}^{i-1}, N_{H_2}^{i-1} N_{CO_2}^{i-1}$. This feed composition corresponds to the retentate composition after the separation stage of (i-1)th block. At equilibrium, Δc_i moles of CO react with Δc_i moles of H_2O to produce Δc_i moles of CO_2 and Δc_i moles of H_2. The equilibrium concentrations are:

$$N_{CO,eqm}^{i} = N_{CO}^{i-1} - \Delta c_i \tag{6.16}$$

$$N_{H_2O,eqm}^{i} = N_{H_2O}^{i-1} - \Delta c_i \tag{6.17}$$

$$N_{H_2,eqm}^{i} = N_{H_2}^{i-1} + \Delta c_i \tag{6.18}$$

$$N_{CO_2,eqm}^{i} = N_{CO_2}^{i-1} + \Delta c_i \tag{6.19}$$

The K_P Equation 3.27 becomes:

$$K_P = \frac{(N_{CO_2,eqm}^{i})(N_{H_2,eqm}^{i})}{(N_{CO,eqm}^{i})(N_{H_2O,eqm}^{i})} \tag{6.20}$$

At $T_{Carnot,WGS}$ of 974.67 K, $K_P = 1.6191$. Thus, Δc_i is the only unknown in the above equation and is calculated. The product composition is then calculated, and this is the feed to the first sub-stage of the separation stage i.

Effect of increasing the operating pressure of the WGS MR

The operating pressure of the WGS MR only has an effect due to "Sievert's law"; the "K_P equation" (Equation 6.20) is unaffected by operating pressure. This is because the pressure term does not appear in the "K_P equation" used to predict conversion. Thus, in contrast to the SMR MR, increasing the operating pressure of the WGS MR only increases the conversion by increasing the permeation molar flow rate. The conversion is estimated for different values of C_1 and different operating pressures of the MR. The results are presented in the next section. The Matlab code used is presented in Appendix D.

6.6.1 Results: Estimates of conversion of the WGS MR

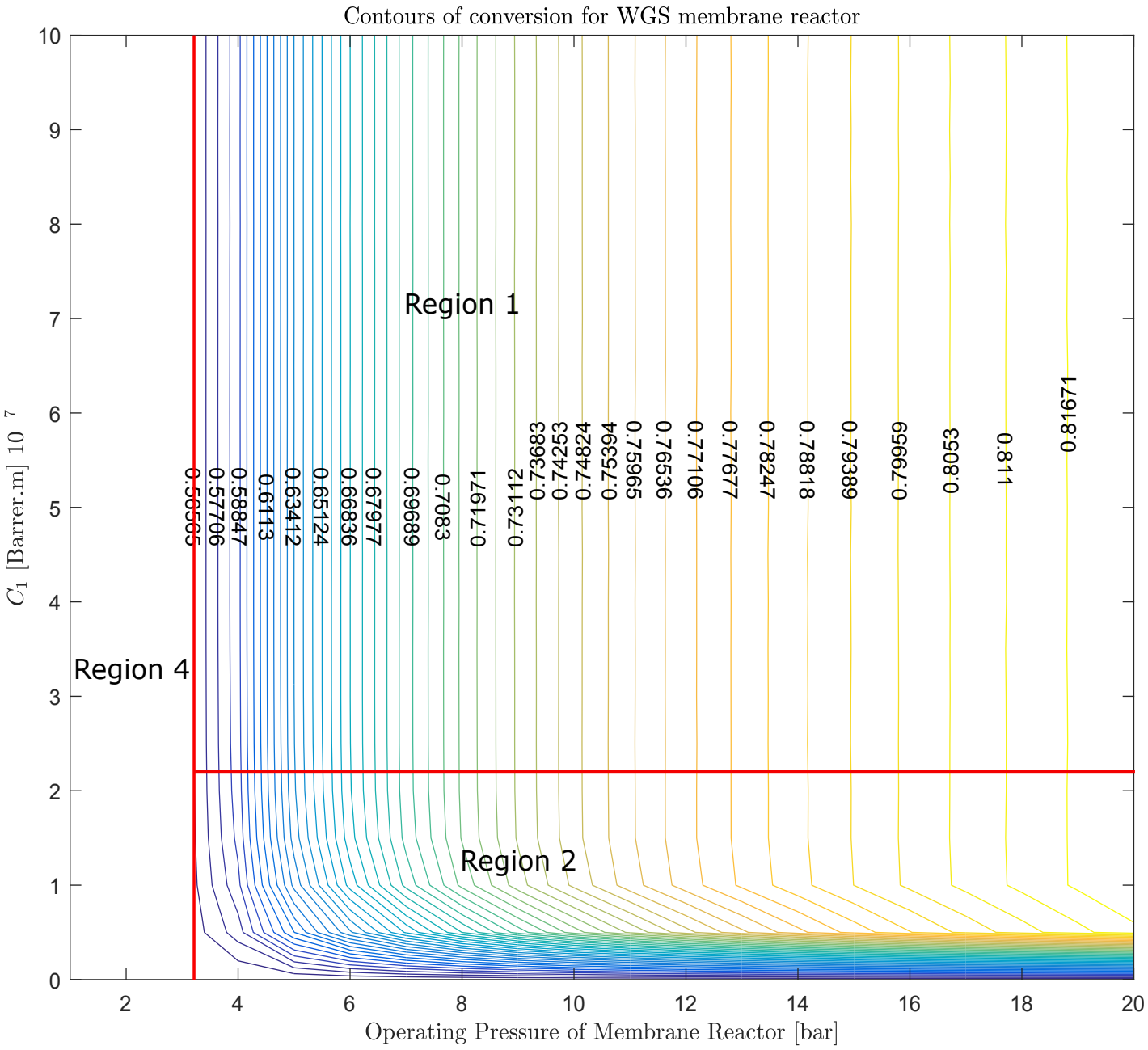

Figure 6.23: Conversion contours of WGS membrane reactor for different operating pressures and C_1 values

6.6.2 Discussion of the results

As can be seen in Figure 6.23, only regions 1, 2 and 4 exist. Region 3 does not exist because there is no effect of "Le-chatelier's principle" and the "K_p equation" in the WGS MR. This is because the WGS reaction occurs without a change in volume, so there is no effect of pressure on conversion in a WGS reaction stage. Increasing the operating pressure only increases the conversion by increasing the permeation molar flow rate according to "Sievert's law".

It can also be seen that in general the range of conversion in a WGS MR is lower than in a SMR MR. This has to do with the lower K_P value at equilibrium resulting from Gibbs free energy calculations.

6.6.3 Area contours of WGS

In this section, the required membrane areas of the WGS MR to achieve targets of conversion are determined. Since the range of conversion is lower, it is reasonable to target for lower conversion values. Figures 6.24, 6.25 and 6.26 correspond to conversion targets of 0.65, 0.70 and 0.75. The discussion of results and the recommended design decisions made in the SMR MR section are relevant in this section as well.

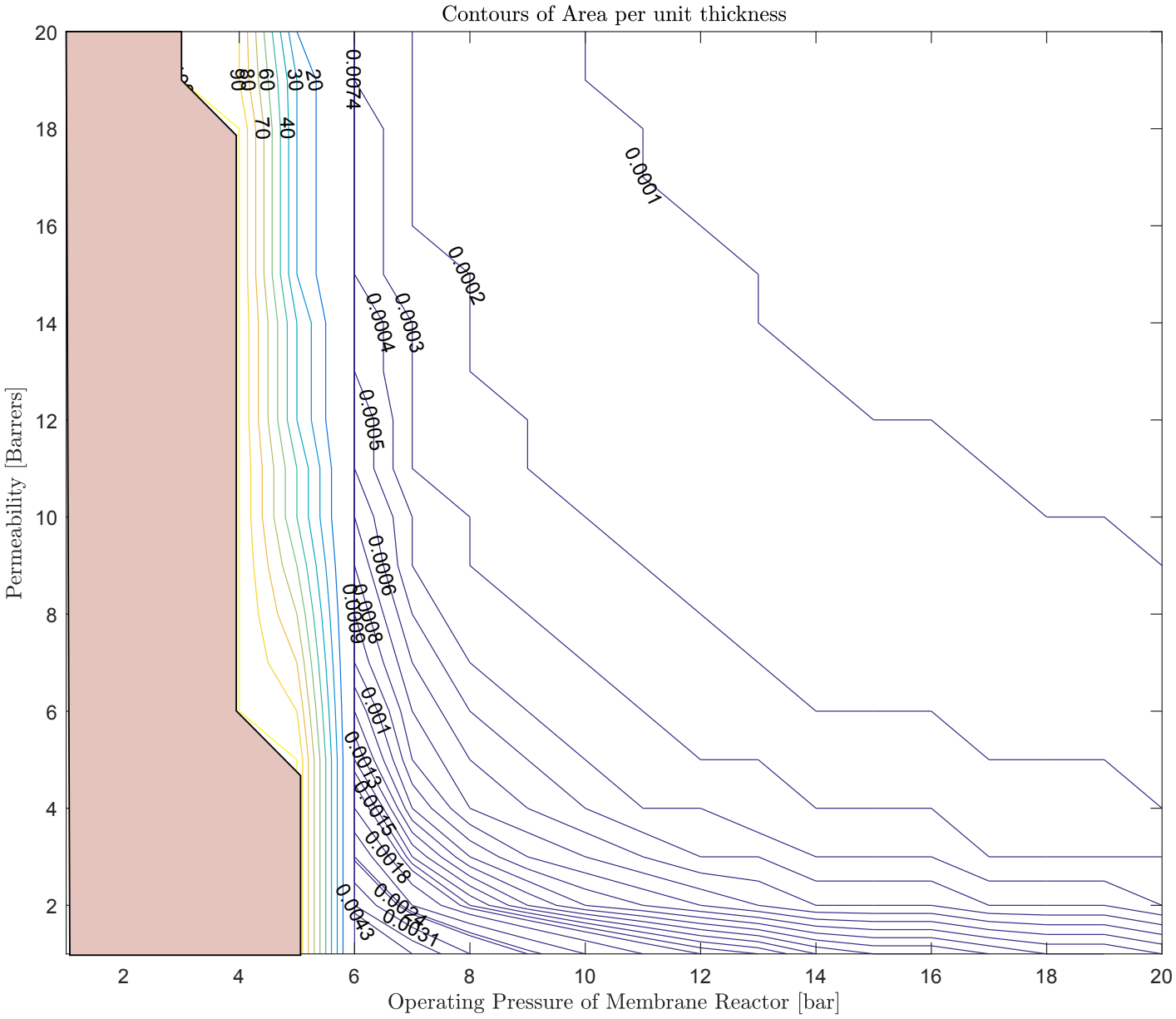

Figure 6.24: Area contours for a target conversion of 0.65 in a WGS MR

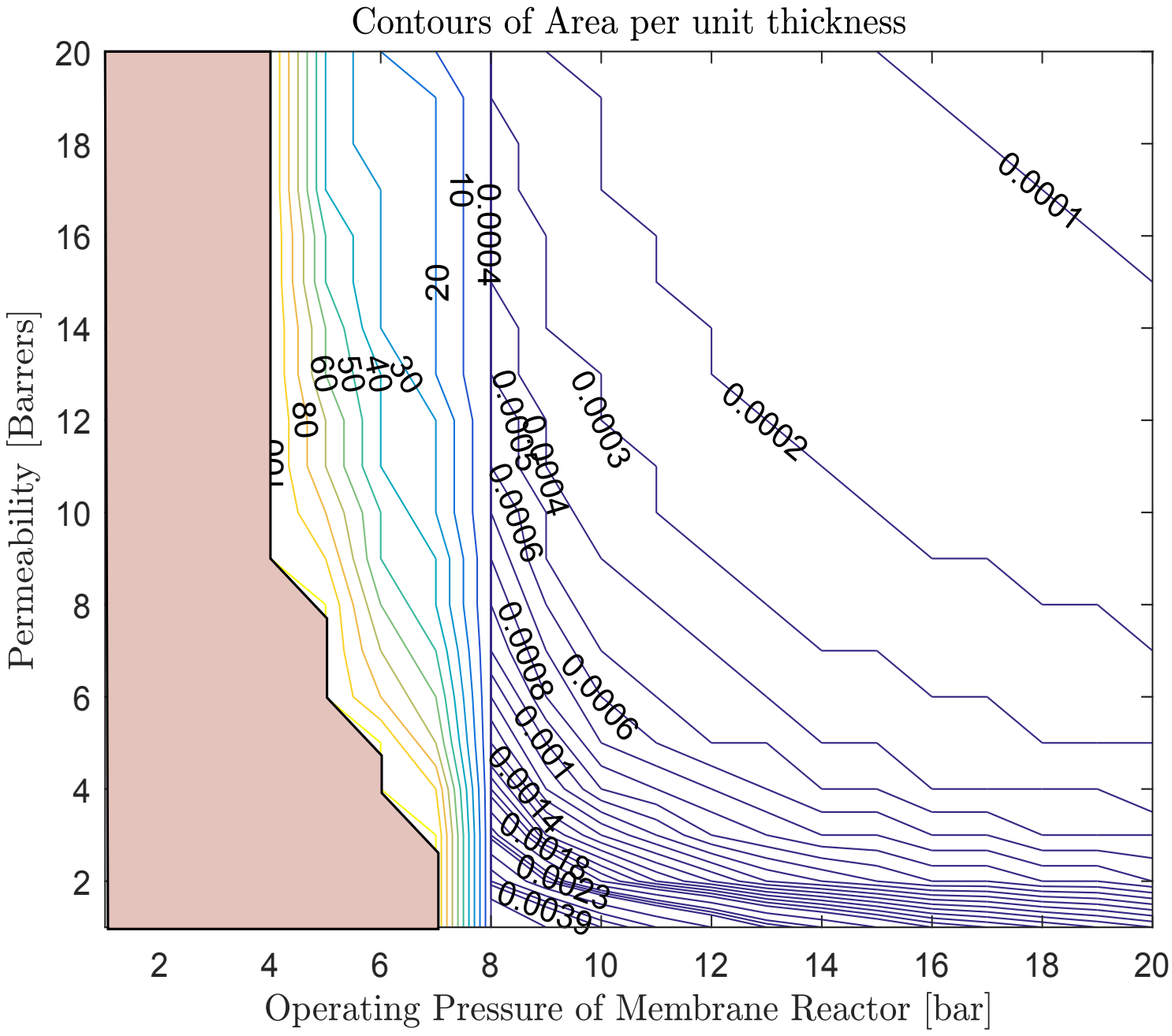

Figure 6.25: Area contours for a target conversion of 0.70 in a WGS MR

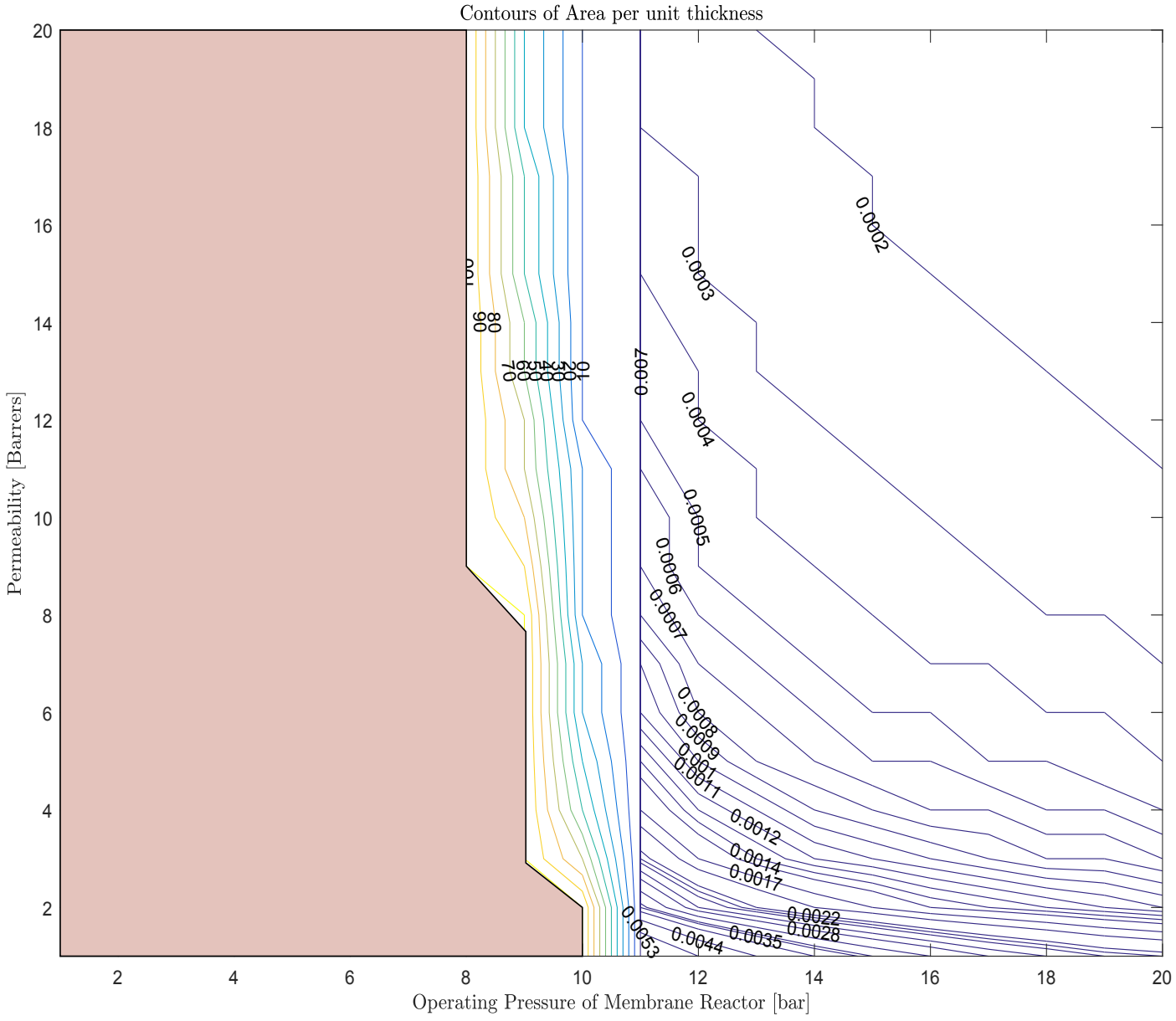

Figure 6.26: Area contours for a target conversion of 0.75 in a WGS MR

6.7 Constant Minimum Flux Model

6.7.1 Motivation for the model

In the previous sections (6.3 to 6.6), Sievert's law for hydrogen permeation through a Palladium membrane was used as a permeation model to estimate the conversion. Section 6.33 shows the assumptions made in the permeation model. Making those assumptions overestimates the conversion of the MR compared to an actual MR. Thus, the results obtained in the case studies in Sections 6.5 and 6.6 give an upper-bound estimate for the conversion of the SMR MR and the WGS MR. In order to get a more balanced picture of the expected conversion, it is necessary to determine the lower-bound estimate for the conversion as well. The objective of this section is to develop a fixed minimum flux model to estimate this lower-bound of conversion. This permeation model is then applied to a case study of the SMR MR and WGS MR. Since this section relies on concepts already discussed rigorously in sections 6.3 to 6.6, the presentation is more concise.

A lower conversion in a MR arises as a result of a lower flux through the membrane. This corresponds to a lower permeation molar flow rate F_i in each separation stage. This implies that if the permeation molar flow rate F_i through each membrane stage is fixed to be a minimum (i.e. the most conservative case), the corresponding conversion calculated would also be the lower-bound estimate. Let $F_{min,i}$ denote this minimum permeation molar flow rate in each separation stage. In this permeation model, $F_{min,i}$ is assumed to be a constant for all the separation stages in the MR. Thus, the subscript i can be dropped to give F_{min}. In a later section, a permeation model (called the Variable Minimum Flux Model) is developed to study the case in which $F_{min,i}$ is not a constant but varies in each separation stage.

6.7.2 Determining the constant minimum permeation molar flow rate (F_{min})

Implementing the constant minimum flux model requires information on the F_{min} value. Kotowicz and Balicki [40] developed a method to determine the minimum flux through a membrane in a separation process. Insight from this method is used to determine the minimum permeation molar flow rate (F_{min}) value in each separation stage of the membrane reactor. Kotowicz and Balicki assume certain partial pressure profiles and use these to determine the minimum flux value. Figure 6.27 is used to illustrate this procedure.

Figure 6.27 shows the partial pressure profile for both the feed (p_h) and permeate (p_l) side of the membrane in separation stage i. It is important to note that these partial pressure profiles are used to set up the constant minimum flux model - they are not the resulting partial pressure profiles of the MR obtained after implementing the constant minimum flux model. In other words, insight from Figure 6.27 is used to determine the F_{min} value which is then implemented in the constant minimum flux model described later on using Figure 6.28. After this implementation, the resulting partial pressure profiles can be determined and these will be different from the ones assumed in Figure 6.27. For this reason, the set up described in Figure 6.27 can be thought of as a precursor model to the constant minimum flux model described using Figure 6.28.

The assumptions of the sequential model listed in Section 6.33 are still assumed to hold for the precursor. Further assumptions are:

- Since the number of blocks, N, is large, the area of each separation stage is sufficiently small such that the partial pressure at the feed side (p_h) decreases linearly along the length of the membrane.
- The partial pressure at the permeate side (p_l) is constant along the length of the membrane. This is consistent with the previous assumption in Section 6.32 of a cross-flow membrane regime .

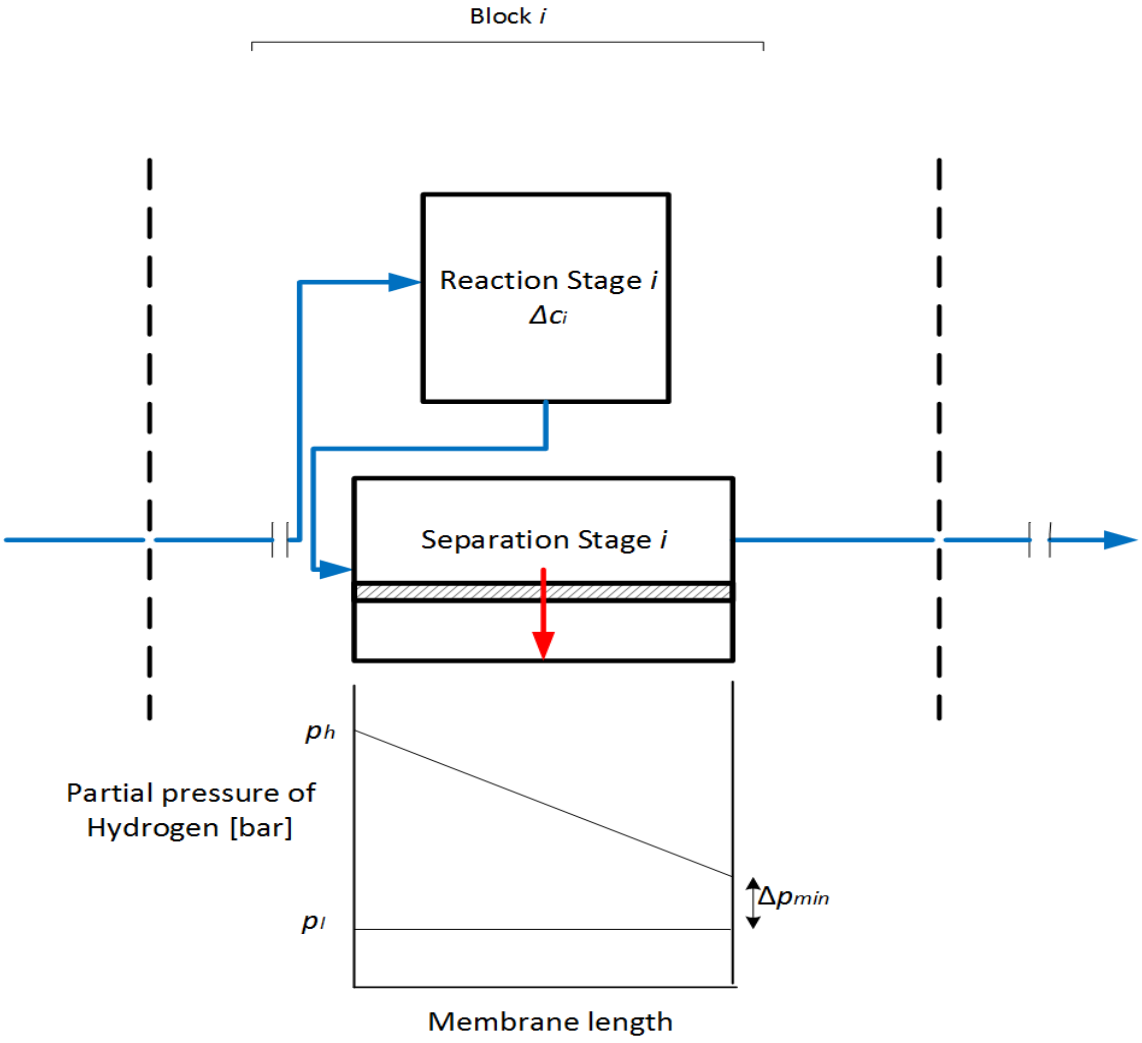

Figure 6.27: Partial pressure profile of both the feed (p_h) and permeate (p_l) side for separation stage i of the precursor model

The driving force behind the permeation through the membrane is the difference between the partial pressure of hydrogen at the feed and permeate side. Thus, driving forces are proportional to the gap between the upper and lower lines in Figure 6.27. As can be seen in the figure, driving forces decrease along the membrane length and reach a minimum at the end of the membrane. Minimum driving forces correspond to Δp_{min} as labeled in Figure 6.27.

Since the flux is proportional to the driving force, it implies that the minimum flux (J_{min}) occurs at the end of the membrane and corresponds to the driving forces labeled Δp_{min}. This minimum flux can be calculated using Sievert's law as done in Equation 6.21 with the same definition of terms as in Equation 6.1:

$$J_{min} = \frac{P[p_{h,min}^n - p_l^n]}{L} \tag{6.21}$$

Since $p_{h,min} = p_l + \Delta p_{min}$,

$$J_{min} = \frac{P[(p_l + \Delta p_{min})^n - p_l^n]}{L} \tag{6.22}$$

The next step is to fix that this calculated minimum flux (J_{min}) occurs through the entire area of the separation stage (A_{stage}) not just at the end of the membrane. This assumption corresponds to the most conservative case; in an actual MR, the flux through any point is greater than or equal to this calculated minimum flux (J_{min}). This can be used to get an expression for the minimum permeation molar flow rate in the separation stage, F_{min}. F_{min} is calculated using Equation 6.23:

$$F_{min} = J_{min} A_{stage} = C_2[(p_l + \Delta p_{min})^n - p_l^n] \tag{6.23}$$

where: $C_2 = \frac{PA_{stage}}{L}$.

Note that Sievert's law is not applied to model the permeation through the entire separation stage as in Section 6.4. Sievert's law is applied only to calculate the minimum flux (J_{min}), and this flux is assumed to occue for the entire separation stage. In the next sections, the constant minimum flux model is implemented in case studies to estimate the conversion of the SMR MR and the WGS MR. The Matlab code used is presented in Appendix D.

6.8 Estimating conversion in the SMR MR with the constant minimum flux model

The reaction stage is identical to that used in Section 6.5 so is not presented here. As discussed in Section 6.7, the separation stage is different. Figure 6.28 shows a MR with a constant minimum permeation molar flow rate F_{min} through each separation stage. The order of processes in this model is as follows: The reactant of the MR is fed to first reaction stage where the conversion Δc_1 occurs. The products from this reaction stage are fed to the first separation stage. A constant permeation molar flow rate (F_{min}) is assumed in the membrane separation stage. The retentate forms the feed to the second reaction stage in block 2, while the permeate containing pure hydrogen is collected as the valuable product of the membrane reactor. In order to enable comparison with the results obtained in Section 6.5, an identical "standard stoichiometric feed" is used. and the total number of blocks N is also assumed to be equal to 100.

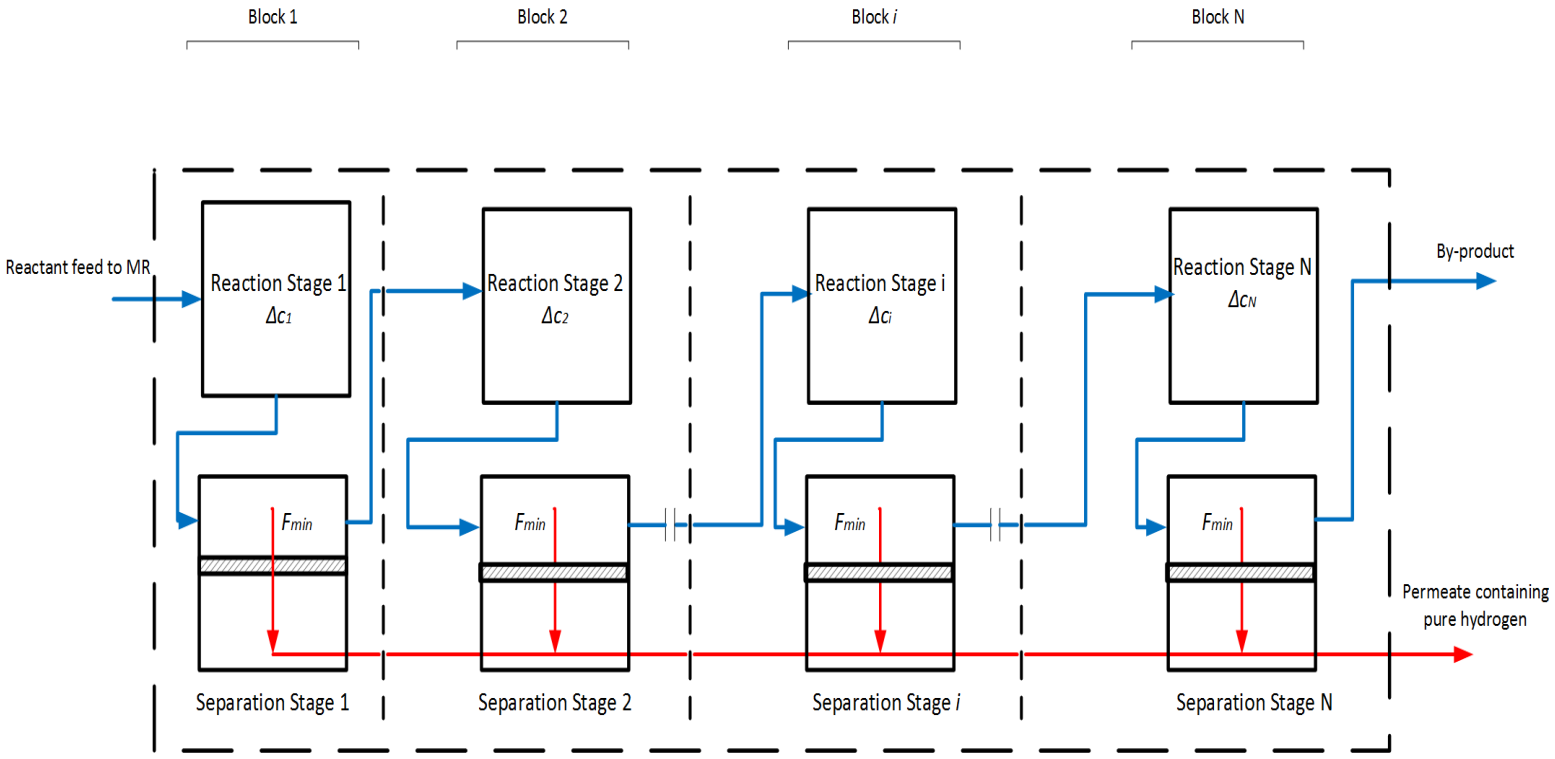

Figure 6.28: Membrane Reactor with constant minimum permeation molar flow rate F_{min} through each separation stage

6.8.1 Results: Estimate of conversion of the SMR MR

Figure 6.29 shows the contours of conversion of the SMR MR for $\Delta p_{min} = 0.15$ bar. In order to enable comparison with the results presented in Section 6.5, it is necessary to express the C_2 value in terms of the C_1 value. In Section 6.5, 1000 sub-stages were assumed thus A_{stage}=1000A_{sub}, implying:

$$C_2 = \frac{PA_{stage}}{L} = \frac{1000PA_{sub}}{L} = 1000C_1 \tag{6.24}$$

In addition, similar to Section 6.5, area contours for certain conversion targets can also be drawn. However, in the interest of brevity, these area contours are not presented in this section.

6.8.2 Discussion of Results

The subdivision of Figure 6.29 into regions 1-4 and discussion of the regions is not done in this section for the sake of brevity. The discussion of Section 6.5 and the recommended design decisions are applicable here as well.

As expected, the range of estimated conversion values in Figure 6.29 is lower than the range of estimated conversion values in Figure 6.6 in Section 6.5. This is intuitive because Figure 6.29 represents the lower-bound estimate of conversion while Figure 6.6 represents the upper-bound estimate of conversion. For example, a MR with a C_1 value of 10 and an operating pressure of 20 bar has a conversion of 0.7962 with the constant minimum flux model, and a conversion of 0.9186 with

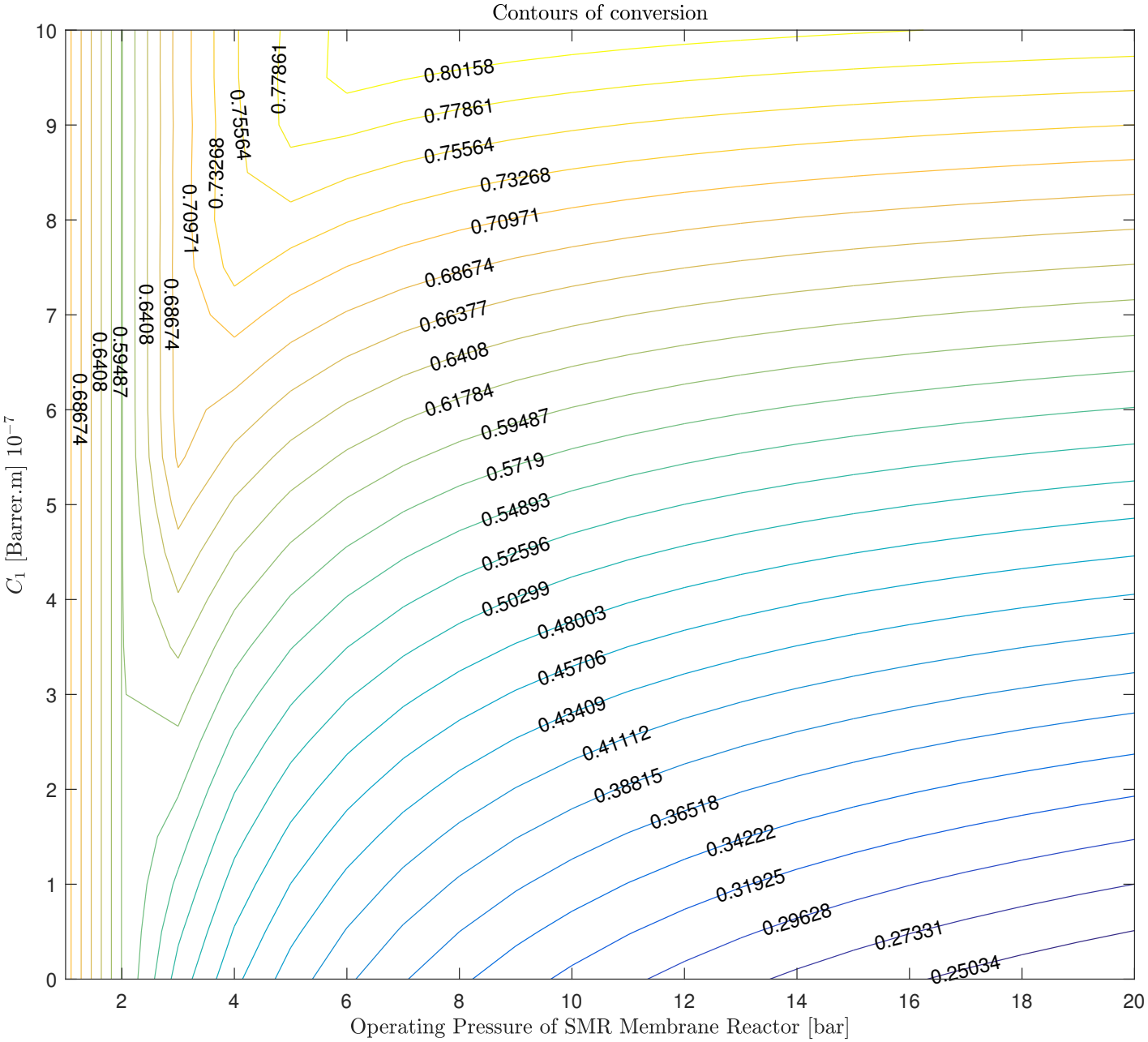

Figure 6.29: Conversion contours of the SMR membrane reactor for different operating pressures and C_1 values. The Δp_{min} values is 0.15 bar

the Sievert's law model for hydrogen permeation through a palladium membrane. These two values provide the range of the expected conversion in an actual SMR MR with the given operating conditions.

Although this constant minimum flux model is valuable in estimating the lower-bound of conversion, it has three drawbacks as explained next.

- The first drawback is the difficulty in accurately estimating the Δp_{min} value

of the MR. The flux through each separation stage F_{min} is a strong function of the Δp_{min}; thus, an inaccurate Δp_{min} would change the estimated conversion value significantly. The solution to this drawback is carry-out rigorous experimental studies in order to quantify the Δp_{min} value of membranes used in the separation stage of the MR.

- The second drawback is the assumption that the minimum flux is constant through all the separation stages of the MR. In an actual MR, this assumption would not necessarily hold. For instance, a majority of the conversion may occur closer to the entrance of the MR compared with the end of the MR. As a result, the flux closer to the entrance of the MR may be much higher than the flux closer to the exit of the membrane reactor. Thus, modeling the entire MR to have a constant minimum permeation molar flow rate (F_{min}) may be too conservative, and thus not representative of the the functioning of an actual MR. A novel permeation model (called the Variable Minimum Flux Model) is developed in Section 6.10 to address this drawback.

- The third drawback discussed arises from a scenario in which this permeation model gives an incorrect trend. The work of Kotowicz and Balicki [40] is focused on modeling membranes in solely separation processes, not in membrane reactor processes in which a reaction stage occurs resulting in a change in the feed partial pressure of hydrogen. In addition, the work in [40] is focused on a single membrane separation stage not several membrane separation stages as in this permeation model. Thus, insight from [40] may not always be directly applicable.

  Figures 6.30 and 6.31 showing the conversion contours for Δp_{min} values of 0.30 bar and 0.45 bar respectively are used to illustrate this incorrect trend. In both figures, the estimated conversion values in the contours are higher than the corresponding estimates in Figure 6.29 which has Δp_{min}= 0.15 bar. For example, consider the estimated conversion of a MR with C_1 value of 10 and an operating pressure of 20 bar. If Δp_{min} is 0.15 bar, the conversion is 0.7962; if Δp_{min} is 0.30 bar, the conversion is 0.8825; and if Δp_{min} is 0.45 bar, the estimated conversion is 0.8674.

  This trend of estimated conversion increasing with higher Δp_{min} values is contradictory to intuition: It is normally desired to design a membrane with as low a Δp_{min} value as technologically and economically feasible, and membranes with low Δp_{min} values are considered "better" membranes. Thus, the prediction that conversion is decreased by using a better membrane in the MR is incorrect, and exposes a flaw in this permeation model.

  The central reason for this flaw is the application of Sievert's law in Equation 6.23. It can be seen that using a higher Δp_{min} value in Equation 6.23 gives a higher F_{min} value. This higher minimum permeation molar flow rate results in a higher overall conversion. Intuitively, the opposite should be true: A higher Δp_{min} value should give a low permeation molar flow rate (F_{min}) value and lower conversion in the MR. This drawback also motivates the development of a novel permeation model (called the Variable Minimum Flux Model) in Section 6.10 that does not use Sievert's law to determine the minimum flux value.

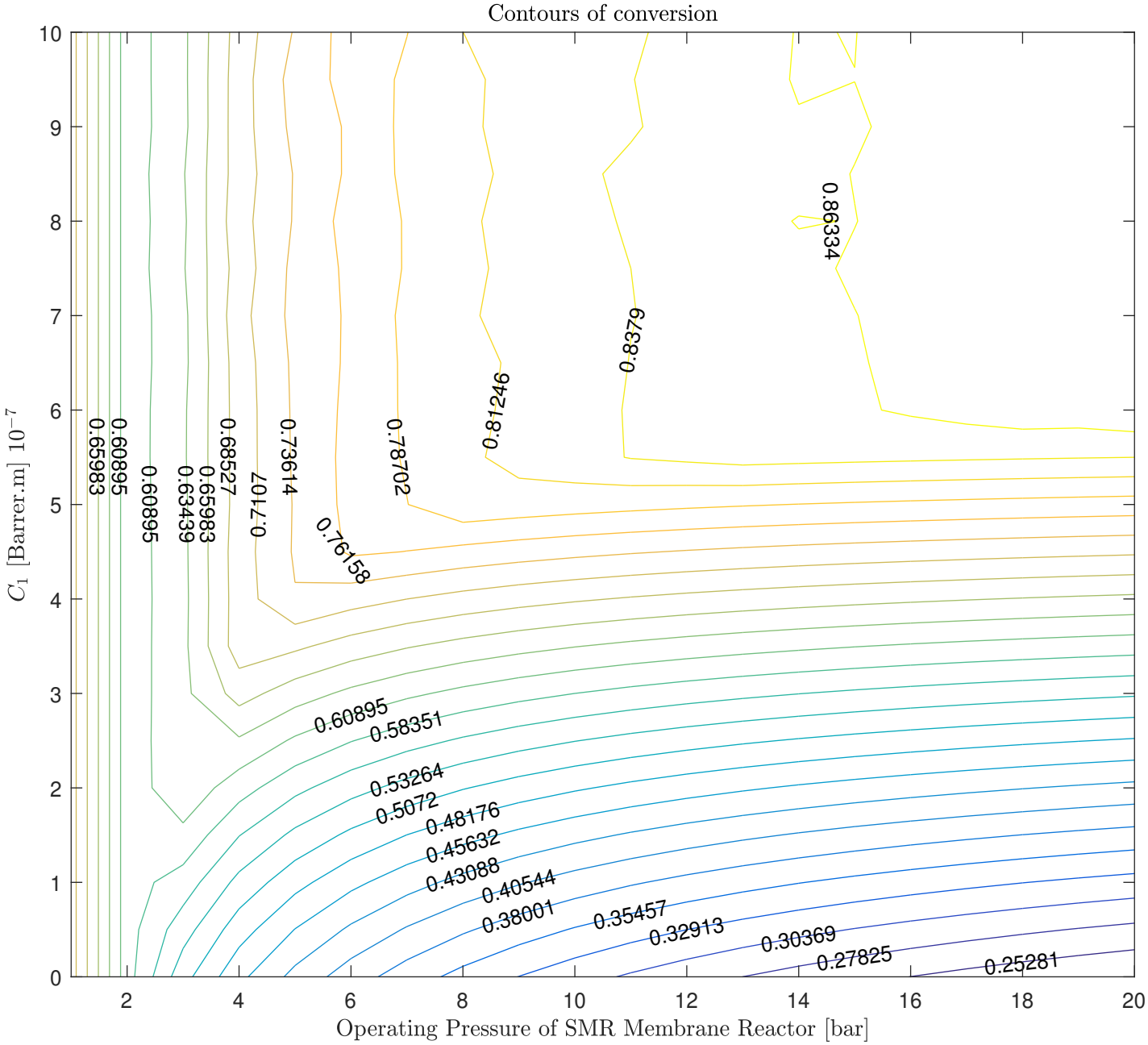

Figure 6.30: Conversion contours of the SMR membrane reactor for different operating pressures and C_1 values. The Δp_{min} values is 0.30 bar

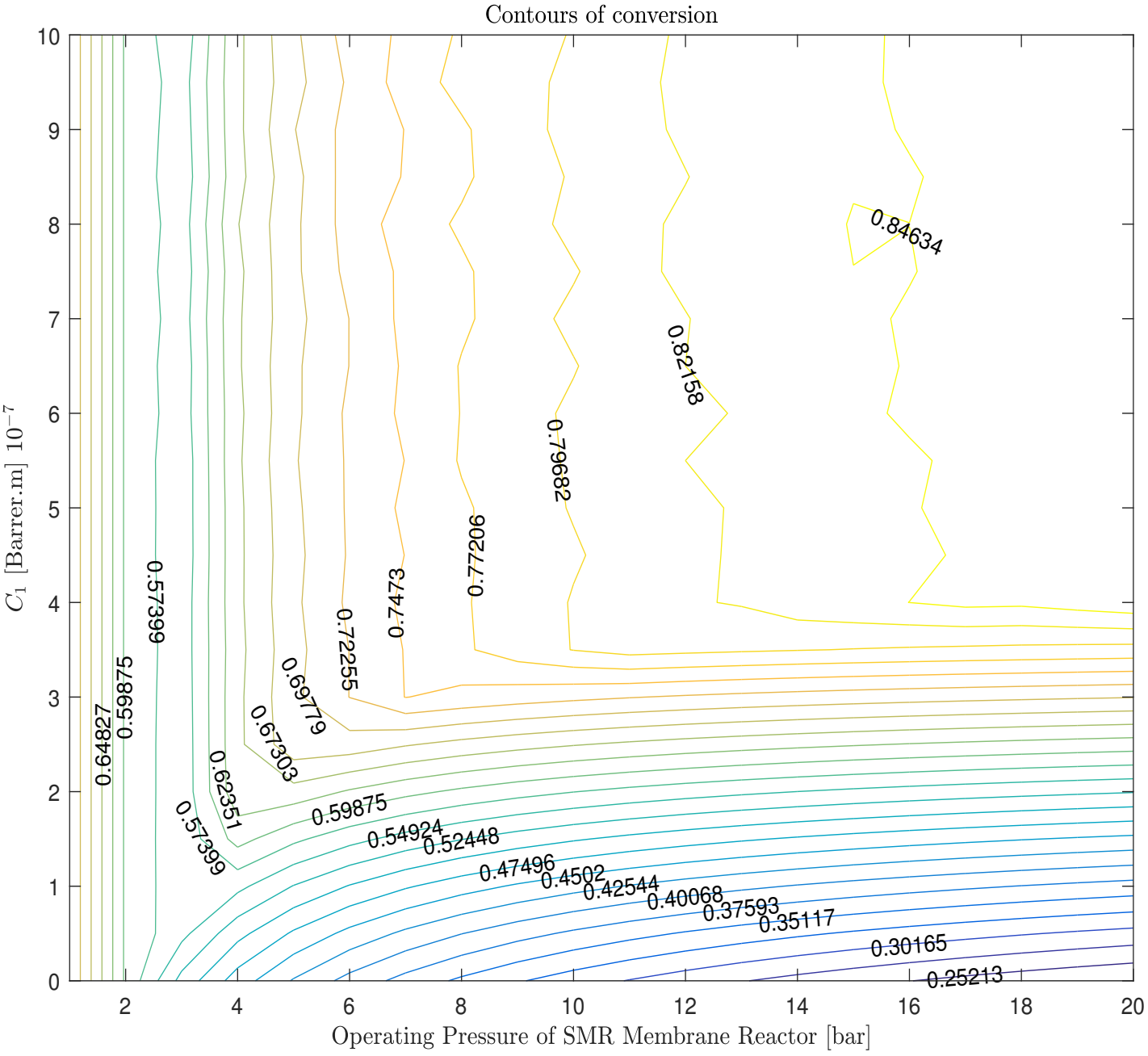

Figure 6.31: Conversion contours of the SMR membrane reactor for different operating pressures and C_1 values. The Δp_{min} values is 0.45 bar

6.9 Estimating conversion in the WGS MR with the constant minimum flux model

The reaction stage is identical to that used in Section 6.6 so is not discussed. Similarly, the separation stage is identical to that used in Section 6.8.

6.9.1 Results: Estimate of conversion of the WGS MR

Figure 6.32 shows the contours of conversion of the WGS MR for $\Delta p_{min} = 0.15$ bar, varied with operating pressure of the WGS MR and C_1 value. Area contours can also be drawn but are not included for brevity.

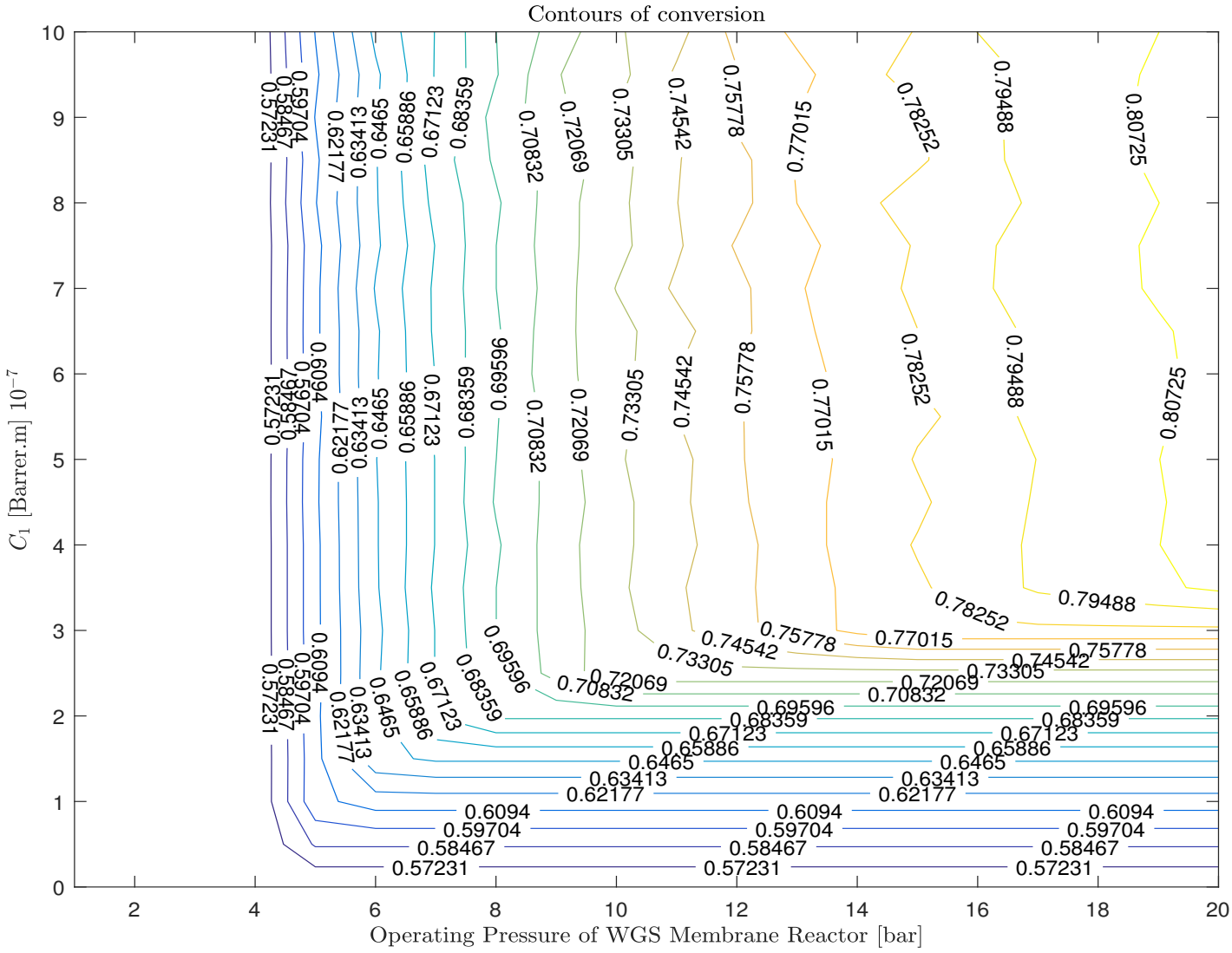

Figure 6.32: Conversion contours of the WGS membrane reactor for different operating pressures and C_1 values. The Δp_{min} values is 0.15 bar

The discussion of results given in Section 6.8, and the drawbacks discussed are

also valid for this section. Figure 6.32 gives a lower-bound estimate for the conversion of a WGS MR while Figure 6.23 in Section 6.6. gives the upper-bound estimate. For example, a WGS MR with a C_1 value of 10 and an operating pressure of 20 bar has a conversion of 0.8196 with the constant minimum flux model, and a conversion of 0.8824 with the Sievert's law model for hydrogen permeation through a palladium membrane as used in Section 6.6.

6.10 Variable Minimum Flux Model analogous to a Heat Exchanger

6.10.1 Motivation for the model

As mentioned in Section 6.8, the drawbacks of the constant minimum flux model motivate the development of a novel permeation model. To the best of my knowledge, such a permeation model has not been developed to study and estimate the conversion of a membrane reactor using a Process Systems Engineering point of view. The two major drawbacks mentioned are: The minimum molar permeation ($F_{min,i}$) in each separation stage may not be constant, and using Sievert's law equation to calculate the F_{min} value in Equation 6.23 gives an incorrect trend of the variation of the estimated conversion with the Δp_{min} value. Since Sievert's law gives incorrect results, this model uses a different equation to determine the $F_{min,i}$ value. This equation is developed by making an analogy between a single membrane separation stage and a heat exchanger, as explained below.

6.10.2 Developing the equation to determine the $F_{min,i}$ values

Figure 6.33 is used to show the analogy between a heat exchanger and a single membrane separation stage of the sequential MR model. Note once again that the partial pressure profiles presented in Figure 6.33 are used to set up the variable minimum flux model - they are not the resulting partial pressure profiles after the variable minimum flux model has been implemented. Thus, Figure 6.33 is used to explain the procedure to determine the $F_{min,i}$ values which are then implemented in the variable minimum flux model described using Figure 6.35.

The following parameters are analogous between a heat exchanger and a single membrane separation stage:

- Driving forces: Temperature in the heat exchanger is analogous to the partial pressure of hydrogen in the membrane separation stage. The temperature profile of the hot stream is analogous to the partial pressure profile on the high pressure side of the membrane. Similarly, the temperature curve of the cold stream is analogous to the partial pressure profile of the permeate side.

- The quantity of heat exchanged between the hot and cold streams (Q) is analogous to the permeation molar flow rate ($F_{min,i}$). Thus, the well-known relationship between Q and the temperature driving forces can be extrapolated to the case of permeation through the membrane separation stage.

  For a heat exchanger:

  $$Q = mc_p(T_{hot,in} - T_{hot,out}) \tag{6.25}$$

  where: m is the mass flow rate and c_p is the specific heat capacity of the hot stream.

  The analogous permeation molar flow rate equation can be written by introducing a constant C_3:

  $$F_{min,i} = C_3(p_{h,in} - p_{h,out}) \tag{6.26}$$

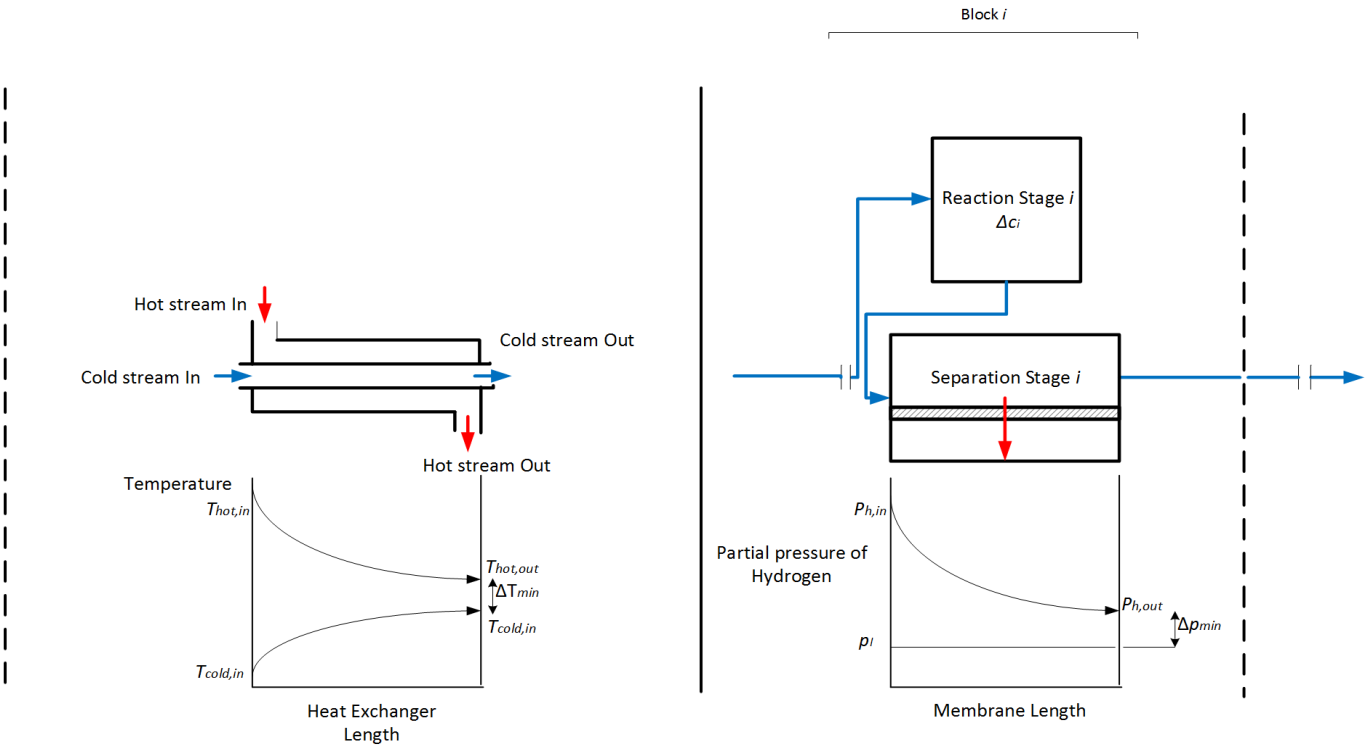

Figure 6.33: Figure to demonstrate the analogy between a heat exchanger and a single separation stage of the membrane reactor. Heat exchanger diagram is adapted from [10].

Equation 6.26 addresses the drawback associated with using the Sievert's law as in Equation 6.23. As can be seen in Figure 6.33, a membrane with a larger Δp_{min} value would also have a larger $p_{h,out}$ value, given that the partial pressure of the permeate side is a constant in a cross-flow membrane regime. From Equation 6.26, this would give a lower $F_{min,i}$ value. Thus, Equation 6.26 gives the intuitive result that a membrane separation stage with a higher Δp_{min} value has a lower flux, and a "better" membrane with a low Δp_{min} value has higher flux.

6.10.3 Accounting for variable minimum flux values

An immediate question not yet addressed is how to determine the partial pressure profile at the high pressure side of the membrane separation stage that is given by the curve in Figure 6.33. Specifically, it is necessary to determine the $p_{h,in}$ and $p_{h,out}$ values of each separation stage so as to substitute these into Equation 6.26 to get the $F_{min,i}$ value.

One solution is to use the partial pressure profiles determined using the Sievert's law permeation model in Sections 6.4 - 6.6. The partial pressure at the feed to the separation stage can be determined and plotted for all the separation stages. This was already done in Sections 6.5 and 6.6, for example in the third subplot of Figure 6.10. This partial pressure profile gives the $p_{h,in}$ values since it corresponds to the feeds of the separation stages. To get the $p_{h,out}$ values, the partial pressure profile at the retentate from the different separation stages can also be plotted. Figure 6.34 gives an example of the plots of both the $p_{h,in}$ and $p_{h,out}$ values for all the separation stages.

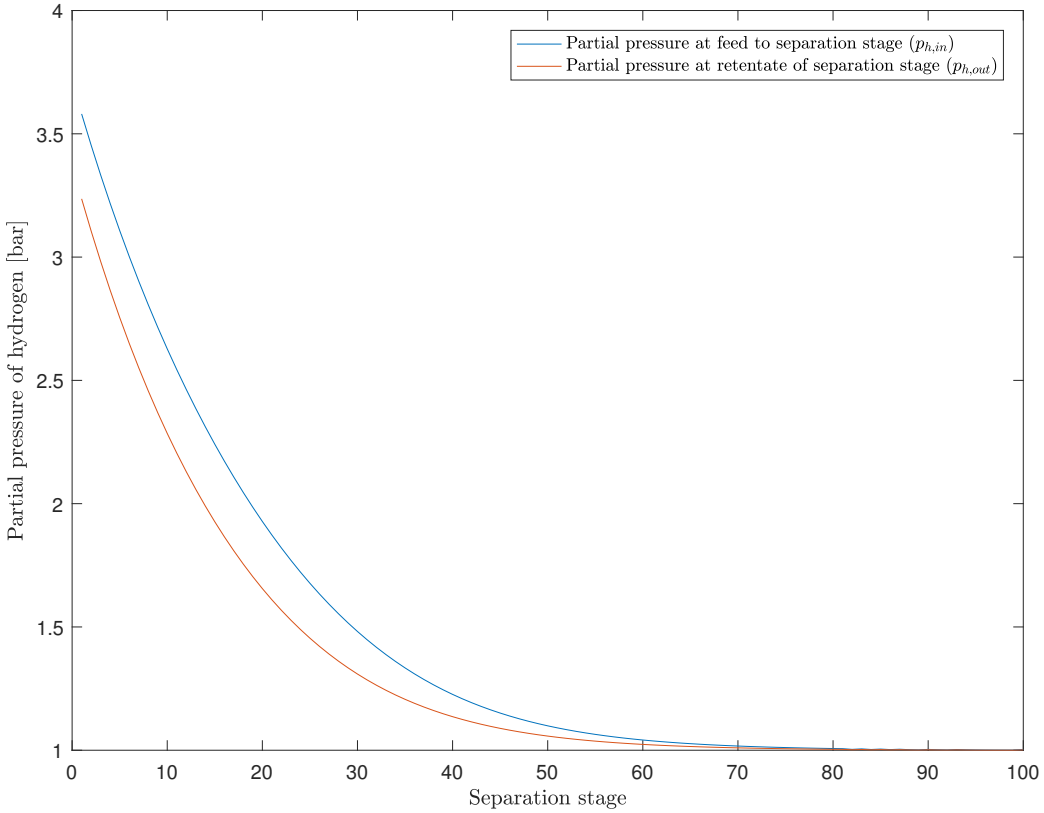

Figure 6.34: Example of partial pressure profiles used to calculate $F_{min,i}$ values in Equation 6.26

At each separation stage i, the corresponding $p_{h,in}$ and $p_{h,out}$ values are read off from Figure 6.34. The $F_{min,i}$ values are then calculated using Equation 6.26. These $F_{min,i}$ values can be calculated for all 100 stages and stored within the computer code. During the simulation of the variable minimum flux model, these stored $F_{min,i}$ values can then be accessed. A case study of using this variable minimum flux model to estimate the conversion of the SMR and WGS MR is presented in Sections 6.11 and 6.12. The Matlab code used is presented in Appendix D.

6.11 Estimating conversion in the SMR MR with the variable minimum flux model

The reaction stage is identical to that used in Section 6.5 so is not presented here. The separation stage is different. Equation 6.26 is used to calculate the permeation molar flow rate at each stage. Figure 6.35 shows a MR with a variable minimum permeation molar flow rate $F_{min,i}$ through each separation stage. The order of processes in this model is as follows: The reactant of the MR is fed to first reaction stage where the conversion Δc_1 occurs. The products from this reaction stage are fed to the first separation stage. The variable minimum permeation molar flow rate ($F_{min,1}$) is calculated using Equation 6.26 with $p_{h,in}$ and $p_{h,out}$ values read off from Figure 6.34 for the first stage. The retentate forms the feed to the second reaction

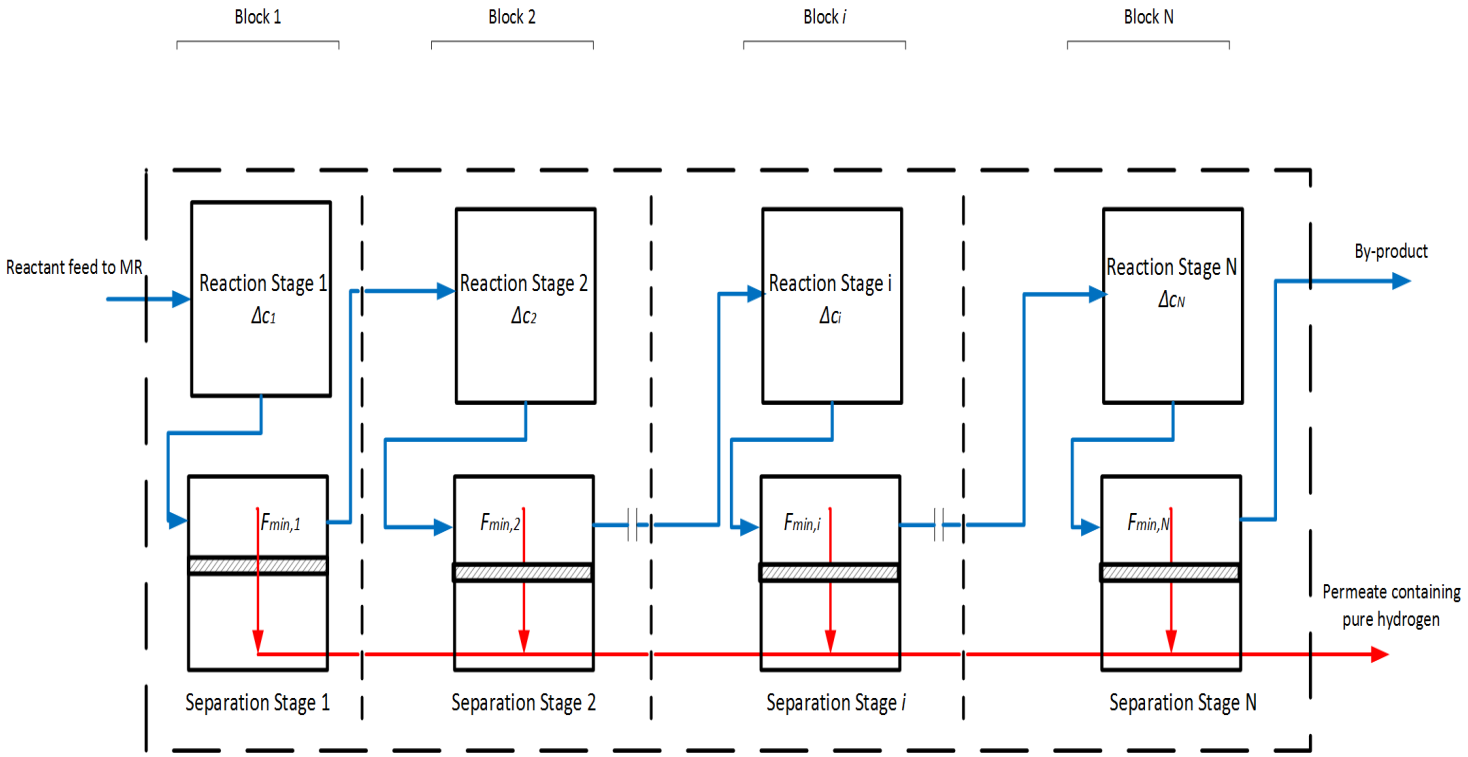

Figure 6.35: Membrane Reactor with variable minimum permeation molar flow rate $F_{min,i}$ through each separation stage

stage in block 2, while the permeate containing pure hydrogen is collected as the valuable product of the membrane reactor.

6.11.1 Results: Estimate of conversion of the SMR MR

Figure 6.36 shows the contours of conversion of the SMR MR for different C_3 values and operating pressures. In addition, similar to Section 6.5, area contours for certain conversion targets can also be drawn. However, in the interest of brevity, these area contours are not presented.

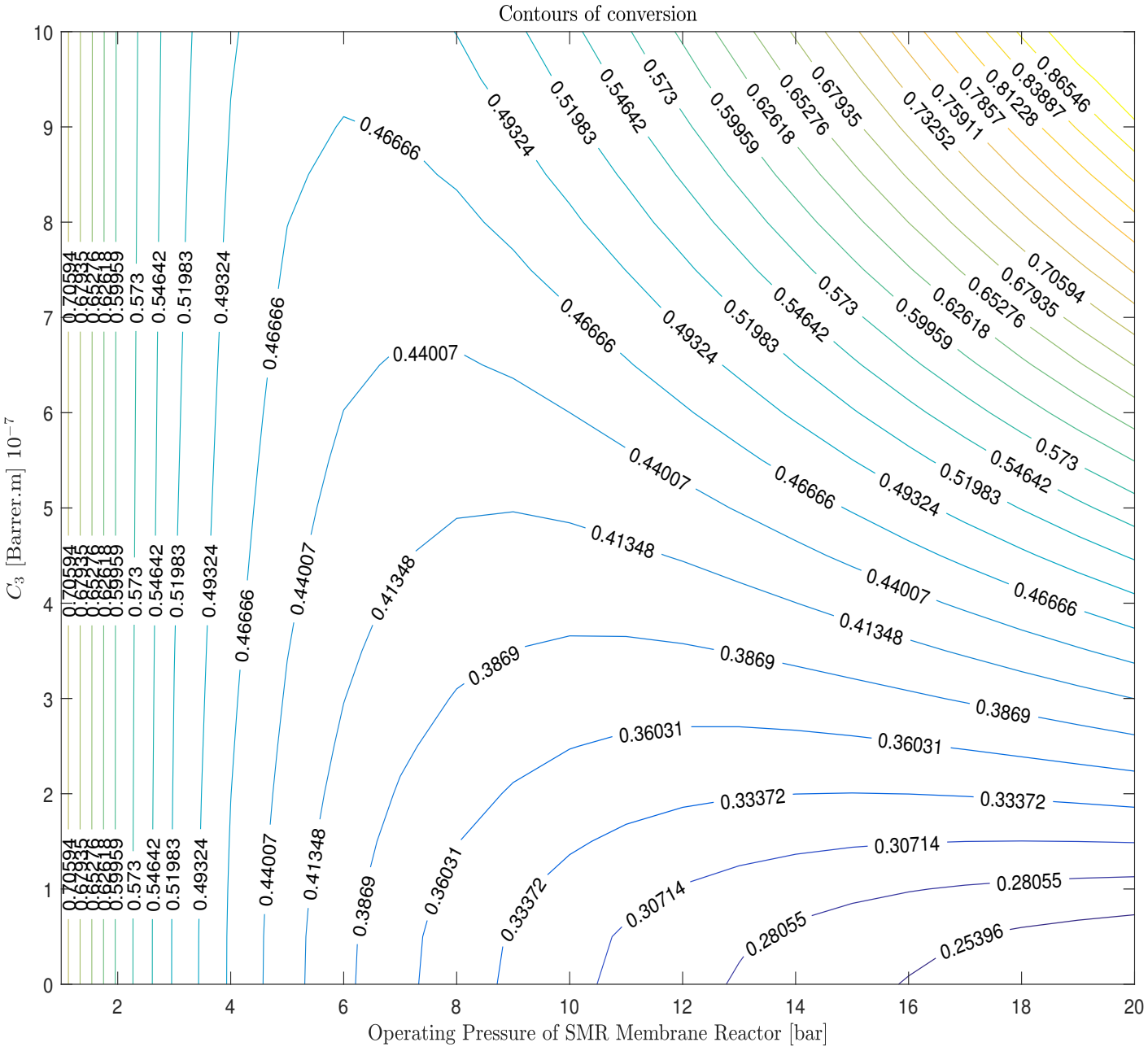

Figure 6.36: Conversion contours of the SMR membrane reactor for different operating pressures and C_3 values.

6.11.2 Discussion of Results

The subdivision of Figure 6.36 into regions 1-4 and discussion of the regions is not done in this section for the sake of brevity. The recommended design decisions in Section 6.5 are applicable here as well. While this model gives an intuitively correct trend, there are two drawbacks:

- First, since a novel model was developed, it is necessary to validate it with rigorous experimentation. This experimental work would provide further insight on which membranes operate according to Equation 6.26 and which membranes do not. Further, experimentation is also necessary to be able to quantify accurate values of C_3 for different membranes.
- The second drawback of this model is that it is not clear how to compare the estimated conversion results with those determined in Sections 6.5 - 6.10. This is because the conversion contours drawn for those sections have a C_1 variable on the y-axis, while a C_3 variable is used in the variable minimum flux model.

One may make a further criticism of this variable minimum flux model: One may note that Equation 6.26 only considers the partial pressure profile on the feed side to argue that this model is incorrect in that it is independent of the permeate pressure. However, the permeate pressure is taken into consideration in generating the partial pressure profiles in Figure 6.34. As mentioned, these partial pressure profiles were generated using the Sievert's law permeation model in Sections 6.4 to 6.6, which does include the permeate pressure in the procedure. Thus, this variable minimum flux model can be thought of as a hybrid model which combines insight obtained by making analogies with a heat exchanger with partial pressure profiles obtained using the Sievert's law permeation model.

6.12 Estimating conversion in the WGS MR with the variable minimum flux model

The reaction stage is identical to that used in Section 6.6 so is not discussed. Similarly, the separation stage is identical to that used in Section 6.11.

6.12.1 Results: Estimate of conversion of the WGS MR

Figure 6.37 shows the contours of conversion of the SMR MR for different C_3 values and operating pressures. Area contours can also be drawn.

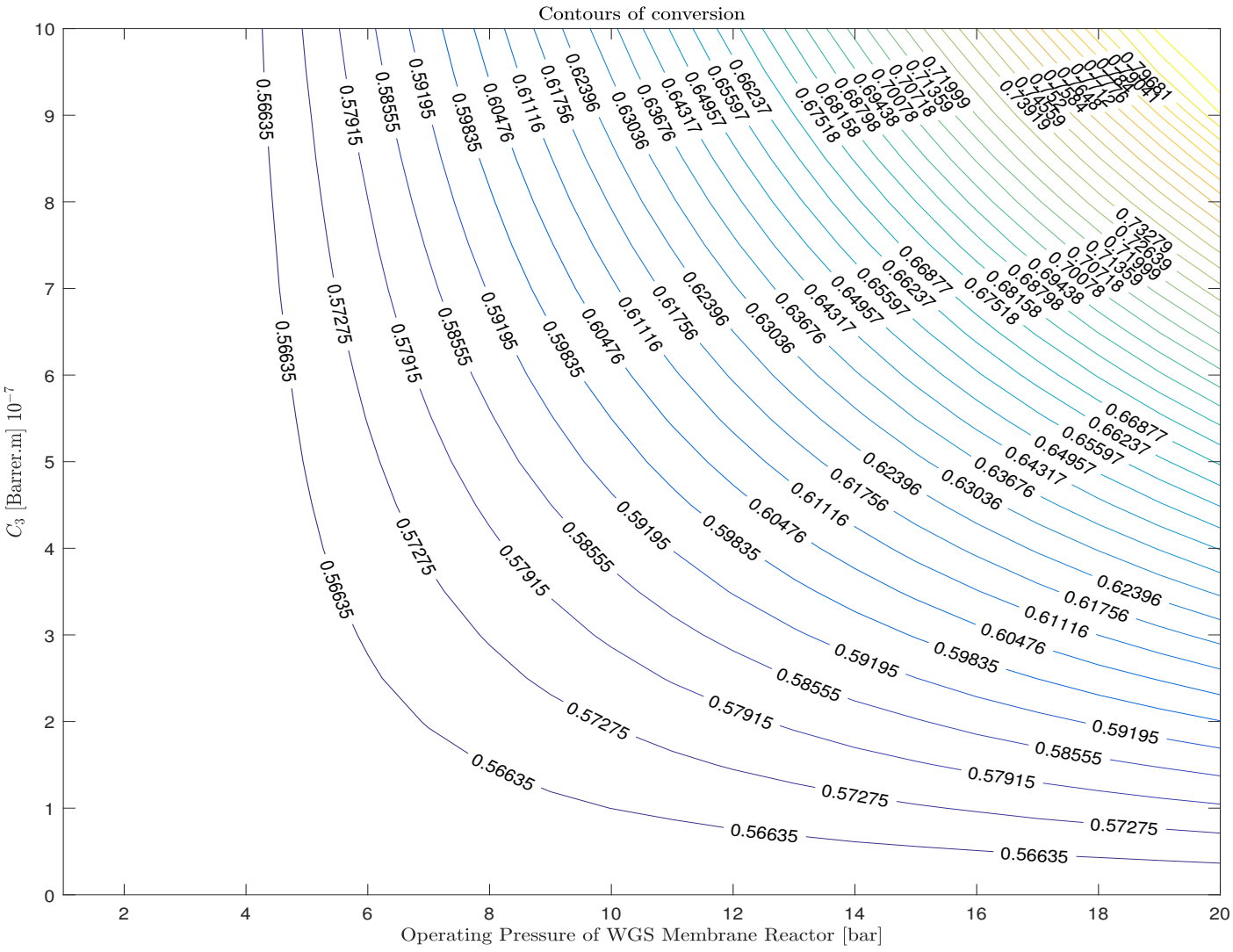

Figure 6.37: Conversion contours of the WGS membrane reactor for different operating pressures and C_3 values.

The discussion of results given in Section 6.11 is valid in this section as well.

6.13 Hydrogen Production Process using membrane reactors for the SMR and WGS reactions

Sections 6.2 - 6.12 show different procedures to estimate the conversion of the SMR and WGS MRs. Any permeation model can be used; the conversion estimates are then read off from the respective figures. In this case study, the Sievert's law permeation model of hydrogen through a palladium membrane is used. The rationale for using this model is that Palladium membranes are readily available and widely studied for use in hydrogen membrane reactors [35]. Thus, this permeation model is closest to the state-of-the-art in terms of hydrogen membrane reactors.

These conversion estimates can then be used in the G-H methodology to design a hydrogen production process that uses the SMR MR and WGS MR. In Chapter 4, the G-H methodology was extended to include cases in which the conversion was less than 1. A new term (the "multiple of the simplest stoichiometric feed" f) was coined for convenience in order to take the conversion into account. In order to design a hydrogen production process using a SMR MR and WGS MR, the conversion estimates from Sections 6.5 and 6.6 are used in the extended G-H methodology described in Chapter 4, with a minor modification. This modification deals with choosing the operating pressure of the overall process. In the extended G-H methodology of Chapter 4, the overall operating pressure was calculated in Step 7 (after conversion had already been taken into account in Step 3) so as to extract all the work available from the process. However, for the case of membrane reactors, the overall operating pressure is chosen first, and then the estimated conversion is read off from the conversion contours plotted in Sections 6.5 and 6.6. The procedure for process design is presented in the next sections. Step 1 and Step 2 are unchanged from Chapter 3, Step 3 onwards changes.

6.13.1 Step 3: Choose the overall operating pressure

It is desired to run the membrane reactor so as to give as high a conversion as possible without requiring excessively high membrane areas or permeabilities. From the design decisions recommended in Section 6.5, membrane reactor operating conditions are chosen such that the membrane operates in region 2. Region 1 is avoided because it is wasteful in terms of membrane area and permeability. Region 4 is also avoided because the operating pressure is too low to have any flux, and Region 3 is avoided because it has a lower range of conversion than region 2. In this case study, the operating pressure is chosen to be 10 bar for both the SMR and WGS MR. The $\frac{A_{total}}{L}$ value of 0.005 is chosen such that the membrane reactor operates in Region 2. Increasing the permeability always increases conversion. However, an excessively high permeability would entail high membrane manufacture costs. Considering this trade-off a permeability of 10 is chosen. With these operating conditions the conversion is estimated. The result are summarized in Table 6.5

Table 6.5: Operating conditions of the SMR MR and WGS MR and respective estimated conversions

		SMR MR	WGS MR
Operating Temperature	K	960.83	974.67
Operating Pressure	bar	10	10
$\frac{A_{total}}{L}$	m	0.005	0.005
Permeability	Barrer	10	10
C1	Barrer.m 10^{-7}	5	5
Conversion		0.8827	0.7465

6.13.2 Step 4: Obtain relations between reaction extents

This step is similar to Step 3 done in Chapter 3. Performing material balances for all the individual species, in moles:

$$N_{CH_4} = N^0_{CH_4} - f_{SMR}.c_{SMR} - e_{comb} \tag{6.27}$$

$$N_{H_2} = N^0_{H_2} + 3f_{SMR}.c_{SMR} + f_{WGS}.c_{WGS} \tag{6.28}$$

$$N_{CO} = N^0_{CO} + f_{SMR}.c_{SMR} - f_{WGS}.c_{WGS} \tag{6.29}$$

$$N_{CO_2} = N^0_{CO_2} + f_{WGS}.c_{WGS} + e_{comb} \tag{6.30}$$

$$N_{H_2O} = N^0_{H_2O} - f_{SMR}.c_{SMR} - f_{WGS}.c_{WGS} + 2e_{comb} \tag{6.31}$$

$$N_{O_2} = N^0_{O_2} - 2e_{comb} \tag{6.32}$$

The superscript "0" shows the number of moles of that component fed to the overall process, and the final number of moles out of the overall process is given by N without the superscript.

The following design decisions are made for individual unit operations:

- It is assumed that the only feed materials are: CH_4, H_2O and O_2. Thus: $N^0_{H_2} = N^0_{CO} = N^0_{CO_2} = 0$
- The methane feed is chosen to be: $N^0_{CH_4} = 1$. This can be any molar units, but mol/s is used for consistency. The overall process scales with this methane feed. Also, it is desired that all the methane is used up in the process, so $N_{CH_4} = 0$.

$$e_{comb} = 1 - f_{SMR}.c_{SMR} \tag{6.33}$$

- Since the WGS MR does not achieve complete conversion, N_{CO} is not equal to 0. Thus, Equation 6.29 cannot be utilized to derive a relationship between f_{WGS} and f_{SMR}. However noting that the WGS reaction uses carbon monoxide

produced from the SMR MR, the feed of CO to the WGS MR should be equal to the produced CO in the SMR MR. Thus:

$$f_{WGS} = f_{SMR}.c_{SMR} \tag{6.34}$$

Since complete conversion cannot be achieved in the WGS membrane reactor, there will be some unreacted carbon monoxide and steam after the WGS. In this case study, since it is desired to only use membrane reactors and no recycling, this unreacted feed is not utilized, and is disposed off.

- The amount of steam produced in the phase change reaction and in the combustion reactor should equal the sum of the steam reacting in the SMR MR and the steam fed into the WGS MR. Thus:

$$e_{phase} + 2f_{comb} = f_{SMR}.c_{SMR} + f_{WGS} \tag{6.35}$$

$$e_{phase} = f_{SMR}.c_{SMR} + f_{WGS} - 2f_{comb} \tag{6.36}$$

$$e_{phase} = 4f_{SMR}.c_{SMR} - 2 \tag{6.37}$$

6.13.3 Step 5: Choose overall adiabatic operating conditions

This step is similar to step 4 done in Chapter 3.

Overall heat and work balance:

$$\begin{pmatrix}\Delta H_{overall}\\ \Delta G_{overall}\end{pmatrix} = \begin{pmatrix}\Delta H_{SMR}\\ \Delta G_{SMR}\end{pmatrix}(f_{SMR}.c_{SMR}) + \begin{pmatrix}\Delta H_{WGS}\\ \Delta G_{WGS}\end{pmatrix}(f_{WGS}.c_{WGS}) + \begin{pmatrix}\Delta H_{phase}\\ \Delta G_{phase}\end{pmatrix}(e_{phase}) + \begin{pmatrix}\Delta H_{comb}\\ \Delta G_{comb}\end{pmatrix}(e_{comb}) \tag{6.38}$$

Express in terms of single variable f_{SMR}.

$$\begin{pmatrix}\Delta H_{overall}\\ \Delta G_{overall}\end{pmatrix} = \begin{pmatrix}\Delta H_{SMR}\\ \Delta G_{SMR}\end{pmatrix}(f_{SMR}.c_{SMR}) + \begin{pmatrix}\Delta H_{WGS}\\ \Delta G_{WGS}\end{pmatrix}(f_{SMR}.c_{WGS}.c_{SMR}) + \begin{pmatrix}\Delta H_{phase}\\ \Delta G_{phase}\end{pmatrix}(4f_{SMR}.c_{SMR} - 2) + \begin{pmatrix}\Delta H_{comb}\\ \Delta G_{comb}\end{pmatrix}(1 - f_{SMR}.c_{SMR}) \tag{6.39}$$

Substitute in values:

$$\begin{pmatrix}\Delta H_{overall}\\ \Delta G_{overall}\end{pmatrix} = \begin{pmatrix}206.12\\ 142.16\end{pmatrix}(0.8827f_{SMR}) + \begin{pmatrix}-41.19\\ -28.59\end{pmatrix}(0.8827 * 0.7465 * f_{SMR}) + \begin{pmatrix}44.01\\ 8.56\end{pmatrix}(4(0.8827)f_{SMR} - 2) + \begin{pmatrix}-802.35\\ -800.71\end{pmatrix}(1 - 0.8827f_{SMR}) \tag{6.40}$$

Choosing operating conditions to correspond to an overall adiabatic process, $\Delta H_{overall} = 0$ kW. Thus, the value of f_{SMR} can be obtained by solving Equation 6.40. The extents of all the other reactions can be obtained from this f_{SMR} value, the results are given in Table 6.6.

The negative sign of ΔG implies that the overall process produces work. Thus, the amount of work that can be extracted $W = 80.25$ kW.

Table 6.6: Heat and Work balance after Step 5

Unit operation		SMR	WGS	Water phase change	Combustion	Overall Process
Temperature	K	960.83	974.67	453.35	145,866.25	
Pressure	bar	10	10	10	10	
f		0.8743	0.7717	1.0868	0.2283	
c		0.8827	0.7465	1	1	
e=f.c		0.7717	0.5761	1.0868	0.2283	
ΔH	kW	159.06	-23.73	47.83	-183.17	0.00
ΔG	kW	109.71	-16.47	9.30	-182.79	-80.25

6.13.4 Step 6: Use realistic operating temperatures

For identical reasons as listed in Chapter 4, a lower combustion temperature of 1200.0 K is used rather than the Carnot temperature of 145,866.25 K. The maximum work that can be produced by the combustion reaction at 1200.0 K is 603.01 kJ/mol CH_4 as calculated in Step 5 of Chapter 4. The updated heat and work balance is given in Table 6.7.

Table 6.7: Heat and Work balance after Step 6

Unit operation		SMR	WGS	Water phase change	Combustion	Overall Process
Temperature	K	960.83	974.67	453.35	1200.0	
Pressure	bar	10	10	10	10	
f		0.8743	0.7717	1.0868	0.2283	
c		0.8827	0.7465	1	1	
e=f.c		0.7717	0.5761	1.0868	0.2283	
ΔH	kW	159.06	-23.73	47.83	-183.17	0.00
ΔG	kW	109.71	-16.47	9.30	-137.66	-35.12

6.13.5 Step 7: Include separation work

In Chapter 2, it was assumed that the work required for separation of the product from the reactor into its pure components is negligible. However, in a realistic process, this separation work is significant and needs to be included. Thus, Equation 2.14 is used to get the separation work of the product streams into pure components. Note that the hydrogen stream that is the permeate of the MR is already a pure stream. This implies that the separator is only used to partition the unreacted feed from the by-product. The results are given in Table 6.8

Table 6.8: Work balance including separation work after Step 7

$W_{sep,SMR}$	$W_{sep,WGS}$	$W_{sep,comb.}$	Total separation Work	Total recoverable Work
kW	kW	kW	kW	kW
1.5973	2.2901	1.0806	4.9680	30.1520

In Chapter 4, the operating pressure of the overall process was a degree of freedom that could be set to recover some of the available work from the process. However, for membrane reactors, the overall process operating pressure is not a degree of freedom since it was chosen in Step 3. For instance, in this case study, the overall operating pressure was chosen to be 10 bar in Step 3. Thus, all required degrees of freedom are fixed and the block flow diagram of the process can be drawn in Figure 6.38. The process flowsheet is presented in Figure 6.39. The stream data for both the material streams and the energy streams is provided in Appendix C.

It can be seen from Figure 6.38 that $n_{in} = 1.4566$ mol/s and $n_{out} = 1$ mol/s implying work is added to the process rather than recovered from the process. The amount of this work can be calculated:

$$W_{in} = (n_{in} - n_{out})RT_0 ln(P_{overall}/P_0) \tag{6.41}$$

$$W_{in} = (1.4566 - 1)(\frac{8.314}{1000})298.15 ln(\frac{10}{1.01325}) = 2.591\text{kW} \tag{6.42}$$

The process flowsheet was simulated in Aspen HYSYS, and an exergy analysis performed in order to provide a comparison with the other hydrogen production process designs.

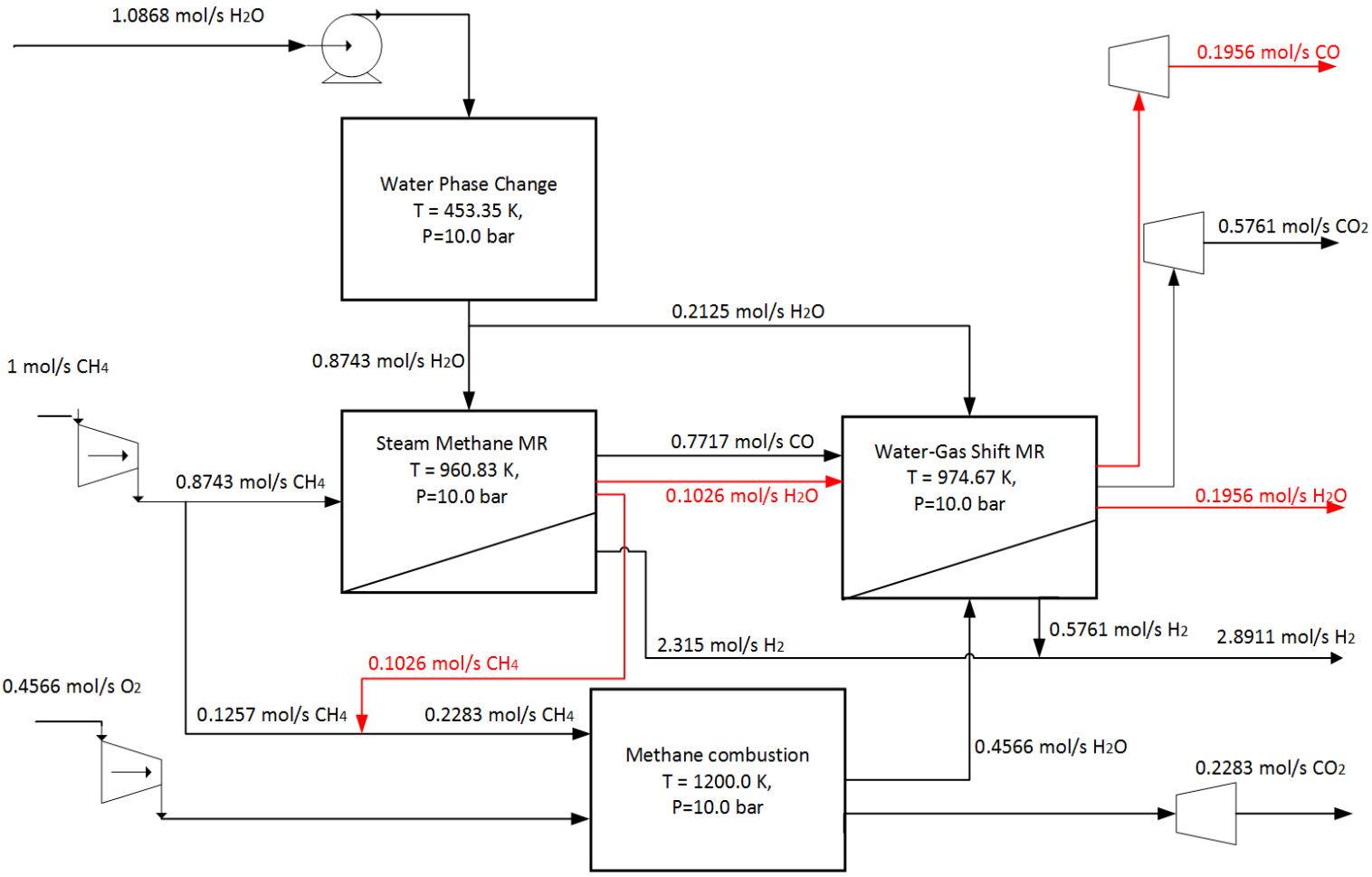

Figure 6.38: Block flow diagram of Hydrogen production process with SMR MR and WGS MR unit operations

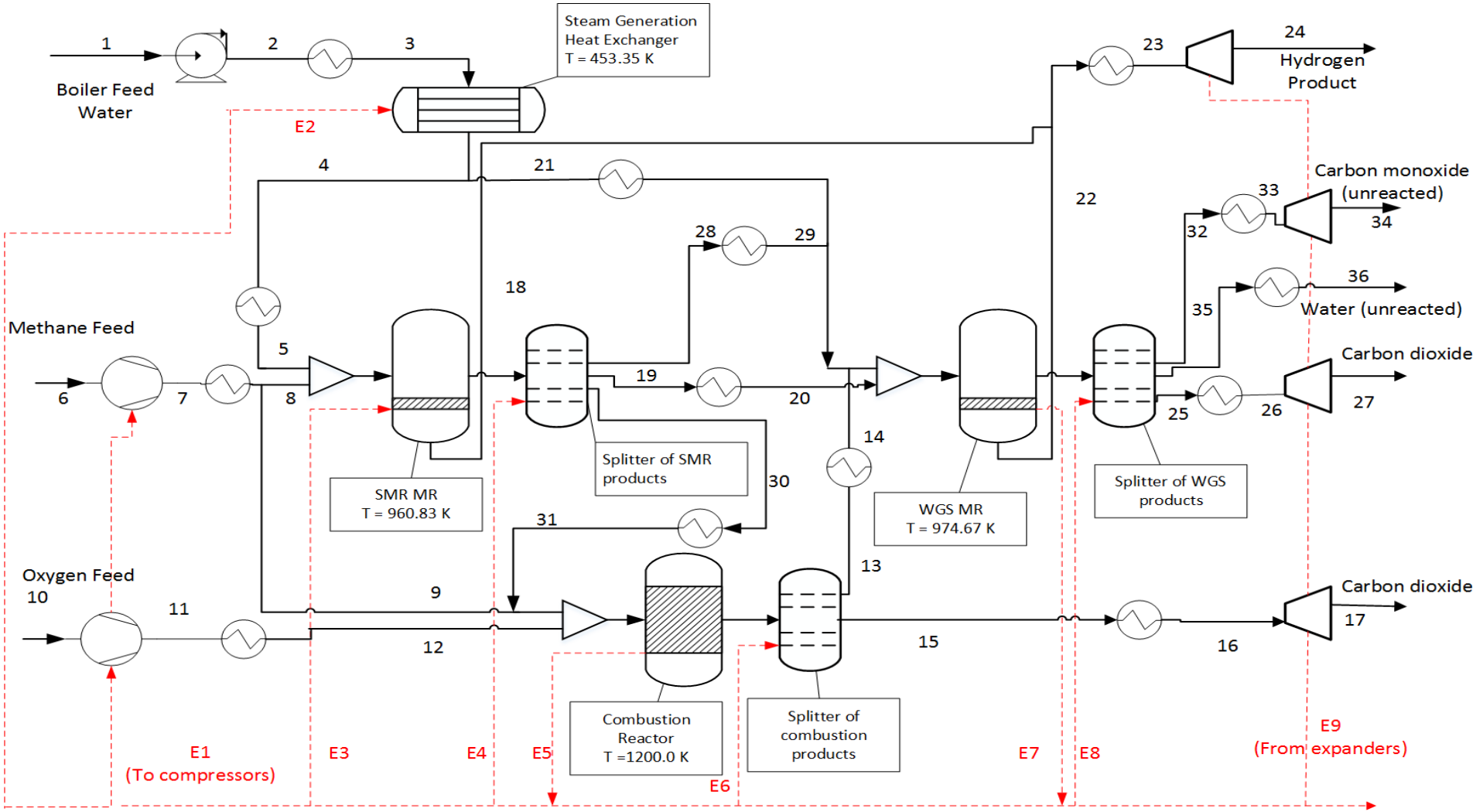

Figure 6.39: Flowsheet of Hydrogen production process with SMR MR and WGS MR unit operations

6.13.6 Overview of Exergy Analysis Results

Table 6.9 shows the exergy destroyed in the different unit operations of the hydrogen production process with the SMR MR and the WGS MR. A comparison with the state-of-the-art process described in Section 1.2 is also provided.

Table 6.9: Exergy Analysis of unit operations

Process: Component group	MRs Exergy destroyed kW/kmol CH_4	Percentage	State-of-the-art Exergy destroyed kW/kmol CH_4	Percentage
Steam Generation HX	780.00	0.87	44848.99	20.89
Feed mixers	5944.00	6.39	10223.17	4.76
Reformer	7025.00	3.61	29466.63	13.72
Water-Gas Shift	3540.00	5.38	16273.75	7.58
Furnace	45272.00	49.74	101829.91	47.42
Separation processes	12858.00	40.00	12096.83	5.63
Total Exergy Destroyed	75419.00		214739.27	

An exergy analysis of the overall process can also be performed. Table 6.10 shows the exergy analysis results of the overall process with the SMR MR and WGS MR, and the calculation of the overall process exergetic efficiency using Equation 1.4. Table 6.10 can be visualized in a pie chart as done in Figure 6.40. kW/kmol CH_4

Table 6.10: Exergy Analysis of overall process

Stream	Units	Methane In	BFW	Oxygen In	Qin	H_2 Out
Temperature	°C	25	25	25		25
Pressure	bar	10	10	10		1
Physical Exergy	kW/kmol CH_4	5637.58	23.30	2585.59		94.40
Mixing Exergy	kW/kmol CH_4	0.00	0.00	0.00		0.00
Chemical Exergy	kW/kmol CH_4	831650.00	978.12	1812.70		682551.25
Total Exergy	kW/kmol CH_4	837287.58	1001.43	4398.30	7633.00	682645.65
			Exergy In	850320.30	Exergy Out	682645.65
				Exergetic	Efficiency =	80.28

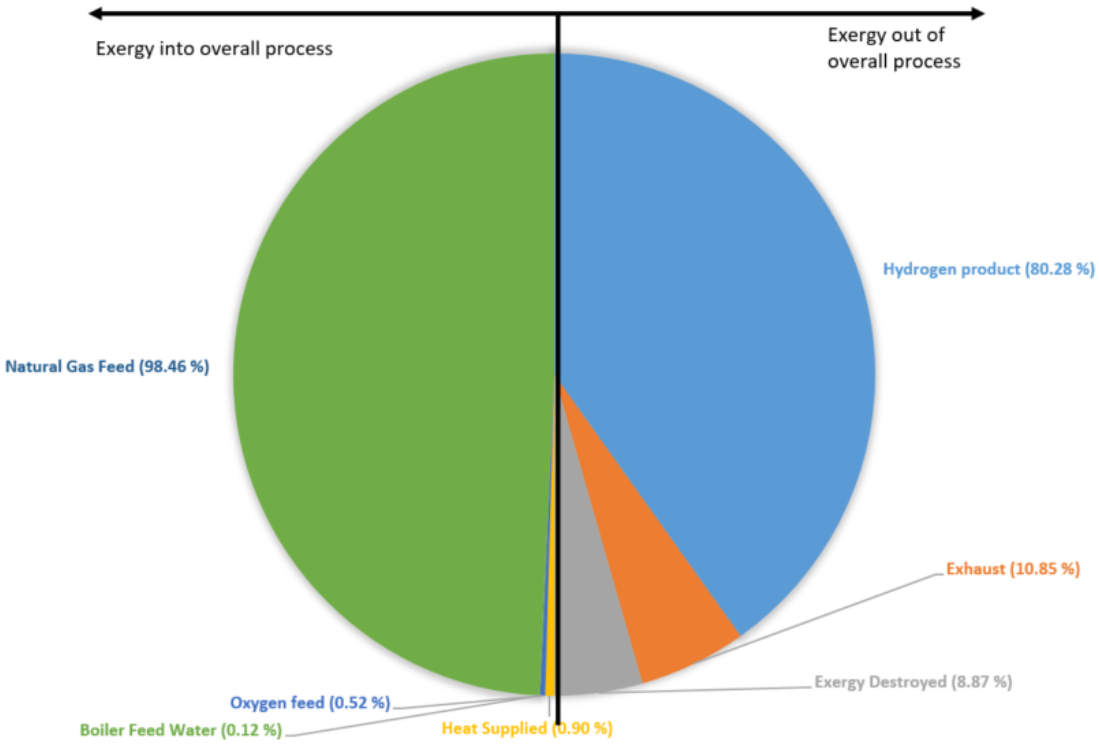

Figure 6.40: Pie chart to visualize the exergy analysis results of the overall hydrogen production process with SMR and WGS MRs

6.13.7 Discussions

This section is brief since several of the discussions made in Section 4.2.5 are applicable here as well. The caveats 1 - 5 also hold in this section. The following comments can be made with respect to Table 6.9:

- The total exergy destroyed is less than the state-of-the art process. Less exergy is destroyed because the SMR and WGS act more reversibly since they operate at their Carnot temperatures. Less exergy is destroyed in the furnace as well. The furnace is still the largest source of inefficiency due to identical reasons as in Section 4.2.5.

- The amount of exergy destroyed in the separation process is comparable with the corresponding exergy destruction in the state-of-the-art process. Compared with the exergy destruction values in separation for the processes with 100 % recycle and 80 % recycle in Chapter 4, this value is lower. The reason for this is that the membrane reactor produces a pure hydrogen product stream in the permeate. Thus, the separation process is only used to separate the unreacted feed from the by-product.

Table 6.10 shows the results of performing the exergy analysis on the entire overall process. The following comments can be made:

- The overall exergetic efficiency is lower (80.28 %) compared to the process with 80 % recycle (83.07 %) and the process with full recycle (87.28 %). This is

because the conversion in the WGS reaction is lower (at 0.7465) implying more exergy is lost in the exhaust stream containing the unreacted feed compared to the processes designed in Chapter 4. Approximately 26 % of the unreacted feed to the WGS reaction is disposed off in the exhaust stream, and thus does not form the valuable hydrogen product.

- The above point can also be made by comparing the exergy lost in the exhaust stream: This process loses 10.85 % of exergy in the exhaust stream which is higher than the process with 80 % recycle (6.8 %), and the process with 100 % recycle (1.08 %).

- The discussion on the heat supplied made in Section 4.2.5 is applicable here as well. The work supplied to the process (W_{in}) is included within the Q_{in} value in Table 6.10.

- Considering that the exergy lost in the exhaust stream decreases with increase in conversion, it is recommended to use membrane reactors that give as high a conversion as possible. However, this comes with a trade-off in terms of membrane reactor operating pressure, and membrane permeability and area: A membrane reactor with higher permeability and area, as well as higher operating pressure is more expensive in terms of investment costs but has a higher conversion. This implies that less exergy is lost as unreacted feed in the exhaust stream which in turn results in a higher overall process exergetic efficiency. Thus, there is a trade-off between membrane reactor investment cost and exergetic efficiency attainable. Optimization is necessary to determine the most suitable process operating points. This is left for later iterations in the detailed design phase.

6.14 Concluding remarks

In this chapter, both a methodological contribution as well as a process design contribution was made. The methodological contribution involved two aspects. First, a novel sequential model was formulated to estimate the conversion of a membrane reactor for three different permeation models. Both a lower-bound estimate as well as an upper-bound estimate of the conversion was determined. Second, this estimated conversion was used in the extended G-H methodology to include a membrane reactor unit operation in process design right from the conceptual design phase. The process design contribution was a case study used to demonstrate the methodological contributions. A conceptual stage hydrogen production process that used membrane reactors for the SMR and WGS reactions was designed. The extended G-H methodology was used to determine the relevant operating conditions: Operating Pressure, operating temperature, permeate pressure, membrane permeability, feed flow rate and composition, and total membrane area to thickness ratio. A flowsheet showing the process was presented and simulated in Aspen HYSYS, and an exergy analysis performed on the process.

The results of the exergy analysis showed that the process designed in this chapter had significantly lower exergy destruction values compared to the state-of-the-art process. The reason for the lower exergy destruction is that the SMR and WGS processes were running at their Carnot temperatures. In addition, a different combus-

tion reaction was used in the furnace and this resulted in lower exergy destruction as well. However, it was noted that the furnace is still responsible for the greatest exergy destruction; it is expected that this will continue in future designs because most combustion reactions of fossil fuels are inherently irreversible.

The overall exergetic efficiency (80.28 %) was higher than the state-of-the-art (75.03 %) but lower than the process with 100 % recycle (87.28 %) and the process with 80 % recycle (83.07 %). However, it is useful to note that the membrane reactor is an instance of process intensification implying that the hydrogen separation process is integrated within the reactor resulting in fewer units. This benefit of process intensification in terms of lower capital cost may out-weigh the impact of lower exergetic efficiency.

Lastly a trade-off exists between the membrane reactor investment cost and the exergy destruction: Higher conversion can be achieved by investing more in membrane area and permeability, as well as operating the process as higher pressure and this will reduce the exergy lost in the exhaust stream containing the unreacted feed.

Chapter 7

Using a highly intensified 1-step reaction

7.1 Introduction

In the previous sections, the modifications to the G-H methodology start after Step 3. The four reactions considered in Step 1 (the SMR reaction, the WGS reaction, the water phase change reaction and the combustion reaction) are unchanged. However, there may be other reactions, starting with a methane feed, that can be used in a hydrogen production process. Thus, a modification is made right from Step 1.

7.2 Step 1: Define the chemical reactions

An example of an alternative chemical reaction for hydrogen production from methane is presented in Equation 7.1. This reaction is termed hereafter as the "1-step reaction" .

$$\mathrm{CH_4(g) + 2\,H_2O\,(l) \rightleftharpoons CO_2(g) + 4\,H_2(g)} \tag{7.1}$$

The standard enthalpy and standard Gibb's energy of reaction are given as $\Delta H_{1,step} = 252.95$ kJ/mol, $\Delta G_{1,step} = 130.69$ kJ/mol (calculated using values in [6]). The 1-step reaction is also a reversible reaction.

The rationale for using the 1-step reaction for hydrogen production from methane is explained next:

- The 1-step reaction is an instance of process intensification. This is because the 1-step reaction is a combination of the SMR reaction, the WGS reaction and the phase change reaction: The 1-step reaction (Equation 7.1) can be obtained by adding the SMR reaction (Equation 1.1) to the WGS reaction (Equation 1.2) to twice the water phase change reaction (2* Equation 3.3). The corresponding ΔH and ΔG values are also added up. In practice, the summation of the three reactions to form the 1-step reaction is equivalent to housing the three different reactors in one unit operation. Thus, by using the 1-step reaction, the benefits of process intensification such as fewer units, lower capital and operating costs etc. can be attained.

- The Carnot temperature of the 1-step reaction is relatively low. As is calculated in later sections, $T_{Carnot,1step}$=616.86 K. This is much lower than the Carnot temperature of the SMR or WGS reactions. Since it is technologically feasible to run reactors at 616.86 K, it implies that is possible to design a 1-step reactor that is reversible.

From Equation 7.1, it can be seen that the 1-step reaction requires heat and work in order to proceed. Similar to previous chapters, this heat and work is supplied by using the exothermic methane combustion reaction.

$$\mathrm{CH_4(g) + 2\,O_2(g) \rightleftharpoons CO_2(g) + 2\,H_2O\,(g)} \tag{7.2}$$

The standard enthalpy and standard Gibbs energy of reaction are given as $\Delta H_{comb} = -802.35$ kJ/mol, $\Delta G_{comb} = -800.71$ kJ/mol [6].

7.3 Step 2: Plot reactions as vectors in G-H space. Determine Carnot temperatures.

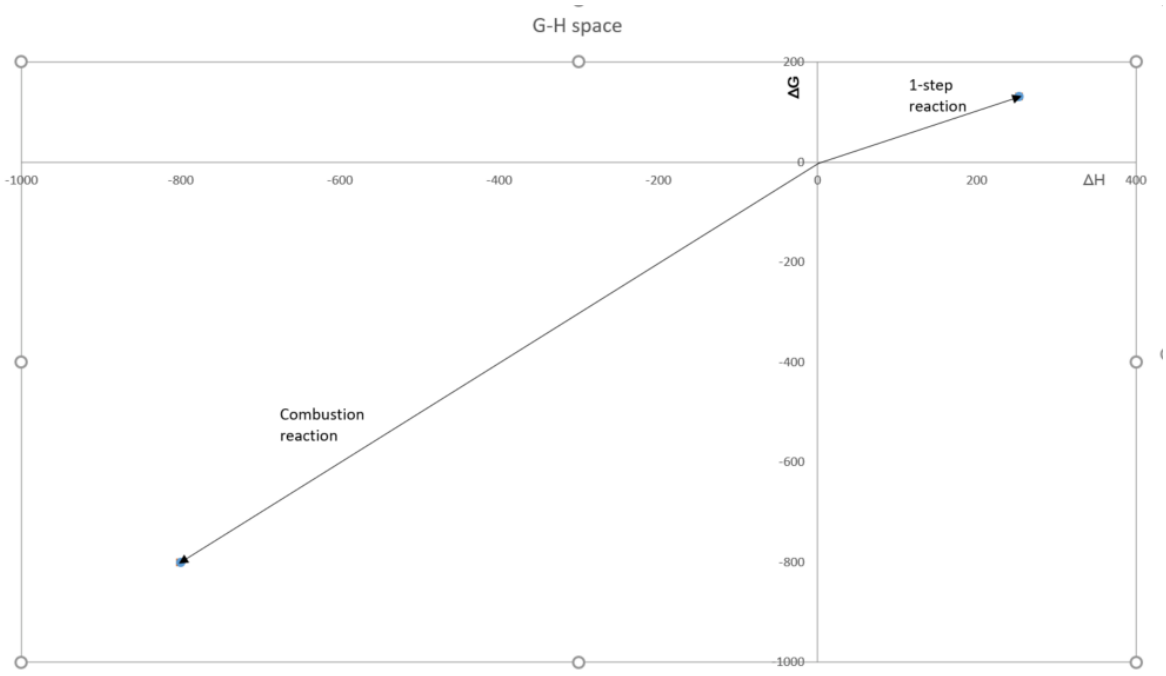

Figure 7.1: Plotting the 2 reactions on the G-H space

Equation 2.11 can be used to determine the Carnot temperatures of the reactions in Step 1. The Carnot temperature of the 1-step reaction $T_{Carnot,1step}$=616.86 K. The Carnot temperature of the methane combustion reaction is unchanged at $T_{Carnot,comb}$=145866.25 K.

7.4 Step 3: Obtain relations between reaction extents

This step is similar to Step 3 done in Chapter. It is desired that 100 % conversion is achieved. The method used to achieve this complete conversion is full recycle of unreacted feed as in Section 4.2. Since complete conversion is assumed, there is no need to use the extended G-H methodology developed in Chapter 4 - the basic G-H methodology presented in Chapter 3 is sufficient.

Performing material balances for all the individual species, in moles:

$$N_{CH_4} = N^0_{CH_4} - e_{1,step} - e_{comb} \tag{7.3}$$

$$N_{H_2O(l)} = N^0_{H_2O(l)} - 2e_{1,step} + 2e_{comb} \tag{7.4}$$

$$N_{CO_2} = N^0_{CO_2} + e_{1,step} + e_{comb} \tag{7.5}$$

$$N_{O_2} = N^0_{O_2} - 2e_{comb} \tag{7.6}$$

$$N_{H_2} = N^0_{H_2} + 4e_{1,step} \tag{7.7}$$

The superscript "0" shows the number of moles of that component fed to the overall process, and the final number of moles out of the overall process is given by N without the superscript.

The following design decisions are made for individual unit operations:

- It is assumed that the only feed materials are: CH_4, $H_2O(l)$ and O_2. Thus: $N^0_{H_2} = N^0_{CO_2} = 0$
- The methane feed is chosen to be: $N^0_{CH_4} = 1$. This can be any molar units, but mol/s is used for consistency. The overall process scales with this methane feed. Also, it is desired that all the methane is used up in the process, so $N_{CH_4} = 0$.

$$e_{comb} = 1 - e_{1,step} \tag{7.8}$$

7.5 Step 4: Choose overall adiabatic operating conditions

This is similar to Step 4 done in Chapter 3.

Overall heat and work balance:

$$\begin{pmatrix} \Delta H_{overall} \\ \Delta G_{overall} \end{pmatrix} = \begin{pmatrix} \Delta H_{1,step} \\ \Delta G_{1,step} \end{pmatrix} (e_{1,step}) + \begin{pmatrix} \Delta H_{comb} \\ \Delta G_{comb} \end{pmatrix} (e_{comb}) \tag{7.9}$$

Express in terms of single variable $e_{1,step}$.

$$\begin{pmatrix}\Delta H_{overall}\\ \Delta G_{overall}\end{pmatrix} = \begin{pmatrix}\Delta H_{1,step}\\ \Delta G_{1,step}\end{pmatrix}(e_{1,step}) + \begin{pmatrix}\Delta H_{comb}\\ \Delta G_{comb}\end{pmatrix}(1 - e_{1,step}) \tag{7.10}$$

Substitute in values:

$$\begin{pmatrix}\Delta H_{overall}\\ \Delta G_{overall}\end{pmatrix} = \begin{pmatrix}252.95\\ 130.69\end{pmatrix}(e_{1,step}) + \begin{pmatrix}-802.35\\ -800.71\end{pmatrix}(1 - e_{1,step}) \tag{7.11}$$

Choosing operating conditions to correspond to an overall adiabatic process, $\Delta H_{overall} = 0$ kW. Thus, the value of $e_{1,step}$ can be obtained by solving Equation 7.11. The extents of the combustion reaction can be obtained from this $e_{1,step}$ value, the results are given in Table 7.1. At this step, both reactions are fixed to operate at their Carnot temperatures.

The negative sign of ΔG implies that the overall process produces work. Thus, the amount of work that can be extracted $W_{out} = 92.57$ kW.

Table 7.1: Heat and Work balance after Step 4

		1-step reaction	Combustion	Overall Process
Operating temperature	K	616.86	145,866.25	
Operating pressure	bar	1	1	
e		0.7603	0.2397	
ΔH	kW	192.32	-192.32	0.00
ΔG	kW	99.36	-191.93	-92.57

7.6 Step 5: Use realistic operating temperatures

The combustion reaction has a Carnot temperature of 145,866.25 K, which is unrealistically high. In Chapter 4 an operating temperature of 1200 K was chosen for the combustion reaction. This operating temperature was used to supply heat and work to the WGS reaction at 974.67 K and the SMR reaction at 960.83 K. Thus, the choice of combustion operating temperature was constrained to be greater than or equal to 974.67 K.

However in this chapter, the combustion reaction is only used to provide heat and work to the 1-step reaction at 616.86 K. A lower operating temperature can be chosen as long as it greater than or equal to 616.86 K. In this step, the combustion temperature was chosen to be 616.86 K. Thus, the operating temperature of the combustion reaction is chosen to be identical to that of the 1-step reactor. The rationale for this choice is to include the possibility of housing the 1-step reactor and combustion reactor within the same unit operating at the same temperature. This would be a further example of process intensification: The combined process

would be an "auto-thermal 1-step process" meaning that the heat and work required for the 1-step process is provided by an in-situ methane combustion reaction. This further example of process intensification has the benefits of reducing the number of units as well as lowering capital and operating costs.

The maximum work that can be produced from a combustion reaction at 616.86 K can be obtained by substituting into Equation 4.1:

$$W_{comb} = 802.35(1 - \frac{298.13}{616.86}) = 414.57\text{kW} \tag{7.12}$$

Table 7.2 shows the updated heat and work balance:

Table 7.2: Heat and Work balance after Step 5

		1-step reaction	Combustion	Overall Process
Operating temperature	K	616.86	616.68	
Operating pressure	bar	1	1	
e		0.7603	0.2397	
ΔH	kW	192.32	-192.32	0.00
ΔG	kW	99.36	-99.37	0.01

7.7 Step 6: Include separation work

In Chapter 2, it was assumed that the work required for separation of the product from the reactor into its pure components is negligible. However, in a realistic process, this separation work is significant and needs to be included. Thus, Equation 2.12 is used to get the separation work of the product streams into pure components.

Table 7.3: Work balance including separation work after Step 6

$W_{sep,1step}$	$W_{sep,comb.}$	Total separation Work	Total recoverable Work
kW	kW	kW	kW
4.72	1.13	5.85	-5.84

The total recoverable work is negative implying that work has to be added to the overall process. This is undesirable. Since it is desired that the overall process does not depend on supplying work from outside, it is necessary to increase the temperature of the combustion process to supply this separation work. Equation 4.1 is used to calculate the new combustion temperature. Substituting values:

$$W_{comb} = 802.35(1 - \frac{298.15}{T_{comb.}}) = 414.57 + 5.84 = 420.41\text{kW} \tag{7.13}$$

Solving:

$$T_{comb} = 626.35K \tag{7.14}$$

Note that this combustion temperature is now no longer identical to the 1-step reactor temperature of 616.86 K, implying that the two processes can no longer be

intensified and housed in one unit. However, since the difference in temperature is small, it may be useful to run the 1-step reactor at 626.35 K in order to provide the option for process intensification. Thus, it may be useful to run the 1-step reaction at a temperature other than its Carnot temperature in order to gain the benefits of process intensification such as fewer units and lower capital and operating costs. This implies that there is a trade-off: The 1-step reactor becomes more irreversible as it is moved away from its Carnot temperature, but the number of reactor units decreases. This possibility is left open to be considered in later detailed design stages - in this chapter, the 1-step reaction is run at its Carnot temperature and process intensification is not considered.

With this combustion temperature there is no work available to be recovered; the process does not supply or require work. Since there is no work to be recovered, the operating pressure is 1 bar: There is no need for compression of feed and expansion of products.

Thus, all the required degrees of freedom are fixed and the block flow diagram of the process can be drawn in Figure 7.2. The process flowsheet is presented in Figure 7.3. The stream data for both the material streams and the energy streams is provided in Appendix C. The process flowsheet was simulated in Aspen HYSYS, and an exergy analysis performed in order to provide a comparison with the other hydrogen production process designs.

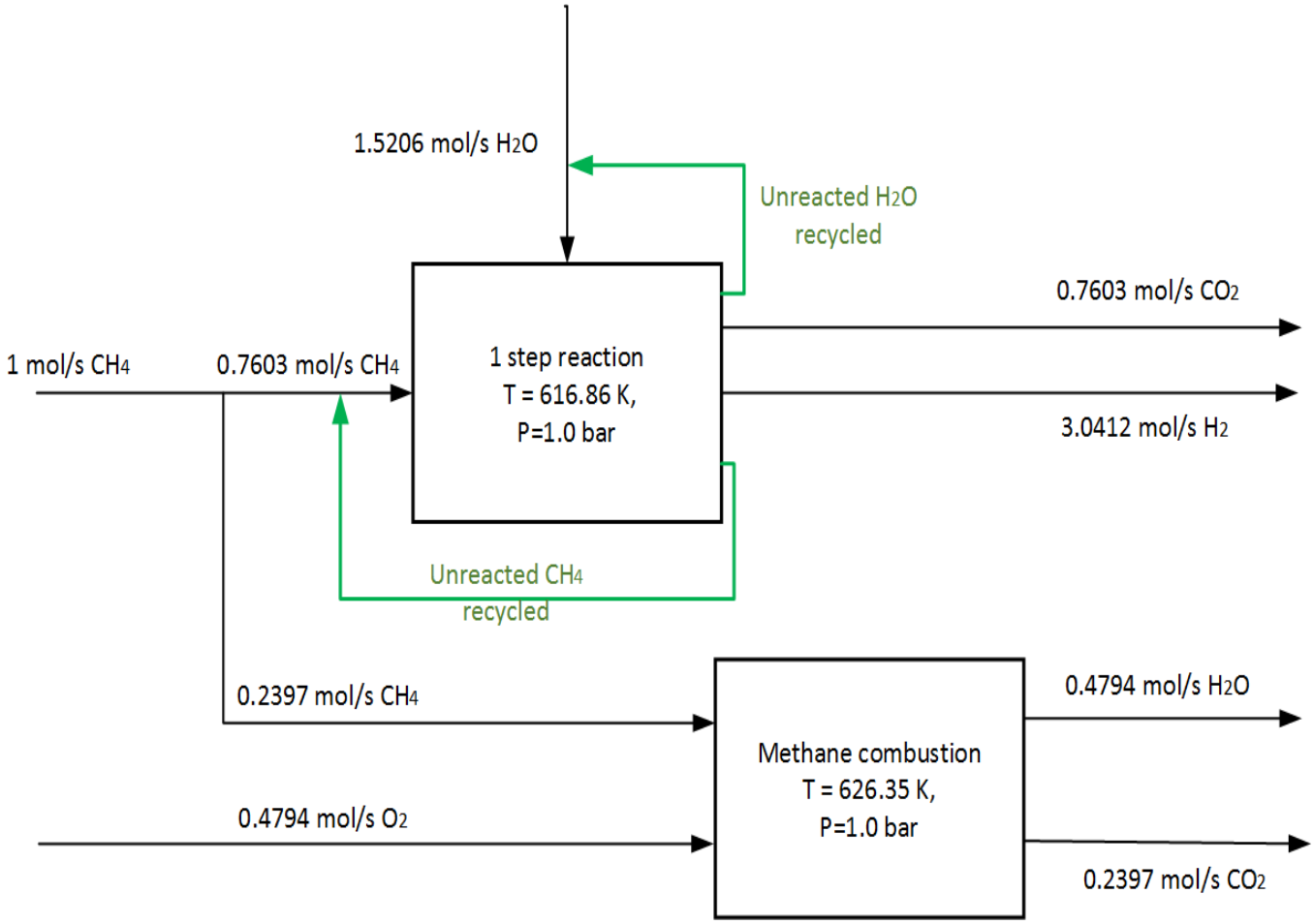

Figure 7.2: Block diagram of Hydrogen production process using the 1-step reaction

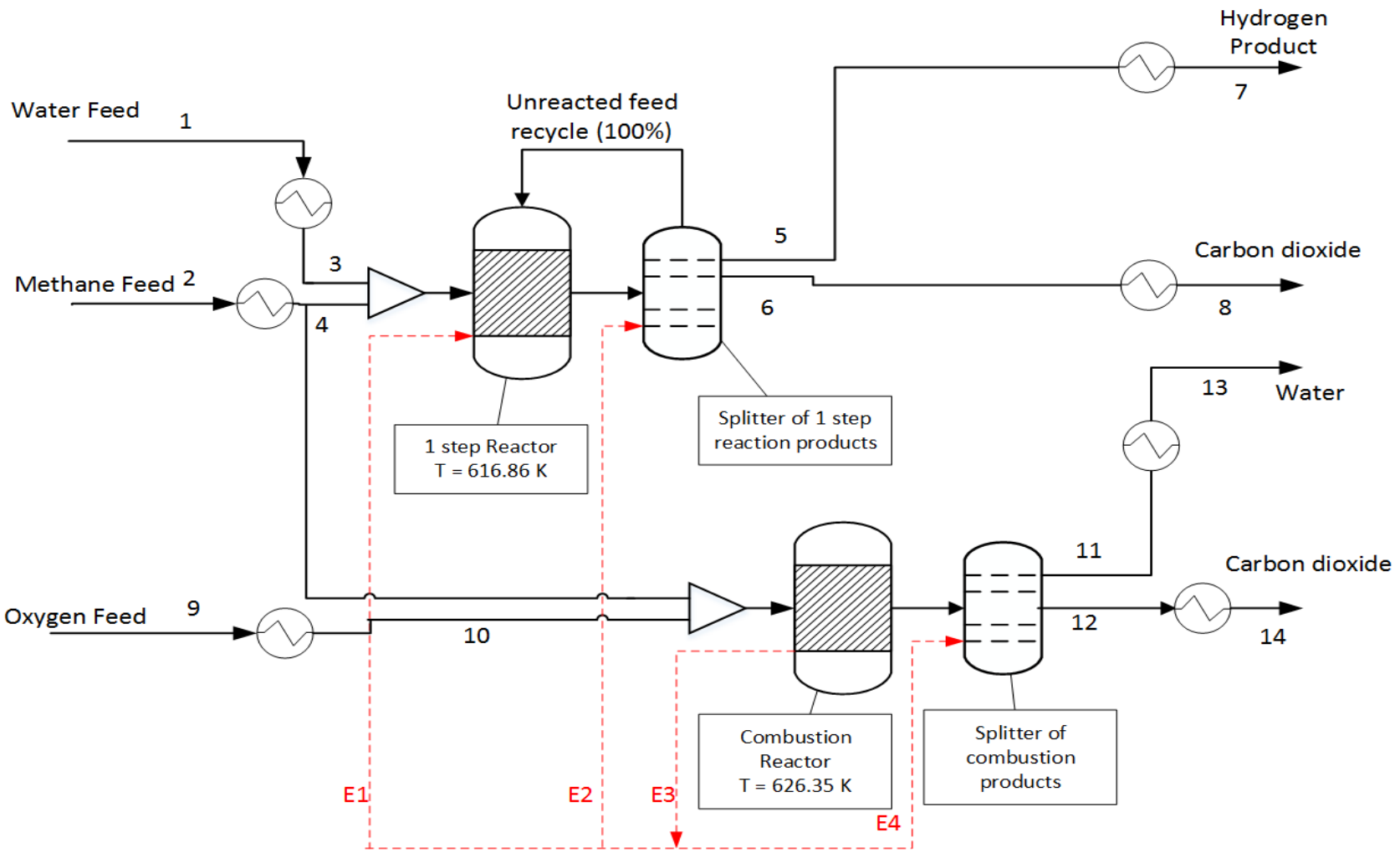

Figure 7.3: Flowsheet of Hydrogen production process using the 1-step reaction

7.8 Overview of Exergy Analysis Results and Comparisons with other processes

Since this is this is the last hydrogen production process designed in this Master's thesis, this section also includes a comparison with other processes presented in Chapters 4 - 6, as well as the state-of-the-art process. Table 7.4 shows the exergy destroyed in the different unit operations of the hydrogen production process for the 5 different processes.

An exergy analysis of the overall process with the 1-step reaction can also be performed. Table 7.5 shows the exergy analysis results of the overall process with the 1-step reaction, and the calculation of the overall process exergetic efficiency using Equation 1.4. Table 7.5 can be visualized in a pie chart as done in Figure 7.4. The overall process exergetic efficiency values for all the 5 processes are presented in Table 7.6

Table 7.4: Exergy Analysis results for the 5 different processes

Process:	State-of-the-art	100% recycle	80 % recycle	Membrane Reactor	1-step process
Component group	Exergy destroyed kW/kmol CH_4	Exergy destroyed kW/kmol CH_4	Exergy destroyed kW/kmol CH_4	Exergy destroyed kW/kmol CH_4	Exergy destroyed kW/kmol CH_4
Steam Generation HX	44849	821	792	780	-
Feed mixers	10223	6343	5798	5944	4732
Reformer	29466	7771	3272	7025	8824
Water-Gas Shift	16274	10290	4886	3540	
Furnace	101830	43927	45108	45272	91348
Separation processes	12097	35388	30834	12858	32564
Total Exergy Destroyed	214739	104540	90690	75419	137468

Table 7.5: Exergy Analysis of overall process with 1-step reaction

Stream	Units	Methane In	BFW	Oxygen In	Qin	H2 out
Temperature	°C	25	25	25		25
Pressure	bar	1	1	1		1
Physical Exergy	kW/kmol CH_4	0	0	0		0
Mixing Exergy	kW/kmol CH_4	0	0	0		0
Chemical Exergy	kW/kmol CH_4	831617.43	1368.54	1887.58		717928.02
Total Exergy	kW/kmol CH_4	831617.43	1368.54	1887.58	38058.00	717928.02
			Exergy In	872931.55	Exergy Out	717928.02
						82.24

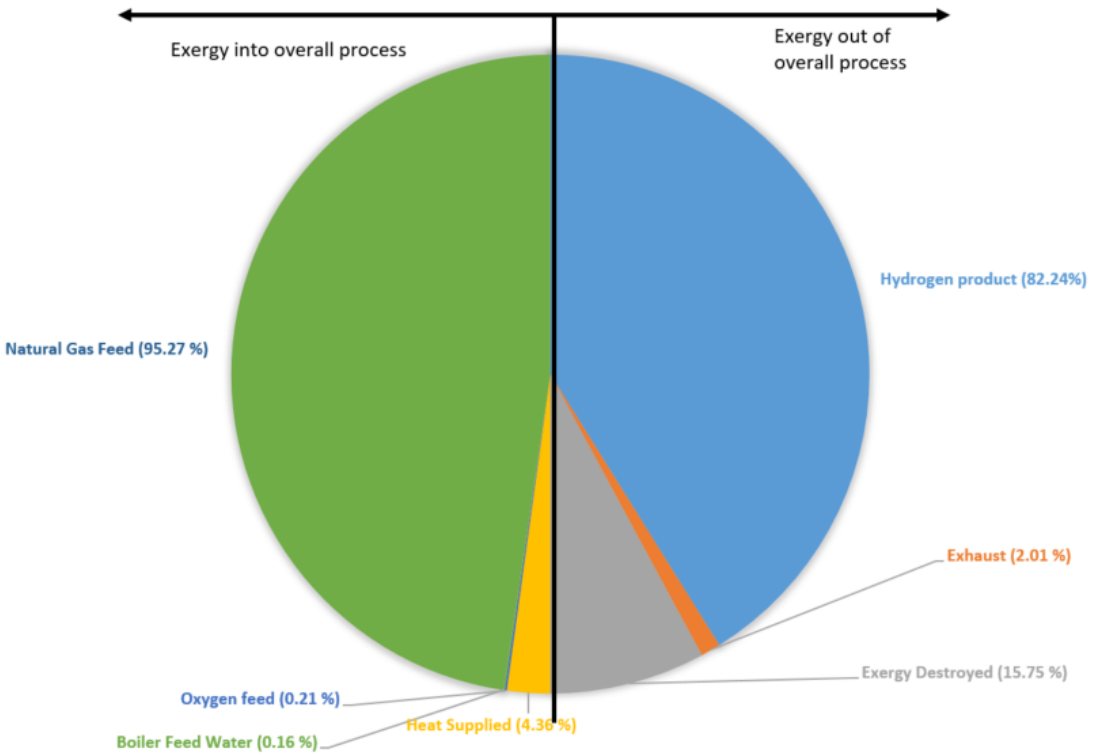

Figure 7.4: Pie chart to visualize the exergy analysis results of the overall hydrogen production process with 80 % recycle

Table 7.6: Comparison of the exergetic efficiencies of the different processes

Process:	State-of-the-art	100% recycle	80 % recycle	MR	1-step process
Exergetic efficiency (%)	75.03	87.28	83.07	80.28	82.24

7.8.1 Discussions

Several of the discussions made in Section 4.2.5 are applicable here as well. The caveats 1 - 5 also hold in this section. The following comments can be made with respect to Table 7.4:

- The total exergy destroyed is less in the 1-step process than the state-of-the art process. The exergy destroyed in the 1-step reaction is 88224 kW/kmol CH_4. This value has to be compared with the sum of the exergy destroyed in the SMR, WGS and phase change reaction since the 1-step process intensifies all these three processes into one. The exergy destroyed in the 1-step reaction is much lower than this sum because the 1-step process operates at its Carnot temperature. Also the exergy destroyed in the 1-step reaction is lower than the corresponding sum of the three exergy destruction values for all the other processes designed (the process with 100 % recycle, the process with 80 % recycle and the process with SMR and WGS MRs).
- However, the exergy destroyed by the combustion reaction in the 1-step process is much higher than the corresponding exergy destruction for any of the other

designed processes (the process with 100 % recycle, the process with 80 % recycle and the process with SMR and WGS MRs). This can be explained by the the operating temperature of the methane combustion reaction. In the 1-step reaction process, the furnace was set to operate at 626.35 K while in the other three process designs, it was set at 1200.0 K. The Carnot temperature of the methane combustion reaction is unrealistically high at 145,866.25 K - any deviation from this temperature results in exergy destruction. As can be seen, the furnace operating temperature deviates more from the Carnot temperature than the other three processes implying greater exergy destruction.

- The furnace is still the unit operation responsible for the largest source of inefficiency in all the 5 processes. This is expected because the operating temperature of the furnace was changed significantly from its Carnot temperature in the designed processes. It is thought that the furnace process will continue to be the source of largest exergy destruction because most fossil fuel combustion reactions have unrealistically high Carnot temperatures. Combustion of some fossil fuels such as coal is inherently irreversible because the Carnot temperature is negative.

  Future design efforts should focus on figuring out alternatives to methane combustion for providing the heat and work required for the other unit operations. One possibility that can be studied is to recover heat from hot streams available in the background process. For instance, heat integration could be done with the high temperature flue gas from power generation plants.

- The table also shows that the exergy destroyed in a unit operation is proportional to the conversion in that unit operation, all other operating conditions kept constant. This can be seen by studying the exergy destroyed in the WGS reaction in the process with 100 % recycle, 80 % recycle and with MRs: The exergy destruction is greatest in the process with 100 % recycle (complete conversion), followed by the process with 80 % recycle (conversion of 0.8) and finally the WGS MR (conversion of 0.7465). This trend can also be seen in the SMR unit operation: the process with 100 % recycle has the greatest exergy destruction, followed by the SMR MR (conversion of 0.8827) and lastly the process with 80 % recycle.

Table 7.5 shows the results of performing the exergy analysis on the entire overall process with the 1-step reaction. The following comments can be made:

- The overall exergetic efficiency is 82.24 %, lower than the two processes with recycle of unreacted feed but higher than the other processes, including the state-of-the-art process. The exergetic efficiency is lower than the processes designed including recycles because more exergy is destroyed in the furnace of the 1-step process as discussed above. However, much less exergy is destroyed compared to the state-of-the-art process.

- Very little exergy is lost in the exhaust stream because complete conversion is achieved in the 1-step process implying no unreacted feed is lost in the exhaust.

- The discussion on the heat supplied made in Section 4.2.5 is applicable here as well. This heat supplied addresses the assumptions made in formulating the G-H methodology in Section 2.1.

Table 7.6 shows the results of performing the exergy analysis on the entire overall process with the 1-step reaction. The following comments can be made:

- All the 4 processes designed in this Master's thesis have a higher overall exergetic efficiency than the state-of-the-art process. The reason for this is the SMR, WGS or 1-step reaction unit operations are operating at their Carnot temperature resulting in more reversible overall processes. In addition, the furnace destroys less exergy compared to the state-of-the-art. As elaborated upon in Chapter 4, this comparison entails several caveats arising from the fact that the state-of-the-art process corresponds to a detailed design phase while the other process are at the conceptual design phase. Thus, after detailed design, several irreversibilities will be added to the conceptual designs resulting in lower overall exergetic efficiency.

- Despite the fact that the 1-step process and the process with SMR and WGS membrane reactors have lower exergetic efficiencies compared to the two processes with recycling, they also are highly intensified processes. These intensified processes may be desired because they have fewer units and lower investment costs. For instance, the 1-step process has only 2 reactors compared to 4 reactors in other processes. For this reason, the 1-step reaction shows great promise for energy and cost-efficient hydrogen production.

- It can also be seen that the greater the conversion, the greater the exergetic efficiency as a result of less exergy loss in the exhaust stream in unreacted feed. Thus, it is desired to aim for as high a conversion as possible.

7.9 Concluding remarks

In this chapter, the 1-step process was designed at the conceptual stage using the G-H methodology. The 1-step reaction represents a highly intensified process in which the SMR, WGS and the phase change reactions are housed in one reactor. In addition, the 1-step process has a realistic Carnot temperature. Hence the 1-step reaction shows great promise for energy efficient hydrogen production. Complete conversion was assumed. A block flow diagram and process flowsheet are presented. The 1-step process was also simulated using Aspen HYSYS and an exergy analysis was performed. A comparison with the exergy analysis results of the other processes was also presented and discussed.

The results of the exergy analysis showed that the 1-step process had a significantly lower exergy destruction value compared to the state-of-the-art process. However, more exergy was destroyed compared to the two processes with 100 % and 80 % recycle, especially in the furnace. This is because the operating temperature of the furnace for the 1-step process has a greater deviation from its Carnot temperature than the furnace operating temperatures of the processes with 100 % and 80 % recycle.

Chapter 8

Conclusions and Future Work

8.1 Conclusions

In this Master's thesis, the G-H methodology was used and extended for conceptual design of energy efficient hydrogen production processes from natural gas. The G-H methodology was presented as a series of steps that culminated in hydrogen production process flowsheets. 5 different processes were designed. 4 of the processes used the SMR and WGS reactions to produce hydrogen. They were distinguished based on the method they used to achieve a certain conversion. These 4 processes were: Hydrogen production using 100 % recycle of unreacted feed to achieve complete conversion, hydrogen production using 80 % recycle of unreacted feed, hydrogen production using different feed ratios obtained by 100 % recycle of only one of the unreacted feed components, and hydrogen production using membrane reactors for the SMR and WGS reactions. The 5th hydrogen production process used a different reaction, termed the "1-step reaction", and achieved complete conversion by 100 % recycle of unreacted feed. These different process flowsheets were simulated using Aspen HYSYS and an exergy analysis performed. The overall process exergetic efficiency was calculated in order to provide a fair basis for comparison between the processes.

The process with 100 % recycle of both unreacted components had the highest overall exergetic efficiency (87.28 %). It corresponded to complete conversion. Thus, the G-H methodology could be directly applied for its design. The high exergetic efficiency comes about as a result of running the SMR and WGS reactions at their Carnot temperatures which results in a more reversible process. In addition, lower exergy is destroyed in the furnace. The higher exergetic efficiency implies that a greater percentage of the methane feed is converted to valuable hydrogen product.

The process with 80 % recycle had a lower conversion. This incomplete conversion implied that the G-H methodology could not be directly applied. An extended G-H methodology was developed to address this issue of incomplete conversion. This process design had the second highest exergetic efficiency (83.07 %). This is lower than the process with 100 % recycle because more exergy leaves the process in the exhaust containing the unreacted feed. Thus, it is recommended to aim for as high a conversion value as possible.

In the third process, the ratio of the feed components was changed in order to increase conversion. Specifically, water was fed in excess in order to increase the conversion of the SMR and WGS reaction. However, the required flowrate of water

to achieve complete conversion was very high making this option impractical. It was pointed out that recycling of water back to the SMR and WGS reactors is an alternative way of achieving complete conversion by changing the feed. This process had operating conditions identical to the process with 100 % recycle of both components of the unreacted feed.

In order to extend the G-H methodology to the case of using membrane reactors (MRs) in the SMR and WGS unit operations, a novel sequential model was developed to estimate the conversion. Different permeation models were used in the MRs and these corresponded to upper-bound and lower-bound estimates of conversion. With these conversion estimates the extended G-H methodology was used to design a hydrogen production process with an SMR and WGS MR unit operation. This process had an exergetic efficiency of 80.28 % - lower than the processes with recycle of unreacted feed because the conversion achieved in the MR is lower implying more exergy is lost in the exhaust containing the unreacted feed. Despite this lower exergetic efficiency, membrane reactors are a promising option because they represent a highly intensified process: The reaction process and the separation process is put together in one unit resulting in fewer total units.

The 1-step reaction also results in a highly intensified process since the phase change, SMR and WGS reactions are housed in the same unit. In addition, the 1-step process has the advantage of having a low Carnot temperature at which the process operates reversibly. The furnace for the 1-step process was chosen to have a lower operating temperature and this resulted in a larger exergy destruction compared to the processes that use recycling. The overall exergetic efficiency was 82.24 %.

With the overall exergetic efficiency results, it is recommended that the process with 100 % recycle of both components of unreacted feed is chosen. However, the 1-step reaction as well as the process with SMR and WGS membrane reactors show great promise as energy and cost-efficient hydrogen production processes.

8.2 Future work

The scope of this Master's thesis was limited to the conceptual design phase using a systems-level approach. Detailed modeling of each unit operation is not done in this stage - instead the process flowsheet is developed at the systems-level to show the interconnections between the different unit operations. The next step is to carry out detailed design of the unit operations such that they operate realistically. For instance, pressure drops can be calculated and implemented in reactors and heat exchangers, and adiabatic efficiencies chosen for the compressors and expanders. Inclusion of these considerations results in a lower exergetic efficiency than that calculated in this thesis. Thus, the flowsheets represent ideal targets that set the direction for the detailed design stages.

At the detailed design stage kinetics considerations are important. Thus, it may be necessary to change the operating conditions (for instance increase the operating pressure) in order to ensure a sufficiently high rate of reaction. It is important to model the different unit operations and investigate the process kinetics. With this aim, it may be necessary to use different catalysts (for instance Palladium or Nickel catalysts) in the reactions taking place.

Finally, future design efforts should focus on figuring out alternatives to methane

combustion for providing the heat and work required for the other unit operations. One possibility that can be studied is to recover heat from hot streams available in the background process. For instance, heat integration could be done with the high temperature flue gas from power generation plants.

Bibliography

[1] International Energy Agency. *Energy Technology Perspectives*. 2016.

[2] Avinash Shankar Rammohan Subramanian. *Novel Concepts for Hydrogen Production from Natural Gas*. Norwegian University of Science and Technology, 2016.

[3] Heinz Hiller, Rainer Reimert, Friedemann Marschner, Hans-Joachim Renner, Walter Boll, Emil Supp, Miron Brejc, Waldemar Liebner, Georg Schaub, Gerhard Hochgesand, et al. "Gas production". *Ullmann's encyclopedia of industrial chemistry* (2006).

[4] Mari Voldsund, Kristin Jordal, and Rahul Anantharaman. "Hydrogen production with CO_2 capture". *International Journal of Hydrogen Energy* (2016).

[5] Ke Liu, Chunshan Song, and Velu Subramani. *Hydrogen and syngas production and purification technologies*. Wiley Online Library, 2010.

[6] James Alistair Fox, Diane Hildebrandt, David Glasser, and Bilal Patel. "A graphical approach to process synthesis and its application to steam reforming". *AIChE Journal* (2013).

[7] Lars Olof Nord. "Pre-combustion CO_2 capture: Analysis of integrated reforming combined cycle". PhD thesis. Norwegian University of Science and Technology, 2010.

[8] Kun Wang and Mari Voldsund. *Hydrogen Production with CO_2 Capture*. SINTEF Energy Research, 2016.

[9] Adam P. Simpson and Andrew E. Lutz. "Exergy analysis of hydrogen production via steam methane reforming". *International Journal of Hydrogen Energy* 18 (2007), pp. 4811–4820.

[10] Robin Smith. *Chemical process design and Integration*. Wiley Online Library, 2016.

[11] Truls Gundersen. "A process integration primer—Implementing agreement on process integration". *Trondheim, Norway: International Energy Agency, SINTEF Energy Research* (2000).

[12] Lorenz T Biegler, Ignacio E Grossmann, and Arthur W Westerberg. "Systematic methods for chemical process design" (1997).

[13] James Alistair Fox, Diane Hildebrandt, David Glasser, Bilal Batel, and Brendon Hausberger. "Process flow sheet synthesis: Reaching targets for idealized coal gasification". *AIChE Journal* (2014).

[14] Truls Gundersen. *Lecture notes in Energy Utilization and Process Integration*. Jan. 2016.

[15] James Merrill Douglas. *Conceptual design of chemical processes*. McGraw-Hill New York, 1988.

[16] Alexandre C Dimian and Costin Sorin Bildea. *Chemical process design: computer-aided case studies*. John Wiley & Sons, 2008.

[17] Gijsbert Korevaar. *Sustainable Chemical Processes and Products: New Design Methodology and Design Tools*. Eburon Uitgeverij BV, 2004.

[18] Ignacio E Grossmann, Jose Antonio Caballero, and Hector Yeomans. "Advances in mathematical programming for the synthesis of process systems". *Latin American Applied Research* (2000).

[19] Mahmoud M El-Halwagi. *Process integration*. Academic Press, 2006.

[20] Bilal Patel. "Fundamental targets for the synthesis and evaluation of chemical processes". PhD thesis. Faculty of Engineering and the Built Environment, University of Witwatersrand, Johannesburg, 2007.

[21] Yunus A Cengel and Michael A Boles. *Thermodynamics: an engineering approach*. 1994.

[22] Adrian Bejan, Michael J. Moran, and G Tsatsaronis. *Thermal Design and Optimization*. 1996.

[23] Jan Szargut, David R Morris, and Frank R Steward. *Exergy Analysis of Thermal, Chemical, and Metallurgical Processes*. 1988.

[24] Tadeusz Jozef Kotas. *The exergy method of thermal plant analysis*. Elsevier, 2013.

[25] Bilal Patel, Diane Hildebrandt, David Glasser, and Brendon Hausberger. "Thermodynamics analysis of processes. 1. Implications of work integration". *Industrial & engineering chemistry research* (2005).

[26] Bilal Patel, Diane Hildebrandt, and David Glasser. "An overall thermodynamic view of processes: Comparison of fuel producing processes". *Chemical Engineering Research and Design* (2010).

[27] Baraka Celestin Sempuga, Brendon Hausberger, Bilal Patel, Diane Hildebrandt, and David Glasser. "Classification of chemical processes: a graphical approach to process synthesis to improve reactive process work efficiency". *Industrial & Engineering Chemistry Research* (2010).

[28] Truls Gundersen. "An introduction to the concept of exergy and energy quality". *Norwegian University of Science and Technology, Version* (2011).

[29] Ira N. Levine. *Physical Chemistry*. McGraw-Hill, 2002.

[30] R Smith and B Linnhoff. "The design of separators in the context of overall processes". *Chemical engineering research & design* (1988).

[31] Jacob A Moulijn, Andrzej Stankiewicz, Johan Grievink, and Andrzej Górak. "Process intensification and process systems engineering: a friendly symbiosis". *Computers & Chemical Engineering* (2008).

[32] Juan Gabriel Segovia-Hernández and Adrián Bonilla-Petriciolet. *Process Intensification in Chemical Engineering: Design Optimization and Control*. Springer, 2016.

[33] David Reay, Colin Ramshaw, and Adam Harvey. *Process Intensification: Engineering for efficiency, sustainability and flexibility*. Butterworth-Heinemann, 2013.

[34] Samhun Yun and S Ted Oyama. "Correlations in palladium membranes for hydrogen separation: a review". *Journal of membrane science* (2011).

[35] Marcello De Falco, Luigi Marrelli, and Gaetano Iaquaniello. *Membrane reactors for hydrogen production processes*. Springer, 2011.

[36] Anjan Kumar Tula, Deenesh K Babi, Jack Bottlaender, Mario R Eden, and Rafiqul Gani. "A computer-aided software-tool for sustainable process synthesis-intensification". *Computers & Chemical Engineering* (2017).

[37] Philip Lutze, Alicia Román-Martinez, John M Woodley, and Rafiqul Gani. "A systematic synthesis and design methodology to achieve process intensification in (bio) chemical processes". *Computers & Chemical Engineering* (2012).

[38] Genyin Ye, Donglai Xie, Weiyan Qiao, John R Grace, and C Jim Lim. "Modeling of fluidized bed membrane reactors for hydrogen production from steam methane reforming with Aspen Plus". *International journal of hydrogen energy* (2009).

[39] G Camera-Roda, V Loddo, L Palmisano, F Parrino, and F Santarelli. "Process intensification in a photocatalytic membrane reactor: Analysis of the techniques to integrate reaction and separation". *Chemical Engineering Journal* (2017).

[40] Janusz Kotowicz and Adrian Balicki. "Enhancing the overall efficiency of a lignite-fired oxyfuel power plant with CFB boiler and membrane-based air separation unit". *Energy Conversion and Management* (2014).

[41] Danahe Marmolejo Correa. "Analysis and Design of Low Temperature Processes with Focus on LNG: Developing new Thermodynamics based Tools and introducing Exergy in Design Methodologies". PhD thesis. Norwegian University of Science and Technology, 2013.

[42] A. P. Hinderink, F. P J M Kerkhof, A. B K Lie, J. De Swaan Arons, and H. J. Van Der Kooi. "Exergy analysis with a flowsheeting simulator - I. Theory; calculating exergies of material streams". *Chemical Engineering Science* (1996).

[43] Joseph Kestin. *A course in thermodynamics*. Vol. 1. CRC Press, 1979.

[44] YVC Rao. *Chemical engineering thermodynamics*. Universities Press, 1997.

[45] Farzad Abdollahi-Demneh, Mohammad Ali Moosavian, Mohammad Reza Omidkhah, and Hossein Bahmanyar. "Calculating exergy in flowsheeting simulators: A HYSYS implementation". *Energy* (2011).

[46] ABK Lie. "ExerCom: calculating exergies in Aspen (PC-version) user manual". *Stork Comprimo report* (1994).

Appendices

Appendix A

This Appendix contains a summary of the procedure and results of the exergy Analysis of an state-of-the-art Hydrogen Production process. The state-of-the-art process used in this case study is described in Chapter 1. This appendix is a summary from the specialization project [2].

A.1 General Background

A.1.1 Motivation for Exergy Analysis

The 2nd law of thermodynamics can be used to provide greater insight into the sources of process inefficiencies. The 1st law of thermodynamics only considers the "quantity" of energy: It views all the different forms such as chemical energy, heat, work, electrical energy, etc. as equally useful. However, this is not the case: For instance, it can be shown that even an ideal heat engine cannot convert all the available thermal energy to work. Thus, energy has a "quality" as well as a "quantity" as demonstrated by the 2nd law of thermodynamics [21]. Exergy is the term that encompasses both the quality and quantity aspect of energy. Exergy is defined as the "maximum useful work that can be obtained from a system at a given state in a specified environment" [21]. Thus, Exergy (also called "available energy") shows how much of the energy is available to be extracted as work through an ideal process.

Tsatsaronis et al. remark that: "Exergy Analysis provides insights that elude a purely first-law approach" [22]. They mention that "Exergy Analysis ... is well suited for furthering the goal of more effective energy resource use, for it enables the location, cause, and true magnitude of waste and loss to be determined" [22]. Performing the 1st law Energy Balance calculations gives the energy lost as heat to the environment as the only source of process inefficiencies. However, this reasoning does not reveal the true source of process inefficiencies. Thus, it is necessary to use Exergy Analysis to zero in on the actual cause of the process inefficiencies.

The 2nd law of thermodynamics provides these further insights by making a distinction between "reversible" processes and "irreversible" processes as explained in detail in [21]. Work-producing devices operating reversibly deliver the most work while work-consuming devices operating reversibly consume the least work. Thus, reversible processes provide the theoretical limit of efficiency for any process while irreversibilities destroy the exergy of a process. This concept of exergy destruction and irreversibilities is applied in this case study to determine the true source of process inefficiencies.

A.1.2 Classification of Exergy

As mentioned above, exergy is defined as: "maximum useful work that can be obtained from a system at a given state in a specified environment". Different interactions can be used to extract this work by changing the system from its initial state to equilibrium with the environment. These include: thermal, mechanical and chemical interactions [24].

- Thermal interactions: These occur when the temperature (T) at the given state of the system is different from the temperature of the reference environment state (T_0). An (ideal) heat engine can be used to convert some of the heat energy exchanged between these two states into work.
- Mechanical interactions: This involves using the difference between the pressure at the given state of the system (P) and the pressure at the reference environment state (P_0) to produce work for instance through an expansion process.
- Chemical interactions: This involves using the difference in chemical components or composition between the given state of the system and the reference state of the environment to produce work. The details of these interactions are explored in the following sections.

Many different classifications of exergy exist. Before defining the different types of exergy, it is necessary to first specify the type of equilibrium that exists between the system and the environment.

States of Equilibrium with the Environment

A system can be in two different states of equilibrium with the environment: The Restricted Dead State and the Unrestricted Dead State.

- The Restricted Dead State: When a system is in restricted equilibrium with the environment, its temperature and pressure are equal to the environment temperature (T_0) and pressure (P_0). Thus, the system is in thermo-mechanical equilibrium with its environment i.e. no further work can be extracted from the system using thermal or mechanical interactions. However, a barrier prevents chemical interactions between the system and the environment.
- The Unrestricted Dead State: When a system is in unrestricted equilibrium with the environment, it has identical temperature (T_0), pressure (P_0) and chemical composition with the environment. Thus, the system is in thermal, mechanical and chemical equilibrium with the environment and cannot use any of these three interaction modes to produce useful work. Hence, the system and environment are said to be in an unrestricted dead state.

  A practical definition of this unrestricted dead state is given by Szargut et al. in [23]. It is intuitive that all parts of this unrestricted dead state are themselves in thermo-mechanical and chemical equilibrium with each other. However, it is difficult to practically define such a dead state on the earth since different sections of the earth are not in equilibrium with each other. For this

reason, Szargut et al. defined three different dead states: Atmospheric Air, Seawater and the Earth's crust [23]. In each of these dead states, they defined a set of "reference species" with respect to which exergies are calculated. Within the scope of this project, it is sufficient to consider only reference species in atmospheric air. Szargut et al. list ten reference species in atmospheric air: $O_2(g), CO_2(g), H_2O(l), N_2(g), Ar(g), Xe(g), Ne(g), Kr(g), He(g)$ and D_2O and define their reference compositions in the unrestricted dead state [23]. Thus, the exergy of a system can be further specified as the "maximum useful work that can be produced by a process that changes the system from its initial state to the unrestricted dead state at which it is in thermo-mechanical equilibrium (i.e. is at temperature (T_0) and pressure (P_0)) as well as chemical equilibrium with the dead state (i.e. it has an identical composition to the reference composition of species in atmospheric air as defined in [23])".

Szargut et al. and Kotas propose classifications of exergy that are fully illustrated in [41]. Gundersen also proposes a classification that is shown in Figure A.1 [28]. Other different classifications are also shown in [41]. In this project, the simpler classification (shown in Figure A.2) suggested by Hinderink et al. [42] is used. Below, a definition of the terms in Figure A.2 is given, with further details in Section ... A comparison of Gundersen's classification and the classification shown in Figure A.2 is given at the end of section ...

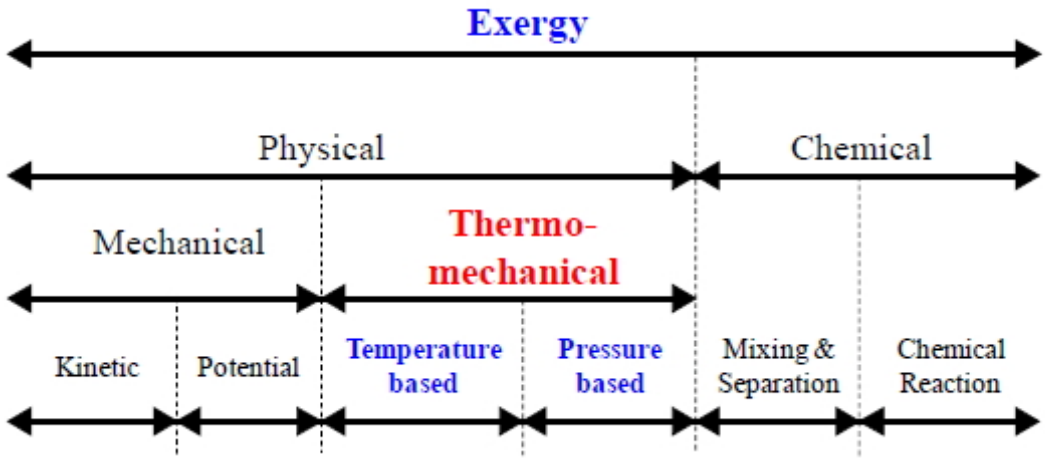

Figure A.1: Classification of Exergy proposed by Gundersen [28].

- The physical (or thermo-mechanical) exergy of a system is the maximum obtainable amount of useful work when this system is brought from its initial state at temperature T and pressure P using only reversible processes to thermo-mechanical equilibrium with its environment, which is a temperature T_0 and pressure P_0. This state of thermo-mechanical equilibrium is the Restricted Dead State. Thus the thermo-mechanical exergy of a system represents its ability to produce useful work as a result of thermal and mechanical interactions.

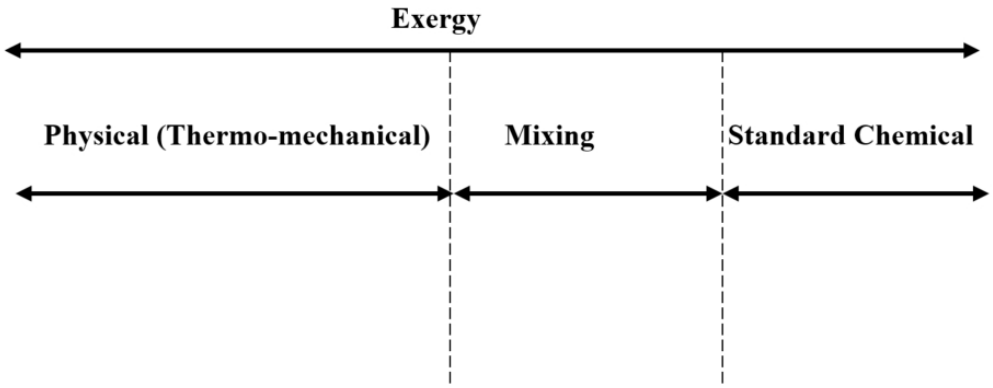

Figure A.2: Classification of Exergy used in this project.

- The mixing exergy of a system is best defined by considering a material stream. The mixing exergy of a material stream represents the exergy destroyed when individual constituent components of the material stream mix at constant temperature (T_0) and pressure (P_0) to form the material stream mixture.
- The standard chemical exergy of a material stream is the maximum amount of useful work attainable in bringing pure components at the Restricted Dead State to the Unrestricted Dead State both at temperature T_0 and pressure P_0 through reversible processes. In the Unrestricted Dead State, the material stream is in full thermo-mechanical, compositional and chemical equilibrium with its environment and thus has no more potential to provide useful work.

A.2 Methodology to perform exergy analysis

The first step in performing an exergy analysis on the case study is to obtain values of the physical, mixing and chemical exergy of relevant material streams. Szargut et al. propose a procedure that involves systematically converting the material stream through a number of intermediate hypothetical processes until it is identical in composition with the reference environment (at the unrestricted dead state) [23]. Each of these hypothetical processes should be ideal (reversible) i.e. should themselves not destroy any exergy. These hypothetical reversible processes are shown schematically in Figure A.3.

The following subsection describes the methodology to obtain these different exergies. First, a theoretical framework is described and then ways to implement this framework into flowsheeting software are explored.

A.2.1 Theoretical framework to calculate the physical exergy of a material stream

The physical exergy of a material stream can be subdivided into pressure-based exergy and temperature-based exergy, but this distinction is not important in this project. If the enthalpy and entropy of the material stream at its initial state are

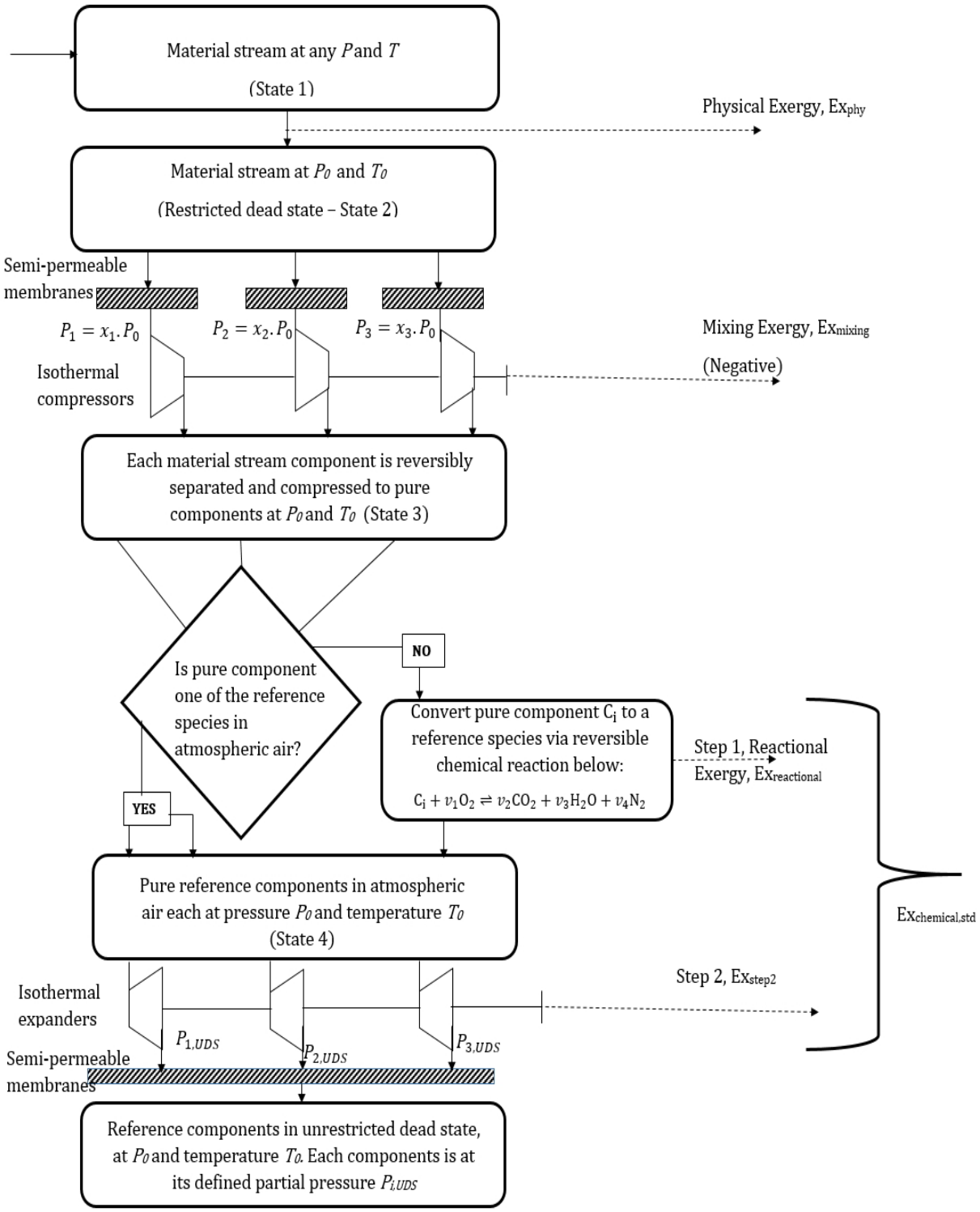

Figure A.3: Procedure to obtain physical, mixing and standard chemical exergy of a material stream. Note that the rhombus represents a decision box, not that the streams are mixing

given by H and S, and its enthalpy and entropy at the restricted dead state is given by H_0 and S_0, then the expression for physical exergy (Ex_{phy}) is:

$$Ex_{phy} = (H - H_0) - T_0(S - S_0) \tag{A.1}$$

This exergy is obtained by changing the state of the material stream from State 1 to State 2 on Figure A.3. The physical exergy does not take into account the chemical composition of the material stream - this is considered in mixing and chemical exergies.

A.2.2 Theoretical framework to calculate the mixing exergy of a material stream

Material streams commonly consists of more than one component. However, it is convenient to perform exergy calculations on a single, pure component stream rather than one containing a mixture of several components. For this reason, the first step is to separate (or split) the mixture into its pure component streams. This separation process itself requires work, and this work is equivalent to the mixing exergy of the material stream. Since work has to be input to split the material stream, the mixing exergy has a negative value.

In order to follow the requirement of reversibility of the intermediate hypothetical processes (i.e. that the hypothetical processes used to obtain exergy values should not themselves destroy exergy), it is necessary to conceive of an ideal device to carry out the separation process. Van't Hoff introduced the notion of a semi-permeable membrane that lets one component pass through completely unhindered while blocking all the other components [43]. This semi-permeable membrane, at least conceptually, offers a way to carry out reversible splitting of the material stream into its components [44]. The pressure of the single component in the permeate is equal to its partial pressure (P_i) in the material stream mixture given by the Gibb's-Dalton Equation A.2, where x_i is the mole fraction of component i in the material stream mixture.

$$P_i = x_i.P_o \tag{A.2}$$

Each of these single component streams is then isothermally and reversibly compressed to the pressure P_o with reversible heat exchange to the environment. The work supplied to the ideal compressors is the mixing exergy of the material stream. That means that this work input is used to compensate for the exergy destruction of mixing (as a result of entropy generation by mixing) when the material stream was formed from its constituent components [24]. Figure A.3 illustrates this on a material stream with three components. The derivation of an expression for Ex_{mixing} is presented below:

Applying the first law of thermodynamics to the control volume of the isothermal reversible compressor at steady-state conditions, ignoring kinetic and potential energies:

$$\dot{W}_{in} = \Delta\dot{H} + \dot{Q}_{out} \tag{A.3}$$

From the second law of thermodynamics

$$\dot{Q}_{out} = -T_o\Delta\dot{S} \tag{A.4}$$

So

$$\dot{W}_{in} = \Delta\dot{H} - T_o\Delta\dot{S} \tag{A.5}$$

It is assumed that there is no enthalpy or entropy change in the semi-permeable membranes. Thus, the above equation can be extended to represent the change in state from the mixed material stream (State 2 in Figure A.3) to the pure component streams (State 3 in Figure A.3). Writing the above equation for n pure components of the material stream:

$$\dot{W}_{in} = (\sum_{i=1}^{n}(x_i.\dot{H}_i)_{State3} - \dot{H}_{State2}) - T_o(\sum_{i=1}^{n}(x_i.\dot{S}_i)_{State3} - \dot{S}_{State2}) \tag{A.6}$$

So

$$Ex_{mixing} = -\dot{W}_{in} = (\dot{H}_{State2} - \sum_{i=1}^{n}(x_i.\dot{H}_i)_{State3}) - T_o(\dot{S}_{State2} - \sum_{i=1}^{n}(x_i.\dot{S}_i)_{State3}) \tag{A.7}$$

A.2.3 Theoretical framework to calculate the standard chemical exergy of a material stream

The standard chemical exergy of a material stream is defined here as the maximum amount of useful work attainable in bringing pure components at the restricted dead state to the unrestricted dead state both at temperature T_0 and pressure P_0 through ideal reversible processes.

This standard chemical exergy is calculated in two steps. First, if the pure component under consideration is not one of the defined reference species, it is converted to a reference species via a hypothetical reversible chemical reaction. This part of the standard chemical exergy is also termed "reactional exergy", and corresponds to the "Chemical Reaction" term in Gundersen's classification in Figure A.1. Thus, if the pure component is one of the defined reference species, it has zero reactional exergy. This hypothetical reversible chemical reaction is given in Equation A.8 [23],[45]. For a pure component (C_i) that is not a reference species:

$$\begin{aligned}\mathrm{C}_i + \mathrm{v}_1\mathrm{O}_2(\mathrm{g}) \rightleftharpoons\ & \mathrm{v}_2\mathrm{CO}_2(\mathrm{g}) + \mathrm{v}_3\mathrm{H}_2\mathrm{O}(\mathrm{l}) + \mathrm{v}_4\mathrm{N}_2 + \mathrm{v}_5\mathrm{S}_{\mathrm{solid}} + \mathrm{v}_6\mathrm{Ar}(\mathrm{g}) + \mathrm{v}_7\mathrm{Xe}(\mathrm{g}) \\ & + \mathrm{v}_8\mathrm{Ne}(\mathrm{g}) + \mathrm{v}_9\mathrm{Kr}(\mathrm{g}) + \mathrm{v}_{10}\mathrm{He}(\mathrm{g}) + \mathrm{v}_{11}\mathrm{D}_2\mathrm{O}\end{aligned} \tag{A.8}$$

Thus, the pure component C_i is reversibly reacted with oxygen to produce products that lie within the set of reference species. v_j represents the stoichiometric coefficients for the 11 species (other than C_i) that take part in the equation.

The change in Gibb's energy for the above chemical reaction is given by the equation:

$$\Delta G^0_{Reaction,C_i} = \sum_{2}^{11}(v_j.G^0_{f,j})_{products} - \sum_{1}(v_j.G^0_{f,j})_{reactants} \tag{A.9}$$

where $G^0_{f,j}$ is the standard Gibbs energy of formation of species j. For reversible reactions taking place at constant temperature and pressure, the change in standard Gibb's free energy is equivalent to the change in exergy thus:

$$Ex_{reactional,C_i} = \Delta G^0_{Reaction,C_i} \tag{A.10}$$

This gives the reactional exergy of the pure component stream C_i. Summing up the reactional exergy of all the n components, each of mole fraction x_i in the material stream, gives the total reactional exergy of the stream:

$$Ex_{reactional} = \sum_{i=1}^{n} x_i.\Delta G^0_{Reaction,C_i} \tag{A.11}$$

After step 1, all the pure components that are not reference components are converted to pure reference components (State 4 in Figure A.3). Thus, the second step deals solely with reference components.

The second step to calculate the standard chemical exergy is to use a hypothetical process to change the state of the pure reference components (State 4 in Figure A.3) from each having an individual pressure of P_0 to their conventional partial pressure in the unrestricted dead state $P_{i,UDS}$ (State 5 in Figure A.3). This conventional partial pressure corresponds to a composition that is identical to the composition of the reference elements in the unrestricted dead state as defined by Szargut et al. [23]. This process has to be reversible and isothermal, only involving heat and work exchange with the environment. It is essentially the opposite procedure carried out to obtain the mixing exergy in the previous section. Thus the pure components are expanded in isothermal reversible expanders to their partial pressure in the unrestricted dead-state ($P_{i,UDS}$) and then they undergo reversible mixing by passing the different streams through a semi-permeable membrane to State 5 in Figure A.3. There is no enthalpy or entropy change across the semi-permeable membrane i.e. it ensures that the mixing process does not result in exergy destruction. In this way, this hypothetical mixing process meets the requirement that no exergy should be destroyed in the intermediate processes used to calculate exergy.

The useful work produced in the reversible expanders is given by equation A.12

$$\dot{W}_{out} = (\dot{H}_{UDS,State5} - \sum_{i=1}^{n}(x_i.\dot{H}_i)_{State4}) - T_o(\dot{S}_{UDS,State5} - \sum_{i=1}^{n}(x_i.\dot{S}_i)_{State4}) \tag{A.12}$$

Thus,

$$Ex_{step,2} = (\dot{H}_{UDS,State5} - \sum_{i=1}^{n}(x_i.\dot{H}_i)_{State4}) - T_o(\dot{S}_{UDS,State5} - \sum_{i=1}^{n}(x_i.\dot{S}_i)_{State4}) \tag{A.13}$$

Therefore the total standard chemical exergy is given by

$$Ex_{chemical,std} = Ex_{reactional} + Ex_{step,2} \tag{A.14}$$

Szargut et al. published tables of these standard chemical exergies using conditions of $T_0 = 25$ °C and $P_0 = 1.01325$ bar in [23]. It is convenient to use these published values in the case study exergy analysis

Having elaborated on the theoretical frameworks used to obtain the different exergies, the classification used in Figure A.2 can be compared with the classification proposed by Gundersen in Figure A.1. The following distinctions are made:

- The Kinetic and Potential exergies are assumed to negligible in Figure A.2 compared to Figure A.1. Thus "Mechanical" exergy is assumed to negligible.

- The "Mixing and Separation" exergy of Figure A.1 is different from the "Mixing" exergy of Figure A.2. Gundersen's Mixing and Separation exergy (also called compositional exergy) would add both Ex_{mixing} and $Ex_{step,2}$ yet "Mixing" exergy of Figure A.2 only contains Ex_{mixing}.

- The "Standard Chemical" exergy is different from Gundersen's "Chemical" Exergy as the Standard Chemical exergy does not contain Ex_{mixing}.

The rationale for choosing the different classification shown in Figure A.2 is that the classification is easier to implement using programming into flowsheeting simulator software. This is discussed in the next section.

A.3 Performing Exergy Analysis with flowsheeting simulators

The above methodology to perform exergy analysis can be integrated with flowsheeting simulators such as Aspen Plus and Aspen HYSYS. This computer-aided exergy calculation makes exergy analysis more accessible and enables rapid analysis of the nature of irreversibilities of different process designs [42], [45]. The methodology is implemented in the simulators by manually programming subroutines to extract stream data from the simulators and perform the exergy calculation steps.

A.3.1 Automation in Aspen Plus using ExerCom

A generally available software for performing the exergy analysis called "ExerCom" has been developed and licensed by Stork Comprimo (Amsterdam, the Netherlands), [42] [46] to work with Aspen Plus. The order in which the exergy calculations is performed is presented in Figure A.4. The internal calculation path used by Exercom is also presented in Figure A.5.

ExerCom performs the exergy calculations congruently with the mass and energy balance calculations performed by the flowsheeting simulator. The definitions of the output results "CHEMEX", "FYSEX" and "MIXEX" given when using ExerCom correspond exactly with the chemical exergy, physical exergy and mixing exergy derived in the theoretical framework.

A.3.2 Automation in Aspen HYSYS using User-Defined Functions

Aspen HYSYS has an advantage over Aspen Plus in that it uses an equation based engine to solve for the thermodynamic properties as soon as all the input degrees of freedom are satisfied while Aspen Plus uses a sequential modular format. As a result of this advantage, it was desirable to model the process using Aspen HYSYS over Aspen Plus. In order to automate the exergy analysis using Aspen HYSYS, User-Defined Functions were programmed using Visual Basic. These user-defined functions obtained the necessary thermodynamic information of the material streams from the corresponding objects in HYSYS and performed calculations on these to output the mixing, physical and chemical exergy.

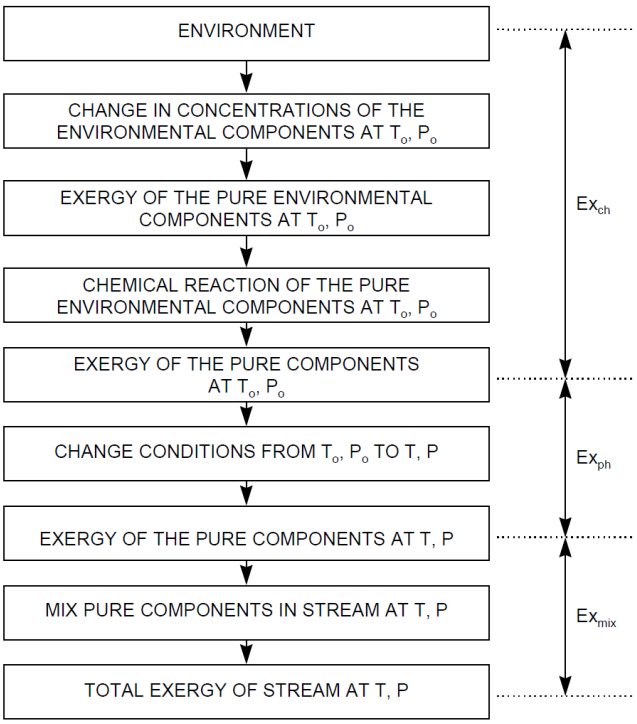

Figure A.4: Procedure to perform exergy calculations used in Exercom [46]

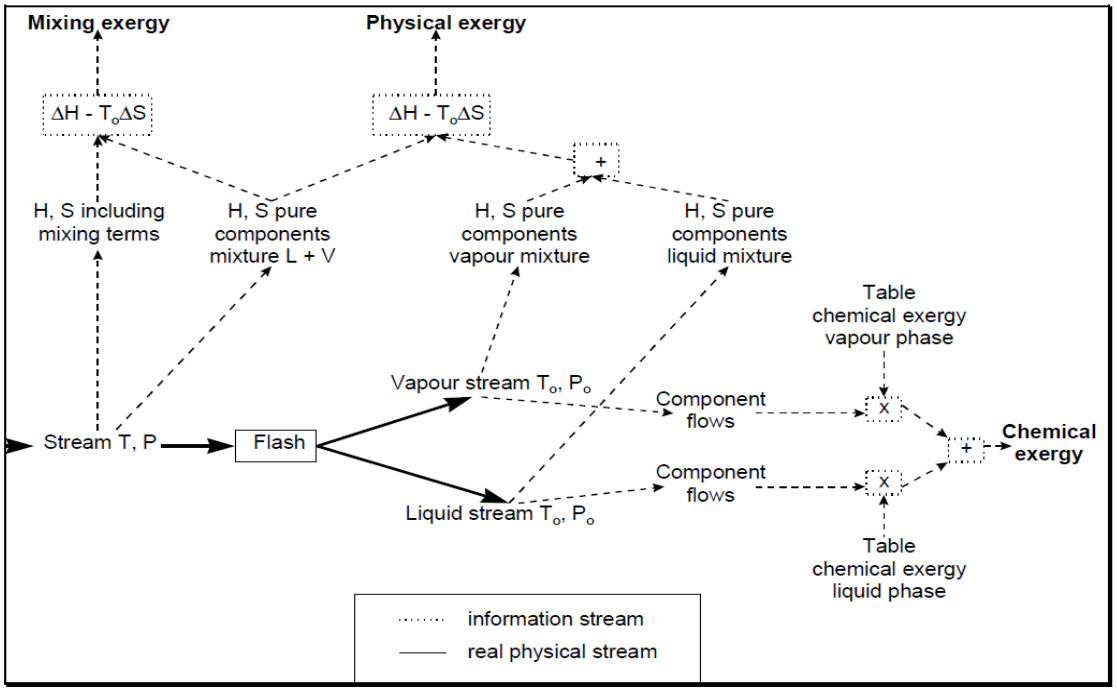

Figure A.5: Internal calculation path to perform exergy calculations used in Exercom [46]

The values of the standard chemical exergy published by Szargut et al. in [23] are input for each component as user-defined properties. Figure A.6 shows how this is done within the Aspen HYSYS environment. Figure A.7 shows the interface for

implementation of user-defined variables in the Aspen HYSYS environment.

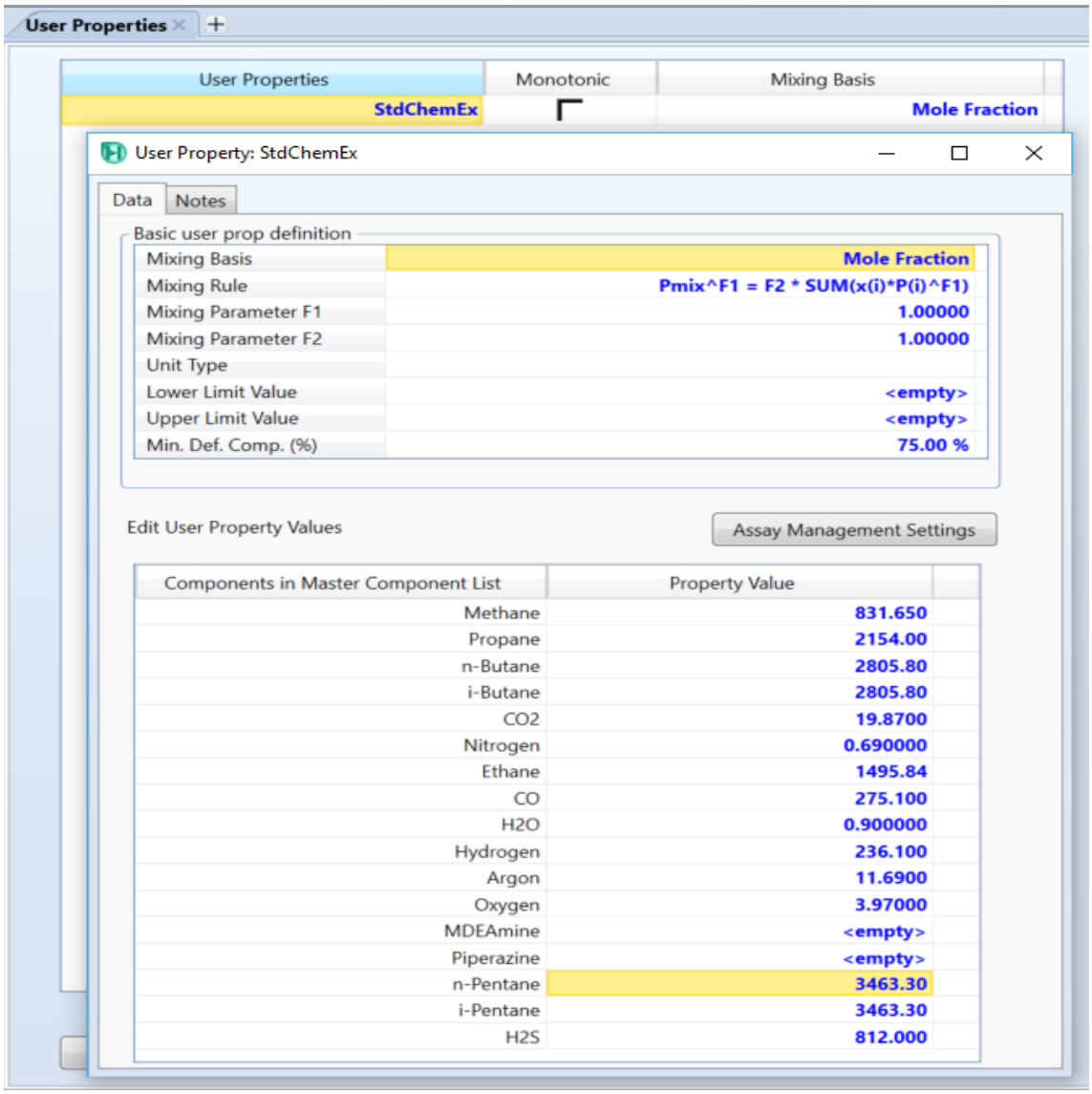

Figure A.6: User-defined properties for each component in the simulation basis manager of HYSYS

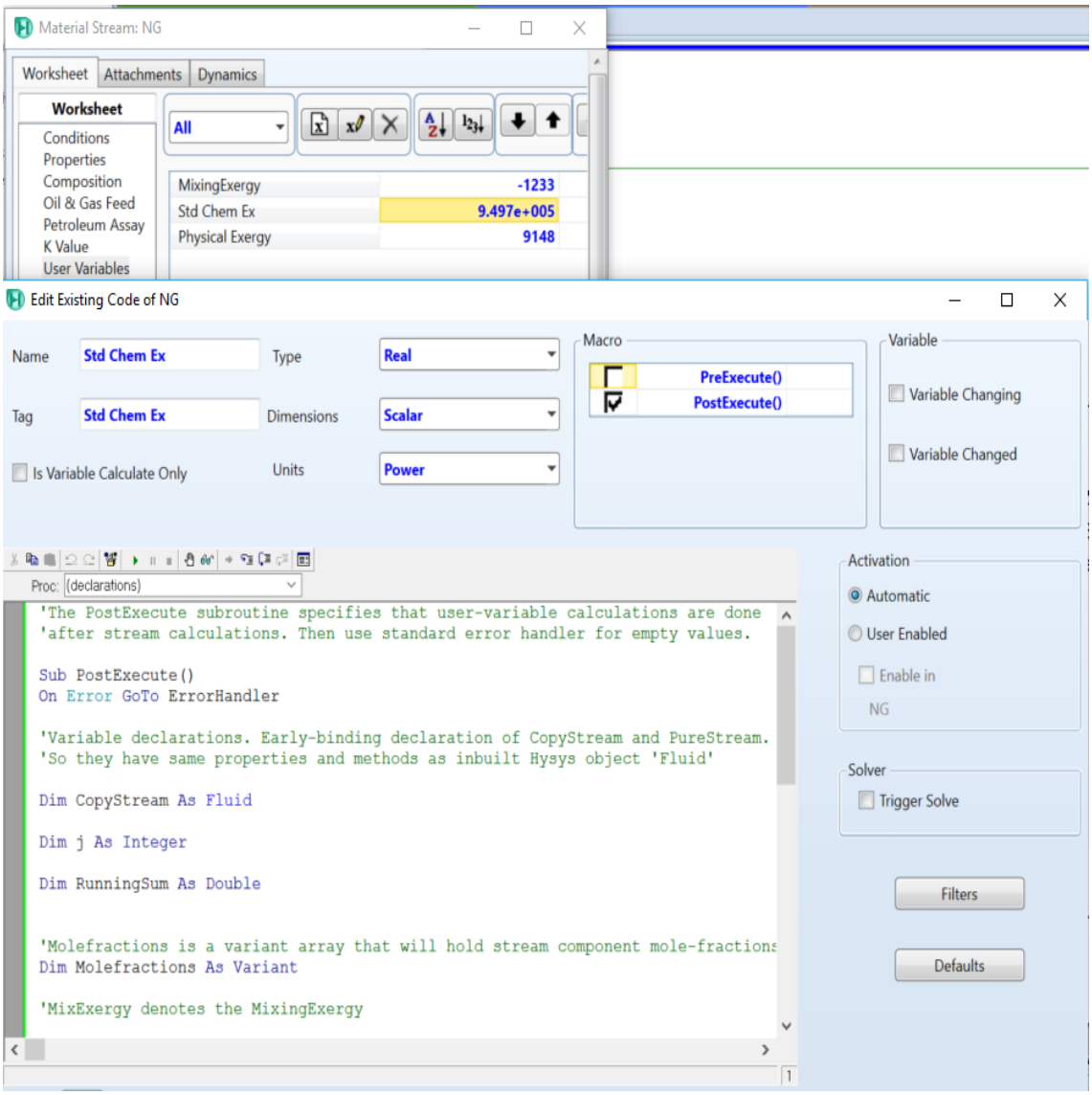

Figure A.7: Interface for implementation of user-defined variables in the Aspen HYSYS environment

A.3.3 Exergy as a state function

Exergy is by definition a state function since it only depends on enthalpy and entropy values which are themselves state functions. Thus, the exergy of a material stream only depends on the initial state of the material stream and the state of the reference environment, not on any of the in-between hypothetical processes. As a result of this property, it is possible to design the hypothetical processes according to convenience for implementation as a sub-routine in the flowsheeting simulator. Three different paths are chosen and implemented using user-defined variables in Aspen HYSYS. It is shown in this section that while the resulting total exergy value is constant, the proportion of thermo-mechanical exergy and mixing exergy is dependent on the path chosen.

Path 1

The first path chosen is shown in Figure A.8. The thermo-mechanical exergy is first obtained by a reversible process that changes the state of the material stream from its temperature T and pressure P to the restricted dead state at temperature T_0 and pressure P_0. Then the stream is separated and Equation A.7 is used to obtain the mixing exergy at the restricted dead state, followed by using the published tables to obtain standard chemical exergy [23]. The order of execution of the sub-routines is similar to that used in Abdollahi-Demneh et al. [45], and corresponds exactly with Figure A.3.

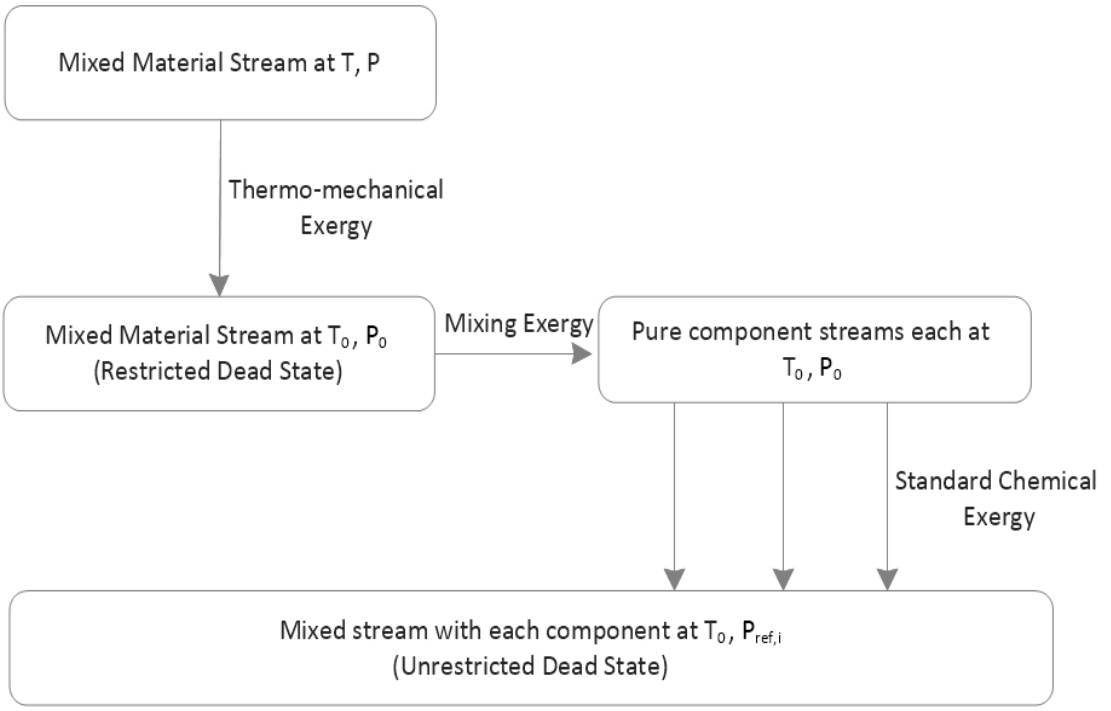

Figure A.8: Path 1 to obtain total exergy. First thermo-mechanical exergy, then mixing exergy and finally standard chemical exergy

Path 2

The second path chosen is shown in Figure A.9. The stream is first separated into its pure components at its temperature T and pressure P. The thermo-mechanical exergy is then obtained for each of the pure components as they undergo a reversible process that changes their state from temperature T and pressure P to the restricted dead state at temperature T_0 and pressure P_0. The total thermo-mechanical exergy is the sum of the thermo-mechanical exergy of each individual pure component stream. Finally, the standard chemical exergy of each pure stream is obtained from published tables. The order of execution of the sub-routines is similar to that used in Hinderink et al. [42] and in Exercom [46],[45].

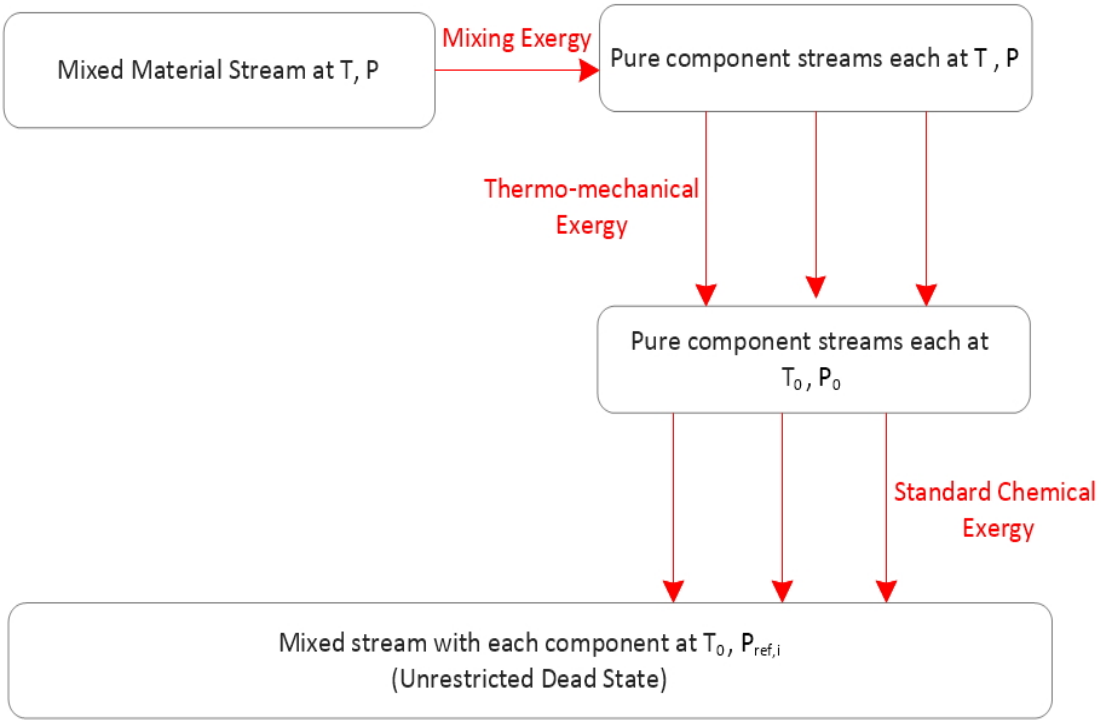

Figure A.9: Path 2 to obtain total exergy. First mixing exergy, then thermo-mechanical and then standard chemical exergy

Path 3

The motivation for the third path is to have only one phase present in the material stream when separating it into its individual components. Thus the material stream first undergoes a hypothetical reversible heating process at constant pressure until it reaches a temperature T_{high} in which the material stream exists only in vapour phase. The exergy change is $\Delta Ex.1$. Then the material stream is separated into its constituent components that also exist only in their vapour phase. As a result there is no need to account for possible formation of liquid phase during the separation. In addition, the material stream behaves as an ideal gas at T_{high} so the value obtained for the separation exergy $\Delta Ex.2$ can be compared with the values for exergy destruction during ideal gas mixing obtained from the known equation below [21]:

$$\Delta Ex.2 = \sum_{i=1}^{n} x_i.nRT_0ln(x_i) \tag{A.15}$$

The pure component streams are then cooled with reversible heat exchange with the surroundings to the original stream temperature T, and the work produced is $\Delta Ex.3$. The mixing exergy is then equal to the sum, accounting for sign convention of $\Delta Ex.1$, $\Delta Ex.2$ and $\Delta Ex.3$.

$$Ex_{mixing} = \Delta Ex.1 + \Delta Ex.2 + \Delta Ex.3 \tag{A.16}$$

The thermo-mechanical and standard chemical exergies are then calculated in ways identical to Path 2, as shown in Figure A.10. The visual basic code is omitted in this report since it is similar to the code of path 2,

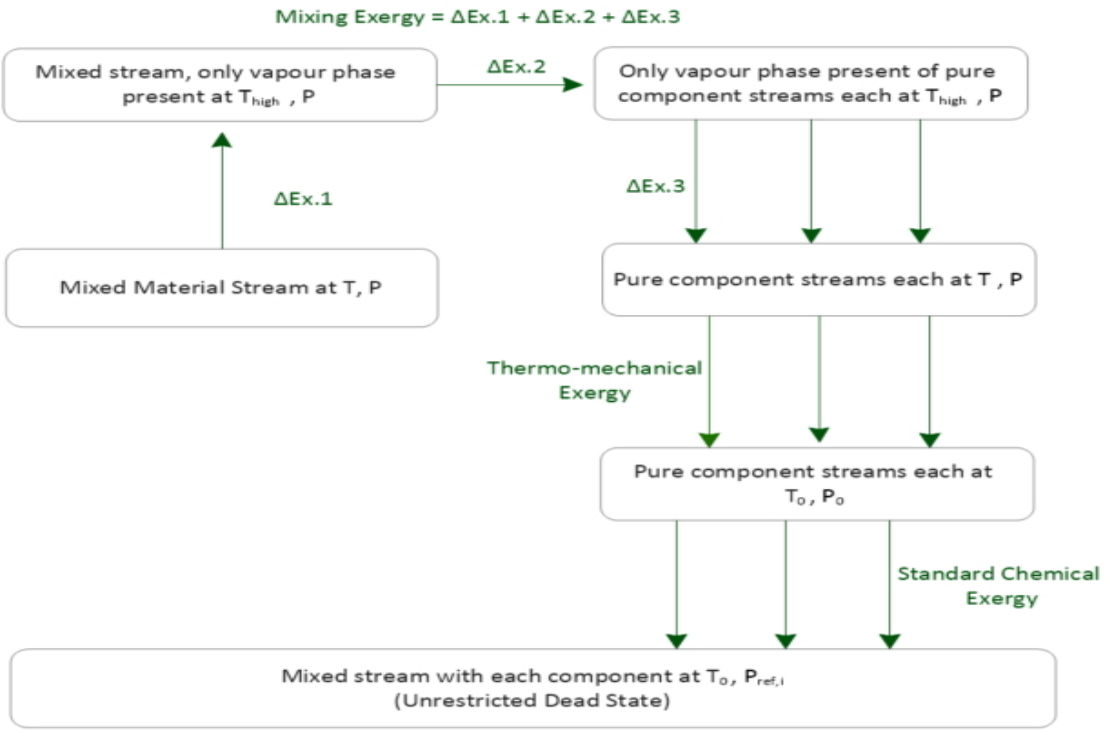

Figure A.10: Path 3 to obtain total exergy. First mixing exergy of pure vapour phase mixture and components, then thermo-mechanical exergy, then standard chemical exergy

The three paths, as expected, give the same total exergy as seen in the table below. However, they give different values for the thermo-mechanical and mixing exergy depending on which path is chosen, though the sum of the two exergies is independent of process path. This result suggests a need to define precisely the meaning of "physical" or "mixing" exergies when they are presented. For instance, it is important to distinguish whether "physical" exergy of a material stream has been obtained from bringing the mixed material stream from T and P to T_0 and P_0, or from bringing each of the constituent components of the material stream from T and P to T_0 and P_0.

Table A.1: Exergy results of the three paths for a sample material stream

Path		Path 1	Path 2	Path 3
Physical Exergy	KW	10,880	11,000	10,880
Mixing Exergy	KW	-1140	-1260	-1140
Standard Chemical Exergy	KW	949,700	949,700	949,700
Total Exergy	KW	959,440	959,440	959,440

A.4 Exergy Analysis Results

The results for only the furnace are provided to give an indication of the procedure. The overview of results is available in Chapter 1.

Control volumes containing major relevant unit operations of the case study simulation model were chosen and Exergy Analysis perfomed on these. The physical, mixing and standard chemical exergies of the inlet and outlet material streams into the control volume are presented. A comparison with the values obtained using ExerCom are shown side-by-side.

The Exergy destroyed in each control volume is given by the equation:

$$Ex_{destroyed} = \sum Ex_{in} - \sum Ex_{out} \tag{A.17}$$

These are calculated using the HYSYS user-defined functions using Path 1. The inlet and outlet exergies could be in material streams, heat (Q) or work (W).

Furnace

Table A.2: Exergy Analysis of Furnace

Component		Furnace						
Stream		Purge Gas (in)		Air (in)		Flue Gas (out)		Q (out)
Temperature	°C	137.8		363.9		1050		
Pressure	bar	1.013		1.013		1.013		
		HYSYS	Exercom	HYSYS	Exercom	HYSYS	Exercom	
Physical Exergy	KW	1008.7	947.2	14121.7	13577.3	124583.1	124405.0	
Mixing Exergy	KW	-4911.3	-4911.5	-6153.7	-6153.8	-12998.6	-12996.0	
Chemical Exergy	KW	381698.4	381210.0	5949.9	6392.2	26975.2	27962.5	
Total Exergy	KW	377795.8	377245.7	13917.9	13815.7	138559.7	139371.5	161667.6
Exergy Destroyed	KW	91486.4						

Appendix B

The expression for the Carnot temperature is derived. An entropy balance is performed on the control volume (represented by the dotted lines) which contains the reactor.

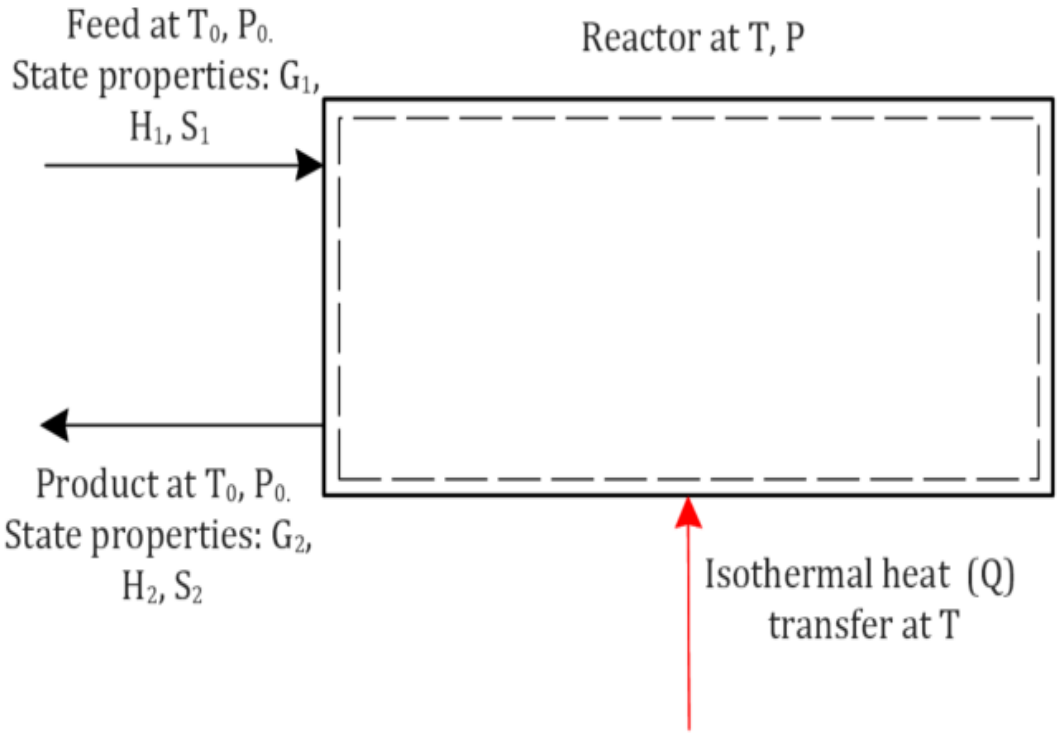

Figure B.1: Control volume of simple chemical process

Entropy is transferred to the control volume by means of heat transfer (Q) and mass transfer of the inlet and outlet streams. For a steady process, the entropy balance is given by:

$$\dot{Q}/T + \sum(\dot{m}_i s_i)_{inlet} - \sum(\dot{m}_e s_e)_{outlet} + \dot{S}_{gen} = dS_{CV}/dt \tag{B.1}$$

For steady flow processes: $dS_{CV}/dt = 0$. Thus equation becomes:

$$\dot{Q}/T + \dot{S}_{gen} = \dot{S}_2 - \dot{S}_1 \tag{B.2}$$

It is desired to find a condition for which the simple chemical process is internally reversible. Thus assume that the entropy generated $(\dot{S}_{gen}) = 0$. Note that making

this assumption implies that the chemical reaction is also assumed to be reversible - this is not always realistic since chemical reactions are commonly a source of irreversibilities. Also, the heat transfer (Q) is assumed to be isothermal so as not to be a source of irreversibilities - this is also not realistic since heat transfer requires a finite temperature difference to occur. These realities will be considered at a later stage of the G-H space methodology; at this early conceptual stage, the process is designed to be as reversible as possible. By definition:

$$G_1 = H_1 - T_0 S_1 \tag{B.3}$$

and

$$G_2 = H_2 - T_0 S_2 \tag{B.4}$$

Subtracting and rearranging:

$$\dot{S}_2 - \dot{S}_1 = ((\dot{H}_2 - \dot{H}_1) - (\dot{G}_2 - \dot{G}_1))/T_0 = (\Delta\dot{H} - \Delta\dot{G})/T_0 \tag{B.5}$$

The "dot" denoting time derivatives are dropped for convenience, since all the following equations are in dimensions of power e.g. KW.

It desired that the heat supplied is used to match the process ΔH requirements, so $Q = \Delta H$. With these conditions, the reactor temperature T is defined as the Carnot temperature or the reversible temperature. Thus, $T = T_{carnot}$. The equation becomes:

$$\Delta H/T_{Carnot} = (\Delta H - \Delta G)/T_0 \tag{B.6}$$

Rearrange to give:

$$\Delta G = \Delta H(1 - T_0/T_{Carnot}) \tag{B.7}$$

This equation is re-arranged to give the equation used in Chapter 2.

Appendix C

C.1 100 % recycle

Table C.1: Material stream data for process with 100 % recycle

Material Stream	T (C)	T (K)	p (bar)	Molar flow rate (mol/s) CH4	H20	CO	CO2	O2	H2	Total
1	25	298.15	1	-	1.1152	-	-	-	-	1.1152
2	25	298.15	62.9	-	1.1152	-	-	-	-	1.1152
3	279	552.15	62.9	-	1.1152	-	-	-	-	1.1152
4	279	552.15	62.9	-	0.7788	-	-	-	-	0.7788
5	687.68	960.83	62.9	-	0.7788	-	-	-	-	0.7788
6	25	298.15	1	1	-	-	-	-	-	1
7	25	298.15	62.9	1	-	-	-	-	-	1
8	687.68	960.83	62.9	0.7788	-	-	-	-	-	0.7788
9	687.68	960.83	62.9	0.2212	-	-	-	-	-	0.2212
10	25	298.15	1	-	-	-	-	0.4424	-	0.4424
11	25	298.15	62.9	-	-	-	-	0.4424	-	0.4424
12	687.68	960.83	62.9	-	-	-	-	0.4424	-	0.4424
13	687.68	960.83	62.9	-	0.4424	-	-	-	-	0.4424
14	701.52	974.67	62.9	-	0.4424	-	-	-	-	0.4424
15	687.68	960.83	62.9	-	-	-	0.2212	-	-	0.2212
16	25	298.15	62.9	-	-	-	0.2212	-	-	0.2212
17	25	298.15	1	-	-	-	0.2212	-	-	0.2212
18	687.68	960.83	62.9	-	-	-	-	-	2.3364	2.3364
19	687.68	960.83	62.9	-	-	0.7788	-	-	-	0.7788
20	701.52	974.67	62.9	-	-	0.7788	-	-	-	0.7788
21	701.52	974.67	62.9	-	0.3364	-	-	-	-	0.3364
22	701.2	974.35	62.9	-	-	-	-	-	0.7788	0.7788
23	25	298.15	62.9	-	-	-	-	-	3.1152	3.1152
24	25	298.15	1	-	-	-	-	-	3.1152	3.1152
25	701.52	974.67	62.9	-	-	-	0.7788	-	-	0.7788
26	25	298.15	62.9	-	-	-	0.7788	-	-	0.7788
27	25	298.15	1	-	-	-	0.7788	-	-	0.7788

Table C.2: Energy stream data for process with 100 % recycle

Energy Stream	Heat	Work
Wout = E9-E1	-	27.35
E2	49.07	9.55
E3	160.52	110.71
E4	-	4.34
E5	-177.51	-133.41
E6	-	1.05
E7	-32.08	-22.26
E8	-	2.68

Table C.3: Material stream data for process with 80 % recycle

Material Stream	T (C)	T (K)	p (bar)	CH4	H20	CO	CO2	O2	H2	Total
1	25	298.15	1	-	1.0927	-	-	-	-	1.0927
2	25	298.15	92.26	-	1.0927	-	-	-	-	1.0927
3	305.35	578.5	92.26	-	1.0927	-	-	-	-	1.0927
4	305.35	578.5	92.26	-	0.9665	-	-	-	-	0.9665
5	687.68	960.83	92.26	-	0.9665	-	-	-	-	0.9665
6	25	298.15	1	1	-	-	-	-	-	1
7	25	298.15	92.26	1	-	-	-	-	-	1
8	687.68	960.83	92.26	0.9665	-	-	-	-	-	0.9665
9	926.85	1200	92.26	0.0335	-	-	-	-	-	0.0335
10	25	298.15	1	-	-	-	-	0.4536	-	0.4536
11	25	298.15	92.26	-	-	-	-	0.4536	-	0.4536
12	926.85	1200	92.26	-	-	-	-	0.4536	-	0.4536
13	926.85	1200	92.26	-	0.4536	-	-	-	-	0.4536
14	701.52	974.67	92.26	-	0.4536	-	-	-	-	0.4536
15	926.85	1200	92.26	-	-	-	0.2268	-	-	0.2268
16	25	298.15	92.26	-	-	-	0.2268	-	-	0.2268
17	25	298.15	1	-	-	-	0.2268	-	-	0.2268
18	687.68	960.83	92.26	-	-	-	-	-	2.3196	2.3196
19	687.68	960.83	92.26	-	-	0.7732	-	-	-	0.7732
20	701.52	974.67	92.26	-	-	0.7732	-	-	-	0.7732
21	701.52	974.67	92.26	-	0.1262	-	-	-	-	0.1262
22	701.2	974.35	92.26	-	-	-	-	-	0.6185	0.6185
23	25	298.15	92.26	-	-	-	-	-	2.9381	2.9381
24	25	298.15	1	-	-	-	-	-	2.9381	2.9381
25	701.52	974.67	92.26	-	-	-	0.6185	-	-	0.6185
26	25	298.15	92.26	-	-	-	0.6185	-	-	0.6185
27	25	298.15	1	-	-	-	0.6185	-	-	0.6185
28	687.68	960.83	92.26	-	0.1933	-	-	-	-	0.1933
29	701.52	974.67	92.26	-	0.1933	-	-	-	-	0.1933
30	687.68	960.83	92.26	0.1933	-	-	-	-	-	0.1933
31	926.85	1200	92.26	0.1933	-	-	-	-	-	0.1933
32	701.52	974.67	92.26	-	-	0.1547	-	-	-	0.1547
33	25	298.15	92.26	-	-	0.1547	-	-	-	0.1547
34	25	298.15	1	-	-	0.1547	-	-	-	0.1547
35	701.52	974.67	92.26	-	0.1547	-	-	-	-	0.1547
36	25	298.15	1	-	0.1547	-	-	-	-	0.1547

Table C.4: Energy stream data for process with 80 % recycle

Energy Stream	Heat	Work
Wout = E9 - E1	-	27.6745
E2	48.09	9.35
E3	159.37	109.92
E4	-	4.3111
E5	-181.98	-136.77
E6	-	1.0735
E7	-25.48	-17.68
E8	-	2.1254

Table C.5: Material stream data for process with SMR and WGS MRs

Material Stream	T (C)	T (K)	p (bar)	CH4	H20	CO	CO2	O2	H2	Total
1	25	298.15	1	-	1.0868	-	-	-	-	1.0868
2	25	298.15	10	-	1.0868	-	-	-	-	1.0868
3	180.2	453.35	10	-	1.0868	-	-	-	-	1.0868
4	180.2	453.35	10	-	0.8743	-	-	-	-	0.8743
5	687.68	960.83	10	-	0.8743	-	-	-	-	0.8743
6	25	298.15	1	1	-	-	-	-	-	1
7	25	298.15	10	1	-	-	-	-	-	1
8	687.68	960.83	10	0.8743	-	-	-	-	-	0.8743
9	926.85	1200	10	0.1257	-	-	-	-	-	0.127
10	25	298.15	1	-	-	-	-	0.4566	-	0.4566
11	25	298.15	10	-	-	-	-	0.4566	-	0.4566
12	926.85	1200	10	-	-	-	-	0.4566	-	0.4566
13	926.85	1200	10	-	0.4566	-	-	-	-	0.4566
14	701.52	974.67	10	-	0.4566	-	-	-	-	0.4566
15	926.85	1200	10	-	-	-	0.2283	-	-	0.2283
16	25	298.15	10	-	-	-	0.2283	-	-	0.2283
17	25	298.15	1	-	-	-	0.2283	-	-	0.2283
18	687.68	960.83	10	-	-	-	-	-	2.315	2.315
19	687.68	960.83	10	-	-	0.7717	-	-	-	0.7717
20	701.52	974.67	10	-	-	0.7717	-	-	-	0.7717
21	701.52	974.67	10	-	0.2125	-	-	-	-	0.2125
22	701.2	974.35	10	-	-	-	-	-	0.5761	0.5761
23	25	298.15	10	-	-	-	-	-	2.8911	2.8911
24	25	298.15	1	-	-	-	-	-	2.8911	2.8911
25	701.52	974.67	10	-	-	-	0.5761	-	-	0.5761
26	25	298.15	10	-	-	-	0.5761	-	-	0.5761
27	25	298.15	1	-	-	-	0.5761	-	-	0.5761
28	687.68	960.83	10	-	0.1026	-	-	-	-	0.1026
29	701.52	974.67	10	-	0.1026	-	-	-	-	0.1026
30	687.68	960.83	10	0.1026	-	-	-	-	-	0.1026
31	926.85	1200	10	0.1026	-	-	-	-	-	0.1026
32	701.52	974.67	10	-	-	0.1956	-	-	-	0.1956
33	25	298.15	10	-	-	0.1956	-	-	-	0.1956
34	25	298.15	1	-	-	0.1956	-	-	-	0.1956
35	701.52	974.67	10	-	0.1956	-	-	-	-	0.1956
36	25	298.15	1	-	0.1956	-	-	-	-	0.1956

Table C.6: Energy stream data for process with SMR and WGS MRs

Energy Stream	Heat	Work
Wout = E9 - E1	-	30.152
E2	47.83	9.3
E3	159.06	109.71
E4	-	1.5973
E5	-183.17	-137.66
E6	-	1.0806
E7	-23.73	-16.47
E8	-	2.2901

Table C.7: Material stream data for 1-step

				Molar flow rate (mol/s)						
Material Stream	T (C)	T (K)	p (bar)	CH4	H20	CO	CO2	O2	H2	Total
1	25	298.15	1	-	1.5206	-	-	-	-	1.5206
2	25	298.15	1	-	1	-	-	-	-	1
3	343.71	616.86	1	-	1.5206	-	-	-	-	1.5206
4	353.2	626.35	1	-	0.2397	-	-	-	-	0.2397
5	343.71	616.86	1	-	3.01412	-	-	-	-	3.01412
6	343.71	616.86	1	-	-	-	0.7603	-	-	0.7603
7	25	298.15	1	-	3.01412	-	-	-	-	3.01412
8	25	298.15	1	-	-	-	0.7603	-	-	0.7603
9	25	298.15	1	-	-	-	-	0.4794	-	0.4794
10	353.2	626.35	1	-	-	-	-	0.4794	-	0.4794
11	353.2	626.35	1	-	0.4794	-	-	-	-	0.4794
12	353.2	626.35	1	-	-	-	0.2397	-	-	0.2397
13	25	298.15	1	-	0.4794	-	-	-	-	0.4794
14	25	298.15	1	-	0.2397	-	-	-	-	0.2397

Table C.8: Energy stream data for 1-step

Energy Stream	Heat	Work
E1	192.32	99.36
E2	-	4.72
E3	-192.32	-99.37
E4	-	1.13

Appendix D

D.1 Main code

```
clear all
clc

%Membrane reactor parameters

global Opressure Rpressure Kp Otemperature R

Otemperature=960.83; %SMR MR operating temperature in K
R=8.314/1000; %Universal Gas constant in Kj/mol K

Rpressure = 100000; % This is the permeate pressure
%Pi=Opressure/Rpressure;

% n_i is the number of membrane and reactor stages.
n_i= 100;

% m_i is the number of substages in the membrane
m_i = 1000;

%Index for rate determining step
n = 0.5;

%Reactor parameters
Kp= 8.025;
t=0;
% Separator parameters:
%for Opressure = 100000:10000:20000
Opressure=1000000;
    j=0;
   t=t+1;
    Opressure
%for Ceff = 0.0:0.005:0.1
Ceff=0.05;
    j=j+1;
X(t,j)=Opressure/100000;
Y(t,j)=Ceff*100;




Feed=zeros(4,1);

%In component molar concentration vector, the order of components is:
% 1) CH_4
% 2) H20 (g)
% 3) H2
% 4) CO


% This fixes the feed compositions to the membrane reactor. The units is
% mol\s
Feed(1)=1;
Feed(2)=1;
Feed(3)=0;
Feed(4)=0;

%dA is the area of 1 membrane stage
dCeff = Ceff/n_i;
```

```
for b=1:1:n_i
% The function reaction takes in feed mole composition and returns the
% conversion and product mole compostions
b;
Feed;
Stage(b)=b;
[dc(b),Product]=reaction_robust_Pa(Feed);
Ph(b)=((Product(3))/sum(Product))*Opressure;
c(b)=sum(dc);
% % separation step. Use feed and retentate.
[retentate,permeate(b)]=separationCeff(Product,dCeff,m_i,n);
[dG(b)]=dGi_separation(Product,permeate(b));

Feed=retentate;
end

c_end=sum(dc);
dG_SMR_sep = sum(dG);


Z(t,j)=c_end;

figure(1)
contour(X,Y,Z,85,'ShowText','on')
xlabel('Operating Pressure of Membrane Reactor [bar]','interpreter','latex')
ylabel('$C_1$ [Barrer.m] $10^{-7}$','interpreter','latex')
title('Contours of conversion in region 4','interpreter','latex')
```

D.2 Code for reaction process

```
function [d_conversion, moleProduct]=reaction_robust(moleFeed,dcPrev)
global Opressure Kp
Opressure;
Kp;
for i=1:1:4
    if (moleFeed(i)<0)
       warning('Feed is negative_reaction')
        d_conversion=0;
        moleProduct=moleFeed;
        return
    end
end
Pressure=Opressure/100000;

    Ntotal=sum(moleFeed);

fun=@(x)(Kp-(((Pressure/(Ntotal+2*x))^2)*((moleFeed(3)+3*x)^3)*(moleFeed(4)+x))...
   /((moleFeed(1)-x)*(moleFeed(2)-x)));
%     x0=[0,1];
    c=fzero(fun,0.5);

        if (abs(c)<1e-4)
   c = 0;
   %warning('fzero function not accurate')
```

```
        end

%
    if ((abs(c)<1))
d_conversion = abs(c);
moleProduct(1)=moleFeed(1)-d_conversion;
moleProduct(2)=moleFeed(2)-d_conversion;
moleProduct(3)=moleFeed(3)+3*d_conversion;
moleProduct(4)=moleFeed(4)+d_conversion;

    else
        warning('fzero function does not work')
        [d_conversion,moleProduct]=reaction(moleFeed);
    end

    for i=1:1:4
    if (moleProduct(i)<0)
 %       warning('Feed is used up_reaction')
         d_conversion=0;
        moleProduct=moleFeed;
        return
    end
    end

end
```

D.3 Code for separation process

```
function [retentate, permeate]=separationCeff(feed_m,dCeff,m_i,n)
global Opressure Rpressure
% feed_m
%m_i is the number of substages we want to use.

% A is the area of each membrane sub-stage.
A = dCeff/m_i;

% Initialize retentate and permeate
retentate=feed_m;
permeate = 0;

for i = 1:1:m_i
    for j=1:1:4
    if (feed_m(j)<0)
       warning('Separation Feed is negative')
        J(i)=0;
 %       permeate = permeate + J(i);
        return
    end
end
sumfeed=sum(feed_m);
Ph(i)=(feed_m(3)/sumfeed)*Opressure;
if (Ph(i)>Rpressure)
    flux=A*((Ph(i)^n)-(Rpressure^n));
J(i)=A*((Ph(i)^n)-(Rpressure^n));
%warning('normalroute')
```

```
if (J(i)>feed_m(3))
    J(i)=feed_m(3);
    warning('Full separation!')
end
else
 %  warning('No partial pressure difference')
    J(i)=0;
end

SubStage(i)=i;
retentate(3)=feed_m(3)-J(i);
permeate = permeate + J(i);
feed_m(3) = retentate(3);

for j=1:1:4
    if (feed_m(j)<0)
       warning('Separation end is negative')
        J(i)=0;
 %       permeate = permeate + J(i);
        return
    end
end
end
```